THE UNIVERSITY OF HULL

Development of Microfluidic Devices for Analysis of Cardiac Tissue *ex vivo*

being a Dissertation submitted in partial fulfilment of

the requirements for the Degree of

Doctor of Philosophy

in the University of Hull

by

Lih Tyng, Cheah
BSc (Hons)

March 2012

Abstract

Polydimethylsiloxane (PDMS)–based (Generation 1) and glass–based (Generation 2) microfluidic devices for heart tissue maintenance have been developed. Rat and human heart biopsies were electrically–paced in a 37 ^{o}C environment constantly perfused with oxygenated media, and waste products were continuously removed, mimicking the *in vivo* conditions. Tissue damage was indicated by assaying the lactate dehydrogenase (LDH) activity in the effluent samples. Heart tissues were kept viable in the biomimetic microenvironment within these devices once optimised, for up to 3.5 hours (human, Generation 1); 5 hours (rat, Generation 1), and 24 hours (rat, Generation 2). Mechanical contraction was observed in some of the tissue biopsies, suggesting that they were functioning as it is in the body.

Sensitive, accurate and robust electrochemical analytical probes were established to measure the total reactive oxygen species (ROS) and creatine kinase MB (CK–MB) concentration in the effluent from the tissue biopsies. The total ROS probe was integrated with the Generation 1 microfluidic device to give a real–time measurement of the tissue insult. Both of these devices were also used to investigate the effects of on–chip ischaemia reperfusion (IR) procedures on the expression levels of a series of genes, which were analysed off–chip by semi–quantitative PCR.

In addition, mixing within the Generation 1 microfluidic device was induced by redox–magnetohydrodynamics (redox–MHD), where a redox species, hexamineruthenium (III) chroride (Ruhex) and magnet were used to generate a magnetic force, thus causing the fluid to rotate around the electrodes. Qualitative microscopy recordings on polystyrene microbeads movement were provided in the supplementary DVD, showing the effects of MHD and Ruhex–MHD. This application could be of particular importance when the tissue sample is exposed to certain therapeutic drugs during perfusion for defined periods of time, to test the responsiveness of cardiac tissue to treatment.

This proof–of–principle microfluidic technique will hopefully serve as a platform technology for future cardiac research and may also be exploited and modified for investigation of other clinical tissues, hence reducing reliance on animal models. The full potential of this technology remains to be discovered as other groups adopt this approach to analyse diseased and normal tissues.

Acknowledgements

First and foremost, I would like to express my deep and sincere gratitude to my supervisors, Professor John Greenman, Dr Anne Marie Seymour, and Professor Stephen Haswell for their understanding, encouragement and personal guidance during my times in the PhD pursuit. I will never forget their valuable assistance in the preparation and completion of this study.

I owe my sincere thanks to Dr Yuehua Dou and Dr Jay Wadhawan for their valuable advice and demonstration of the electrochemistry microelectrode fabrication work. Their kind support and patience have been of great value in this study and my first published paper. I also wish to thank Professor Ingrid Fritsch from USA, who has visited and worked with me at the end of 2010 on MHD studies on–chip. The extensive and interesting discussions around our work have offered me a great insight into the potential microfluidic integration.

I would also like to extend special thanks to Mrs Jenny Foster and Mrs Kathleen Bulmer for their invaluable technical support. In particular, I am grateful to Dr Steve Clark for building the microfluidic devices, Mr John Hebden for manufacturing the incubator box and Mr Steven Griffin for providing the human sample biopsies.

I gratefully acknowledge the funding source, the Heart Research UK, that made my PhD work possible. Not forgetting also the Oversea Research Scholarship offered by The University of Hull.

Lastly, I would like to thank my family for all their love and support in all my pursuits. Also, I express my thanks to my colleagues and friends at the University who make my life in Hull enjoyable and colourful.

Table of Contents

Pages

List of Figures

Pages

Chapter 1. Introduction

Chapter 2. Materials and Methods

List of Tables

Pages

Chapter 1. Introduction

Chapter 2. Materials and Methods

Chapter 4. Ischaemia Reperfusion in Generation 1 Device

Chapter 6. Ischaemia Reperfusion in Generation 2 Device

List of Equations

Pages

Abbreviations

$\Delta\Psi$	Membrane potential
1,3 BPG	1, 3–bisphosphoglycerate
ACC	Acetyl–coenzyme A carboxylase
ACL	ATP citrate lyase
Acetyl–CoA	Acetyl–coenzyme A
AD	Adenosine deaminase
ANOVA	Analysis of variance
ANT	Adenosine nucleotide translocase
AMI	Acute myocardial infarction
Apaf–1	Apoptotic protease activating factor–1
AR	Aldose reductase
A_{temp}	Annealing temperature
ATP	Adenosine triphosphate
Bak	Bcl–2 homologous antagonist killer
Bax	Bcl–2 associated X protein
Bcl–2	B cell lymphoma gene 2
Bcl–xL	B cell lymphoma–extra large
Bio–MEMS	Bio–microelectromechanical system
β–ME	β–mercaptoethanol
BNP	Brain natriuretic peptide
BSA	Bovine serum albumin
CABG	Coronary artery bypass graft
Calcein AM	Calcein–acetoxymethyl ester
Caspases	Cysteine aspartate–specific proteases
cDNA	Complementary DNA
cFLIP	Cellular FLICE inhibitory protein
CICR	Calcium–induced calcium release
CK	Creatine kinase
CK–BB	Creatine kinase–brain type
CKmito	Mitochondrial creatine kinase
CK–MB	Creatine kinase heterodimer
CK–MM	Creatine kinase–muscle type
$CoQH_2$	Coenzyme QH_2
Cr	Creatine
Cu-ZnSOD	Copper–zinc superoxide dismutase
CycV	Cyclic voltammetry
CV	Coefficient of variation
Cx 43	Connexin 43
CyP–D	Cyclophilin–D
Cyt c	Cytochrome c
dATP	Deoxyadenosine triphosphate
dCTP	Deoxycytidine triphosphate
dGTP	Deoxyguanosine triphosphate
DHBA	8–hydroxydeoxyguanosine, 2,3–dihydroxybenzoic acid
DIABLO	Direct IAP binding protein with low pl
DMF	Dimethylformamide

dNTP	Deoxyribonucleotide triphosphate
DTT	Dithiothreitol
dTTP	Deoxythymidine triphosphate
EC	Excitation–contraction
ECIA	Electrochemical immunoassays
ECM	Extracellular matrix
EDC	Ethyl(dimethylaminopropyl) carbodiimide
EDTA	Ethylenediaminetetraacetic acid
EIA	Enzyme immunoassay
ELISA	Enzyme–linked immunosorbent assay
ETC	Electron transport chain
eNOS	Endothelial nitric oxide synthase
F	Faraday constant (96485.34 C/mol)
F6P	Fructose–6–phosphate
FADD	Fas–associated death domain
$FADH_2$	Reduced form of flavin adenine dinucleotide
FAS	Fatty acid synthase
Fc–CHO	**Ferrocene–carboaldehyde**
FIA	Fluorescence immunoassay
FITC	**Fluorescein isothiocyanate**
G6P	**Glucose–6–phosphate**
G6PD	**Glucose–6–phosphate dehydrogenase**
GAPDH	Glyceraldehyde 3–phosphate dehydrogenase
gDNA	Genomic deoxyribonucleic acid
GK	Glycerol kinase
GLUT	Glucose transporter
GPO	Glycerol–3–phosphate oxidase
GPx	Glutathione peroxidase
GSH	Glutathione
HK	Hexokinase
HMG–CoA	3–hydroxy–3–methylglutaryl–coenzyme A
HRP	Horseradish peroxidase
hsCRP	High sensitivity C–reactive protein
HSF–1	Heat shock factor protein–1
HSP	Heat shock protein
HX	Hypoxanthine
ID	Inner diameter
IgG	Immunoglobulin G
IMM	Inner mitochondrial membrane
iNOS	Inducible nitric oxide synthase
I_0	Oxidation current
i_p	Peak current
IR	Ischaemia reperfusion
KHBB	Krebs–Henseleit bicarbonate buffer
LA	Left atrium
LAD	Left anterior descending
L–Arg	L–arginine
I_{ca}	L–type Ca^{2+} channel
L–Cir	Citrate
LDH	Lactate dehydrogenase

L-NAME	L–nitro–arginine methyl ester
LOC	Lab–on–a–chip
LV	Left ventricle
Mcl–1	Induced myeloid leukemia cell differentiation protein–1
MHD	Magnetohydrodynamic
MI	Myocardial infarction
MitoCaU	Mitochondrial Ca^{2+} uniporter
M–MLV	Moloney murine leukemia virus
MnSOD	Manganese–superoxide dismustase
mPTP	Mitochondrial permeability transition pore
mRNA	Messenger ribonucleic acid
NAD^+	Oxidised form of nicotinamide adenine dinucleotide
NADH	Reduced form of nicotinamide adenine dinucleotide
NADH dehyd	Nicotinamide adenine dinucleotide dehydrogenase
NADPH	Nicotinamide adenine dinucleotide phosphate
Na–HX	Sodium–proton exchanger
NBT	Nitro blue tetrazolium
NCX	Na^+/ Ca^{2+} exchanger
NdFeB	Neodymium iron boron
NF–IL6	Nuclear factor for interleukin 6
nNOS	Neuronal nitric oxide synthase
NO	Nitric oxide
NOS	Nitric oxide synthase
NTP	Nucleoside triphosphate–AMP transphosphorylase
NT–proBNP	N–terminal pro brain natriuretic peptide
$O^{\bullet-}$	Superoxide anion
OD	Outer diameter
OH•	Hydroxyl
Oligo $(dT)_{15}$	Oligodeoxythymidylic acid (15 nucleotides)
OMM	Outer mitochondrial membrane
PBS	Phosphate buffered saline
PCr	Phosphocreatine
PCR	Polymerase chain reaction
PDH	Pyruvate dehydrogenase
PDMS	Polydimethylsiloxane
PEEK	Polyether ether ketone
PEP	Phosphoenolpyruvate
PFK1	Phosphofructokinase–1
PFKFB	6–phosphofructo–2–kinase/fructose–2,6–biphosphate
PGI	Phosphoglucose isomerase
Pi	Inorganic phosphate
PI	Propidium iodide
PIC	Phosphate carrier
PK	Pyruvate kinase
PLB	Phospholamban
PMF	Proton motive force
PMS	Phenazine methosulfate
pO_2	Partial pressure of oxygen
POC	Point–of–care
PPP	Pentose phosphate pathway

Pt	Platinum
PVO–Os–HRP	Polyvinylpyridine–osmium–wired horseradish peroxidase
Q	Ubiquinone
R	Gas constant (8.314 J/K/mol)
RA	Right atrium
Re	Reynolds number
RIA	Radioimmunoassay
ROS	Reactive oxygen species
RT	Reverse transcription
Ruhex	Hexammineruthenium (III) chroride
RV	Right ventricle
RyR	Ryanodine receptor
SDH	Sorbitol dehydrogenase
SE	Stimulation electrode
SERCA	SR Ca^{2+} ATPase
Si–O–Si	Siloxane bonds
Si–OH	Silicone hydroxide
SMAC	Second mitochondrial–derived activator of caspase
SOD	Superoxide dismutase
SR	Sarcoplasmic reticulum
STAT	Signal transducer and activator of transcription
Sulpho–NHS	N–hydroxysulphosuccinimide
TBE	Tris/Borate/EDTA
tBid	Truncate BH3 interacting domain death agonist
TC	Tissue chamber
TCA	Tricarboxylic acid
TRAIL	TNF–related apoptosis–inducing ligand
Tris	Tris(hydroxymethyl)aminomethane
Tn	Troponin
TNF–α	Tumour necrosis factor–alpha
TRAIL	TNF–related apoptosis–inducing ligand
TUNEL	Terminal deoxynucleotidyl transferase–mediated dUTP *in situ* nick–end labeling
µTAS	Micro total analysis system
UCP	Uncoupling protein
UV	Ultraviolet
VDAC	Voltage–dependent anion channel
X	Xanthine
XDH	Xanthine dehydrogenase
XIAP	X–linked inhibitor of apoptosis protein
XO	Xanthine oxidase

Chapter 1

Introduction

1.1. The heart – An important pumping machine

The mammalian heart consists of four chambers, left atrium (LA) and right atrium (RA), left ventricle (LV) and right ventricle (RV; Figure 1.1). The heart consists primarily of terminally differentiated cardiomyocytes, and supportive fibrovascular connective tissue (Opie, 2004), with an average cell density of 1 – 10 x 10^8 cells/cm^3 (Murthy *et al*., 2006). Cardiomyocytes contribute about 20 – 40 % of all the heart cells, but they occupy 80 – 90 % of its volume (Nag, 1980). The atria have relatively thin walls and serve as the collection chambers for blood entering the heart, while the thicker ventricles, especially the LV, act as the pump to eject blood into the pulmonary and systemic circulation. On average, the wall thicknesses for human RA and LA are 2 mm and 3 mm; for RV and LV, these are up to 5 mm and 15 mm, respectively (Berry and Billingham, 2007).

1.1.1. Calcium handling

Ca^{2+} is the central regulator of myocardium contraction which involves the mutual sliding of thick and thin filaments (Figure 1.2). Myosin heavy and light chains are found in the thick filament, whilst the thin filament contains actin, troponin (Tn) complex (TnI, TnC, and TnT) and tropomyosin. Regulation of myocardial contractility is an important aspect of normal cardiovascular function. Cardiac excitation–contraction (EC) coupling is used to describe the process from the electrical excitation of cardiomyocyte to the contraction of the heart.

The cellular surface of a cardiomyocyte has T–tubules which run transversally from the sarcolemma across cardiomyocytes (Brette and Orchard, 2003). EC coupling is triggered when the cell is depolarised by an action potential (Bers, 2002). Subsequently, Ca^{2+} enters the cell through depolarization–activated L–type Ca^{2+} channels (I_{ca}; Figure 1.3). This influx of Ca^{2+} is detected by ryanodine receptors (RyR) in the footpad of the sarcoplasmic reticulum (SR) membrane, triggering the release of Ca^{2+} stored in this organelle (Fabiato, 1983).

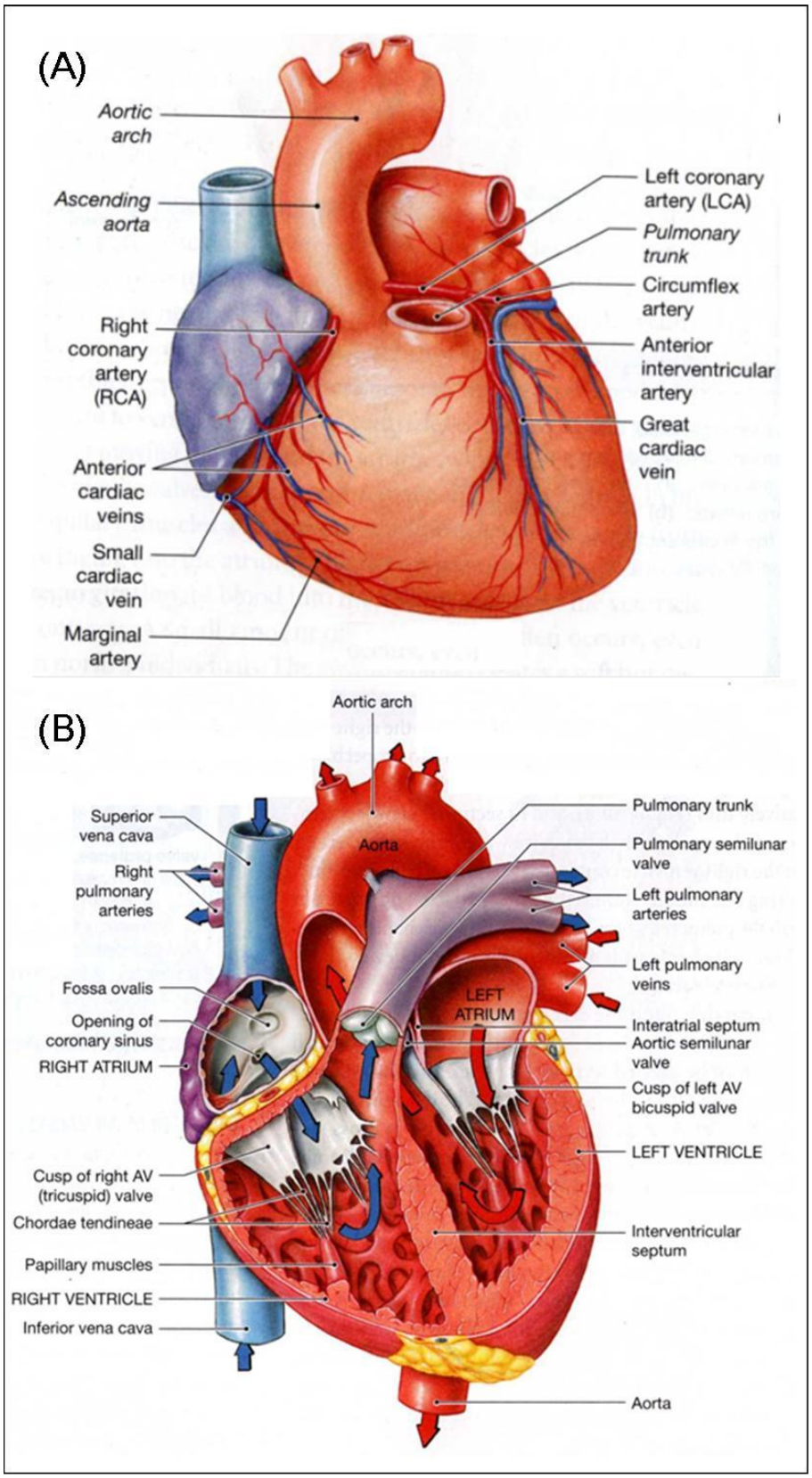

Figure 1.1. Anatomy of the mammalian heart: (A) anterior (B) sectional views. (Martini and Bartholomew, 2010)

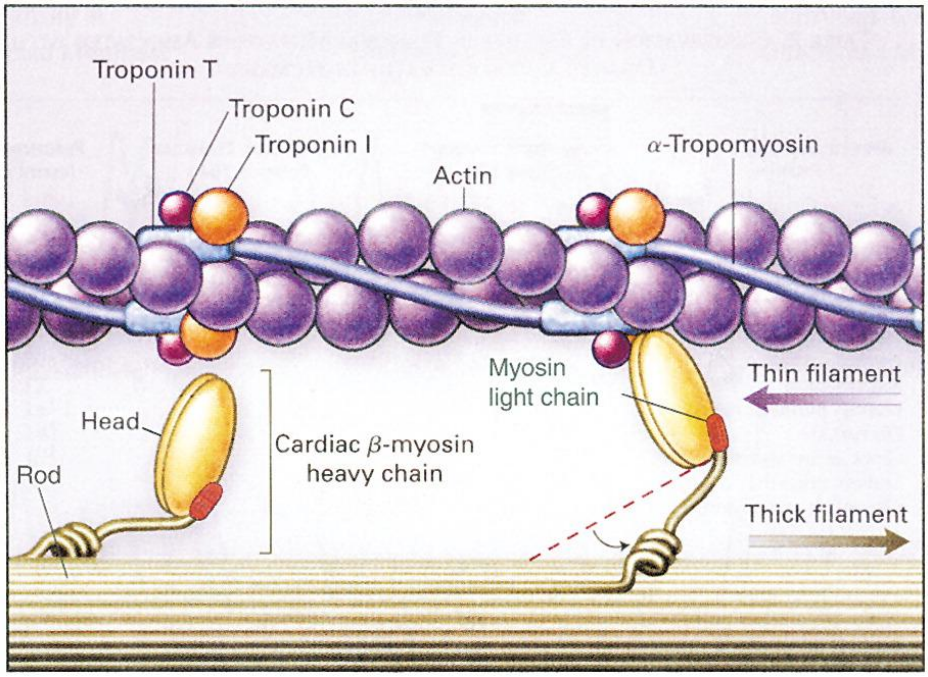

Figure 1.2. Components of thin and thick filaments. (Seidman and Seidman, 2001)

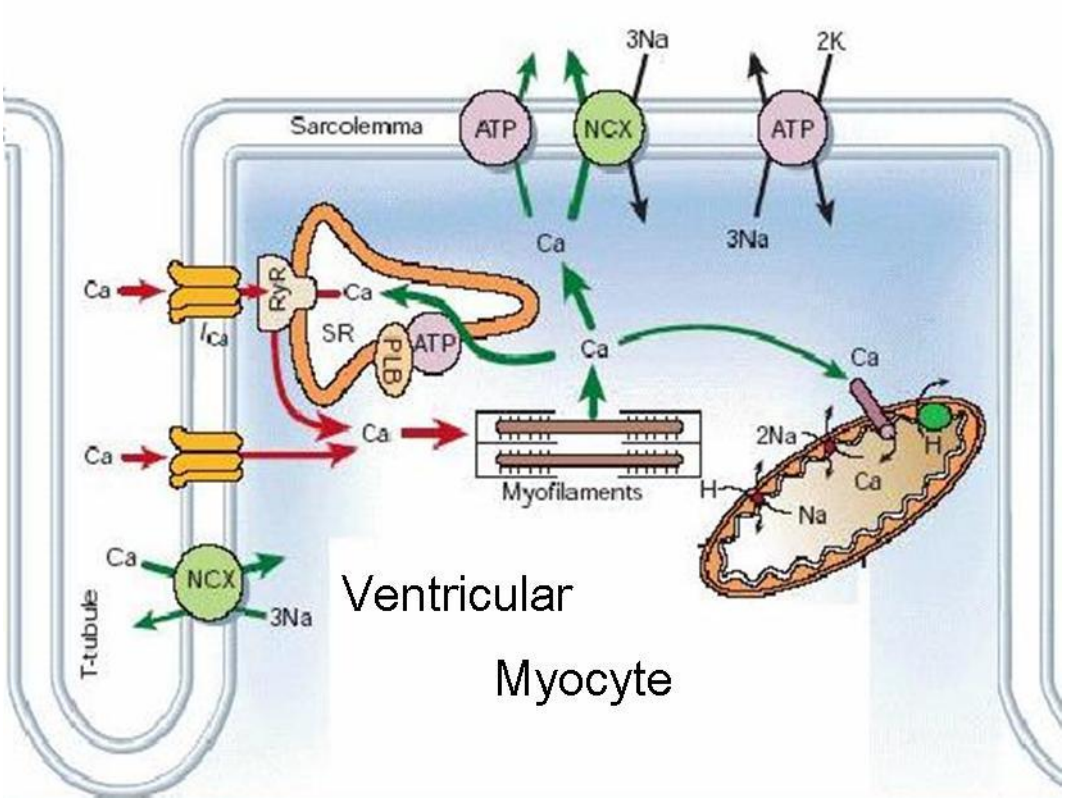

Figure 1.3. Excitation–contraction coupling. (Bers, 2008)

ATP, adenosine triphosphate; NCX, Na^+/Ca^{2+} exchanger; PLB, phospholamban; RyR, ryanodine receptor; SR, sarcoplasmic reticulum.

The process is known as calcium–induced calcium release (CICR). The opening of the cardiac RyR is the greatest when the [Ca^{2+}] is about 100 µM, and this decreases at very high [Ca^{2+}] (5 – 10 mM; Xu *et al*., 1998, Bers, 2008). The combination of Ca^{2+} influx, together with SR Ca^{2+} release increases the cytosolic [Ca^{2+}] (Huxley, 1957), facilitating the binding of Ca^{2+} to TnC of the thin filaments. This in turn results in conformational changes in TnI which expose a site on the actin molecules for the binding of the myosin head which contains ATPase (Figure 1.4). By using the energy produced from adenosine triphosphate (ATP) hydrolysis, the myosin head forms a cross bridge with the actin filaments active site, pulling the actin filament toward the centre of the sarcomere, hence shortening the sarcomere length. The resultant ADP and inorganic phosphate (Pi) are then dissociated from the myosin.

The strength of contraction relies on the extent of SR Ca^{2+} release, which in turn depends on Ca^{2+} influx and SR Ca^{2+} content (Bassani *et al.,* 1995). Half–maximal activation of contraction requires approximately 60 µM Ca^{2+} influx to reach 600 nM $[Ca^{2+}]_i$, i.e. ~ 100 : 1 buffering of $[Ca^{2+}]_i$ (Bers, 2008). Under physiological conditions, the SR Ca^{2+} content is in the range of 50 – 150 µmol/L cytosol (Bers, 2008). A typical contraction in rabbit ventricular myocytes involves the release of ~ 50 % of the SR Ca^{2+} content (Bassani *et al*., 1995).

For myocardial relaxation to occur, $[Ca^{2+}]_i$ must be sequestered, to allow dissociation of Ca^{2+} ions from TnC. This can occur in four possible mechanisms: (i) SR Ca^{2+}–ATPase (SERCA) which is under the inhibitory control of phospholamban (PLB), (ii) sarcolemmal Na^+/Ca^{2+} exchanger (NCX), (iii) sarcolemmal Ca^{2+}–ATPase and (iv) mitochondrial Ca^{2+} uniporter (MitoCaU; Bassani *et al.,* 1994; Figure 1.3). Contributions of SERCA and NCX in Ca^{2+} removal from the cell during relaxation are about 68.5 % and 30 % in rabbit ventricular myocytes, respectively (Bers, 2008), consistent with a study conducted by Bassani's group using rat and rabbit models (SERCA: 70 %, NCX: 28 %; Bassani *et al*., 1994). The sarcolemmal Ca^{2+}–ATPase and

MitoCaU contributed less than 1 % each for Ca^{2+} removal in both studies. However, in rat myocytes, SERCA contributed 92 % of Ca^{2+} removal, while it was 7 % for NCX (Bassani *et al.,* 1994). The variation in contribution was mainly due to the species differences. The reduction in $[Ca^{2+}]_i$ induces a conformational change in the Tn complex, allowing TnI to inhibit the binding of myosin to actin. An ATP molecule then binds to the myosin head and the initial sarcomere length is restored (Figure 1.4).

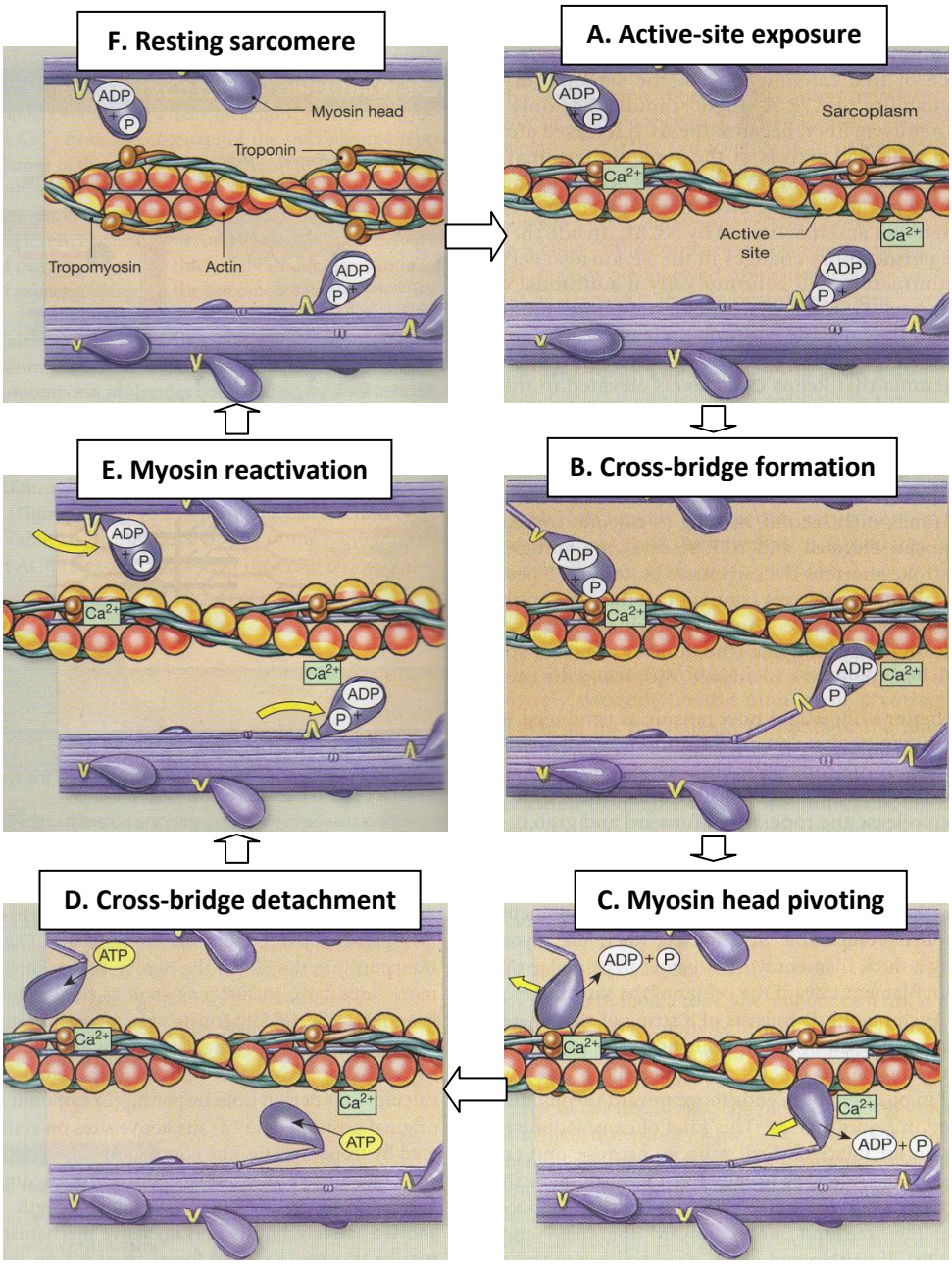

Figure 1.4. Molecular events occuring during the contraction cycle. (Martini and Nath, 2009)

ADP, adenosine diphosphate; ATP, adenosine triphosphate; P, phosphate.

1.1.2. Energy production

The cardiac energy metabolism consists of: substrate utilization (from food) followed by oxidative phosphorylation and energy transfer/utilization in the creatine kinase (CK) system (Figure 1.5).

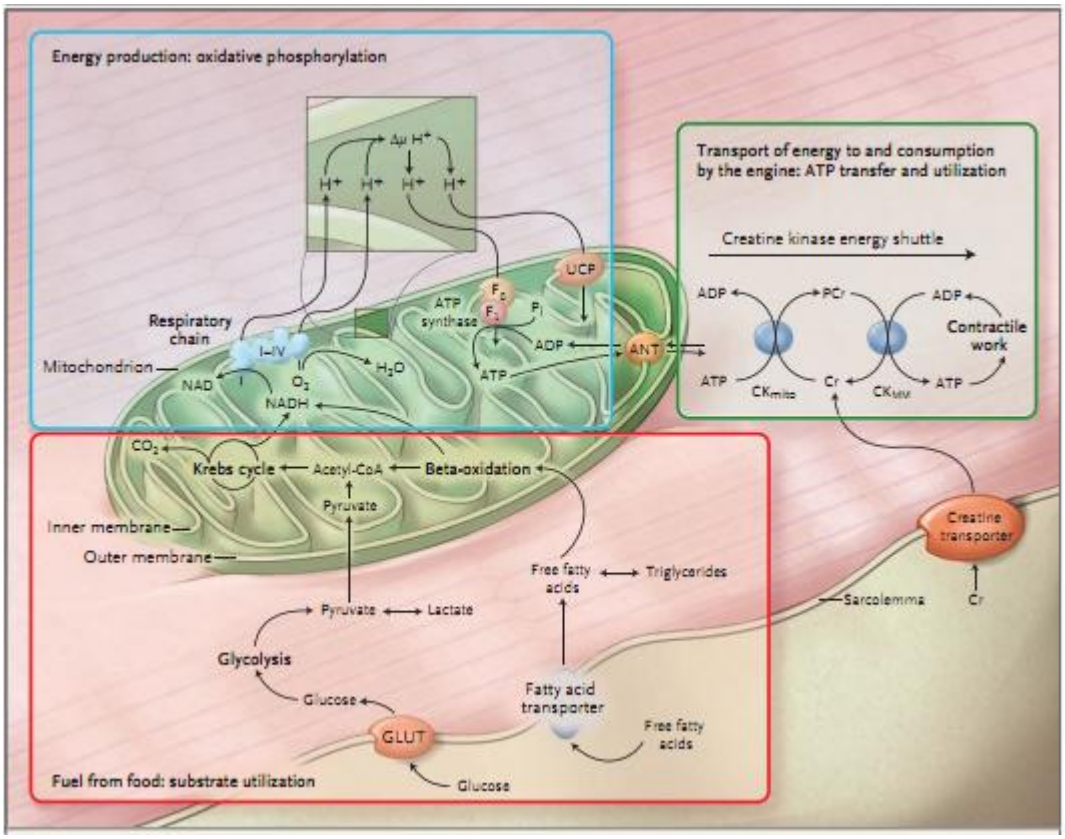

Figure 1.5. Cardiac energy metabolism. (Neubauer, 2007)

ADP, adenosine diphosphate; ANT, adenine nucleotide translocase; ATP, adenosine triphosphate; CKmito, mitochondrial creatine kinase; Cr, creatine; GLUT, glucose transporter; NAD, oxidised nicotinamide adenine dinucleotide; NADH, reduced nicotinamide adenine dinucleotide; PCr, phosphocreatine; UCP, uncoupling protein.

The heart has an ATP content of 5 µmol/g wet weight, and an ATP hydrolysis rate of ~ 0.5 µmol/g wet weight/second at rest, hence there is a complete turnover of the myocardial ATP pool at about 10 seconds under normal conditions (Ingwall, 2002). Therefore the heart requires a constant supply of ATP from fuels, such as glucose, lactate, fatty acids or ketone bodies, to maintain its pump function. The release of energy from these compounds via oxidation involves step–by–step processes of enzymatically controlled fuel metabolism and mitochondrial oxidative phosphorylation

(Taegtmeyer, 2000). About 95 % of ATP comes from mitochondrial oxidative phosphorylation (Stanley *et al*., 2005, Lopaschuk *et al*., 2010).

In the normal adult heart, fatty acid β–oxidation is the predominant source of ATP generation (Sambandam and Lopaschuk, 2003), the remaining being produced by oxidation of glucose, lactate and ketone bodies. Fatty acids generate more ATP molecules than carbohydrates on a per carbon atom basis. For instances, oxidation of one 18–carbon oleic acid produces 146 ATP (8.1 ATP/carbon), whereas oxidation of glucose liberates 36 ATP (6 ATP/carbon). A two–carbon fragment acetyl–coenzyme A (acetyl–CoA), produced as the result of substrate oxidations mentioned above, enters the tricarboxylic acid (TCA) cycle within the mitochondria (Figure 1.6). Under normal conditions, approximately 60 – 90 % of acetyl–CoA, which enters the TCA cycle, comes from β–oxidation of fatty acids, and 10 – 40 % from oxidation of pyruvate, which comes from the glucose (Scolletta *et al*., 2011).

The TCA cycle is closely linked to ATP generation via mitochondrial oxidative phosphorylation (Mitchell, 1972). The reduced forms of nicotinamide adenine dinucleotide (NADH) and flavin adenine dinucleotide ($FADH_2$), produced by substrate oxidations and the TCA cycle, feed into the electron transport chain (ETC), where a series of protein complexes (I – IV) are located on the inner mitochondrial membrane (IMM; Figure 1.7). NADH and $FADH_2$ pass electrons into the ETC which is coupled to ATP synthesis via the proton pumping activity of complexes to generate a proton motive force (PMF) across the inner mitochondrial membrane. Protons are extruded for electron passing from NADH and $FADH_2$ to oxygen (Brand, 2005, Hinkle, 2005). PMF consists of a membrane potential ($\Delta\Psi$) and a pH gradient (Equation 1; Breeuwer and Abee, 2004). The redox span across the entire ETC is about 1100 mV with the maximal PMF maybe 180 – 220 mV across the IMM (Brand and Nicholls, 2011). This force is used by ATP synthase to synthesize ATP from ADP and Pi.

$$PMF\ (\Delta p) = \Delta\Psi - Z\,\Delta pH \qquad \textbf{Equation 1}$$

Where Z = 2.3RT/F; R is the gas constant, F is the Faraday constant, and T is the temperature.

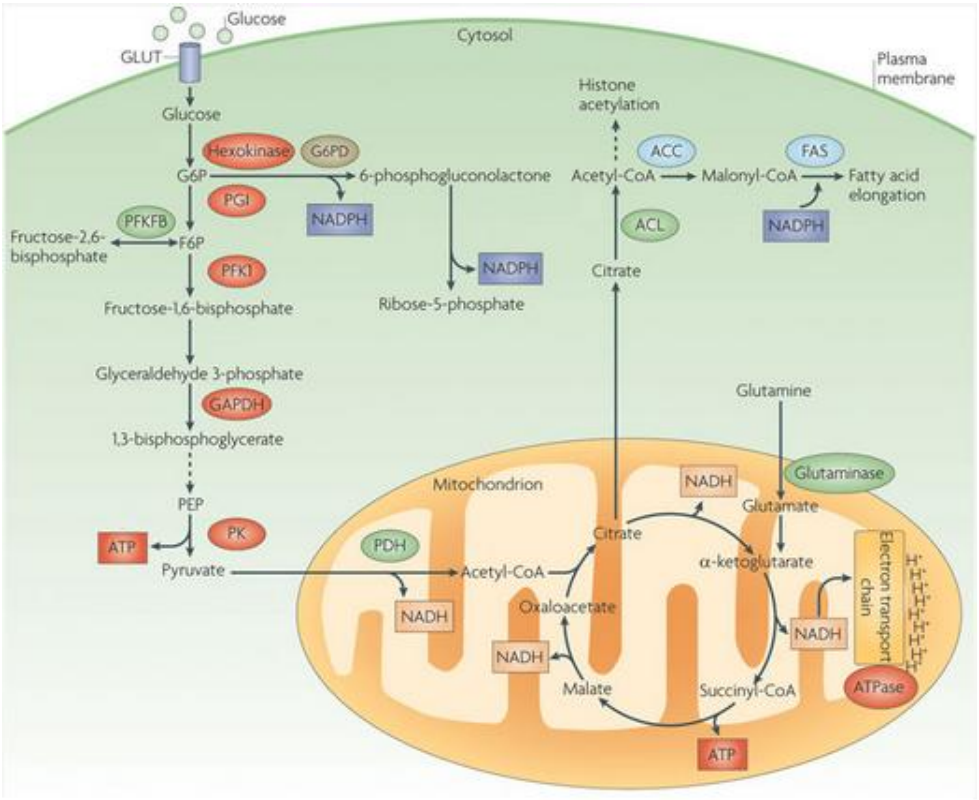

Figure 1.6. Overview of glycolysis and TCA cycle. (Buchakjian and Kornbluth, 2010)

ACC, acetyl–CoA carboxylase; ACL, ATP citrate lyase; ATP, adenosine triphosphate; F6P, fructose–6–phosphate; FAS, fatty acid synthase; G6P, glucose–6–phosphate; G6PD, glucose–6–phosphate dehydrogenase; GAPDH, glyceraldehydes 3–phosphate dehydrogenase; GLUT, glucose transporter; PDH, pyruvate dehydrogenase; PEP, phosphoenolpyruvate; PGI, phosphoglucose isomerase; PFK1, phosphofructokinase–1 ; PFKFB, 6–phosphofructo–2–kinase/fructose–2,6–biphosphatase; PK, pyruvate kinase; NADH, reduced nicotinamide adenine dinucleotide; NADPH, reduced nicotinamide adenine dinucleotide phosphate.

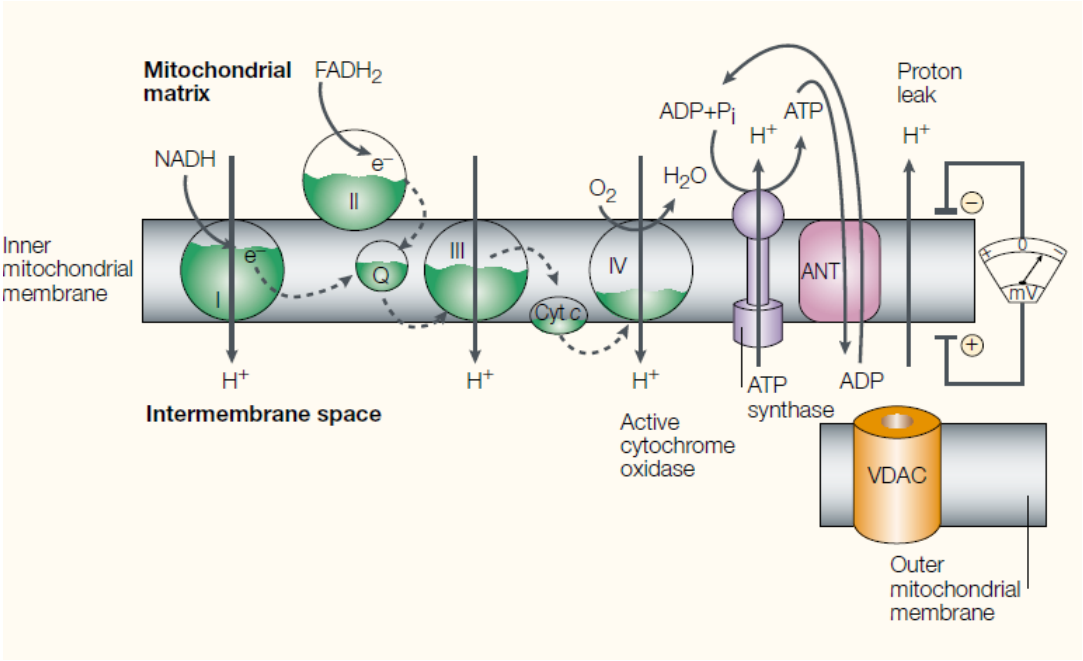

Figure 1.7. Electron transport chain in mitochondria. (Moncada and Erusalimsky, 2002)

ADP, adenosine diphosphate; ANT, adenosine nucleotide translocase; ATP, adenosine triphosphate; Cyt c, cytochrome c; NADH, nicotinamide adenine dinucleotide; $FADH_2$, reduced form of flavin adenine dinucleotide; Pi, inorganic phosphate; Q, ubiquinone; VDAC, voltage–dependent anion channel; I, II, III, IV refer to the protein complexes of the electron transport chain.

Under high ATP demand, cardiomyocytes use the energy reserve i.e. the phosphocreatine (PCr) and creatine kinase (CK) reaction within the heart (Ingwall, 2009). This system serves as an energy buffer and transporter of high energy phosphate bonds from the sites of energy production to the sites of usage, particularly in the heart (Figure 1.5). The rate of ATP synthesis in the CK reaction in the rat heart is 10 mM/second, compared with mitochondrial oxidative phosphorylation which is 0.7 mM/second (Ingwall, 2002). Two isoforms of CK can be found in a cell, mitochondrial CK (CKmito) and cytosolic CK. There are two CKmito isoenzymes: the ubiquitous and sarcomeric form. Ubiquitous CKmito is expressed in brain, smooth muscle and sperm, whereas sarcomeric CKmito is expressed solely in cardiac and skeletal muscle (Schlattner *et al*., 2006). Cytosolic CK enzyme exists as a homo or heterodimer consisting of a combination of either B (brain type) or M (muscle type): CK–MM, CK–BB, and CK–MB. The ratio of isoenzymes varies

within muscle type: cardiac muscle (70 – 80 % CK–MM, 20 – 30 % CK–MB), skeletal muscle (98 % CK–MM, 2 % CK–MB), and brain has predominantly CK–BB (Sood, 2006).

CKmito is located on the outer mitochondrial membrane (OMM) coupled to adenine nucleotide translocase (ANT), linked by cardiolipin molecules, and directly interacts with voltage–dependent anion channel (VDAC; Schlattner *et al*., 2009), where it catalyzes the transfer of a high energy phosphate bond from ATP to creatine to form PCr. In contrast, cytosolic CK associates with cellular structures in close proximity to ATP–requiring processes (Schlattner *et al*., 2006), e.g. contractile apparatus, and catalyzes the reverse transfer of a phosphate group to ADP, liberating creatine and ATP (Neubauer, 2007). CK catalyzes the phosphorylation of approximately 2/3 of total creatine pool in the heart, where the remaning 1/3 remains as free creatine. When energy demand exceeds energy supply, PCr levels decline in order to restore ATP level to the normal range (Ingwall, 2002).

1.2. Myocardial infarction

Myocardial infarction (MI) is a result of acute occlusion of a coronary artery (Figure 1.1.A) for more than 20 – 40 minutes. Timely reperfusion is the definitive solution for the acute MI (AMI) where restoration of blood flow to the ischaemic zone of myocardium is elicited (Figure 1.8); however, this reintroduction of blood flow may itself induce or exacerbate lethal tissue injury in addition to that generated by ischaemia alone (Yellon and Hausenloy, 2007), including arrhythmias, contractile dysfunction (stunning), microvascular impairment, and irreversible damage via apoptosis and necrosis (Moens *et al*., 2005). Despite optimal reperfusion, the mortality rate after an AMI approaches 10 % (Keely *et al*., 2003). Such ischaemia reperfusion (IR) episode is a clinical problem associated with procedures, for example thrombolysis, coronary bypass graft (CABG) surgery, and angioplasty which are generally used to generate blood reflow and reduce the damage of the myocardium following severe ischaemia (Venugopal *et al*., 2009a and b).

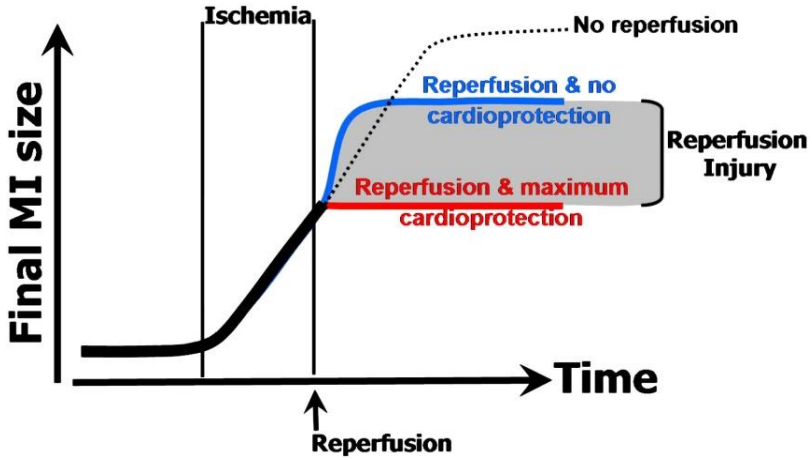

Figure 1.8. Effect of myocardial ischaemia and reperfusion on final infarct size. (Adapted from García-Dorado and Piper, 2006)
MI, myocardial infarction.

1.2.1. Metabolic changes

During coronary artery occlusion, oxygen supply to the myocardium is limited and mitochondrial oxidative phosphorylation is interrupted. PCr and ATP are reduced subsequently. In a model of myocardial ischaemia simulated by a 60 % reduction in coronary blood flow for 1 hour, [PCr] and [ATP] were decreased by 75 % and 50 %, respectively (Salem *et al*., 2002).

Corresponding increase in [Pi] is also found in ischaemic myocardium. In paced, isolated rabbit hearts, [Pi] increased 6 – fold when the mean coronary flow was reduced from 25 to 1 ml/minute for 15 minutes (Ferrari, 2001). When coronary flow is completely occluded, [Pi] can increase > 10 – fold compared to the normoxic concentrations. During acute ischaemia, where the left anterior descending (LAD) artery was ligated, [P_i] was increased to approximately 3.1 mM and 5.1 mM, 22 s and 36 s after the occlusion, respectively. Increased [P_i] favours the opening of mitochondrial permeability transition pore (mPTP; discussed below), and leads to apoptosis (Lim *et al*., 2007, Di Lisa *et al*., 2011).

As oxidative phosphorylation is impaired during IR, metabolic intermediates in the form of reducing equivalents and protons accumulate, for example the cytoplasmic NADH and the relative ratios of redox couples, NADH/NAD^+ increases by 13 – fold (Salem *et al*., 2002). This increase can depress SR Ca^{2+} release by over 50 % in ventricular cardiomyocytes, as NADH mediated direct and indirect inhibition on the activities of RyR channel and SERCA, respectively (Zima *et al*., 2004). Therefore, significant changes in the NADH/NAD^+ ratio play a crucial role in the impairment of CICR and EC coupling during myocardial IR.

In addition, a shift from aerobic mitochondrial metabolism to anaerobic glycolysis appears to be an adaptation to reduced oxygen availability during ischaemia (Ramirez *et al*., 2007). Such a shift can occur over different timescales via a variety of mechanisms, allowing cardiomyocytes to cope

with the energy demand (Gohil *et al*., 2010). Pyruvate generated by glycolysis is not oxidised in the mitochondria, instead it is reduced to lactate in the cytosol. Hence, lactate was shown to be a specific but relatively insensitive diagnostic marker of myocardial ischaemia in the clinical settings in early studies (Buffon *et al*., 2000). During ischaemia, lactate and its associated H^+ accumulate in the cardiomyocytes leading to intracellular acidosis, contributing to contractile dysfunction in the ischaemic myocardium. The cytoplasmic pH reduced from 7 to 5.5 – 6 during 30 minutes of low–flow or 20 minutes of zero–flow ischaemia in isolated perfused rat heart (Trueblood *et al*., 2000). It has been demonstrated that intracellular lactate produced during ischaemia reduced the glycolytic rate indirectly by increasing $NADH/NAD^+$ ratio (Cross *et al*., 1995), whereas reduced intracellular pH directly and indirectly decreased pyruvate production by inhibition of phosphofructokinase (Figure 1.6), which in turn inhibited glycolysis (Ichai *et al*., 2008).

Reperfusion of ischaemic myocardium causes a rapid alteration in the ionic fluxes, and normalization of pH may enhance cytotoxicity (Turer and Hill, 2010). Studies using acidotic postconditioning have demonstrated cardioprotective effects (Cohen *et al*., 2007), in that 30 minutes of reperfusion in ischaemic rabbit heart with buffer of pH 7.4 elicited 34.4 ± 2.2 % infarct, whereas 2 minutes of acidosis postconditioning (6 cycles of 10 seconds reperfusion / 10 seconds of occlusion) at reperfusion with buffer of pH 6.9 caused only 15.0 ± 2.6 % infarction. This cardioprotective effect was mainly due to the prevention the mPTP formation (discussed below).

1.2.2. Oxidative stress

Partial reduction of oxygen generates reactive oxygen species (ROS), which include free radicals such as the superoxide anion ($O_2\bullet^-$) and hydroxyl radical (OH•), as well as non–radicals such as hydrogen peroxide (H_2O_2). These species are intermediates that have either unpaired electrons ($O_2\bullet^-$, OH•) or the ability to attract electrons from other molecules (H_2O_2). Furthermore, nitric acid (NO) can react with $O_2\bullet^-$ to form highly reactive

peroxynitrite. Excess ROS production upon reperfusion has been previously reported by many authors (Matsuki *et al*., 2006, Onogi *et al*., 2006). These studies have demonstrated in rat and rabbit models of IR that indicators of oxidative stress such as 8–hydroxydeoxyguanosine, 2,3–dihydroxybenzoic acid (DHBA) and 2,5–DHBA increased during reperfusion. Oxidative stress in rat cardiomyocytes was also shown to be enhanced by approximately 6.8 – fold within 10 minutes of reperfusion (Tang *et al*., 2010). This increase was abolished in the presence of the superoxide scavenger (Tiron) administered during reperfusion.

1.2.2.i. Sources of ROS

Cellular mechanisms of ROS production are illustrated in Figure 1.9. The potential sources of ROS in cardiac IR include xanthine oxidase (XO; in endothelial cells), the complexes I and III of mitochondrial ETC (in cardiomyocytes), NADPH oxidase (in inflammatory cells, endothelial cells, fibroblasts, vascular smooth muscle cells and cardiomyocytes), cyclooxygenase, cytochrome P450 reductases and uncoupled nitric oxide synthases (NOS; Zweier and Hassan Talukder, 2006, Pongnimitprasert, 2009). In parallel, several scavenging mechanisms serve to remove excess ROS under normoxic conditions. Most of the superoxide generated in the mitochondrial matrix and in cytoplasm is removed by manganese–superoxide dismutase (MnSOD) and copper-zinc SOD (Cu-ZnSOD) to H_2O_2, respectively, which readily diffuses through the mitochondrial membranes (Day, 2009; Figure 1.10). The H_2O_2 can then be removed by catalase, glutathione peroxidase and peroxiredoxin, generating water and oxygen. Excessive ROS during IR can overhelm these scavenging mechanisms, leading to cardiac damage.

XO is the interconvertible form of xanthine dehydrogenase (XDH), which normally exists, with very little or no $O_2\bullet^-$ production (Pandey *et al*., 2000). During myocardial ischaemia, XDH is cleaved by Ca^{2+}–dependent proteases and converted to XO under increased Ca^{2+} levels (Bhakuni *et al*., 2005, Raghuvanshi *et al*., 2005). In ischaemic conditions, ATP is catabolised to ADP, AMP, and subsequently to adenosine, inosine, and finally to

hypoxanthine (Zweier and Hassan Talukder, 2006; Figure 1.9). Upon reperfusion, XO converts hypoxanthine to xanthine and subsequently to uric acid, $O_2\bullet^-$ and H_2O_2. XO activity was increased in the blood of MI patients (Raghuvanshi *et al*., 2007) with elevated xanthine and hypoxanthine levels of more than 2 – fold whereas ATP and ADP declined > 66 % in ischaemic (30 minutes) rat heart (Moens *et al*., 2008).

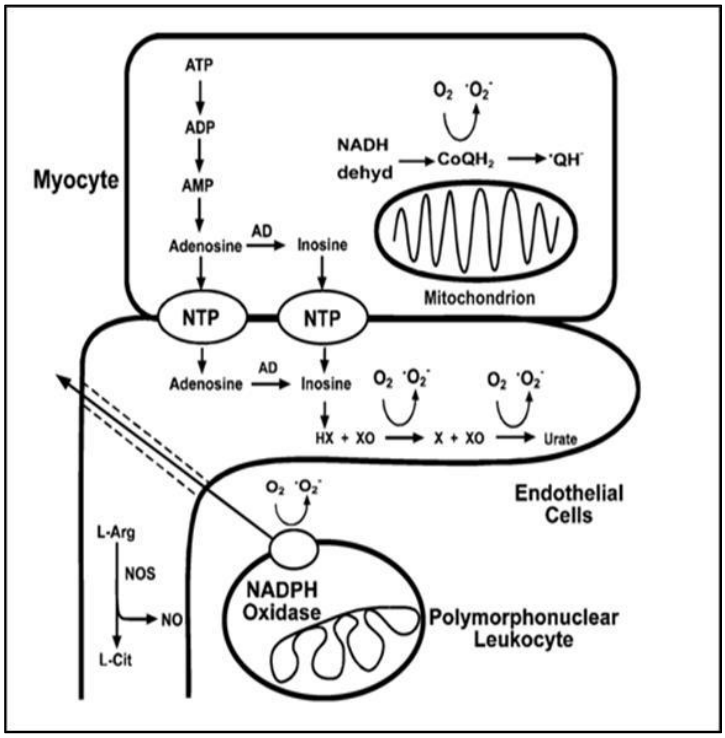

Figure 1.9. ROS production from mitochondrial electron transport chain, xanthine oxidase, and NADPH oxidase. (Zweier and Hassan Talukder, 2006)

AD, adenosine deaminase; ADP, adenosine diphosphate; AMP, adenosine monophosphate; ATP, adenosine triphosphate; $CoQH_2$, coenzyme QH_2; HX, hypoxanthine; L–Arg, L–arginine; L–Cir, citrate; NADH dehyd, NADH dehydrogenase; NO, nitric oxide; NOS, nitric oxide synthase; NTP, nucleoside triphosphate–adenosine monophosphate transphosphorylase; X, xanthine; XO, xanthine oxidase.

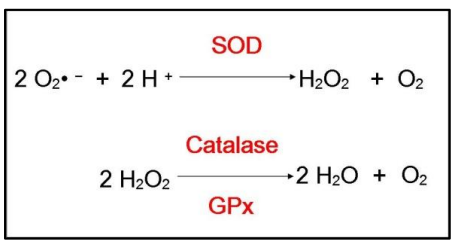

Figure 1.10. Reactions of ROS with scavenging systems.

GPx, glutathione peroxidase; SOD, superoxide dismutase.

Complexes I and III in the ETC have been documented to be the main ROS production sites (Figure 1.7). When treated with rotenone, a complex I inhibitor, there is no increase in H_2O_2 generation in isolated rat mitochondria and isolated rabbit hearts after ischaemia (Chen *et al*., 2003, Lesnefsky *et al*., 2004). Conversely, inhibition of complex III with antimycin A enhanced H_2O_2 production in the mitochondria in the presence of complex I substrate, whereas the presence of rotenone attenuated it (Chen *et al*., 2003, Lesnefsky *et al*., 2004). This is because blocking complex I during ischaemia decreases the electron flow into complex III and reduces electron leak, thereby inducing ROS generation at this site (Chen *et al*., 2006, Aldakkak *et al*., 2008).

Lesnefsky *et al*. (2004) have demonstrated that 25 minutes of global ischaemia caused damage on the ETC, by decreasing the complex III activity, and oxidative phosphorylation via cytochrome oxidase, as well as increasing cytochrome c release in isolated perfused rat heart (Chen *et al*., 2006). Cytochrome c is bound to the IMM by association with the cardiolipin, forming a cardiolipin–cytochrome c peroxidase (Belikova *et al*., 2006). This complex is peroxidized by ROS produced during ischaemia, which simultaneously delocalized cytochrome c from IMM and released into the cytosol. In addition, cytochrome oxidase activity requires a microenvironment enriched with cardiolipin (Paradies *et al*., 2009). The decreased rate of oxidation through cytochrome oxidase was possibly due to the decline in mitochondrial cardiolipin content in isolated ischaemic hearts (Lesnefsky *et al*., 2001).

1.2.2.ii. ROS–induced damage

Many proteins that play an important role in cardiac homeostasis are also modified by ROS. The polyol pathway (Figure 1.11) was activated after 30 minutes regional ischaemia and 45 minutes of reperfusion in isolated rat hearts (Tang *et al*., 2010). The activation of polyol pathway elevated the NADH level as a result of increased sorbital oxidation into fructose catalyzed by sorbital dehydrogenase. The increased NADH stimulated NADH oxidase, which is in close proximity to SR to enhance ROS production (Bassenge *et al*., 2000). In addition, increased levels of peroxynitrite following IR were also observed concomitant with elevated tyrosine nitrosylation and consequent irreversible modification of SERCA, as well as decreased RyR activity (Ramasamy *et al*., 1997, Tang *et al*., 2010). Alterations of these two essential Ca^{2+} handling proteins can lead to the impairment of contractile function during IR.

The oxidative stress in IR hearts was also reported to generate alterations in mitochondrial respiration and oxidative phosphorylation (Makazan *et al*., 2007). Pretreatment with ROS scavenging enzymes (SOD and catalase) was shown beneficial in IR–treated group as it decreased the mitochondrial glutathione (GSH) content, and the GSH : oxidized glutathione ratio, the latter being an index of oxidative stress. Subsequently, the changes in mitochondrial respiration and oxidative phosphoryation activities were attenuated. Additionally, ROS may damage cardiomyocytes by a variety of methods: causing peroxidation of membrane phospholipid (Marnett, 1999, Paradies *et al*., 1999), denaturation of proteins (Stadtman, 2004), and strand breakage in DNA (Dizdaroglu *et al*., 2002), all leading directly or indirectly to mitochondrial dysfunction (Dhalla *et al*., 2000). Alteration of the plasma membrane permeability and fluidity due to lipid peroxidation by ROS triggers loss of membrane integrity, necrosis and subsequently leads to myocardial cell death (Park and Lucchesi, 1999, Levraut *et al*., 2003, Zweier and Villamena, 2003).

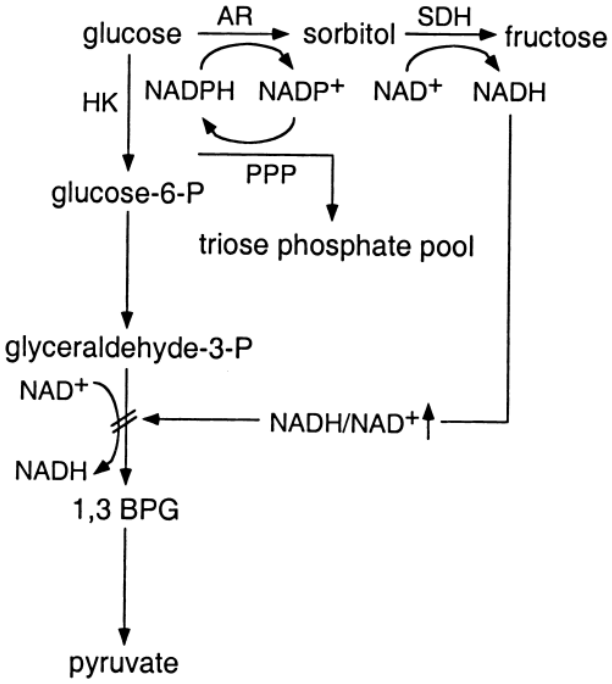

Figure 1.11. The polyol pathway. (Dunlop, 2000)

AR, aldose reductase; 1,3 BPG, 1, 3–bisphosphoglycerate; glucose–6–p, glucose–6–phosphate; glyceraldehyde–3–p, glyceraldehyde–3–phosphate; HK, hexokinase; NAD^+, nicotinamide adenine dinucleotide (oxidised form); NADH, reduced form of nicotinamide adenine dinucleotide; $NADP^+$, oxidised form of nicotinamide adenine dinucleotide phosphate; NADPH, reduced form of nicotinamide adenine dinucleotide phosphate; PPP, pentose phosphate pathway; SDH, sorbitol dehydrogenase.

1.2.2.iii. Antioxidant and ROS scavenger treatment

A number of studies have shown that treatment with antioxidants or scavengers diminished IR injury. For example, Moens *et al*. (2008) demonstrated that folic acid, an antioxidant, ameliorated post–reperfusion injury by preserving high–energy phosphates, particularly promoting ATP and reducing $O_2\bullet^-$ generation. In addition, oral administration of VitaePro, a novel antioxidant mix of xanthine like compounds astaxanthin, lutein and zeaxanthin, could protect rat myocardium from IR injury by decreasing oxidative stress and apoptosis (Adluri *et al*., 2011). There is also growing evidence that flavonoids (Fantinelli *et al*., 2005, Hirai *et al*., 2007, Toufektsain *et al*., 2008, Yamazaki *et al*., 2008) offer protection against myocardial IR injury.

Treatment with uric acid (5 mg/kg intravenous injection) 10 minutes before ischaemia, a peroxynitrite scavenger, has markedly reduced IR–induced peroxynitrite production and infarct size in rat (Ji *et al*., 2010). Additionally, the therapeutic role of L–arginine reduced the XO activity in patients with ischaemic heart disease and led to decreased $O_2•^-$ and H_2O_2 levels (Tripathi and Misra, 2009). Interestingly, molecular hydrogen may react with OH• to produce water (Labiche and Grotta, 2004); and hence can act as an ROS scavenger. Sun *et al*. (2009) and Hayashida *et al*. (2008) have demonstrated that intraperitoneal injection of hydrogen–rich saline and inhalation of hydrogen gas, respectively, in rat myocardium following 30 minutes of LAD occlusion significantly decreased infarct size, attenuated apoptosis and oxidative stress in the area at risk.

However, there are also clinical trial studies that found no beneficial effects of the ROS scavengers and antioxidants against MI. In a clinical trial which involved 120 patients undergoing angioplasty, exogenous administered SOD did not elicit any functional improvement (Kevin *et al*., 2005). This disappointing finding may be owing to the low cellular permeability of the SOD. In addition, numerous randomised controlled trials and meta–analysis showed no significant beneficial effect of vitamin E on myocardial injury and clinical outcome after cardiac surgery (Roncaglioni, 2001, Heart Protection Study Collaborative Group, 2002, Lassnigg *et al*., 2003, Vivekananthan *et al*., 2003), even though improved contractile function and decreased cardiac biomarker release were observed in a randomized trial investigation of the effect of vitamin E in patients undergoing CABG surgery (Yau *et al*., 1994).

Despite most clinical studies with antioxidants against IR injury have been disappointing, the measurement of peroxidation production has demonstrated the evidence of ROS–induced injury (Kevin *et al*., 2005), hence inhibition of excessive ROS production during IR certainly possesses its cardioprotective potential.

1.2.3. Calcium overload

Both ischaemia and reperfusion result in an increase in $[Ca^{2+}]_i$ in cardiomyocytes, which could be due to alterations in normal functions of SERCA, NCX, and PLB. In a patch–clamped study on mouse cardiomyocytes, $[Ca^{2+}]_i$ in term of Fura–2 fluorescence intensity, has increased to 138 ± 7 % during ischaemia (280 seconds), and to 210 ± 11 % after 18 minutes of reperfusion (Wang *et al*., 2007).

SERCA function is impaired during myocardial IR, causing deficient removal of cytosolic Ca^{2+} into SR. Many studies have demonstrated the SERCA activity in isolated rat ventricular myocytes was significantly reduced at the end of 15 minutes of ischaemia (~ 5 versus 7 µmol Pi/mg of protein/hour), whereas 30 minutes of reperfusion returned SERCA activity level to normal (Yu *et al*., 2006). Moreover, SERCA activity in isolated rat cardiomyocytes has been reported to decrease from 35 to 20 nmol/mg/minute after 10 minutes of regional ischaemia but was not further altered after 10 minutes of the reperfusion (Tang *et al*., 2010). Although conflicting results in SERCA activity have been observed which in part may be due to differences in the IR protocol, an overall decreased SERCA activity during ischaemia appears to be a consistent finding.

In addition to reduced SERCA activity, forward (1 Ca^{2+} extrusion, 3 Na^+ influx) and reverse (3 Na^+ extrusion, 1 Ca^{2+} influx) NCX currents are markedly inhibited during ischaemia, and subsequent reperfusion restores and enhances these currents, especially the reverse one. The reverse mode of NCX activity was doubled at 3 minutes of reperfusion compare to that in the pre–ischaemic period (Wei *et al*., 2007). The driving force of reverse NCX comes from the increased $[Na^+]_i$, which could arise from different routes, for example increase Na^+ influx via Na^+/H^+ exchanger (Na–HX; Bers *et al*., 2003), Na^+ channels (Williams *et al*., 2007), and/or decrease in Na^+ extrusion via Na^+–K^+ ATPase (Fuller *et al*., 2003). $[Na^+]_i$ (normal value: 7 – 15 mM) was raised to approximately 3 – fold during myocardial ischaemia to levels in the range of 25 – 40 mM (Murphy and Steenbergen, 2008).

Brief ischaemia (20 – 30 minutes) produced in LAD occluded rats induced marked dephosphorylation of PLB at Ser^{16} and Thr^{17} (Shintani-Ishida and Yoshida, 2011). Reduced SR Ca^{2+} uptake through inactivated SERCA which is caused by PLB dephosphorylation, contributes to the Ca^{2+} overload during IR. Ca^{2+} influx into the cardiomyocytes could also be augmented by ischaemia–induced depolarization of the membrane potential, which in turn activates the sarcolemmal I_{ca} opening (Talukder *et al*., 2009).

A number of therapeutic approaches have targetted Ca^{2+} overload. Ca^{2+} channel blockers such as verapamil, diltiazem and nifedipine markedly attenuated myocardial IR injury with reduced damage as shown by a reduction in release of cardiac markers [CK and lactate dehydrogenase (LDH)], preserved SOD activity and decreased oxidative stress in a rat model (Huang *et al*., 2009). SEA0400 (0.3 µmol/L), a potent NCX inhibitor blocked the change of NCX current and the increase in $[Ca^{2+}]_i$ during IR, especially during reperfusion in mouse cardiomyocytes (Wang *et al*., 2007). Similarly clinical benefit of cariporide, a selective Na–HX inhibitor, has also been observed when administered in patients undergoing CABG (Boyce *et al*. 2003, Mentzer Jr *et al*., 2008). However, MCC–135, another Na–HX inhibitor has been tested clinically but failed to show any reduction of infarct size when given during reperfusion (Bär *et al*., 2006, Jang *et al*., 2008). This failure has been argued to be due to the fact that Na–HX inhibition is most effective during ischaemia (Klein *et al*., 2000, Avkiran *et al*., 2008). Even though the discovery of highly selective therapeutic interventions targeting Ca^{2+} overload is essential, the timing and dosage of administration are innegligible.

1.2.4. Hypercontracture

Hypercontracture is a result of an excessive contractile activation during reperfusion which causes irreversible cell injury by distruption of cytoskeletal structures. Resumption of ATP synthesis during reperfusion as a result of rapid restoration of oxygen and pH was believed to be the main reason contributing to the hypercontracture development (Inserte *et al*., 2008). In the presence of Ca^{2+} overload, uptake of Ca^{2+} into the SR by re–energized SERCA reduces the $[Ca^{2+}]_i$ rapidly, and SR will subsequently release Ca^{2+} load quickly through RyR channel (Piper *et al*., 2006). Ca^{2+} is thus rapidly shifted between cytosol and the SR in an oscillatory manner and Ca^{2+} overload–induced hypercontracture is elicited spontaneously. Hypercontracture in rat myocardium was found at 3.3 ± 0.2 minutes of reperfusion (Inserte *et al*., 2008).

Hypercontraction has been shown to propagate from one reperfused cell to adjacent cells via connexin 43 (Cx 43; Piper *et al*., 2004, Rodríguez-Sinovas *et al.*, 2007), with the formation of contraction bands along the reperfused myocardium (Figure 1.12). Cx 43 is a protein predominantly involved in the formation of gap junctions in the ventricle (Schulz *et al.,* 2007). The permeability and conductance of gap junctions depend on the phosphorylation status of Cx 43. Under normal physiological conditions, Cx 43 is partially phosphorylated (Jeyaraman *et al*., 2003, Schulz *et al*., 2003). During prolonged ischaemia, it becomes dephosphorylated. Mitochondrial and gap junctional Cx 43 dephosphorylation were shown increased after 85 minutes of ischaemia in the porcine myocardium (Totzeck *et al.,* 2008). In addition, phosphorylated Cx 43 was decreased by 83.45 % while dephosphorylated Cx 43 increased 1.62 – fold in mice hearts after 45 minutes of ischaemia and 4 hours of reperfusion *in vivo* (Cao *et al*., 2009).

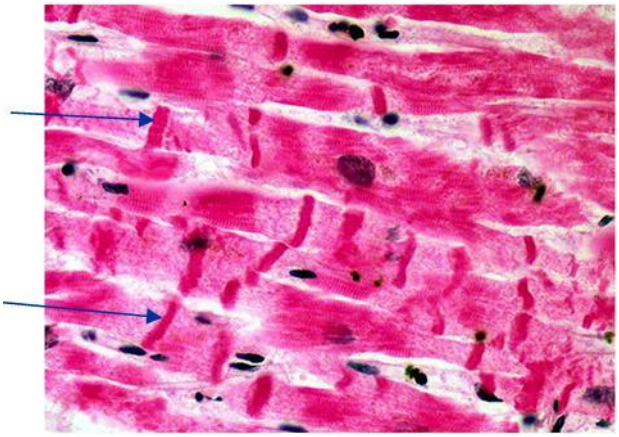

Figure 1.12. Contraction bands in the reperfused myocardium. Contraction band necrosis is visible as dark pink bands spanning the myofibers. (Ibanez *et al*., 2011)

The spread of hypercontraction plays a key role in the continuous expansion of early necrosis via the gap junction–mediated communication between these cells (Ruiz-Meana and García-Dorado, 2009). The hypercontraction propagation is mainly caused by the passage of Na^+ through Cx 43, which in turn induces Ca^{2+} entry via reverse–mode of NCX and drives Ca^{2+} overload. Addition of KB–R7943, a reverse NCX inhibitor, has prevented propagation of hypercontraction (Ruiz-Meana *et al*., 1999). In addition, uncoupling of Cx 43 by heptanol infusion during first 15 minutes of reperfusion in pig hearts following 30 minutes of hypoxia has shown prevention in hypercontracture propagation and reduction in the final infarct size (García-Dorado *et al*., 1997). Therefore, inhibition of Cx 43 formation or its proper functions can be a potential therapeutic target in reducing myocardial IR injury.

1.2.5. mPTP opening

Opening of the mPTP is known to cause both necrotic and apoptotic cardiomycyte cell death (Halestrap, 2006). mPTP is a voltage– and Ca^{2+}–dependent non–specific ion channel in the IMM and is regulated by the proteins on the OMM (Sinha Roy *et al*., 2009, Sileikyte *et al*., 2011). Under normal physiological conditions, the mPTP is closed, and opened under conditions of stress, such as mitochondrial Ca^{2+} overload, oxidative stress, depletion of adenine nucleotides, increase in [Pi], normalisation of pH, and mitochondrial membrane depolarisation (Halestrap *et al*., 2000, 2002, Halestrap, 2002, Borutaite and Brown, 2003, Downey *et al*., 2007). mPTP opening causes a sudden rise in IMM permeability and allows the release of molecules < 1.5 kDalton from the mitochondrial matrix into the cytoplasm (Bernardi *et al.*, 2006). Following mPTP opening, the mitochondrial $\Delta\Psi$ is dissipated, oxidative phosphorylation is uncoupled, and the Ca^{2+} overload augmented (Ruiz-Meana *et al*., 2007).

Despite extensive research, the molecular identity of the protein(s) responsible for the pore has not yet been fully elucidated. Initially, ANT in the IMM (Crompton *et al.*, 1998, Clarke *et al.*, 2002), the VDAC in the OMM (Crompton, 2000, Cesura *et al*., 2003), and cyclophilin–D (Cyp–D) in the matrix (Zamzami and Kroemer, 2001, Crompton *et al*., 2002) were proposed to comprise mPTP (Figure 1.13). VDAC and ANT are proteins that facilitate the efficient transport of ATP and ADP across the membranes (Baines, 2009). Cyp–D is a prolyl isomerase that catalyzes the rotation of proline peptide bonds, hence inducing a conformational change in the target protein (Wang and Heitman, 2005).

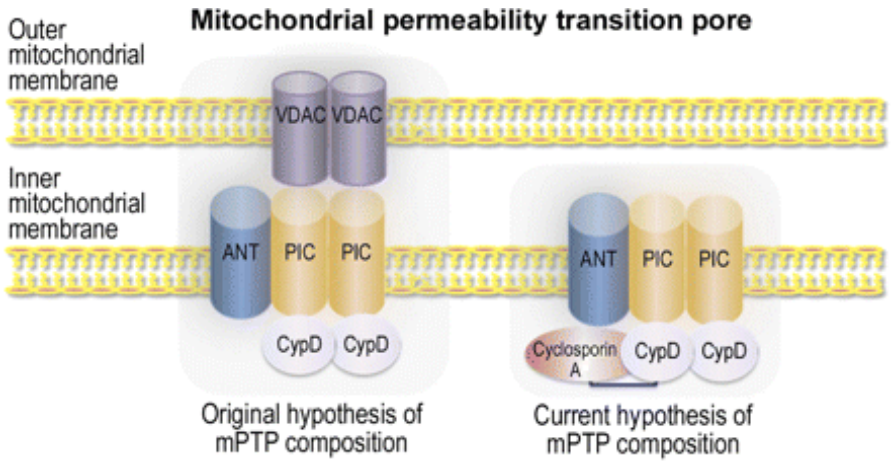

Figure 1.13. Molecular compositions of mPTP in the mitochondrial membranes. (Arbustini and Narula, 2010)

ANT, adenine nucleotide translocase; CypD, cyclophilin D; PIC, phosphate carrier; VDAC, voltage dependent anion channel.

VDAC has been thought to be a critical part of mPTP since 1993, based on the hypothesis made by Zoratti's group (Szabó *et al*., 1993, Szabó and Zoratti, 1993). They proposed that the electrophysiological properties of mPTP were reminiscent of those of the VDAC channel. Surprisingly, the mPTP opening could still be induced in mitochondria from mice deficient for isoforms VDAC1 and VDAC3 (Krauskopf *et al*. 2006; Baines *et al*. 2007). On the other hand, Kokoszka's group (2004) investigated the role of ANT in the mPTP by genetically inactivating two isoforms of ANT in the mouse liver. Mitochondria lacking ANT could still demonstrate opening of mPTP and release of cytochrome c. Mice lacking Cyp–D were protected from IR–induced cell death *in vivo*, whilst Cyp–D overexpressing mice suffered from mitochondrial swelling and cell death (Baines *et al*., 2005, Basso *et al*., 2005, Nakagawa *et al*., 2005, Schinzel *et al*., 2005).

Until recently, phosphate carrier (PIC) has been proposed to be a critical component of mPTP, via interaction with ANT (Leung *et al*., 2008, Halestrap, 2009). Cyp–D can bind to the PIC, and mPTP inhibitors such as N–ethylmaleamide and ubiquinone analogues demonstrated concentration dependent inhibition of PIC. However, the role of PIC in mPTP formation has still not been conclusively established. In light of these findings, ANT is

considered a mPTP regulator, VDAC is dispensable, and only Cyp–D remains as a defined component of the mPTP.

Inhibition of the mPTP opening has been translated to clinical treatment (Gomez *et al*., 2009). A preliminary trial involving 58 patients who were undergoing percutaneous coronary intervention were administered cyclosporine (2.5 mg/kg of body weight; mPTP inhibitor) at the onset of reperfusion (Piot *et al*., 2008). A reduction of infarct size of approximately 40 % was reported in comparison with placebo and there was no adverse effects seen in these patients. However, a larger clinical trial is needed to address whether this treatment may improve clinical outcome in these patients.

1.2.6. Induction of cell death

Two major types of cell death are recognized in the pathology of myocardial injury: necrosis and apoptosis. It has been proposed that mPTP opening contributes to myocardial cell death in reperfusion by initiating both processes (Halestrap, 2006). The morphological features of apoptosis and necrosis are listed in Table 1.1. In mice, hearts subjected to 20 minutes of global ischaemia and 2 hours of reperfusion showed 38 ± 5 % total cell death in the myocardium, but only 4.3 ± 1.7 % of the cell death was apoptotic (Imahashi *et al*., 2004). This is because the development of necrotic cell death occurs at the earlier phase followed by a slower appearance of apoptosis at the later phase (Zhao and Vinten-Johansen, 2002).

Table 1.1. Morphological features of apoptosis and necrosis.

Apoptosis	Necrosis
Single cells/small clusters of cells	Often contiguous cells
Cell shrinkage and convolution	Cell swelling
Intact cell membrane	Disrupted cell membrane
Cytoplasm retained in apoptotic bodies	Cytoplasm released
No inflammation	Inflammation usually present
Active process	Passive process

(Elmore, 2007)

Apoptosis of myocytes has been revealed following IR injury in human, *in vivo* animal, isolated animal hearts and isolated cardiomyocytes, using different IR protocols (Table 1.2). Most of these studies have determined apoptosis primarily or exclusively using the terminal deoxynucleotidyl transferase–mediated dUTP *in situ* nick–end labeling (TUNEL) assays. Apoptosis is mediated by two distinct conserved central death pathways: mitochondria–mediated (intrinsic) and receptor–mediated (extrinsic) apoptosis (Li-Weber, 2010; Figure 1.14). Cytochrome c, a 12 kDalton peripheral protein attached to the IMM, is released into cytosol (Alcalá *et al*., 2008, Leung and Halestrap, 2008) during apoptosis and forms part of the apoptosome complex. This complex is made up of the 700 kDalton adaptor protein apoptotic protease activating factor–1 (Apaf–1), cytochrome c and the cofactor dATP/ATP. It mediates the activation of an initiator caspase (procaspase 9) at the onset of apoptosis (Lavrik, 2010).

ATP levels play an essential role in determining whether ischaemic cardiomyocytes die by necrosis or apoptosis (Tatsumi *et al*., 2003). When an *in vitro* model of cultured neonatal rat cardiomyocytes was exposed to 7 hours of hypoxia in the glucose–depleted medium, the intracellular ATP declined and necrotic cell death was dominant. However when glucose concentration in the hypoxic medium was increased, intracellular ATP levels were increased correspondingly, and cell death changed from necrosis to apoptosis; i.e. apoptosis occurs when ATP is not limited.

Table 1.2. Apoptosis in different models of IR.

Model	Source	I/R duration	Marker of apoptosis used	Reference
Human	Human	4 – 42 d after Acute MI	TUNEL/Caspase 3	Abbate *et al*., 2008
In vivo heart	Dog	2 h / 6 h	TUNEL	Gonzalez *et al.*, 2008
	Mouse	45 m / 4 h	TUNEL	Shan *et al*., 2008
	Mouse	30 m / 3 h	TUNEL/Caspase 3 /DNA laddering	Wang *et al*., 2009
	Pig	1 h / 2 h	TUNEL	Sodha *et al*., 2008
	Pig	1 h / 72 h	TUNEL/Western blot	Sun *et al*., 2010
	Rat	30 m / 2 h	TUNEL/DNA laddering	Lv *et al*., 2008
	Rat	30 m / 6 h	TUNEL	Gao *et al*., 2008
	Rat	30 m / 4 h	TUNEL	Su *et al*., 2007
Isolated heart	Rat	30 m / 2 h	TUNEL	Mukherjee *et al*., 2008
	Rat	30 m /–	Caspase 3	Borutaite *et al*., 2009
	Rat	30 m / 30 m	Caspase 3	Borutaite *et al*., 2009
	Rat	20 m / 2 h	TUNEL	Knight *et al*., 2008
	Rat	30 m / 2 h	TUNEL	Knight *et al*., 2008
	Rat	30 m / 30 m	TUNEL	Dong *et al*., 2011
	Rat	30 m / 1 h	TUNEL	Liu *et al*., 2008
Isolated cardiomyocytes	Rat	3 h / 24 h	Caspase 3	Alloatti *et al*., 2009
	Rat	3 h / 18 h	TUNEL	Qi *et al*., 2011
	Rat	3 h / 1 h	TUNEL/Annexin V/PI	Kempf *et al*., 2006

Caspase, cysteine aspartate–specific protease; d, days; h, hours; I, ischaemia; m, minutes; PI, propidium iodide; R, reperfusion; TUNEL, terminal deoxynucleotidyl transferase mediated dUTP nick–end labelling.

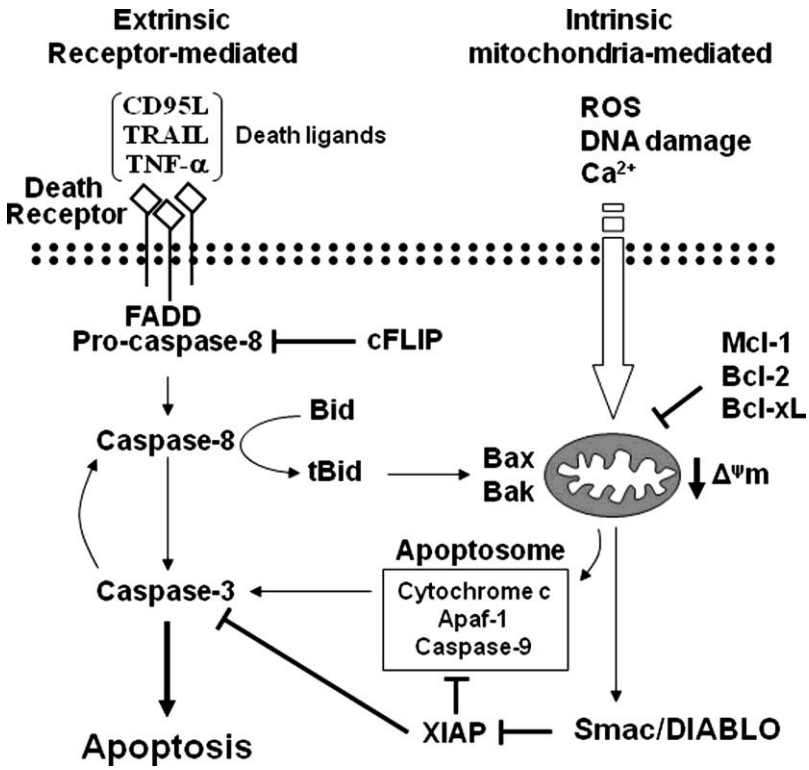

Figure 1.14. Extrinsic and intrinsic pathways leading to apoptosis. (Li-Weber, 2010)

APAF–1, apoptotic protease activating factor–1; Bak, Bcl–2 homologous antagonist killer; Bax, Bcl–2–associated X protein; Bcl–2, B cell lymphoma 2; Bcl–xL, B cell lymphoma–extra large; Caspases, cysteine aspartate–specific proteases; cFLIP, cellular FLICE inhibitory protein; DIABLO, direct IAP binding protein with low pl; FADD, Fas–associated death domain; Mcl–1, induced myeloid leukemia cell differentiation protein; Smac, second mitochondria–derived activator of caspases; tBid, truncate BH3 interacting domain death agonist; TNF–α, tumour necrosis factor–alpha; TRAIL, TNF–related apoptosis–inducing ligand; XIAP, X–linked inhibitor of apoptosis protein.

The loss of viable cardiomyocytes via necrosis or apoptosis will result in progressive cell loss and deterioration of contractile function of the heart, with an increasing load placed on the remaining functioning cardiomyocytes. In addition, cell loss can also cause slippage of muscle bundles, wall thinning, and chamber dilatation (Foo *et al*., 2005), negatively influences the anatomy and haemodynamics of the heart. Therefore, pharmacological interventions to inhibit cell death may help to salvage the myocardium from IR–induced cell loss and contractile dysfunction.

Greater understanding of the mechanisms underlying myocardial IR injury will lead to the development of new pharmacological interventions to confer cardioprotection. Until recently, a list of cardioprotective agents has been proposed in animal models against IR injuries but translation to clinical trials faced certain challenges, including the inadequacy of suitable IR injury animal models used in the preclinical investigations and inappropriate design of the clinical studies (Hausenloy *et al.*, 2010). There are small preliminary clinical studies which have demonstrated cardioprotection (e.g. postconditioning), but this remains to be confirmed in larger clinical trials (Staat *et al*., 2005, Ma *et al*., 2006).

1.3. Diagnosis of myocardiac infarction–Cardiac biomarkers

Myocardial damage and the subsequent loss of membrane integrity lead to the release of cardiac biomarkers into the circulation. The emergence of cardiac biomarkers offers clinician additional information, which is helpful in the decision–making in treating patients with heart disease. The most commonly used biomarkers in cardiac risk stratification are CK–MB, TnT and TnI, and brain natriuretic peptide (BNP; Christenson and Azzazy, 2009). Other biomarkers, including myoglobin, LDH, ischaemia–modified albumin, aspartate aminotransferase have been used in diagnosis of cardiac complications but these are not routine. A multimarker approach has been proposed for comprehensive risk assessment but there are limitations and challenges needed to be recognised (Daniels and Maisel, 2010).

1.3.1. CK–MB

A relatively high level of CK–MB is found in the myocardium (20 – 30 % of total myocardial CK), with only small amount being present in skeletal muscle (about 2 % of total muscle CK; Lewandowski *et al*., 2002). Plasma CK–MB levels increase by 2 – fold within 6 hours and peak within 12 – 24 hours in the range of 39 – 185 ng/ml in the setting of AMI (Figure 1.15). Plasma CK–MB is normally calculated as a percentage of total CK enzyme (total CK activity in units of enzyme per litre; Lewandrowski *et al*., 2002).Serial measurements every 3 hours over 9 hours after emergency department presentation, instead of a single measurement of CK–MB, detect AMI with higher sensitivity (close to 100 %; Gibler *et al*. 1995). CK–MB is also useful in diagnosing reinfarction in patient who has already suffered a MI because of its sudden rise and subsequent early fall; therefore subsequent elevations are indicative of another event (Peela *et al*., 2010).

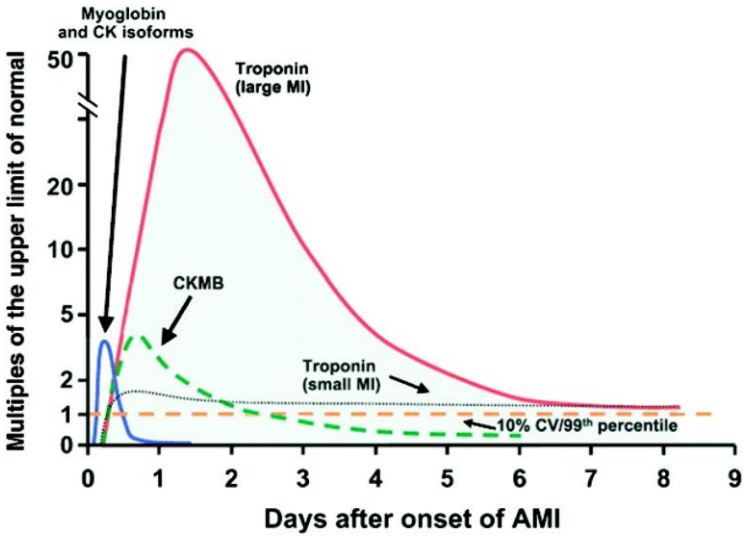

Figure 1.15. Multiple biomarkers release after AMI. Upper limit of normal represents the upper reference limit of the normal range. (Anderson *et al*., 2011)

AMI, acute myocardial infarction; CK, creatine kinase; CKMB, creatine kinase muscle type; CV, coefficient of variation.

1.3.2. TnT and TnI

TnT and TnI are released into the bloodstream when the myocardium is damaged, with levels rising within 4 – 8 hours, peaking at 12 – 24 hours following AMI (Collison, 1998, Frey *et al*., 1998, Wu and Feng, 1998), these remaining elevated for up to 7 – 10 days (TnI) and up to 2 weeks (TnT). Their persistent release is due to slow dissociation of Tn molecules from the actin filaments, giving clinicians a large window for diagnosing recent AMI. Consequently, this prolonged elevation appears to be a superior and sensitive marker for initial MI diagnosis, but has diminished the accuracy in diagnosing reinfarction or extension of infarction. TnI is considered as the gold standard for AMI diagnosis (Alpert *et al*., 2000, Babuin and Jaffe, 2005), with greater specificity compared with CK–MB (100 % versus 90.9 %), but CK–MB is more sensitive (63 % versus 11 %) for AMI diagnosis (Basu *et al*., 2009). TnT lacks specificity because elevations may appear with renal failure and skeletal myopathies as well (Kost *et al*., 1998, Kumar and Connon, 2009).

1.3.3. BNP

BNP is a 32 amino acid neurohormone released in response to increased wall tension and stretch. Its utility in cardiac injury diagnosis is due to the impaired diastolic and systolic functions occur at the onset of ischaemia, which leading to increased left ventricular pressure and volume overload (Daniels and Maisel, 2007). BNP is synthesized as a pre–pro BNP that is enzymatically cleaved into biologically active BNP and N–terminal proBNP (NT–proBNP) remnant (McCullough and Sandberg, 2003). The release of BNP into the blood circulation is in proportion to the degree of heart injury (Maeda *et al*., 1998). Both BNP and NT–proBNP have been described as useful biomarkers for heart failure (Maisel *et al*., 2002, Morrison *et al*., 2002); BNP levels with different heart failure classes are listed in Table 1.3 (Strimike, 2006). A BNP level > 144 pg/ml predicts cardiac dysfunction with 92 % sensitivity and 86 % specificity (McLean *et al*., 2003). BNP levels in patients with LV diastolic dysfunction are normally in the range of 300 – 480 pg/ml, while it is 550 – 280 pg/ml in patient with LV systolic dysfunction. For patients with both systolic and diastolic LV dysfunction, however, BNP levels can reach 800 – 1300 pg/ml or above. BNP is thought to be a good screening tool to rule out cardiac dysfunction, but since it can be elevated in a variety of cardiac conditions, it provides little help in differential diagnosis and has low specificity for detecting specific heart disease (McLean *et al*., 2008).

Table 1.3. BNP levels with different heart failure classes.

Chronic Heart Failure Class	BNP Levels (pg/ml)
Mild	83 – 152
Mild to moderate	235 – 322
Moderate to severe	459 – 590
Severe	960 – 1119

(Strimike, 2006)

1.3.4. Myoglobin

Myoglobin is a 17.8 kDalton cytosolic haem protein found in both skeletal and cardiac muscles (Christenson and Azzazy, 1998). It is a sensitive marker for muscle damage due to its rapid kinetics as it is released during early myocardial injury and can be detected within the circulation in less than 30 minutes (Figure 1.15). Its half-life in plasma is approximately 9 minutes and then quickly excreted by renal clearance (Klocke *et al*., 1982). However, serum myoglobin levels can be raised by conditions unrelated to MI, such as skeletal muscle and neuromuscular disorders, renal failure, strenuous exercise, intramuscular injection, and following several drugs and toxins intake (Plebani and Zaninotto, 1998), compromising its clinical specificity. Besides, patients with renal insufficiency will have increased myoglobin levels owing to the decreased clearance. This limitation can be resolved by the combined assessment of myoglobin and a skeletal specific marker (e.g. carbonic anhydrase III; Beuerie *et al*., 2000) or a cardiac specific marker (creatine kinase; Iqbal *et al*., 2004).

1.4. Detection of cardiac biomarkers

The presence and levels of cardiac biomarkers in the bloodstream can be determined by sensitive assays, such as electrophoresis and immunoassays. The properties of an ideal detection method are: rapid sample analysis time (or rapid turnaround time), simple to perform, and relatively low cost. In 2000, the guidelines for cardiac biomarkers of myocardial necrosis recommended a turnaround time of < 1 hour, but preferably < 30 minutes (Braunwald *et al*., 2000). However, not many hospitals were able to meet this standard (Apple *et al*., 2007). The following section described the most important and clinically useful cardiac biomarker detection methods.

1.4.1. Electrophoresis/Ion exchange column chromatography

CK and LDH isoenzymes were traditionally measured by a labour–intensive electrophoretic method (Griffiths and Handschu, 1977, Leroux *et al*., 1984). However, this technique is error–prone when immunoglobulin–bound CK–BB or other fluorescent drugs migrate close to the CK–MB region (Aleyassine *et al*., 1978, Ljungdahl and Gerhardt, 1978). Although ion exchange column chromatography can be used to separate CK–MB, it is laborious and false–positive results given (Griffiths and Handschu, 1977). These methods have been replaced by more specific and sensitive immunoassays.

1.4.2. Immunoassays

Immunoassays are the most common diagnostic assays currently in use for measuring specific disease–associated proteins. Generally, a monoclonal antibody is initially immobilized onto a well or bead, followed by a blocking step to minimize non–specific binding. When sample is added, an antibody–antigen complex is formed. Subsequently, an enzyme–conjugated secondary antibody is added which binds to a different epitope than the capture antibody. Eventually, an enzyme substrate is added and reaction product is measured. Thorough washing is required between each step to get rid of

excess reagent and non–specifically bound substances. Several immunoassay methologies have been employed, including homogenous/heterogeneous, direct/indirect, and competitive/sandwich assays (Darwish, 2006).

Various immunoassays have been widely used in detecting cardiac biomarkers, for example TnI (Zaninotto *et al*., 1996, Apple *et al*., 1997), CK–MB (Poirey *et al.*, 2000), myoglobin (Delanghe *et al*., 1990), BNP and NT–proBNP (Tamm *et al*., 2008, Liu *et al*., 2010). Enzyme immunoassay (EIA), radioimmunoassay (RIA), and fluorescence immunoassay (FIA) are well established techniques in clinical diagnostic laboratories, but these techniques often require complicated equipment, multiple sample processing steps, and well–trained personnel; hence considerable time (4 – 6 hours) is required for the overall detection.

Electrochemical immunoassays (ECIA) are promising alternatives to the existing immunochemical tests (Fowler *et al*., 2008). The common limitations in RIA are the short half–life of radioactive agents, health hazards and disposal issues, whereas FIA showed limited sensitivity in the analysis of coloured or turbid samples. These complications do not exist in ECIA. The specific binding between antigens (in the sample) and antibodies (immobilized on electrodes) involved the reduction or oxidation of electroactive species and hence generated a measurable electrical signal (Patolsky *et al*., 2001, Limoges *et al*., 2003). With the advantages of simplicity, accuracy, sensitivity, and relatively low cost (Wang, 2006), the use of ECIA in detecting cardiac biomarkers is gradually increasing (Rajesh *et al*., 2010, Saleh Ahammad *et al*., 2011, Zhuo *et al*., 2011).

1.4.3. Point–of–care devices

Due to the continuing clinical demand for rapid analysis (ideally < 30 minutes) of cardiac biomarkers, point–of–care (POC) testing has been implemented in the emergency department in recent years (Lewandrowski, 2009). There are 2 main types of POC testing formats found in the clinical setting bench–top analysers and hand–held devices (Table 1.4). These

devices are predominantly based on immunoassay methods, such as two–site immunometric assay and lateral flow immunoassay. The POC assays are simple, rapid, accurate and proven to be clinically useful (Storrow *et al*., 2006). The median time from blood sampling to reporting of results was 71 minutes for central laboratory versus 24 minutes for POC testing (McCord *et al*., 2001). Similarly, a turnaround time for a POC assay was 20 minutes compared with central laboratory testing of 79 minutes (Collinson *et al*., 2004). POC diagnostic devices also have the capacity to facilitate multiplexed POC cardiac biomarker panels (Table 1.4), thus increasing the accuracy in diagnosing heart complications.

Table 1.4. POC testing currently commercially available.

Assay	Assay type	Specimen	Time (min)	Assay range (ng/ml)	Analytical sensitivity (ng/ml)
Stratus® CS STAT (Dade Behring Inc)	Bench top two-site immunometric assay	Heparinised plasma	15	CK-MB: 0–150 Myoglobin: 0–900 TnI: 0–50	0.3 1 0.03
i-STAT® (Abbott)	Handheld two-site immunometric assay	Whole blood/plasma	10	TnI: 0–50	0.02
Triage® Cardiac Panel (Biosite)	Bench top flow through immunometric assay	Plasma/EDTA whole blood	10–15	CK-MB: ND Myoglobin: ND TnI: 0.04–50 BNP: ND	1 5 0.05 0.02
RAMP® (Response Biomedical Corp)	Bench top lateral flow immunoassay	EDTA whole blood	8–15	CK-MB: ND Myoglobin: ND TnI: 0.03–32	7.2 100 0.2
Cardiac Reader™ (Roche)	Bench top lateral flow immunoassay	150 µl heparinised whole blood	8 12 8 12	Myoglobin: 30–700 TnT: 0.1–2 D-Dimer: 100–4000 NT-proBNP: 0.06–3	70 0.1 500 0.3 (acute HF) 0.125 (chronic HF)
PATHFAST® (Mitsubishi Chemical Europe GmbH)	Bench top chemiluminescent analyser	Whole blood or Heparin/EDTA/citrate plasma	17	CK-MB: 2–500 Myoglobin: 5–1000 TnI: 0.02–50 D-Dimer: 5–5000 NT-proBNP: 0.015–30 hsCRP: 50–30000	2 5 0.02 5 0.015 50

(McDonnell *et al*., 2009)

hsCRP, high sensitivity C–reactive protein; ND, not defined.

1.5. Microfluidics

Microfluidics is the science and technology of systems which manipulate tiny amounts of fluids (nl or µl) using channels with tens to hundreds of µm in dimensions (Whitesides, 2006). Microfluidics has been described as micro total analysis system (µTAS) technology, lab–on–a–chip (LOC) systems, or bio–microelectromechanical systems (Bio–MEMS). The applications of these technologies to molecular biology, biomedicine and analytical chemistry have attracted great attention in the past decade.

The use of microfluidic devices to conduct biological research offers several advantages over other techniques, including (i) the use of a small volume (nl or µl) of sample and reagent, because of the low volume channels, (ii) portability due to reduced size of operating systems, thereby allowing on–site operation and POC analysis, (iii) shorter assay times, and (iv) lower production costs per device hence allowing potential for disposability (Bruus, 2008). These advantages are in contrast to conventional bench–top systems, which are relatively time consuming, tedious, and require expensive equipment.

1.5.1. Fluid flow and transport

The fluid flow through a microfluidic channel is characterized by the Reynolds number (Re), which is originally proposed by Osborne Reynolds in 1883 (Osborne, 1883). Re is defined as follow:

$$\mathrm{Re} = \frac{\rho d v}{\eta}$$ **Equation 2** (Rott, 1990)

Where ρ is the density of the fluid, d is the diameter of the channel, v is the mean velocity of the moving fluid and η is the viscosity of the fluid. A Re > 2300 represents turbulent flow, whilst a Re < 2300 is indicative of laminar flow. Laminar flow regimes dominate as the channels in microfluidic devices are in small dimensions (Ong *et al*., 2008). When two or more streams combine, they flow parallel to each other in organised lamina layers (Figure 1.16) and only mix through convective and molecular diffusion. Takayama's

group (1999) has demonstrated laminar flow patterning of bovine capillary endothelial cells in capillary systems. Cells were adhered and spread in a fibronectin–coated region and perfused with Trypsin/ ethylenediaminetetraacetic acid (EDTA), and media flowing from the designated inlets. Trypsin/EDTA caused the detachment of cells where it flowed. Such partial treatment on cells will give valuable new insight into cell function.

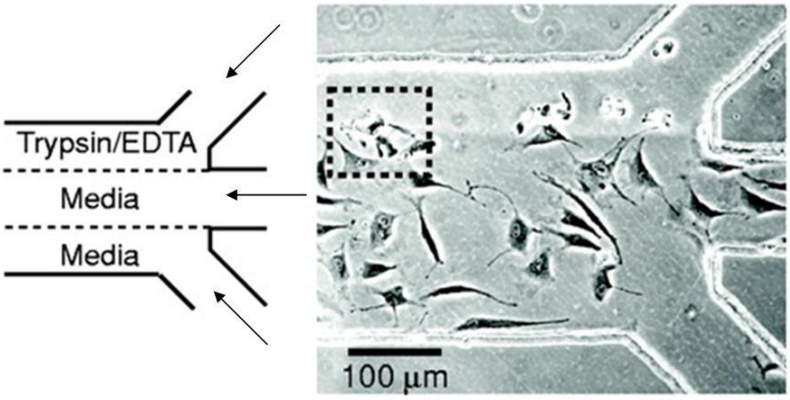

Figure 1.16. Laminar flow patterning of cells in capillary systems. Dashed box shows only portions of a cell exposed to Trypsin/EDTA detached. (Adapted from Takayama *et al*., 1999)

As the time of contact between two individual streams increases, the diffusion between them increases (Figure 1.17). Diffusion can be modelled by

$$d^2 = 2Dt \qquad \textbf{Equation 3}$$

Where d is the distance a particle moves in time t, and D is the diffusion coefficient of the particle. Diffusive mixing becomes critical at the microscale as distance varies to the square power (Tabeling, 2005).

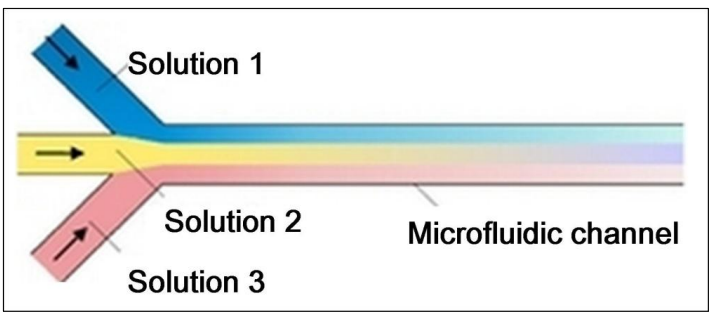

Figure 1.17. Diffusion between parallel streams in a microfluidic channel. (Fang *et al*., 2009)

Mixing is a critical issue in microfluidics. In macro systems, mixing can be achieved by driving propellers or magnetic beads in the fluids. The resultant inertia forces are sufficient to cause turbulence and mixing. In microfluidic devices, however, the inertia forces are very weak and turbulence does not occur, resulting in less homogenous distributions of metabolites and waste products. Various types of micromixers (active and passive) have been designed and shown to work effectively in the microfluidic systems to facilitate mixing (Zhao *et al*., 2002, Panic *et al*., 2004, Park *et al*., 2004).

Fluid transport in microfluidic systems mostly depends on pressure–driven or electrokinetically driven (or electroosmotic pumping) mechanisms (Molho *et al.,* 1998). Pressure–driven flow is induced by a positive or negative displacement pump that is connected via tubing and connectors, to the microfluidic device; whereas electroosmotic pumping is non–mechanical, in this instance an electric field is applied across the channel and the counter ions at the channel wall move towards the electrode of opposite polarity, hence creating fluid motion (Baker, 1995). Typical pressure–driven and electrokinetically driven flow profiles are shown in Figure 1.18. The parabolic flow of fluid driven by an external syringe pump gives higher flow velocities in the centre than at the borders of the channel (Derveaux *et al*., 2008). On the other hand, the pluglike or flat flow profile in electrokinetically driven flow has equal velocities across the entire channel.

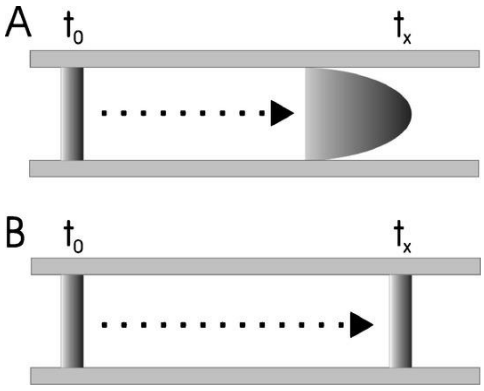

Figure 1.18. Pressure– (A) and electrokinetically driven (B) flow profiles. (Derveaux *et al*., 2008)

1.5.2. Substrate materials for microfluidic devices

Microfluidic devices can be made up from silicon, glass and quartz. The choice of material of these devices is vital as they have varying properties. Glass has been the dominant material for microfluidic device fabrication (Manz *et al*., 1992, Harrison *et al*., 1993), because its fabrication techniques were well developed by the semiconductor industry. In addition, various properties of the glass itself make it an excellent material in microfluidic systems; however the cost of mass production is higher than some of the polymers.

When considering cost, time and labour, a wide range of polymers have been used recently for the manufacture of microfluidic devices. Polydimethylsiloxane (PDMS) has been one of the most actively developed polymers in the field of microfluidics, due to its simple and inexpensive fabrication process (soft lithography), optical transparency which is compatible with optical and fluorescence microscopy, gas permeability that is advantageous for gas exchange over extended culture periods, and non–toxicity (McDonald *et al.*, 2000). PDMS is a silicon–based polymer, with the skeletal atoms comprising of an inorganic siloxane group and organic methyl groups; the repeating unit is depicted in Figure 1.19. Two potential side effects of PDMS microfluidic devices on the cell behaviour exist: adsorption of small hydrophobic molecules into the polymer and leaching of uncured PDMS oligomers into the channels (Regehr *et al*., 2009). A considerable systematic drift in the measurements was found due to the changes of surface chemistry of the PDMS when treated by plasma oxidation (Monahan *et al*., 2002).

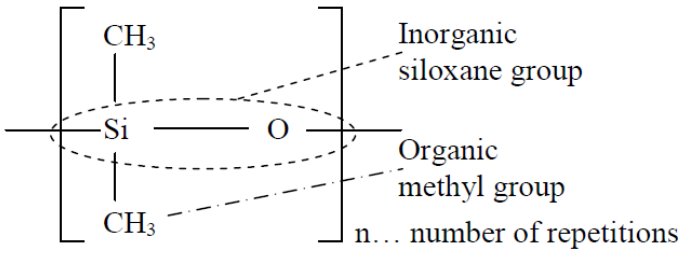

Figure 1.19. Chemical structure of PDMS. (Adapted from Mark *et al*., 2005)

1.6. Microfluidics – Biomimetic microenvironment

Inside any multicellular organism, cells inhabit a closely packed environment with specific physicochemical properties (concentration of growth and other soluble cellular regulatory factors, pH, oxygen tension, temperature, osmolarity), where one cell type is always in contact with many others. Although the major cellular components of the heart are myocytes and fibroblasts, other cell types such as mast cells, macrophages, endothelial cells, smooth muscle cells and lymphocytes are also present. These cells are physically supported and receive important signals from the extracellular matrix (ECM; Bissell, 2003). ECM plays a major role in growth and development of the heart and in response to pathophysiologic stimuli (Goldsmith, 2002). The combination of these biochemical, physical and physicohemical factors constitutes the cell microenvironment, which in turn regulates cell structure, function, behaviour and hence influencing growth, development and repair.

It is important to be able to manipulate mammalian cells *in vitro* whilst retaining their *in vivo*–like cellular microenvironment. The common problem in *in vitro* cell manipulation is that monolayer of cultured cells in culture flasks (or petri dishes and well plates) are extremely likely to behave differently to the *in vivo* situation (Zhang, 2004). Microfluidics, however, can facilitate the study of cell behaviour *in vitro*, by providing tools that create more *in vivo*–like cellular microenvironments than current methodology offers (Khademhosseini *et al*., 2005, Kim *et al.*, 2007, Yeon and Park 2007, Ziółkowska *et al*., 2011). In addition, microfluidic devices mimic the *in vivo* condition, by continuously supplying enriched media to heart tissue biopsy *in vitro* and removing waste products and gases (Hung *et al*., 2005). This allows flow of fluid to resemble the human circulatory system. The well–established cell and tissue culture techniques in general do not offer this essential perfusion, thus waste products are accumulated until a media change, perhaps every 3 days.

1.7. Microfluidics – Cardiac research

Microfluidics in cardiac research is still in its infancy. A number of research groups have developed microfluidic devices to investigate single or populations of cardiomyocytes. The architecture of these devices allows multi–parameter recordings via integration of electrochemical and optical sensors. Li and Li (2005) were the first to develop a microfluidic device to study the contraction of a single cardiomyocyte using fluorescence measurement. A single cardiomyocyte was held at a V–shaped retention structure within the chip. Quantitative analysis of $[Ca^{2+}]_i$ of the cell was measured using the Ca^{2+}–sensitive fluorescent dye, Fluo–4 AM ester, followed by the addition of ionomycin, an intracellular Ca^{2+} stimulant. Li *et al*. (2007) have also developed a microfluidic method to measure the real–time cellular response of a single cardiomyocyte pertaining to drug discovery. They have created a multiple–step liquid delivery system to examine the response of cardiomyocytes to different drugs

Klauke *et al*. (2003) described a microchamber array in which single adult rabbit ventricular myocytes could be stimulated continuously using planar electrodes within a very small volume (100 pl), but microfluidics was not incorporated. Single cardiomyocytes were contained within a limited extracellular volume, simulating the metabolic conditions during myocardial ischaemia. Later, these authors fabricated a microfluidic device with microchannels and positioned two cardiomyocytes in adjacent microchannels to study their extracellular potentials and currents during the course of an action potential (Klauke *et al*., 2006). Sarcomere length and Ca^{2+} transients were monitored by using a fluorescent Ca^{2+} indicator. They further monitored the transmission of Ca^{2+} waves across the intercellular gap junctions between a pair of cardiomyocytes (Klauke *et al*., 2007). Cheng *et al*. (2006) have described a microfluidic platform that allows real–time measurement of ionic and metabolic fluxes from electrically–active, beating cardiomyocytes. Cardiomyocytes were continually paced, while cell length, pH, $[Ca^{2+}]$ as well as intra– and extra–cellular lactate were simultaneously measured on the device.

Using a microfluidic device called NanoPhysiometer, Werdich *et al.* (2004), studied a single cardiomyocyte perfused continuously in a microchamber of 100 pl while the extracellular potential was measured using electroplated platinum black planar microelectrodes. The same device was also used to measure pH in the extracellular environment in a volume of 0.36 nl using electrochemical sensing electrodes for studying the acidification rates in cardiomyocytes in a mouse model of very long chain acyl–CoA dehydrogenase deficiency (Ges *et al*., 2008). Amperometric glucose–sensing electrodes were then incorporated with this device to concurrently measure glucose consumption of cardiomyocytes (Ges and Baundenbacher, 2010).

A dielectrophoresis microfluidic device was fabricated to orientate cardiomyocytes along the direction of the electric field, which was controlled by interdigitated–castellated microelectrodes (Yang *et al*., 2006, Yang and Zhang, 2007), forming a tissue–like structure (Figure 1.20). This research group also looked at the dynamic process of endothelin–1–induced cardiomyocyte hypertrophy in a dielectrophoresis microfluidic device with an impedence sensing system (Yang *et al*., 2007).

It is important to note that physiological heart development and its functioning depend on the response of cardiomyocytes to mechanical stress during haemodynamic loading. A microfluidic cardiac circulation model was developed to mimic the *in vivo*–like mechanical stresses (Nguyen *et al*., 2009). Cardiomyocytes were cultured on a thin flexible silicone membrane and the preload and afterload conditions were dynamically controlled by adjusting the flow rate or manipulating the fluidic resistance of microchannels.

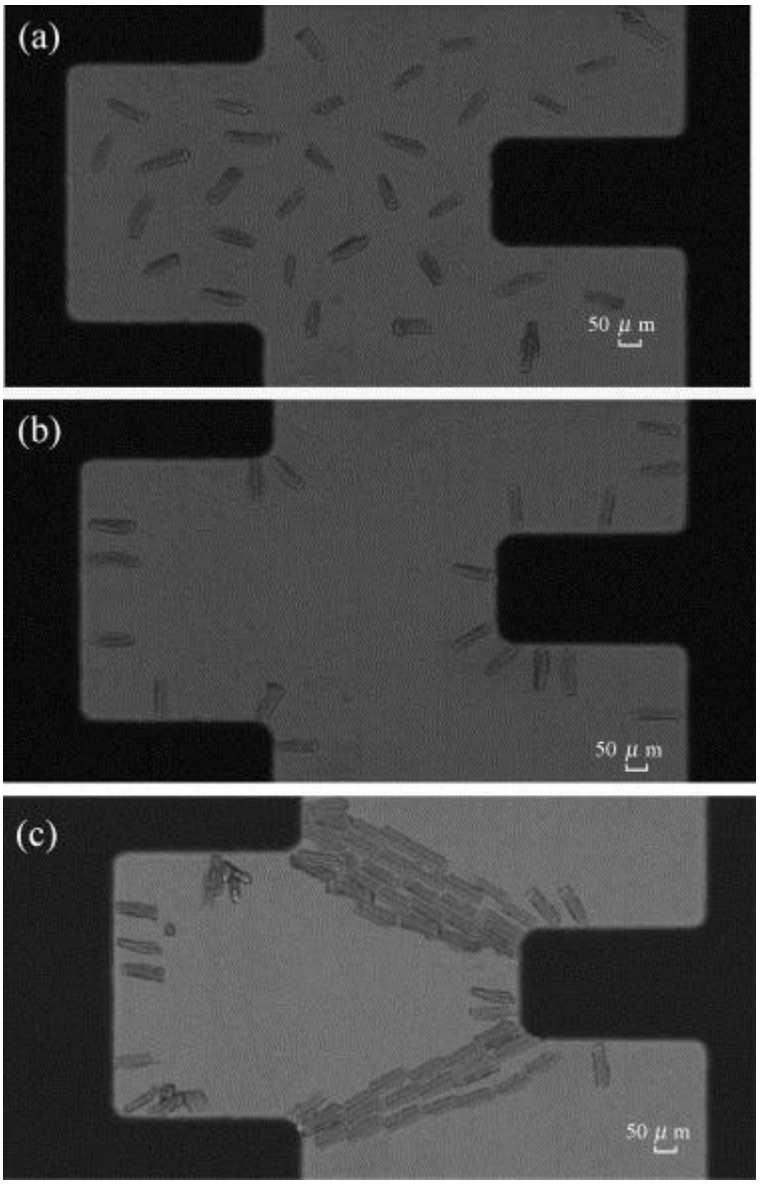

Figure 1.20. Cardiomyocytes orientation in a microfluidic device. (a) No voltage applied, (b) alternating current at 2 V, (c) alternating current at 4 V. (Yang *et al*., 2006, Yang and Zhang, 2007)

Micropatterned cells in microfluidic chambers have also been used for cell toxicity studies, where the response of these cells to localized chemical stimulation was assessed (Kaji *et al*., 2003). The cardiomyocytes were selectively attached to the fibronectin–patterned PDMS areas. Localized flow of octanol, a gap junction inhibitor, inactivated only those cardiomyocytes exposed to the inhibitor, whilst the other part retained spontaneous and synchronous pulsality (Figure 1.21). This approach offers a potential for use in high–throughput drug screening in the future.

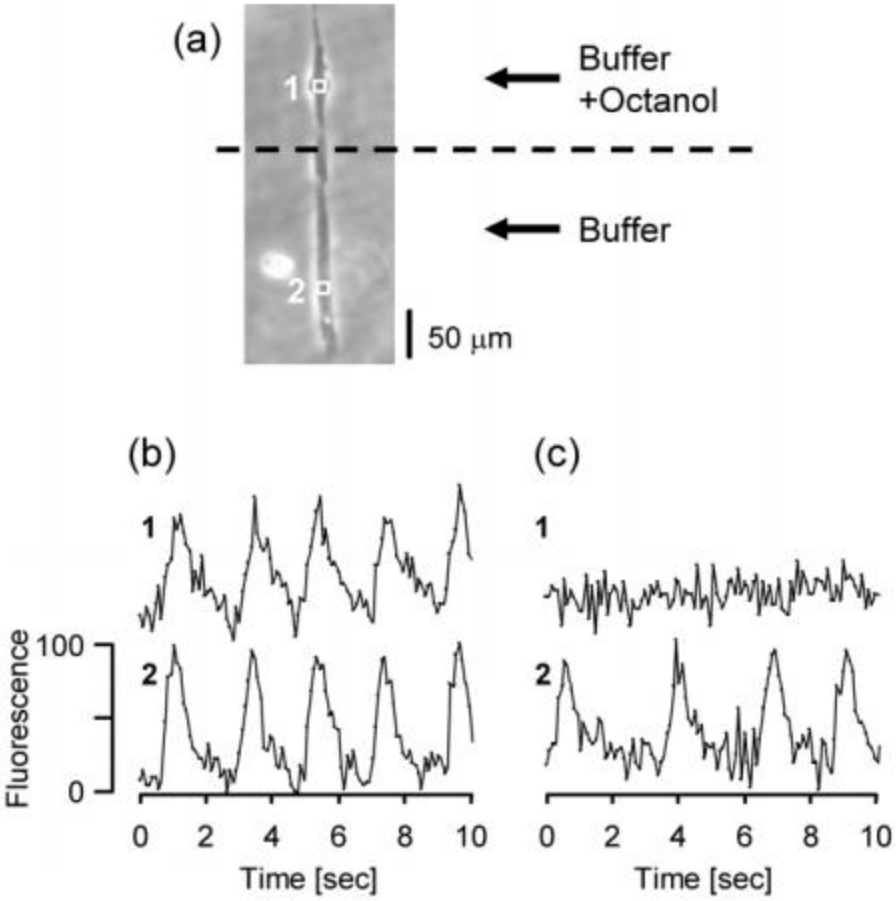

Figure 1.21. Line–patterned cardiomyocytes in the microchannel (a). Part 1 was perfused with buffer and octanol and part 2 with buffer only. Time course of fluorescence of cytosolic Ca^{2+} measured when entire pattern was perfused with buffer (b), followed by localized delivery of 100 μM octanol to part 1 (c). (Kaji *et al*., 2003)

Moreover, microfluidics can also be used for cell sorting and separation. A device has been established to separate myocytes and non–myocytes from neonatal rat myocardium by passing them through microsieves (Murthy *et al*., 2006). Throughout the separation procedure, cell viability was maintained at 70 – 80 %, and an enriched non–myoycte fraction was obtained (~ 13 % myocytes present). This approach provided the least invasive separation method to date as no chemical or biological interactions between cells and device, or mechanical centrifugation and antibody labelling were required.

Microfluidic device design offers the flexibility in incorporating different cell culture compartments for the studies of interactions between multiple cell types. Recently, rat superior cervical ganglion neurons and ventricular cardiomyocytes were co–cultured in separate microcompartments interconnected with microconduits (Takeuchi *et al*., 2011). Connection via these conduits was formed within 3 days of seeding. Electrical stimulations applied to the neurites affected the beating rate of the cardiomyocytes. Another, low shear, microfluidic culture device has demonstrated IR injury of primary porcine cardiomyocytes, by subjecting the cells to 3 – 4 hours of hypoxia, followed by normoxia (Khanal *et al*., 2011), monitoring mitochondrial membrane potential and morphological changes by fluorescence on–chip.

Overall, there are almost limitless potential of microfluidic systems as a research tool, not only in cardiac field, but in all research areas. Integrated microfluidic devices (i.e. combining separate analytical modules on single device) may provide a platform technology for investigating heart pathophysiology, and development of possible therapeutic strategies, since new functionality and experimental paradigms are emerging in recent years.

1.8. Aims of the study

Over the past 6 years, the rapid growth of microfluidic technology has enabled novel miniaturised cell and/or tissue culture systems and assays. However, in cardiovascular research, native heart tissue culture and maintenance in microfluidic devices have not been reported. So far, most of the microfluidic devices have been used to study isolated cardiomyocyte(s) although some research has focused on cardiac tissue engineered from cells. Therefore, this project aims to develop a microfluidic perfusion system that allows the study of both healthy and diseased heart tissues in life–like *in vivo* conditions, and functional changes in response to stress or treatments. Specifically, the work demonstrated here aims to:

- Develop both PDMS– and glass–based devices for perfusion of cardiac sample (rat and human)
- Design and integration of electrochemical modules that allow real–time monitoring of total ROS
- Induce IR damage on–chip and measure gene expression analysis off–chip using reverse transcription (RT)–polymerase chain reaction (PCR) to determine appropriate markers
- Investigate the potential of redox–magnetohydrodynamic (redox–MHD) to give improved control of the mixing around the tissue biopsies
- Develop an electrochemical microsensor for CK–MB measurement

Chapter 2

Materials and Methods

2.1. Experimental Models

2.1.1. Rat model

All studies conform to the UK Animals (Scientific Procedures) Act 1986 and approved by the University of Hull Ethical Review Process. Male Sprague Dawley rats (Charles River Laboratories International, UK) were housed under conditions with a 12:12 hour light–dark cycle and provided with food and water ad libitum. Animals were anaesthetized via intraperitoneal injection of 1 ml / 100 g (body weight) sodium thiopentone (Link Pharmaceuticals, UK) and the hearts were excised under a Schedule 1 procedure.

2.1.2. Human model

Human right atrial tissue biopsies were provided by Mr Steve Griffin (Consultant of Cardiothoracic Surgery, Castle Hill Hospital). The use of tissue biopsies was approved by the Hull and East Yorkshire Local Research Ethics Committee (07/H1304/105) and Hull and East Yorkshire NHS Trust (R0568). After excision, the heart tissue was immersed in cardioplegic solution (Martindale Pharmaceuticals, UK) at 4 ^{o}C, the concentrate was diluted with Ringer's Injection in 1:50 dilutions immediately before use. The cardioplegia solution contains 34 mM $MgCl_2$, 20 mM KCl, 0.14 M NaCl, 2.16 mM $CaCl_2.2H_2O$, and 1.15 M procaine hydrochloride.

Once transported to the laboratory at 4 ^{o}C (within 1 hour), the biopsy was placed in the microfluidic perfusion chamber.

2.2. Design of PDMS microfluidic chamber (Generation 1)

A perfusion chamber with a capacity of 800 µl was designed and made from PDMS (polydimethylsiloxane) and a polystyrene petri dish of 35 mm in diameter (Figures 2.1 and 2.2). The end of a 5 ml plastic syringe was adhered to a petri dish (35 mm) with instant adhesive (Loctite 4850, Loctite, UK) and used as a chamber mould (Figure 2.1). PDMS was prepared from SYLGARD®184 Silicone elastomer kit (Dow Corning, US), composed of curing agent (silicone resin solution) and PDMS monomer. They were evenly mixed in a 1:10 ratio and the mixture (15 g) was subsequently degassed in a vacuum dessicator for 30 minutes. Subsequently, the mixture was poured onto the chamber mould, and the PDMS was left to cure at 75 ^{o}C for two hours.

The cured PDMS slab was carefully removed from the silicon wafer and chamber mould and five apertures punched as shown in Figure 2.3. These holes were used for inlet and outlet tubings, working electrode (Pt), counter electrode (Pt), and reference electrode (AgCl coated Ag wire). The perfusion flow channel was rhombic in shape and contained a circular chamber of 7 mm diameter at the centre. A 2 mm thick PDMS slab was adhered at the bottom of the circular chamber, serving as a holder for the heart tissue biopsy.

The PDMS slabs and petri dish were placed in a beaker of methanol and subjected to ultrasonic cleaning for 5 minutes, followed by washing with distilled water for another 5 minutes and then blow–dried with nitrogen. The PDMS slabs were then treated with oxygen plasma using a SPEEDIVAC coating unit (Model 12E6/1405, Edwards High Vacuum, UK) at 350 V, 20 mA, pO_2 8 mbar for 50 seconds (Ferguson *et al*., 1993). The bonding surfaces of the PDMS slabs were subjected to high energy oxygen plasma which stripped away electrons on the surface and generated exposed silanol (Si–OH) groups (Owen and Smith, 1994), causing them to become hydrophilic (Chaudhury and Whitesides, 1991, Owen and Smith, 1994) and forming strong bonding between PDMS slabs and the petri dish. The bonded PDMS device (Figure 2.2) was placed in a 75 ^{o}C oven for 30 minutes to enhance bonding (McDonald and Whitesides, 2002).

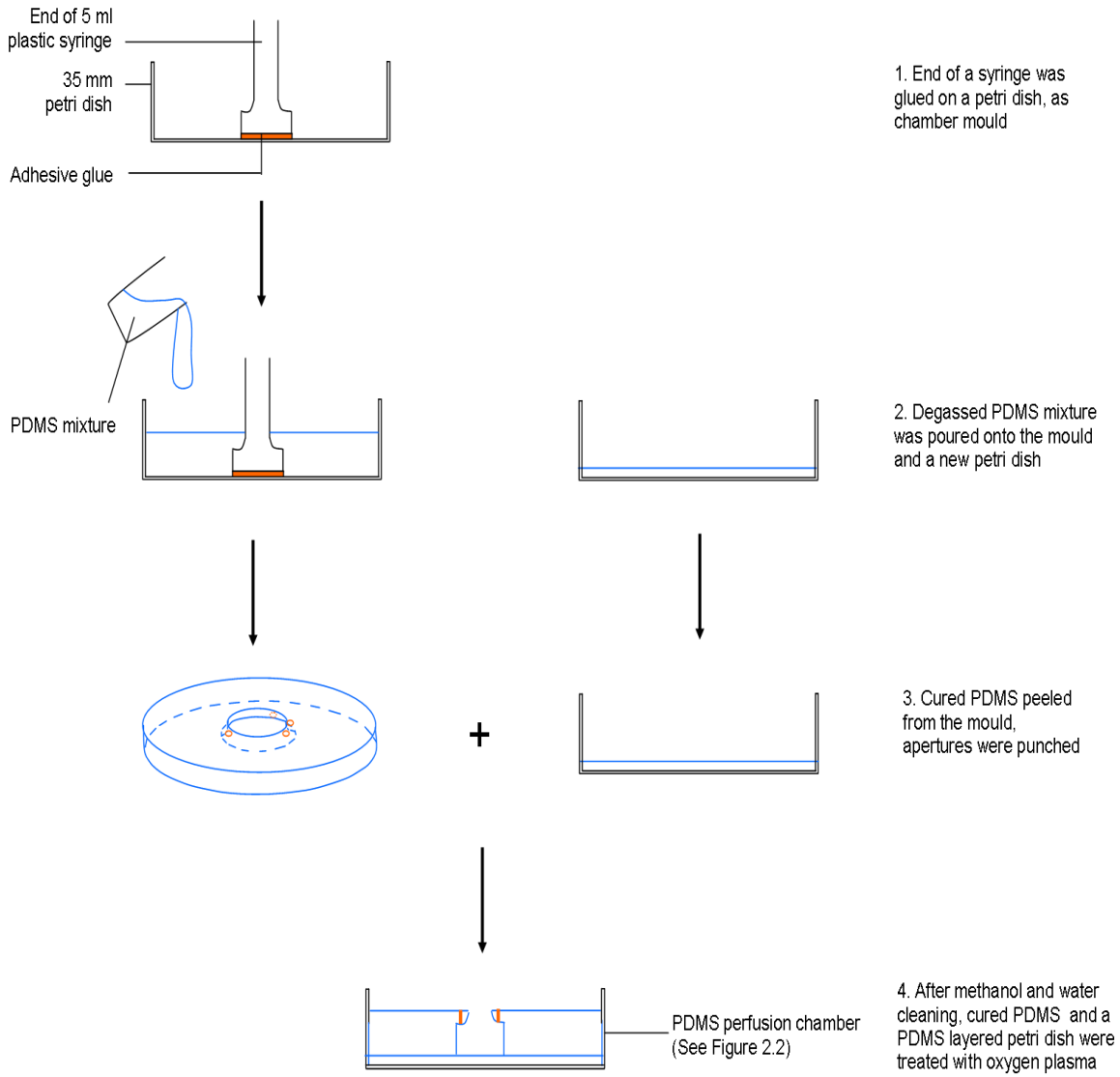

Figure 2.1. PDMS perfusion chamber making procedure.

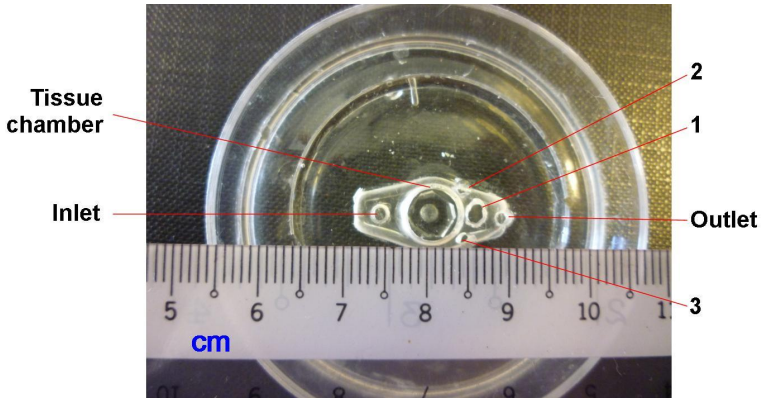

Figure 2.2. PDMS perfusion chamber (top view).

1, Working electrode (Pt); 2, Counter electrode (Pt); 3, Reference electrode (AgCl coated Ag wire)

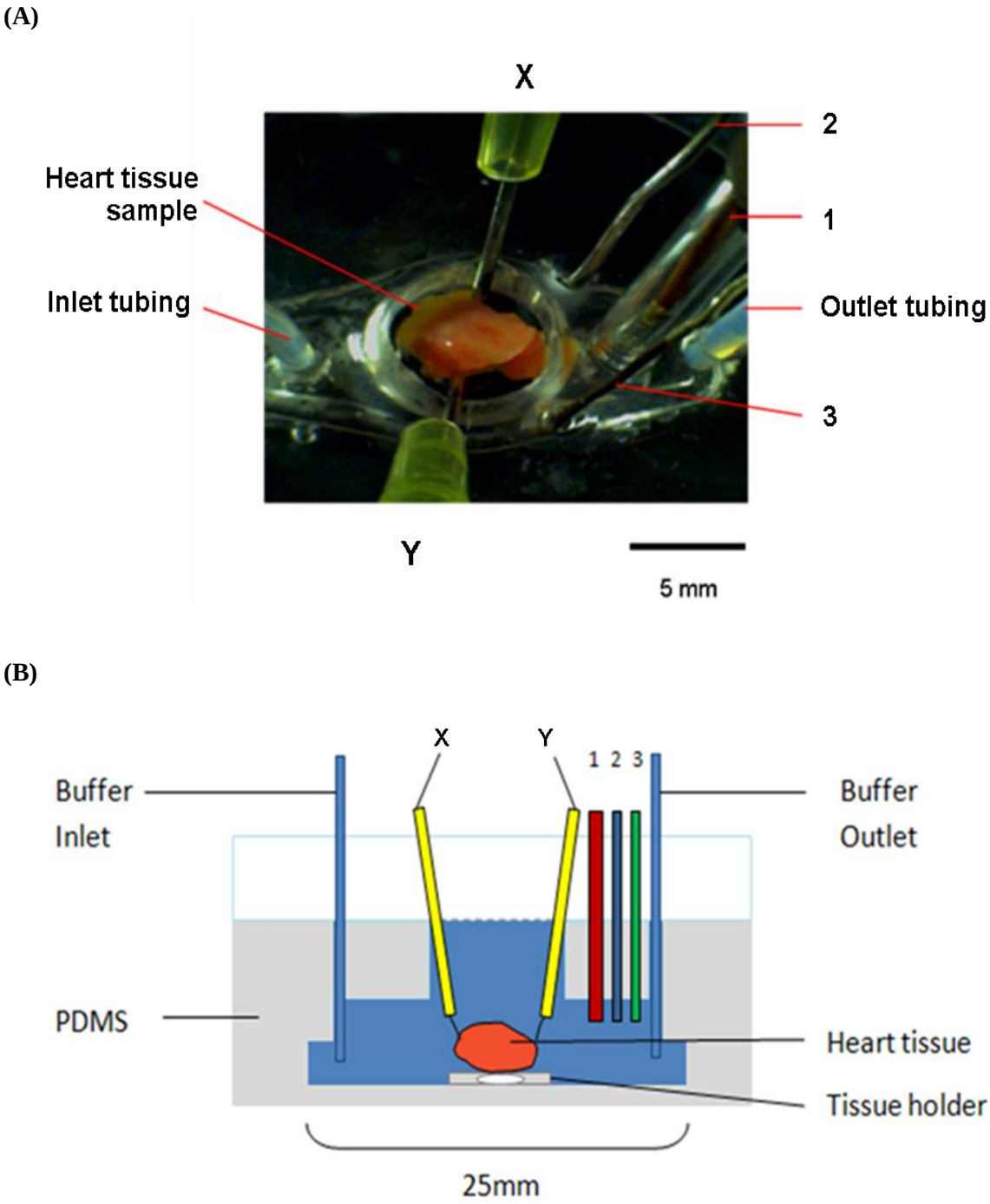

Figure 2.3. PDMS perfusion chamber with heart tissue.

1, Working electrode (Pt); 2, Counter electrode (Pt); 3, Reference electrode (AgCl coated Ag wire); X and Y, stimulation electrodes (Pt)

2.3. Perfusion system setup – PDMS microfluidic chamber

The perfusion system was set up as shown in Figures 2.4 and 2.5. Initially, the microfluidic system was sterilised with 70 % (v/v) ethanol/water by perfusion at 120 µl/minute for 10 minutes and rinsed with sterile double distilled water. The microfluidic device was then primed with Krebs–Henseleit bicarbonate buffer (KHBB; pH 7.4) containing 118 mM NaCl, 25 mM $NaHCO_3$, 4.8 mM KCl, 1.2 mM KH_2PO_4, 1.2 mM $MgSO_4.7\ H_2O$, 2.5 mM $CaCl_2.2\ H_2O$ and 5 mM glucose. The buffer was supplemented with 100 U/ml penicillin and 0.1 mg/ml streptomycin (Sigma–Aldrich, UK) and filtered by passing through a 0.22 µm syringe filter (Millipore Corporation, US) prior to use.

In brief, hearts were rapidly excised and the aorta cannulated on a Langendorff perfusion apparatus (Akki *et al.*, 2008). A section of right ventricular tissue, excised from rat heart or human right atrial tissue biopsy (obtained from the hospital), was placed directly into the chamber of perfusion device after rinsing in KHBB. The perfusion chamber was positioned on a 37 ^{o}C hotplate (World Precision Instruments, UK; Figure 2.4). Buffer was introduced to the chamber via the inlet and was removed through the outlet. In this way, the heart tissue was supplied with fresh nutrients throughout the experiment. Both the inlet and outlet were connected to two Minipuls3 peristaltic pumps (Gilson, France) at a flow rate of 120 µl/minute. KHBB was gassed with 95 % O_2 / 5 % CO_2 (BOC, UK) in a water bath of 37 ^{o}C (Grant Instruments, UK). Heart tissue was electrically stimulated via two platinum wire electrodes using a programmable function generator at 3 - 4 V/cm, 1.5 Hz (Thurlby Thandar Instruments, UK). Contraction of the heart tissue was monitored using a microscopic camera (Veho, UK). The lid of the microfluidic chamber was designed to accommodate ports for fluid inlet and outlet, as well as the stimulating electrodes. Approximately 240 µl effluent (i.e. 2 minutes collection time) was collected from the outlet tubing and stored at – 20 ^{o}C for subsequent LDH or/and H_2O_2 analyses. After an extended period of perfusion, the heart tissue sample was perfused with 2 % (w/v) Triton X100

for at least 30 minutes (or otherwise stated), to induce cell lysis and LDH release.

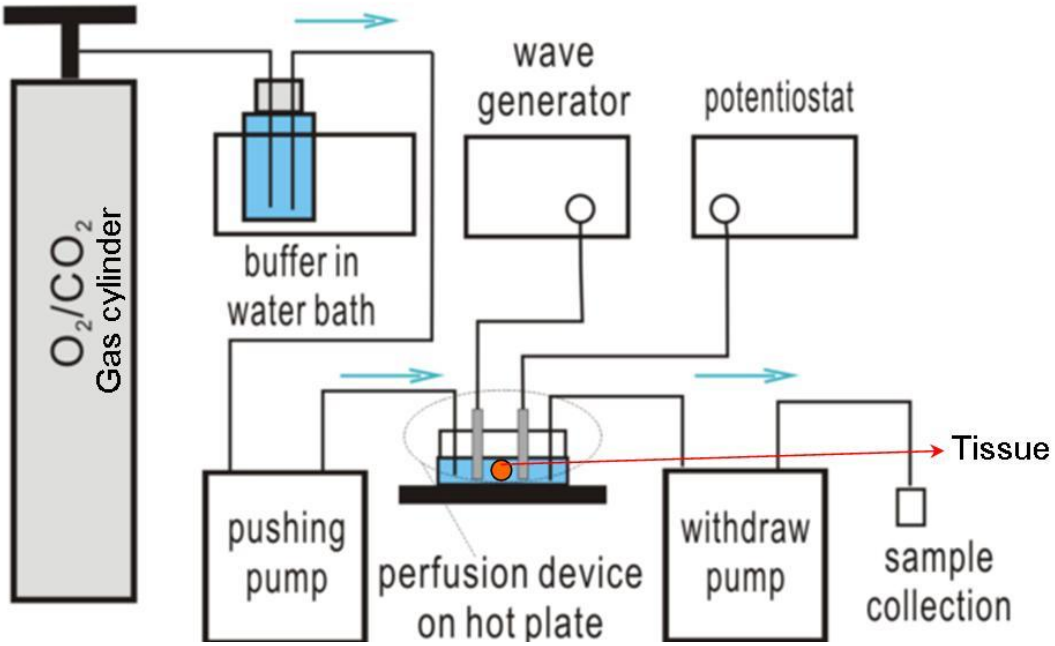

Figure 2.4. Schematic view of the Generation 1 perfusion system.

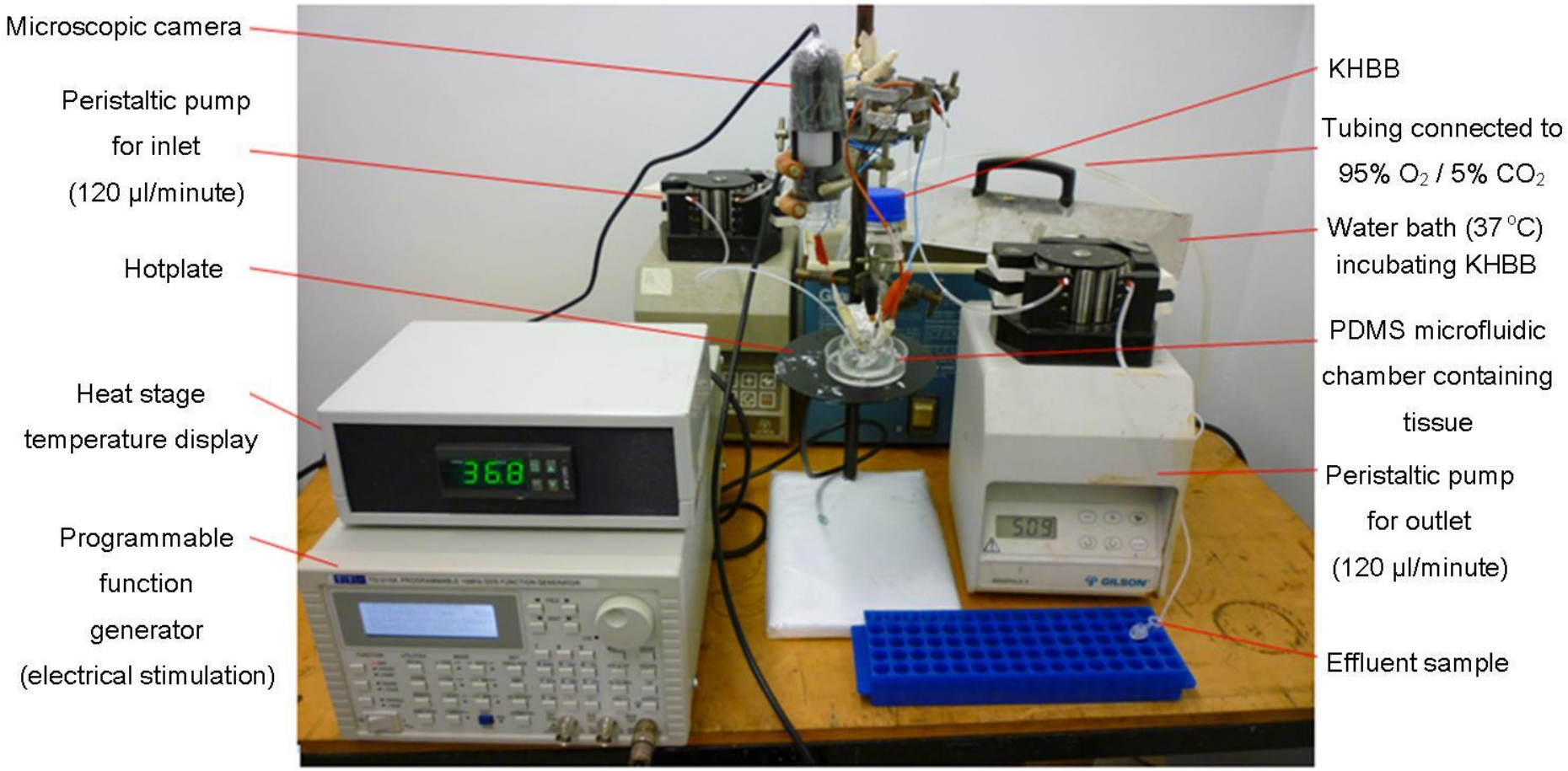

Figure 2.5. Photograph of the Generation 1 perfusion system.

2.4. Design of glass microfluidic device (Generation 2)

A second generation glass microfluidic chip was manufactured by Dr Steve Clark (Department of Chemistry, University of Hull), using standard photolithographic techniques (Figure 2.6).

Briefly, the chrome masked glass plate was coated with photoresist, a liquid polymeric material and then a master mask containing the design layout of the device, i.e. the blueprint of the glass chip, was laid on top. By exposure to ultraviolet (UV) light through the mask and onto the glass plate, individual areas of the photoresist were selectively exposed to light and changed chemically on the glass plate. Subsequently, the glass plate was immersed in a developer solution, dissolving areas of photoresist that were exposed to light and leaving the remaining photoresist patterned with the desired layout of the device. The *Cr* mask and glass were etched simultaneously, in a 1 % hydrofluoric acid/5 % ammonium fluoride solution at 65 ^{o}C, before the *Cr* mask and photoresist were stripped off. Finally, a new glass cover plate was bonded on the etched glass plate, forming the capillary or microchannel of the device.

The design of microfluidic device is given in Figure 2.7, composed of two separate layers; with the top and bottom layers 3 mm and 1 mm thick, respectively. The top layer contained holes of specific diameters (3 mm), whereas the bottom layer was etched with channels, the two layers were then thermally bonded together at 595 ^{o}C for 3 hours. Three 3 mm apertures were drilled on the top layer for a tissue chamber (centre), and two stimulation electrodes. In addition, five 0.8 mm apertures were drilled for polyether ether ketone (PEEK) tubing connection points. Either of the ports, A or B was used as inlet, whilst either port D or E was used as the outlet. Port C was used as a pre–tissue sampling point.

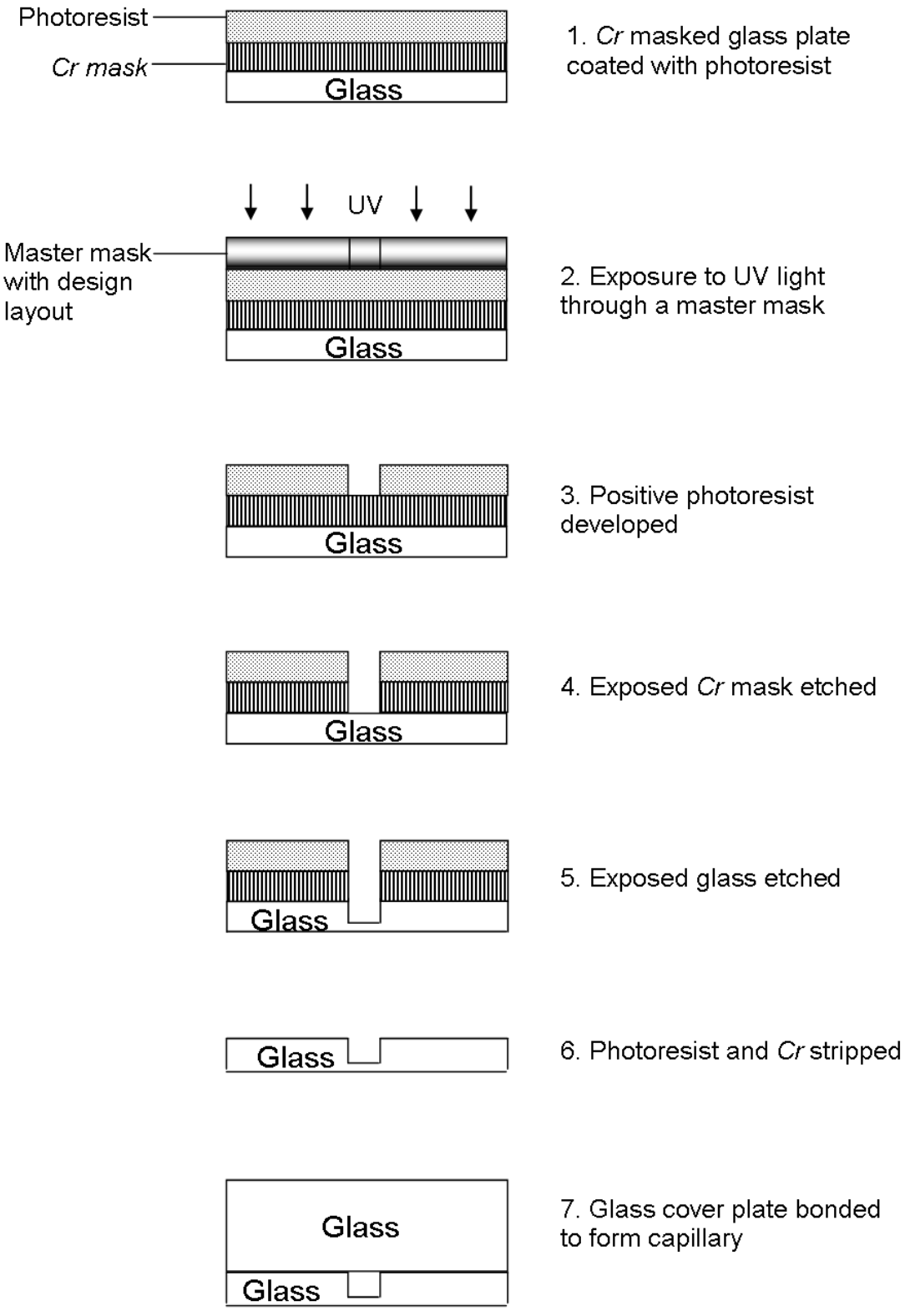

Figure 2.6. The etching process.

Cr, chrome; UV, ultraviolet.

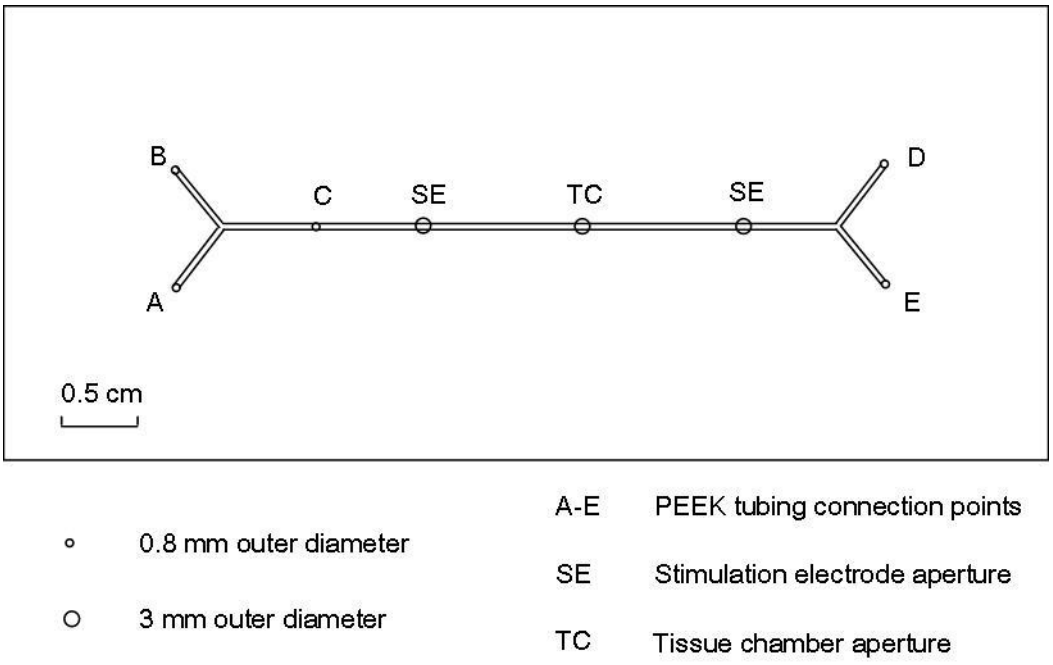

Figure 2.7. Schematic design of the glass microfluidic chip.

Two glass microfluidic chips with different component assemblies have been developed, namely Generation 2.1 and 2.2 (Figures 2.8.A and B, respectively). A nanoport reservoir assembly (Kinesis, UK) was bonded on top of the tissue chamber aperture, according to the company instructions. PEEK tubings (0.8 mm OD x 0.38 mm ID, Kinesis, UK) in Generation 2.1 was bonded onto the glass with ferrules (GC Supplies, Australia) and Araldite adhesive (Bostik Findley, UK). Whereas for Generation 2.2, headless 6–32" coned nanoport assemblies (Kinesis, UK) were used to hold PEEK tubings and stimulation electrodes. Gauge plugs (Kinesis, UK) were used to replace the nanoport nut (Kinesis, UK) at unused ports.

The stimulation electrodes in Generation 2.1 were made from platinum wire sealed in glass capillary (Figure 2.9). First, silver paste (Creativematerials, US) was used to connect one end of the wire (1 cm stripped) to the platinum wire (1 cm) and left overnight for curing at room temperature. The wire was fed through a hollow glass capillary (3 mm outer diameter). Both ends of the glass capillary were sealed with Norland optical adhesive (Norland Products, US), by exposure to UV light (Spectronics Corporations, US; wavelength 365 nm) for 4 hours. The electrodes were polished with polishing pads (Kemet International, UK) to expose a new

platinum surface, and continuity test was performed before the electrodes were bonded onto the chip using Araldite adhesive. Stimulation electrodes in Generation 2.2 were developed by directly placing 2.5 cm platinum wire through the nanoport nut and being glued in place with Araldite adhesive.

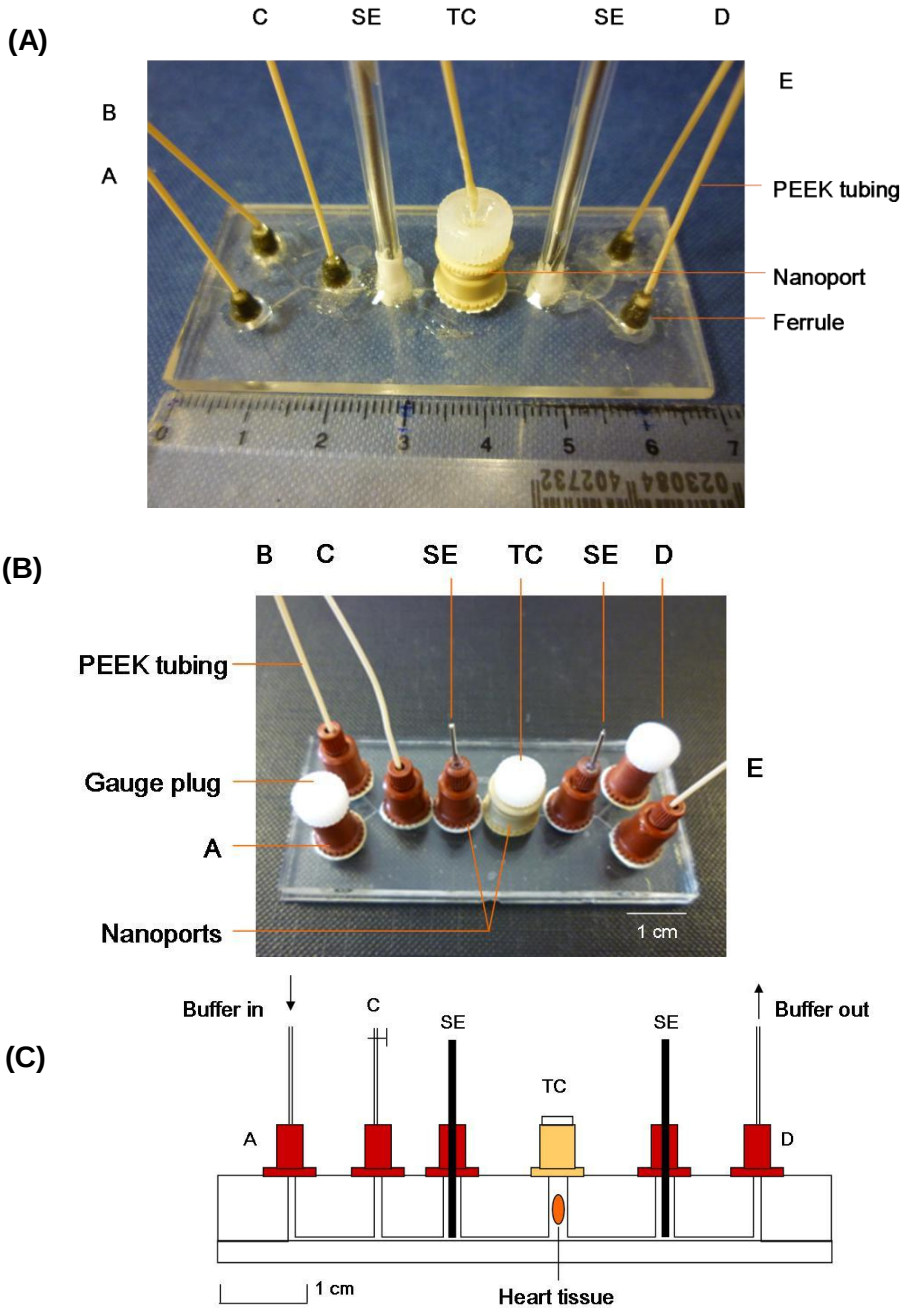

Figure 2.8. Generation 2 glass chips. (A) Generation 2.1, PEEK tubings were bonded to the glass with ferrule and Araldite adhesive. (B) Generation 2.2, nanoports function to hold PEEK tubings in place, gauge plugs were used in unused ports. (C) Side view.

A–D; PEEK tubing connection ports; SE, stimulation electrode; TC, tissue chamber.

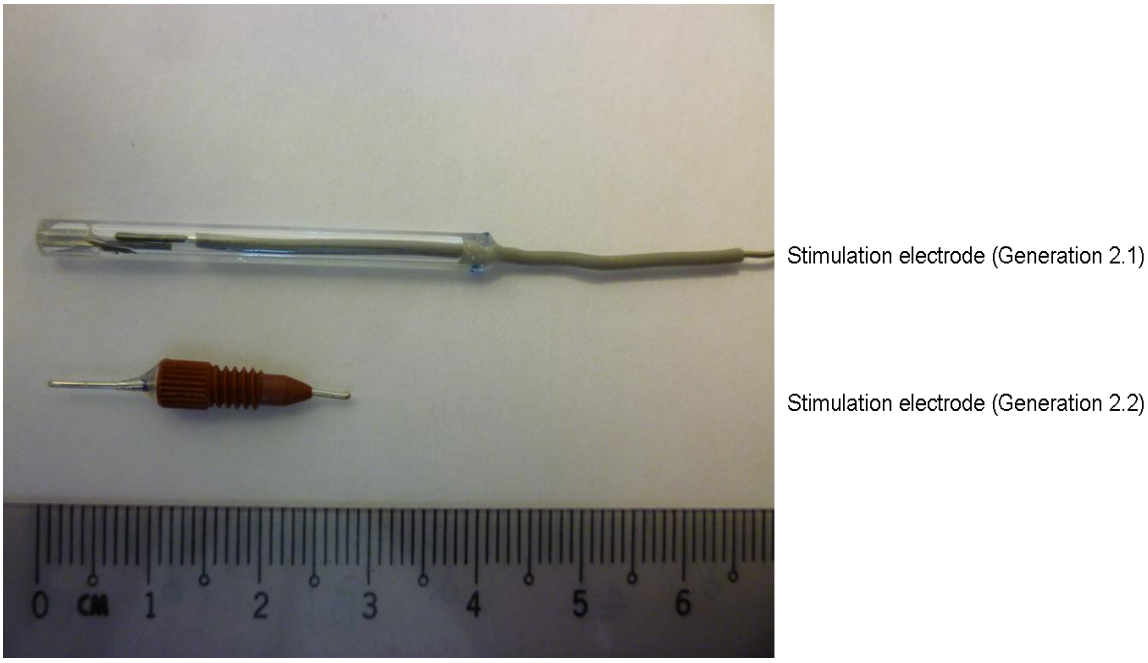

Figure 2.9. Stimulation electrodes for Generations 2 chips.

2.5. Perfusion system setup – Glass microfluidic chamber

The glass microfluidic chip was placed on top of a hotplate (Linkam Scientific Instruments, UK) in an incubator box (Figures 2.10 and 2.11), manufactured from polycarbonate by the Mechanical workshop at University of Hull. The box was designed by myself in collaboration with a clinical colleague, Dr I. Riaz, who is also undertaking a PhD in the group. The internal view of the apparatus arrangement is showed in Figure 2.11.

A type K thermocouple wire (TC Direct, UK) connected to a dual input multi thermocouple type indicator (TC Direct, UK), was placed on top of the glass chip to monitor temperature. The hotplate was connected to a MC 60 controller (Linkam Scientific Instruments, UK) and the temperature was set, so that the glass chip was maintained at 37 ^{o}C. Before experimentation commensed, the glass microfluidic chip was sterilised with 70 % (v/v) ethanol/water by perfusion at 120 µl/minute for 10 minutes and then rinsed with sterile double distilled water. KHBB buffer was gassed with 95 % O_2 / 5 % CO_2 for at least 30 minutes at 37 ^{o}C, before being transferred into a glass syringe which was then positioned in the syringe pump (Harvard Apparatus, UK) and connected to the glass chip via an adapter. The glass chip was primed with oxygenated KHBB for at least 20 minutes before a sample was introduced. The syringe pump was switched on throughout transfer of the tissue sample into the tissue chamber. After an extended period of perfusion, the heart tissue was perfused with 2 % (w/v) Triton X 100 for 30 minutes (or otherwise stated), to cause cell lysis and LDH release.

Approximately 240 µl effluent (i.e. 2 minutes collection time) was collected from the outlet tubing during perfusion and stored at –20 ^{o}C for subsequent LDH analysis off–chip.

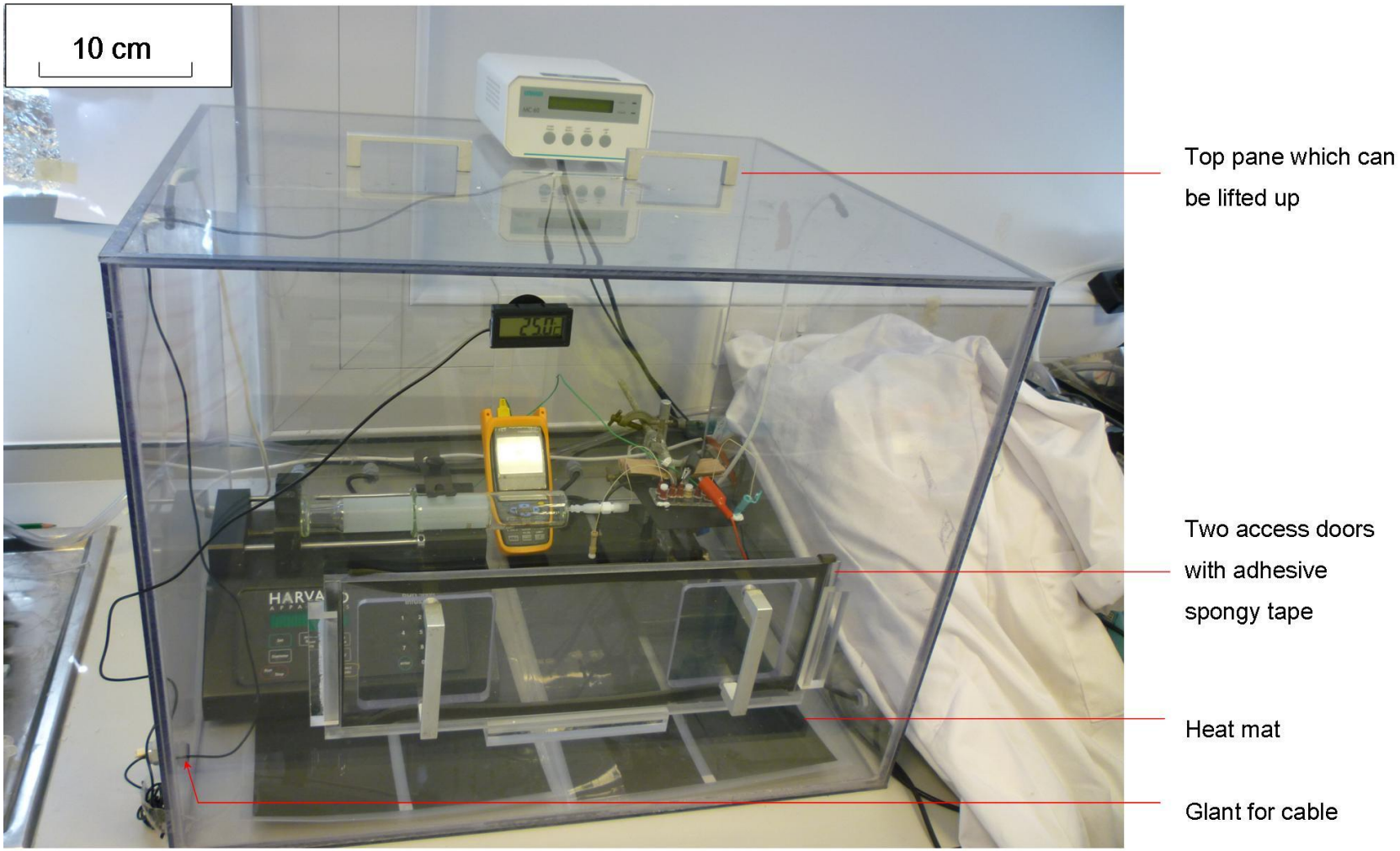

Figure 2.10. Polycarbonate incubator box.

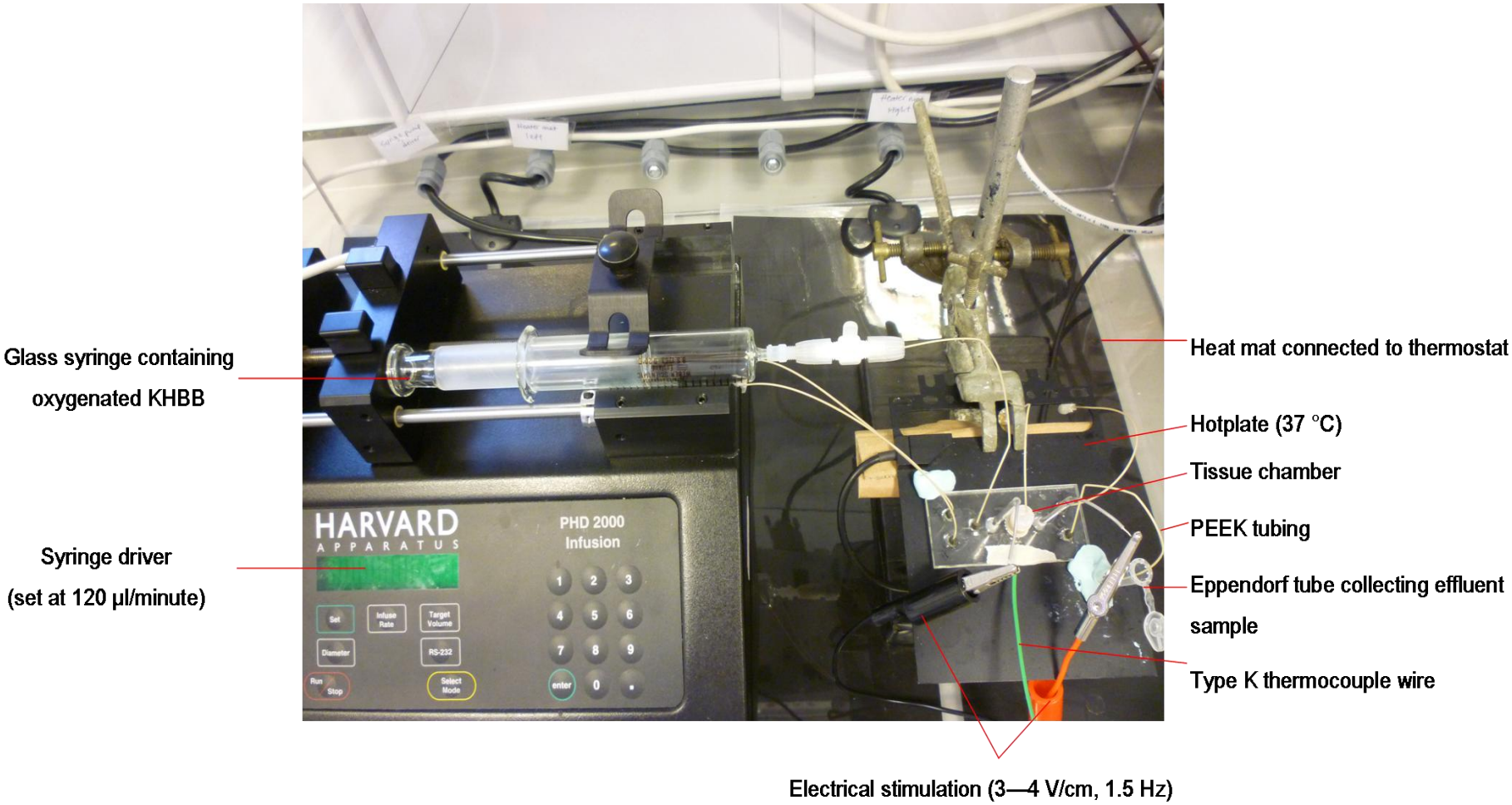

Figure 2.11. Generation 2 perfusion system.

2.6. Measurement of LDH release

To quantify the extent of cell damage, a ubiquitous cytoplasmic enzyme, LDH was assayed using a colourimetric cytotoxicity assay [Cytotoxicity Detection Kit ^{Plus} (LDH), Roche, UK]. Effluent samples were analysed for LDH as shown in Figure 2.12. Serial dilutions of pure enzyme from rabbit muscle (0 – 0.6 U/ml; Sigma–Aldrich, UK) were used as a standard, whereas KHBB served as the control. Rabbit LDH was used thoughout these work as rat LDH was not available. The reaction mixture (50 µl) was added to 50 µl of sample in a 96–well plate, which after gentle shaking was incubated at 37 ^{o}C for 30 minutes. Finally 50 µl of stop solution (1 M HCl) was added into each well and the plate was shaken gently. Absorbance was measured at 490 nm using a microplate reader (BioTek Instruments, US). The results were expressed as the mean determined from triplicate samples. The absorbance value obtained from the control was subtracted from all test values. Absorbance values of the samples were converted to LDH activity (U/ml) according to the LDH standard curve (Figure 2.13). The LDH activity was then divided by the wet weight of heart tissue and presented as U/ml/g in the entire thesis.

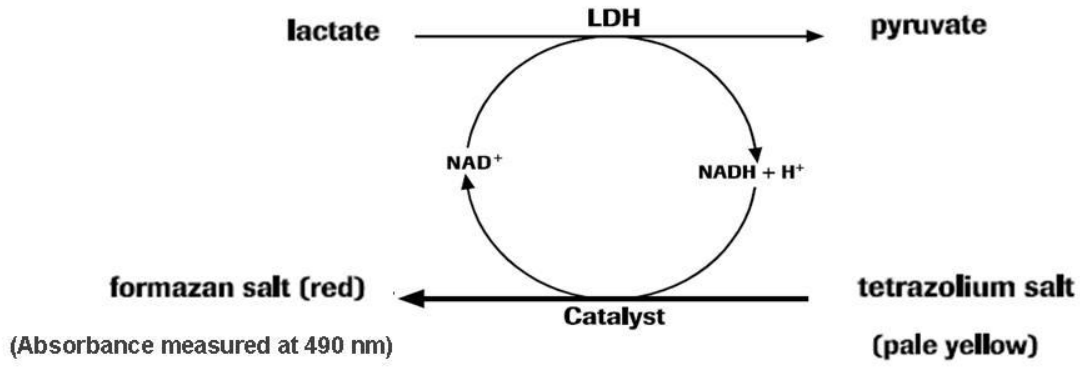

Figure 2.12. Principle of LDH assay.

LDH, lactate dehydrogenase; NAD^{+}, oxidised form of nicotinamide adenine dinucleotide; NADH, reduced form of nicotinamide adenine dinucleotide.

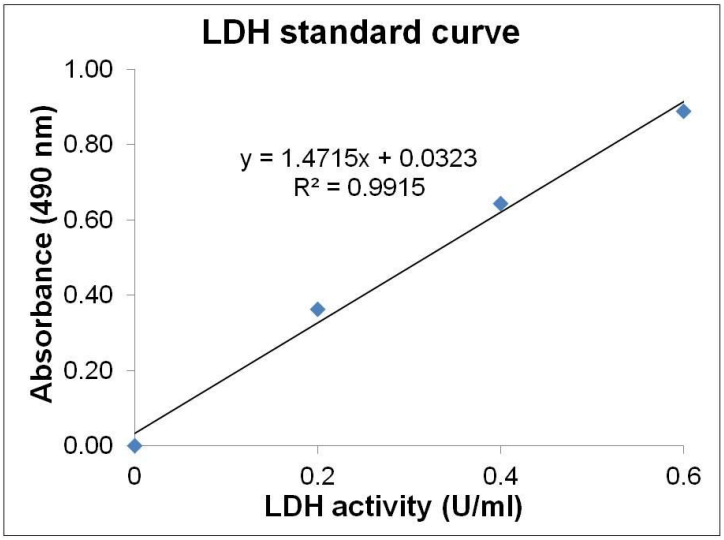

Figure 2.13. Representative LDH standard curve. The absorbance values shown were corrected for background activity. A new standard curve was run for every experiment.

2.7. Viability of heart tissue

Cell viability was evaluated using Calcein–acetoxymethyl ester (Calcein AM; Invitrogen, UK) and Propidium Iodide (PI; Sigma–Aldrich, UK) as described previously (Hattersley *et al*., 2008). Calcein AM is hydrophobic and allows the entry through the plasma membrane of a cell which, when hydrolyzed within a viable cell, becomes a membrane impermeable carboxylate fluorescing at 494 nm (Haugland *et al.*, 1994; Figure 2.14). PI only enters cells with disrupted plasma membranes, intercalates with the DNA and fluoresces at 536 nm (Sasaki *et al.*, 1987), hence providing a measure of dead or dying cells.

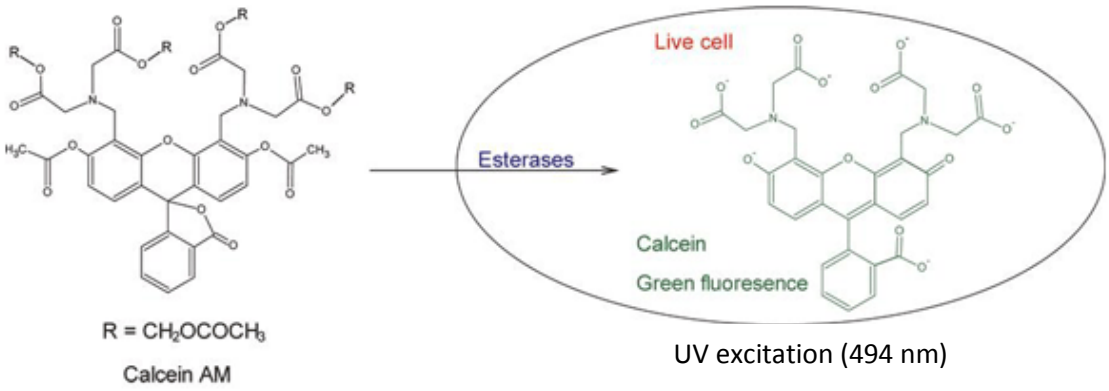

Figure 2.14. Calcein AM for determining cell viability.

Calcein AM was prepared by dissolving in Pluronic F–127 (Invitrogen, UK) before use. Tissue samples after perfused in the microfluidic chamber were initially incubated with 50 µl of 10 µM Calcein AM (λ_{ex} = 494 nm, λ_{em} = 517 nm) in phosphate buffered saline (PBS) for 1 hour. The tissue was then washed with PBS to remove excess probe and subsequently incubated with 50 µl of 3.75 mM PI (λ_{ex} = 536 nm, λ_{em} = 617 nm) for 10 minutes and finally washed again with PBS. The imaging of cardiac tissue was carried out using a laser–scanning inverted confocal microscope (Nikon Eclipse TE2000–E) equipped with Helium/Neon and Argon lasers, and Lazershop 2000 software.

2.8. H_2O_2 measurement

The release of one of the major ROS, H_2O_2, was measured biochemically in the current system for validating the total ROS examined by electrochemical means (Section 2.9).

The concentration of H_2O_2 in the effluent was determined using a commercial Amplex red hydrogen peroxide assay kit (Invitrogen, UK). The principle is given in Figure 2.15. A standard curve ranging from 0 to 5 µM H_2O_2 was generated for each experiment (Figure 2.16). Samples (50 µl) were incubated with 50 µl of reaction mixture containing 100 µM Amplex red reagent and 0.2 U/ml horseradish peroxidase (HRP) for 30 minutes at room temperature. Absorbance at 562 nm was measured using a microplate reader (BioTek Instruments, US). All results were corrected for background absorbance (KHBB alone) and expressed as the average of duplicate samples.

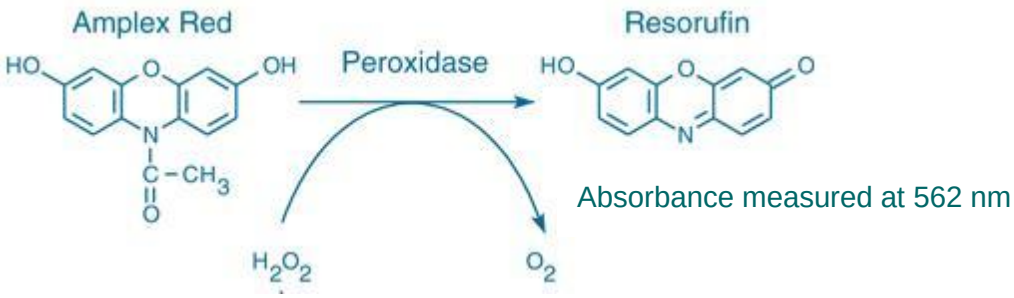

Figure 2.15. Principle of H_2O_2 assay.

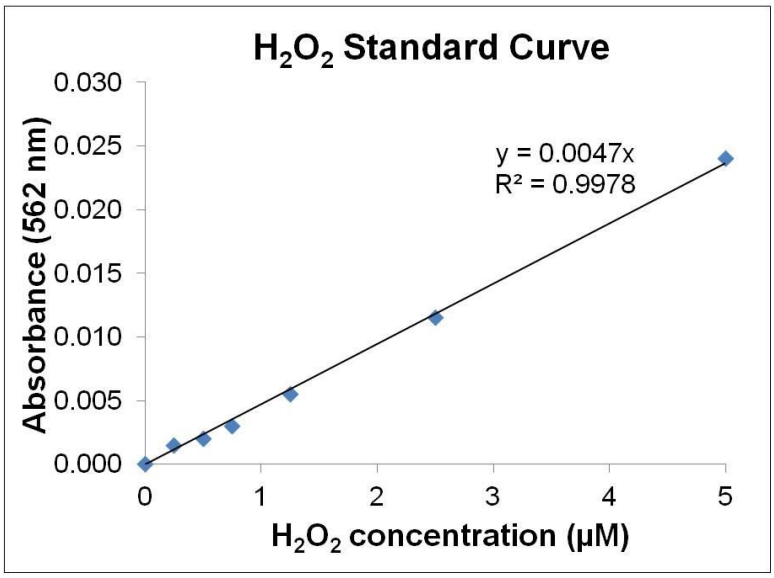

Figure 2.16. Representative standard curve for H_2O_2. The absorbance values shown were corrected for background activity. Standard curves were run for every series of analyses.

2.9. Integrated electrochemical analysis of total ROS

During the perfusion, a three–electrode electrochemical system was integrated into the Generation 1 perfusion chamber via a potentiostat (PalmSens Instruments, Netherland), as shown in Figure 2.3.A, to monitor the level of total ROS. This work was done with the help of Dr Y Dou, a post–doctoral researcher within the department. This system contained a custom–designed Pt electrode (250 µm in diameter) sealed in a glass tube (3 mm outer diameter) which served as a working electrode, a Pt wire as a counter electrode and a Ag wire with a layer of AgCl operating as a quasi–reference electrode. The AgCl layer was electrochemically coated by placing the Ag wire in 100 mM NaCl solution and holding the potential at 0.45 V vs Ag/AgCl (3 M NaCl) for 10 minutes until the oxidation current tailed to a minimum. Prior to use, the working electrode was polished with 0.3 µm and 0.1 µm alumina slurry on polishing pads (Kemet International, UK) simultaneously and then cleaned successively in 10 % (v/v) HNO_3 and water in an ultrasonic bath. By using the potentiostat, cyclic voltammetry (CycV) scans from 0 V to –1.0 V and from 0 V to 1.0 V versus reference electrode were recorded, at the same time as effluent samples were collected for LDH and/or H_2O_2 assays. Oxidation and reduction currents were analysed subsequently.

2.10. Redox–magnetohydrodynamic induced mixing

Redox–magnetohydrodynamics (redox–MHD) can control the fluid flow over a small scale in a redox species containing solution, using electric and magnetic fields (Qian and Bau, 2009). The effect of the redox species and magnet on the heart tissue sample in Generation 1 perfusion system was investigated. The mixing or stirring effect, induced by redox–MHD was followed by the addition of microbeads that demonstrated movement.

2.10.1. Setup of parallel microfluidic perfusion system

A modified Generation 1 perfusion system was designed to perform studies on two tissue samples simultaneously (Figure 2.17). Rat heart tissue handling procedures and perfusion system settings as described in Section 2.3 were followed. Two tubings were attached to each peristaltic pump, connecting parallel Generation 1 perfusion chambers. The tubing lengths between two different components (A and B) of the system were identical so that departure and arrival times of perfusion solutions were the same in both chambers.

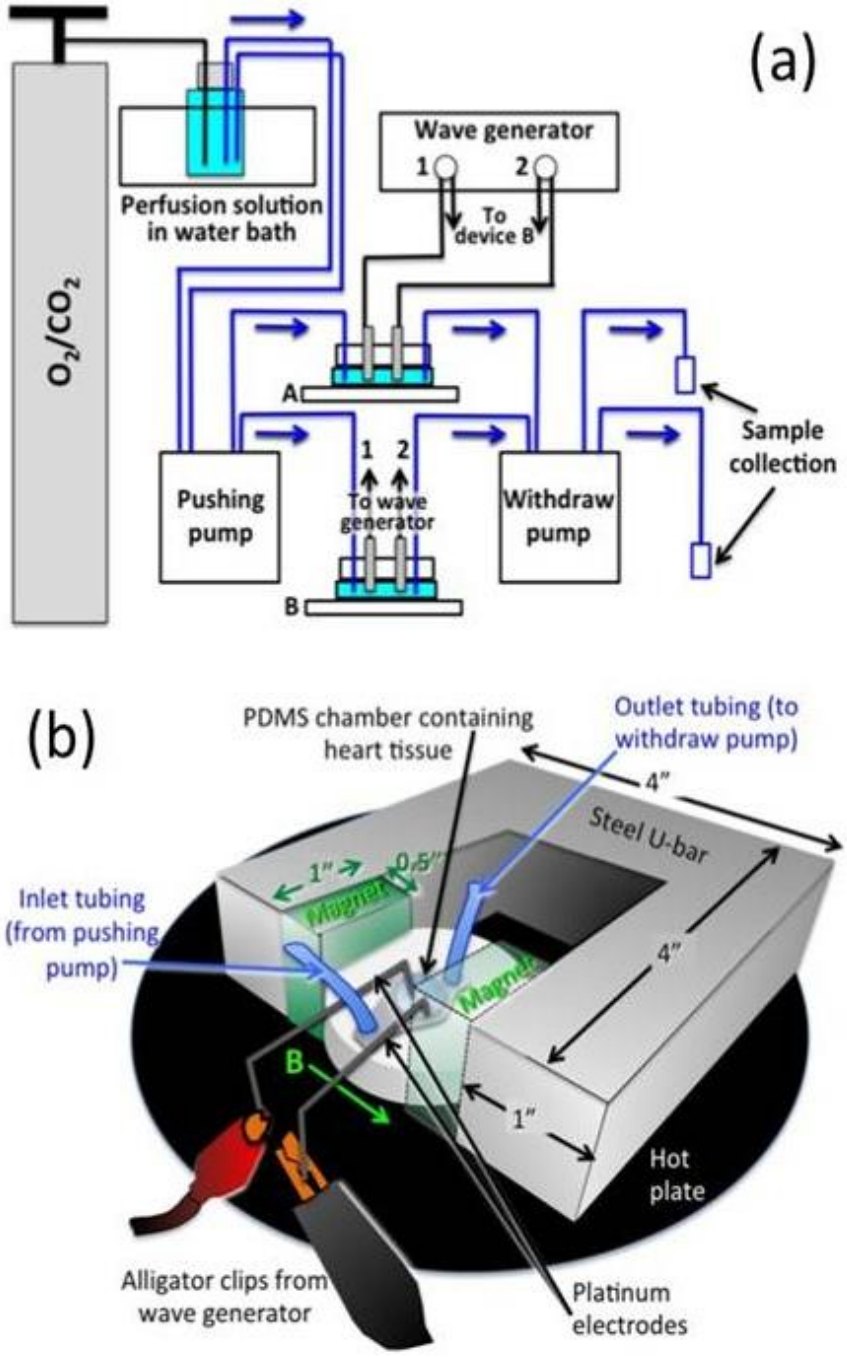

Figure 2.17. Schematics of the experimental setup for MHD studies. (a) A parallel perfusion system simultaneously perfused two tissue chambers (A and B) and a square wave potential was applied to both sets of stimulating electrodes. (b) An enlarged view of the device for studies involving the magnet, showing the positions of hotplate, chamber, perfusion tubing, platinum stimulating electrodes, and clips from wave generator.

2.10.2. Magnet setup

A magnet configuration was chosen to view the bead motion as an indicator of fluid flow in the chamber of the chip, using an inverted microscope (Axiovert S100, Zeiss). A similar setup was also used for viability experiments. Two permanent neodymium iron boron (NdFeB) sintered magnets (1’ x 1’ x 0.5’) were placed at the ends of a steel U–shaped bar in an attracting arrangement with the magnetic field parallel to the plane of the chip (Figure 2.17.b). A direct current magnetometer (AlfaLab, US) was used to measure the magnetic field at the surface of each magnet; this reads 0.39 T (measurement was done by Prof Ingrid Fritsch, a collaborator from University of Arkansas, USA). The magnet apparatus was placed on top of the hotplate, with the chamber centred horizontally between the poles of the magnet and orientated vertically about ¼ the way up from the bottom of the magnet. The chamber was placed over the centre (0.6 cm diameter) of the hotplate to monitor fluid flow (with the inverted microscope) via the beads added to the solution. A curtain was drawn around the chamber during bead studies to minimize disturbance due to air currents which would otherwise have added to the overall convection of the fluid because the chamber did not have a lid due to electrode arrangement.

2.10.3. Measurement of LDH in the presence of redox species

LDH activities in the effluent samples were determined as in Section 2.6, except for those samples which contained redox species, where correction was required to obtain actual LDH activities. The redox species tested in this study included 5 mM Ruhex, 5 mM hydroquinone, or a mixture of 2.5 mM potassium ferricyanide and 2.5 mM potassium ferrocyanide (Sigma–Aldrich, UK). The effect of the presence of these redox species in a series of LDH dilutions on the absorbance at 490 nm was checked (Chapter 7), by plotting the prepared and calculated LDH activities. The calculated LDH activity was derived from the Beer–Lambert Law (Ingle and Crouch, 1988):

$$A = \varepsilon CL \qquad \textbf{Equation 4}$$

Where A is the absorbance, ε is the molar absorptivity, C is the concentration of absorbing species, and L is the path length.

Since the path length is constant in this study, the calculated LDH activity (C) would be respective absorbance divided by molar absorptivity, which is the slope of LDH standard curve (without redox species).

2.10.4. Buffer solutions

Buffer solutions required for the following experiments:

1) KHBB (See Section 2.3)
2) 2 % (w/v) Triton X100 in KHBB (Triton–KHBB)
3) The buffer solution containing 5 mM hexamineruthenium (III) chloride (Ruhex) in KHBB (Ruhex–KHBB).
4) The buffer solution containing 5 mM Ruhex in Triton–KHBB (Ruhex–Triton–KHBB)

2.10.5. Perfusion protocols

A schematic of the perfusion protocol is given in Figure 2.18. After introduction of sample into the microfluidic device, the tissue was perfused with KHBB for 84 minutes, followed by static incubation of KHBB, Triton–KHBB, or Ruhex–Triton–KHBB for 6 minutes in the presence or absence of a magnet. Subsequently, the incubation solution was washed away from the tissue chambers by perfusion with oxygenated KHBB for another 90 minutes. Individual variations in perfusion protocols are described in the appropriate experimental chapter. For the final 30 minutes of all experiments, heart tissues were perfused with Triton–KHBB to induce LDH release if the tissue remained viable. Approximately 240 µl effluent was collected every 5 minutes and stored at –20 ^{o}C for subsequent LDH analysis off–chip (Section 2.6). To monitor the fluid flow caused by MHD and other convection sources (thermal gradients and perfusion) under inverted microscope (Axiovert S100, Zeiss), polystyrene latex microspheres (10 µm diameter; Alfa Aesar, UK) were added to the solution in a 1:30 dilution.

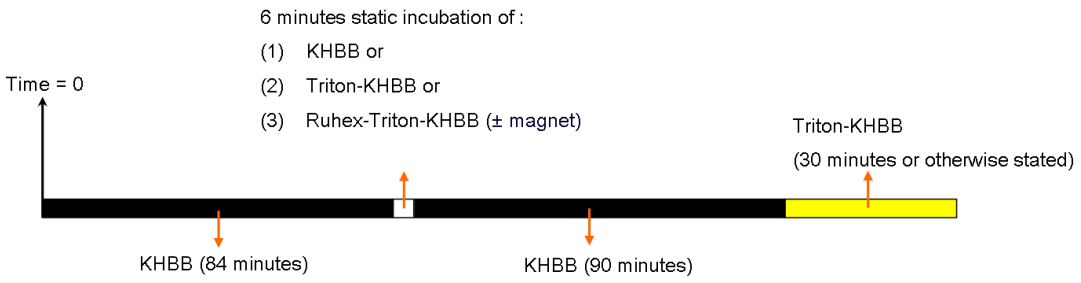

Figure 2.18. Perfusion protocol for redox MHD–induced mixing.

2.11. On–chip ischaemia reperfusion model

IR injury was simulated in the microfluidic perfusion system in two ways: (i) oxygen–deprived ischaemia, and (ii) nitrogen–induced ischaemia. Expression of stress genes [endothelial nitric oxide synthase (eNOS), inducible nitric oxide synthase (iNOS), heat shock protein 72 (HSP 72) and heat shock protein 73 (HSP 73)] were measured using PCR. The expression of additional genes including brain natriuretic peptide (BNP), tumour necrosis factor–alpha (TNF–α), creatine kinase, muscle (CK–M), mitochondrial creatine kinase (CKmito) and troponin T (TnT) were also examined.

2.11.1. Oxygen–deprived IR protocol

The Generation 1 perfusion system was set up as in Section 2.3. Right ventricular tissue biopsies were excised from rat heart and one sample placed directly into the chamber of perfusion device, the rest were kept in cardioplegic solution at 4 ^{o}C until required.

Four phases were investigated (Figure 2.19):

1. A baseline sample was taken at the time of sacrifice.
2. A post–equilibration sample was subjected to 30 minutes equilibration.
3. A post–ischaemia sample was subjected to 30 minutes equilibration and either a 20 or 40 minute ischaemic episode.
4. A post–reperfusion sample was subjected to equilibration (30 minutes), ischaemia (20 or 40 minutes) and 30 (or 120) minutes reperfusion.

In addition, a separate set of samples were perfused for the same length of time as in Figure 2.19, without exposure to ischaemia and reperfusion, as a control.

Ischaemia was induced by cessation of flow (or perfusing with low pO_2 KHBB) and electrical stimulation. A glass slide was used to cover the surface of the PDMS chamber to ensure limited dissolution of oxygen into the buffer

from the atmosphere in the Generation 1 device. The ischaemia treatment lasted for either 20 or 40 minutes.

Reperfusion of the heart tissue was carried out by recommencing perfusion with oxygenated KHBB buffer and electrical stimulation (Section 2.3) for 30 (or 120) minutes. The heart tissue was blotted to remove excess liquid, weighed, and then snap–frozen in liquid nitrogen and stored at –80 ^{o}C for subsequent RNA extraction, and analysis by PCR (Sections 2.11.3 – 2.11.7).

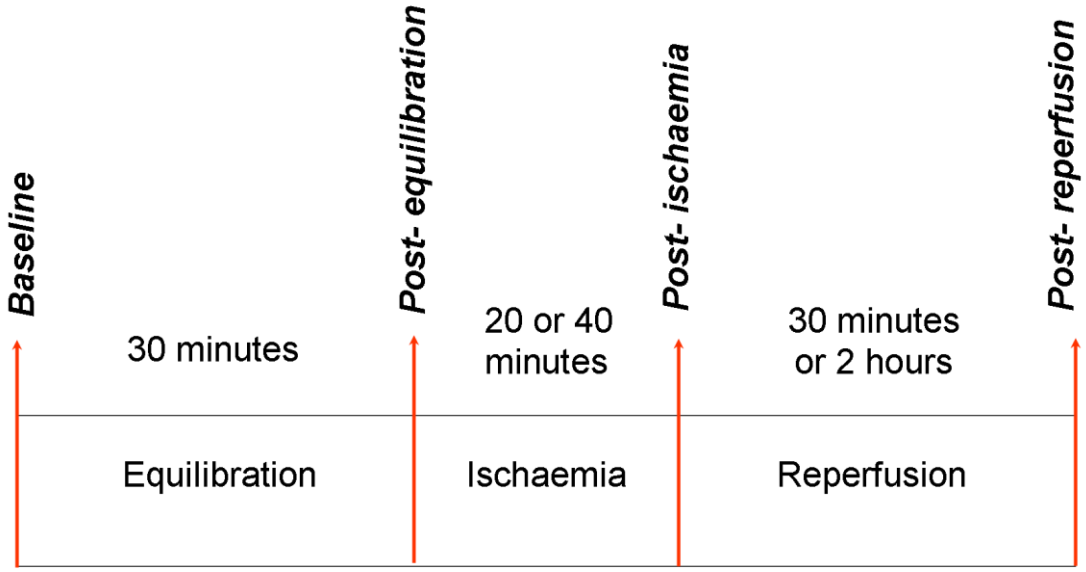

Figure 2.19. Ischaemia reperfusion protocol.

2.11.2. Nitrogen–induced IR protocol

The experimental setup and perfusion protocol were similar to that in Section 2.11.1, except for exposure to a more severe ischaemic episode, induced by perfusing with KHBB gassed with 95 % N_2 / 5 % CO_2 (Energas, UK) for 40 minutes, and 2 hours of reperfusion following ischaemia to allow additional time for gene expression to alter. At the end of the experiment, the perfused heart tissue was dried, weighed, frozen and analysed as previously described.

2.11.3. RNA extraction

RNA was extracted using the RNeasy fibrous tissue mini kit (QIAgen, UK), following the manufacturer's protocol.

In brief, 300 µl of Buffer RLT containing 3 µl of β–mercaptoethanol (β–ME) was added to the frozen heart tissue in a 0.5 ml polypropylene tube and homogenised with a homogenizer (Omni International, US) for ~ 30 seconds. The polypropylene tube was kept in a beaker containing ice during homogenization. Subsequently, 590 µl of sterile RNase–free water was added to the lysate, and 10 µl of proteinase K added to dissociate RNA–protein complexes and digest proteins, such as contractile proteins, connective tissue and collagen. The mixture was incubated at 55 ^{o}C for 10 minutes to inactivate any RNase and DNase still present. The mixture was centrifuged at 10,000 g for 3 minutes at room temperature to pellet the debris.

The supernatant (900 µl) was transferred into a new, clean 1.5 ml microcentrifuge tube and 450 µl of 100 % ethanol added which may precipitate DNA and RNA. Finally, 700 µl of the mixture was transferred into the RNeasy mini spin column within a 2 ml collection tube, and centrifuged at 8,000 g for 15 seconds at room temperature. The flow–through was discarded and the remaining ethanol containing mixture (650 µl) was added into the same column and the centrifugation was repeated. The RNA was bound to the silica membrane of the spin column at this stage.

Wash buffer (RW1, 350 µl) was added to the column and centrifuged at 8,000 g for 15 seconds at room temperature. Again, the flow–through was discarded and 80 µl of DNase I mix was added directly onto the column to digest any traces of DNA in the sample, and incubated at room temperature for 15 minutes.

Subsequently, 350 µl of wash buffer (RW1) was again added to the column and centrifuged at 8,000 g for 15 seconds at room temperature. The flow–through was discarded and 500 µl of wash buffer 2 (RPE) was added to the column to remove any residual DNA, and centrifugation was repeated. The flow–through was discarded and a final wash with 500 µl of wash buffer 2 (RPE) was repeated.

The RNeasy column was finally transferred to a new collection tube and sterile RNase–free water (30 µl) was added directly to elute the RNA. The column was centrifuged at 8,000 g for 1 minute at room temperature and to maximise the RNA yield, the eluate was added back to the column membrane and centrifuged again at 8,000 g for 1 minute at room temperature.

2.11.4. RNA quantification

A GeneQuant II RNA/DNA calculator (Pharmacia Biotech, US) was used to quantify the extracted RNA. Tris.Cl (10 mM, pH 7.5) was used as a reference control. A dilution of 1:50 (1 µl RNA and 49 µl of 10 mM Tris.Cl) was made, mixed well, and spectrophotometric readings were recorded. Total quantity of RNA was calculated using the equation below:

Total RNA quantity = Absorbance at 260 nm X **coefficient of RNA** X **dilution factor** X **total volume of RNA**

Given that coefficient of RNA = 44 µg/ml; dilution factor = 50; total volume of RNA = 0.05 ml

The ratio of absorbances at 260 nm and 280 nm (A_{260} / A_{280} ratio) was used to determine the purity of RNA extraction. Pure RNA has a A_{260} / A_{280} ratio of 1.9 – 2.1 in 10 mM Tris.Cl, pH 7.5. An example of sample analysis is given below.

Table 2.1. Example of a RNA spectrophotometric recording.

A_{260}	0.169
A_{280}	0.084
Ratio	2.021
Concentration	338 µg/ml
Total RNA	16.9 µg

2.11.5. Reverse transcription

RNA (0.5 µg) was reverse transcribed using the Moloney murine leukemia virus (M–MLV) reverse transcriptase kit (Invitrogen, UK). Oligodeoxythymidylic acid [Oligo $(dT)_{15}$] primer (1 µl of 500 µg/ml; Invitrogen, UK) and 1 µl of 10 mM dNTP mix (Invitrogen, UK) were added to 0.5 µg of RNA in a nuclease–free microcentrifuge tube. Sterile RNase free water was added to make up a final volume of 12 µl. The mixture was incubated on a heating block at 65 ^{o}C for 15 minutes and then quickly chilled on ice.

Next, 4 µl of 5 X first strand buffer (250 mM Tris–HCl, 375 mM KCl, 15 mM $MgCl_2$, pH 8.3), 2 µl of 0.1 M dithiothreitol (DTT) and 1.25 µl of RNaseOUT^{TM} recombinant ribonuclease inhibitor (40 units/µl; Invitrogen, UK) were added and incubated for 2 minutes at 37 ^{o}C. After that, 1 µl of M–MLV reverse transcriptase (200 Units/µl) was added into the mixture and reverse transcription was carried out at 37 ^{o}C for 50 minutes. The transcriptase was finally inactivated by heating the mixture at 70 ^{o}C for 15 minutes.

2.11.6. cDNA quantification

Complementary or copy DNA (cDNA) obtained above was quantified using the RNA quantification method (Section 2.11.4), with a coefficient of 50 µg/ml for DNA. cDNA was stored at –20 ^{o}C for use in subsequent PCR analyses.

2.11.7. Polymerase chain reaction

To set up a PCR mix, 12.5 µl of PCR mastermix (Promega, UK) was mixed with 10 mM forward and reverse primers (Eurofins MWG Operon, Germany), and 500 ng of cDNA. The volumes required are given in Table 2.2 and the sequences for the primers listed in Table 2.3. Sterile nuclease free water was added to make up to a final volume of 25 µl. The 2X PCR mastermix contained 50 units/ml of *Thermus aquaticus* (*Taq*) DNA polymerase (pH 8.5), 400 µM dATP, 400 µM dGTP, 400 µM dCTP, 400 µM

dTTP and 3 mM $MgCl_2$. PCR for each gene were performed in a DNA thermal cycler (SLS, UK) with the programmes listed in Table 2.4.

PCR reaction conditions (e.g. amount of DNA/reaction, amount of primer/reaction, annealing temperature) were optimised for efficient amplification of specific targets (Chapter 4).

Table 2.2. Volume of primers required for PCR.

Gene	Volume (µl)
eNOS	1
iNOS	2
nNOS	1
HSP 72	1
HSP 73	1
BNP	2
CK-M	1
CKmito	1
TnT	1
GAPDH	0.5
β- actin	1

N.B. All primers were reconstituted at 10 mM. The primer volume given refers to an equal volume of both the forward and reverse primers e.g., 1µl eNOS primers refers to 1µl of eNOS forward primer and 1µl of eNOS reverse primer.

Table 2.3. Forward and reverse primer sequences.

Primers	Product length (bp)	Sequences (5' – 3')	References
eNOS	164	CGAGATATCTTCAGTCCCAAGC GTGGATTTGCTGCTCTCTAGG	Di Napoli *et al.*, 2002
iNOS	305	TCTGTGCCTTTGCTCATGAC CATGGTGAACACGTTCTTGG	Grilli *et al.*, 2003
nNOS	312	ATCGCACAAAGCTCCGCCCC TCTGGCTTCCGCGTGTGCTG	NCBI
HSP 72	491	TGCTGACCAAGATGAAG AGAGTCGATCTCCAGGC	Nikaido *et al.*, 2004
HSP 73	254	CAATGACTCTCAGCGACAGGCA TGTCAAAGTCTTCTCCGCCCAA	NCBI
BNP	81	GATGATTCTGCTCCTGCTTTTCC GGAGACTGGCTAGGACTTCCC	Ito *et al.*, 2008
CK-M	133	GTCCGTGGAAGCTCTCAACAG CAGAGGTGACACGGGCTTGT	Mizuno *et al.*, 2010
CKmito	126	AGCAAGGATCCACGCTTTTCT TCTACCGATCCGATCTATGTT	Mizuno*et al.*, 2010
TnT	114	AAGGCCAAAGTCACCGGGCG TCGGGTGCCTGGCAAGACCT	NCBI
GAPDH	551	ACCACAGTCCATGCCATCAC TCCACCACCCTGTTGCTGTA	NCBI
β- actin	452	GGGCCGTCTTCCCCTCCATC GTCACGCACGATTTCCCTCTC	Di Napoli *et al.*, 2002

Table 2.4. PCR profile times and temperatures.

Steps / Genes	Initiation (°C / minute)	Denaturation (°C / minute)	Annealing (°C / minute)	Extension (°C / minute)	Final extension (°C / minute)
No of cycle	1	35			1
eNOS iNOS nNOS HSP 73 CK-M CKmito TnT GAPDH β-actin	94 / 2	94 / 1	60 / 1	72 / 1	72 / 7
HSP 72	94 / 2	94 / 1	50 / 1	72 / 1	72 / 7
BNP	94 / 2	94 / 1	56 / 1	72 / 1	72 / 7

2.11.8. Gel electrophoresis

The PCR products were separated on a 2 % (w/v) Ultrapure agarose gel (Invitrogen, US) in 1 X TBE buffer (89 mM Tris–base, 89 mM Boric acid, and 2 mM EDTA), stained with 10 µg/ml ethidium bromide (Bio–Rad Laboratories, US). PCR product (6 µl) was mixed with 6 µl of 1X DNA gel loading buffer (0.042 % (w/v) bromophenol blue, 0.042 % (w/v) xylene cyanol FF, and 5 % (v/v) glycerol in water). The mixture (10 µl) was then loaded into the gel. In addition, DNA ladder (Invitrogen, UK) was loaded to the gel and run at 90 mV for 30 minutes and photographed under UV using Gene Flash Bio Imaging System (Syngene, US). A representative gel image is shown in Figure 2.20, using a 100 bp DNA ladder from Invitrogen.

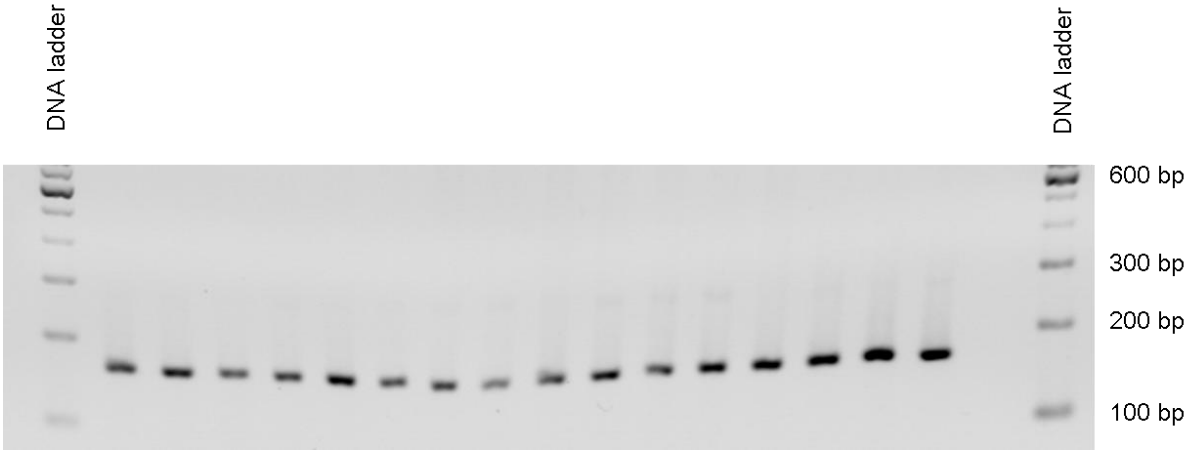

Figure 2.20. Representative gel image.

2.11.9. Statistics

The bands on the gel were analysed and quantified using ImageJ software (version 1.37c). The density for each PCR products was normalized to that of β–actin. Significance was analysed using repeated measures analysis of variance (ANOVA; Miguelez *et al*., 2011, Ohlin *et al*., 2011). Statistical advice was acquired from Mr Adrian Midgley (Department of Sport, Health and Exercise Science, University of Hull).

2.12. Development of creatine kinase MB microsensor

A CK–MB microsensor was made from a carbon fibre microelectrode and CK–MB antibody was adhered onto its surface via ferrocene–carboxaldehyde (Fc–CHO).

2.12.1. Microelectrode fabrication

Single carbon fibres with 7 µm diameter were first separated from a bundle of carbon fibres. Microelectrodes were made by aspirating carbon fibres into 1.65 mm diameter borosilicate glass capillary tubes (Bibby Sterilin, UK; Figure 2.21). Each capillary was then pulled with a micropipette puller (Sutter Instrument, US), and filled with graphite powder (Hopkin and Williams, UK). An insulated wire, with both ends exposed, was inserted into each glass capillary and a seal was achieved by adding adhesive (Permabond Engineering Adhesives, UK). Surface area of exposed carbon fibre is the critical determinant for the CK–MB antibody adherence. However, when visualised by naked eyes, the thickness of several carbon fibres was very similar to one carbon fibre. Therefore, each microelectrode was checked under the microscope, to ensure that only one carbon fibre was trapped in each capillary. The carbon fibre protruding from the glass tip was subjected to electrochemical deposition by poly(oxyphenylene), in 0.4 M allylamine, 0.23 M 2–allylphenol, and 0.23 M 2–butoxyethanol in 1:1 (v/v) water/methanol (Amatore *et al.*, 2008).

In this study, deposition was accomplished by applying potential of +4 V for 3 minutes versus a graphite rod (Amatore *et al.*, 2008). The insulated carbon fibre was transected with a scalpel under a microscope, to expose a disk–shaped electroactive surface prior to antibody adherence. After each experiment, the protruding carbon fibre can be transected to expose a new surface for subsequent experiments (Hu *et al*., 2010); therefore, a microelectrode can be used repeatedly.

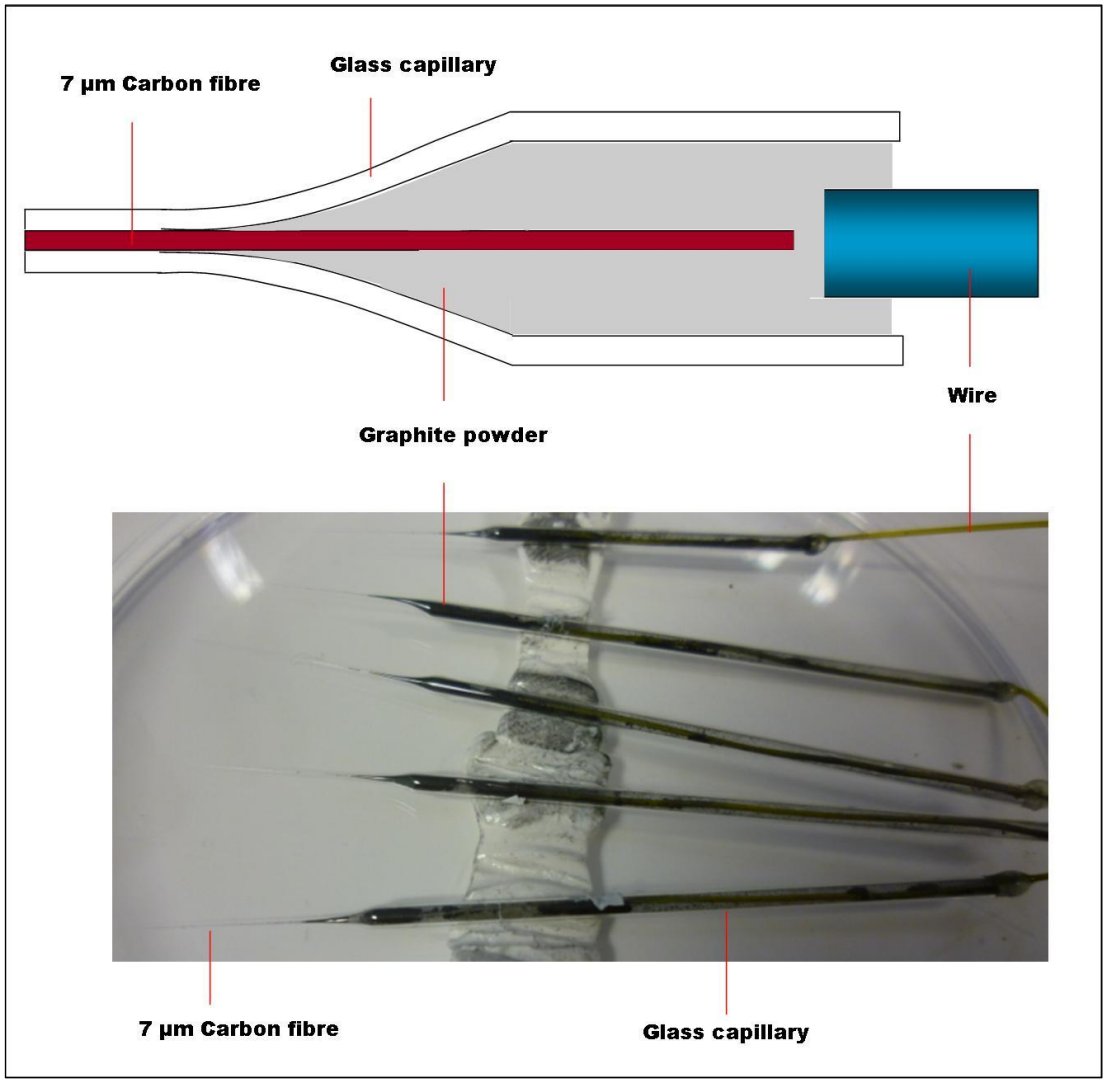

Figure 2.21. Schematic diagram and photo of carbon fibre microelectrode.

2.12.2. Synthesis of Fc–CHO–labelled CK–MB

A rabbit polyclonal IgG specific for CK–MB (40 µl of 200µg/ml; Santa Cruz Biotechnology, Germany) was added into 200 µl of PBS. Then, 40 mg of Fc–CHO (Sigma–Aldrich, UK) was dissolved in 200 µl dimethylformamide (DMF; Sigma–Aldrich, UK), to make a final Fc–CHO concentration of 200 mg/ml. These two mixtures were mixed and the pH was adjusted to 9.3 using 5 % (w/v) K_2CO_3 (Okochi *et al*., 2005; Figure 2.22). After 30 minutes incubation, 2 mg of $NaBH_4$ was added into the mixture to cause reduction to ferrocenemethyl protein and this was incubated for another 10 minutes. The reaction mixture was adjusted to pH 7.3 using 1 M HCl, followed by

ultracentrifugation (12000 g, 10 minutes, 4 ^{o}C) to remove unlabelled ferrocene. The supernatant was subjected to ultracentrifugation (12,000 g, 20 minutes, 4 ^{o}C) in a vivaspin (GE Healthcare, Sweden) to obtain the Fc–CHO–labelled CK–MB antibody.

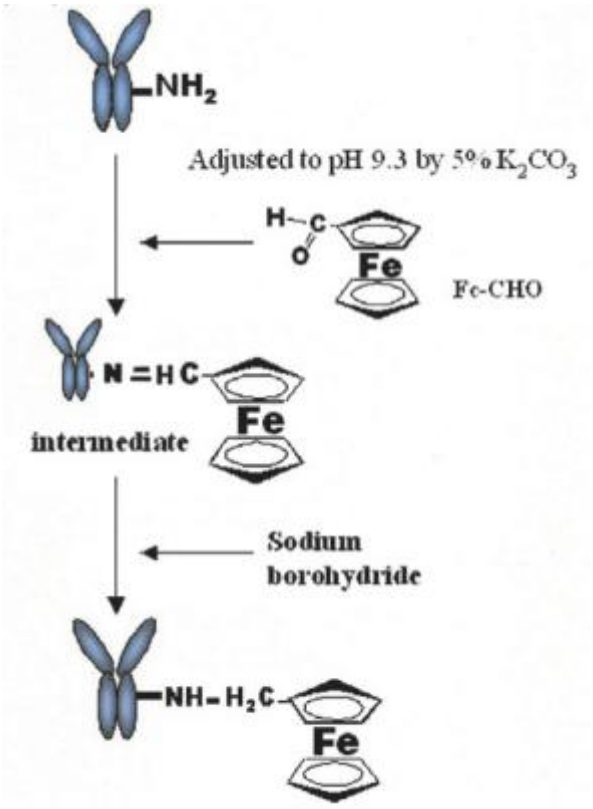

Figure 2.22. Labeling of IgG with Fc–CHO. (Okochi *et al*., 2005)

2.12.3. Immobilization of Fc–CHO–labelled CK–MB onto microelectrode surface

Activation of the carboxyl end of Fc–CHO–labelled CK–MB was achieved by mixing the labelled anti–CK–MB antibody with 2 mM ethyl(dimethylaminopropyl) carbodiimide (EDC; Sigma–Aldrich, UK) and 5 mM N–hydroxysulphosuccinimide (sulpho–NHS; Sigma–Aldrich, UK) activation buffer (1:1, v/v) for 15 minutes. EDC and sulpho–NHS were used as coupling agents to immobilize the antibody onto the microelectrode surface. The microelectrode tip was incubated in 10 µl of activated antibody solution for 18 hours at 4 ^{o}C prior to experimentation.

2.12.4. CK–MB electrochemical measurement

The tip of the microelectrode was washed following antibody immobilization with 0.1 % Tween 20 in 10 mM PBS and dipped in blocking buffer [1 % bovine serum albumin (BSA) in 10 mM PBS, pH 7] for 30 minutes at room temperature. The microelectrode was again washed with Tween 20 and PBS, and tested in PBS for CycV (from –0.2 V to 0.6 V) and square wave voltammetry (SWV; from –0.4 V to 0.6 or 0.8 V) scans using a potentiostat (Palm Instruments, Netherland). Then, it was incubated in solutions containing purified human CK–MB protein (Abcam, UK) or test sample for 10 minutes (for each concentration) at room temperature, before another CycV and SWV scans were carried out. Platinum wire was used as the counter electrode with Ag/AgCl as the reference electrode (Bioanalytical Systems, UK). After each scanning, 0.5 pg/ml CK–MB was added to the test sample, and subsequent washing and scanning were repeated.

2.12.5. Microelectrode surface area determination

Surface area of the microelectrode was worked out using Randles–Sevcik equation (Zanello, 2003, stated below) after electropolymerization.

$$i_p = (2.69 \times 10^5)\, n^{3/2} A\, D^{1/2} C\, v^{1/2} \qquad \textbf{Equation 5}$$

where i_p is the peak current, 2.69×10^{-5} is a collection of constants at 25 ^{o}C, n is the number of electrons appearing in the half–reaction for the redox couple, A is the electrode area (cm^2), D is the analyte's diffusion coefficient (cm^2/second), C is the analyte concentration (mol/cm^3), and *v* is the rate of potential swept (V/second).

Unmodified carbon fibre microelectrode was incubated in 5 mM $K_4Fe(CN)_6$ in 0.1 M KCl and CycV scan was carried out from –0.6 V to 1.2 V. The known functions in Equation 5 are: n = 1, D = 7.6×10^{-6} cm^2/second, C = 5 µmol/cm^3 and *v* = 0.1 V/second. From the cyclic voltammogram, peak current (i_p) can be obtained (as shown in Figure 2.23), and the microelectrode surface area can therefore be worked out.

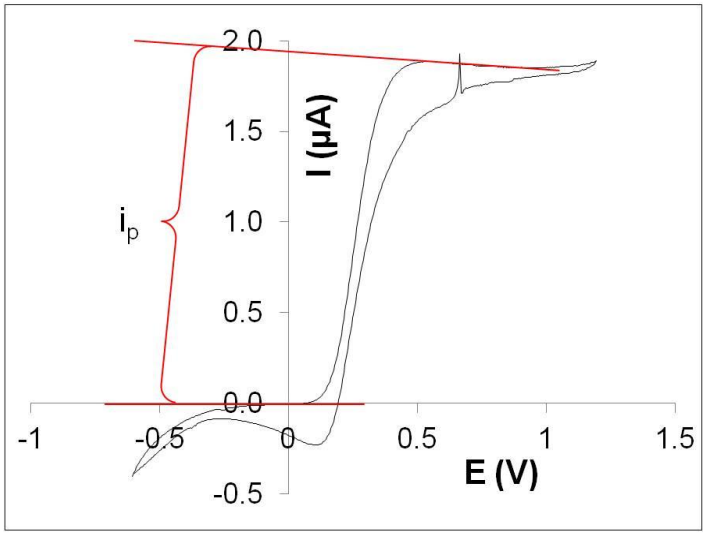

Figure 2.23. An example of cyclic voltammogram showing peak current (i_p) determination.

2.12.6. CK–MB measurement using electrophoretic kit

CK–MB was measured electrophoretically by using a SAS–MX CK VIS–10 Isoenzyme kit (Helena Biosciences, UK), according to the principle illustrated in Figure 2.24. First, the CK isoenzyme activator (1 µl β–ME) was added to 100 µl sample and the mixture was incubated at room temperature for 10 minutes. An agarose gel was blotted on paper towel and a sample application template was aligned at the edge of the gel. A blotter (A) was placed on top of the template and ensured a good contact between the gel and the template. Sample (1 µl) was loaded to each slit. The samples were absorbed for 4 minutes before blotting the template with the blotter (A) again. SAS–MX CK isoenzyme buffer (45 ml) was loaded into each inner section of the electrophoretic tank. The agarose gel was positioned in the electrophoretic tank, with the agarose side down and in contact with the buffer. The electrophoresis unit was run for 20 minutes at 100 V.

A blotter (D) was moistened with water in an incubation chamber at 45 ^{o}C and approximately 3 – 4 minutes prior to incubation, CK isoenzyme reagent was reconstituted in a vial by adding 1 ml of CK diluents and 70 µl of chromogen. The diluent consisted of 2–morpholinoethanesulfonic acid,

sucrose and sodium azide, whereas chromogen contained tetranitro blue tetrazolium and DMF. The gel (with the agarose side upward) was placed on a glass plate following electrophoresis, and CK isoenzyme reagent was poured along the anode side of the gel. The reagent was then spread to the cathode edge by using a serological pipette. After 15 seconds, the pipette was moved towards the anode edge for another 15 seconds. Then, the gel was incubated for 30 minutes at 45 ^{o}C. Subsequently, the gel was immersed in the 10 % acetic acid for 10 minutes, and rinsed with water. Finally the gel was left to dry completely and the bands quantified by densitometry.

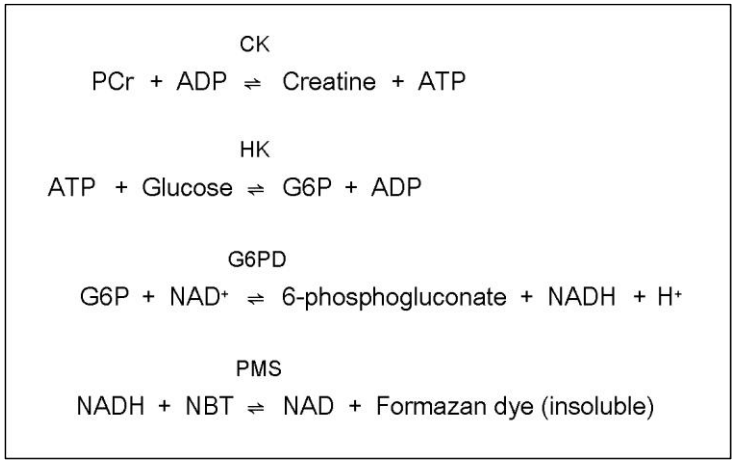

Figure 2.24. Principle for CK electrophoretic assay.

ADP, adenosine diphosphate; ATP, adenosine triphosphate; CK, creatine kinase; G6P, glucose–6–phosphate; HK, hexokinase; NAD^{+}, oxidised form of nicotinamide adenine dinucleotide; NADH, reduced form of nicotinamide adenine dinucleotide; NBT, nitro blue tetrazolium; PCr, phosphocreatine; PMS, phenazine methosulfate.

Chapter 3

Generation 1
Perfusion System

To study the pathophysiology of heart disease, conventional approaches such as *in vitro* cell and tissue culture have been principally used. The traditional Langendorff perfusion set–up has also been widely used to study whole heart physiology and biochemistry (Zimmer, 1998, Sutherland and Hearse, 2000, Akki *et al*., 2008). However, these methodologies all have the limitations in mimicking aspects of the *in vivo* microenvironment or functional properties (Zhang, 2004). Microfluidics, a rapidly developing technology, is proposed to provide a better representation of *in vivo* situation (Yeon and Park, 2007). Perfusion media can be replaced continuously using pumps, the cells or tissue biopsies are supplied with nutrients and gases, whilst waste products are removed, resembling the physiological circulatory system (Hung *et al*., 2005, Yeon and Park, 2007). Heart tissue represents a highly complex structure, and is a better reflection of the heart compared with isolated cardiomyocytes. Therefore, maintaining cardiac tissue under *in vivo*–like conditions hopefully provides a more holistic representation of complex cell: cell and cell: stroma interactions, allowing the effect of interventions to be investigated.

In this chapter, a microfluidic perfusion device for heart tissue maintenance (as described in Section 2.2) was developed and optimised for key parameters, including tissue sample size, electrical stimulation and flow rate. Tissue was maintained in the PDMS microfluidic chamber at 37 ^{o}C and constantly supplied with oxygen throughout the experiment. In addition, the tissue was stimulated electrically using platinum electrodes, resembling the *in vivo* stimulation of sino–atrial and atrio–ventricular nodes. Samples of rat heart were used initially in the optimisation studies, and subsequently human atrial samples were investigated. Effluent levels of LDH were used as a marker of tissue damage during the perfusion period. In addition, Calcein AM and PI were used to label live and dead cells, respectively (Sasaki *et al.*, 1987, Haugland *et al.*, 1994).

ROS play an essential role during tissue injury or disease, and can lead to multiple detrimental consequences (Lesnefsky *et al*., 2001, Droge, 2002). ROS have been reported to lead to oxidation of DNA (Dizdaroglu *et al*., 2002),

membrane phospholipids (Marnett, 1999), as well as proteins (Stadtman, 2004), resulting in impaired mitochondrial function which is important in energy provision for the heart (Dhalla *et al*., 2000). ROS can be measured by various means, including chemiluminescence, colourimetry, fluorometry, and electron spin resonance spectroscopy (Taha, 2003). Electrochemical methods however, provide a direct analytical means to determine the local concentration of ROS in solution, with minimal disturbance to the sample under investigation (McNeil and Manning, 2002). Electrochemical probes allow the conversion of the biological information to a measurable electrical signal, with the distinct advantages of sensitivity (µg/ml to pg/ml) and speed for real–time assessment, *in situ*. For example, the detection limit for DNA is 0.10 pg/ml (Maruyama *et al*., 2002), whereas for H_2O_2, it is 0.34 µg/ml (Scholz *et al*., 2007).

It would be of particular use if real–time measurement of ROS could be obtained to provide dynamic information of tissue responsiveness to injury and treatment (McNeil and Manning, 2002). Here, electrochemical probes were integrated with the perfusion chamber to measure the release of total ROS. Real–time electrochemical analysis was carried out on–chip during the perfusion whereas effluent samples were collected for H_2O_2 analysis which was performed off–chip. H_2O_2 level was assayed because it could be used to validate the electrochemical measurement of total ROS.

The main aim of this part of the study was to establish an optimised microfluidic perfusion device for maintenance of heart tissue, together with real–time measurement of total ROS release using an integrated electrochemical module.

3.1. Optimisation of the size of tissue sample

Reynolds numbers (Re) in microfluidic devices are typically less than 2300, indicating that the flow is predominately laminar with little mixing between two streams of fluids (Figure 1.16). Therefore, mixing in the small scale of the microfluidic channels, normally in the order of 100 μm, relies on diffusion. Hence, the dimensions of the heart tissue have to be optimised so that the tissue was supplied with sufficient oxygen and nutrients. Rat right ventricular tissue was perfused and electrically stimulated within the PDMS microfluidic chamber (Figure 2.2) as described in Section 2.3. Following perfusion, the viability of the tissue was assessed by Calcein AM and PI fluorescent dyes under a laser–scanning inverted confocal microscope (Section 2.7).

Initially, the right ventricular tissue harvested from rat was approximately 6 x 4 x 2 mm^3 (length x width x depth) in volume. Confocal images in Figure 3.2 were taken after a 2 % (w/v) Triton X100 insult following 5 hours perfusion. PI staining was not observed at the edge of the tissue. Optical sectioning of the tissue was then performed using Z–stack and it was found that the centre of the cardiac tissue was mainly stained with PI, while the outer region was stained with Calcein AM (Figure 3.1.A), indicating that the oxygen and nutrient permeation was low. However, when the size of the heart tissue was reduced to approximately 2.5 x 4 x 2 mm^3, the tissue was uniformly stained with Calcein AM and PI (Figure 3.1.B).

Thus, the size of heart tissue was kept at approximately 2.5 x 4 x 2 mm^3 in the following experiments, facilitating permeation issue.

(A)

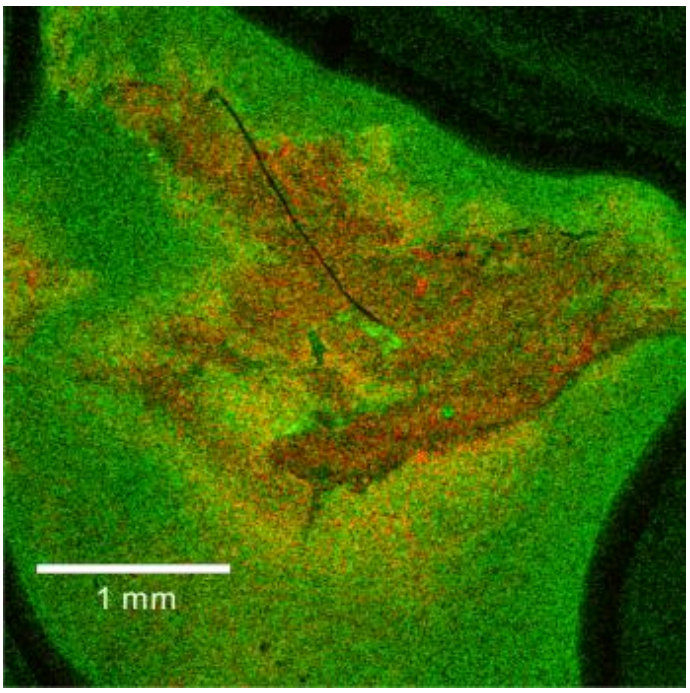

(B)

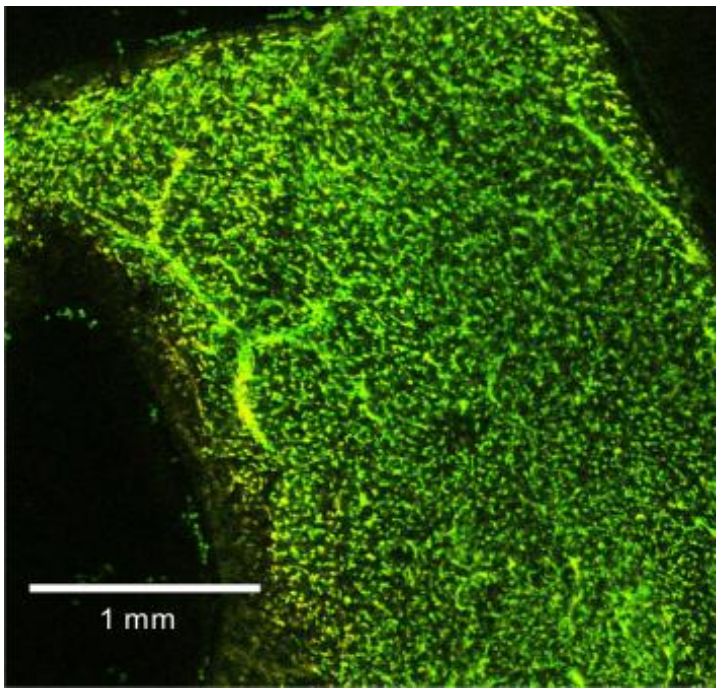

Figure 3.1. Calcein AM (green) and PI (red) treated cardiac tissue. Yellow signal represents cells stained with both dyes. A and B are representative images of two independent experiments. A 10x objective was used. These images were 400 – 500 µm from the bottom surface of the tissue samples.

3.2. Design of PDMS microfluidic chamber

The PDMS microfluidic device was designed to house the heart sample within the tissue chamber. PDMS with the repeating units of $–OSi(CH_3)_2–$ is normally very hydrophobic due to the presence of CH_3 groups on the surface (McDonald *et al*., 2000, Hu *et al.*, 2004). Previous studies have demonstrated that when petri dish material, polystyrene was exposed to plasma, aromatic and alkyl groups were oxidised to carbonyl groups (Zhang *et al*., 2000), improving the hydrophilicity. The PDMS was therefore bonded to the polystyrene base by oxygen plasma treatment (Section 2.2).

Initially, microfluidic chambers for different sizes of the tissue (Figure 3.2) were developed. The tissue chamber as shown in Figure 3.2.A was made by using a 5 ml syringe end as the chamber mould, whereas for Figure 3.2.B, a 1 ml syringe end was used. The diameters of the tissue chambers were 14 mm and 7 mm, respectively. Apertures were made in the device shown in Figure 3.2.B to accomodate inlet and outlet tubings, as well as working, reference and counter electrodes for simultaneous electrochemical analysis during the perfusion.

Since the preliminary chamber with a diameter of 14 mm was too big for the tissue, the smaller microfluidic device with a tissue chamber of 7 mm in diameter was used. In addition, a potential leakage problem was observed between the PDMS and petri dish (Figure 3.2.A) after being used for 3 – 4 times, as hydrophobicity of the oxygen plasma–treated polystyrene surface gradually decreased with time (Occhiello *et al*., 1992). To overcome this problem, a second layer of PDMS (1 – 2 mm thick) was coated on the base of the petri dish, before binding of the PDMS removed from the chamber mould (Figure 3.2.B). Bridging covalent siloxane bonds (Si–O–Si) were formed, producing an irreversible seal between the two PDMS substrates (Figure 3.3). Hence, the Generation 1 microfluidic device used throughout this thesis was prepared by binding the PDMS with the chamber mould onto the petri dish coated with PDMS.

(A)

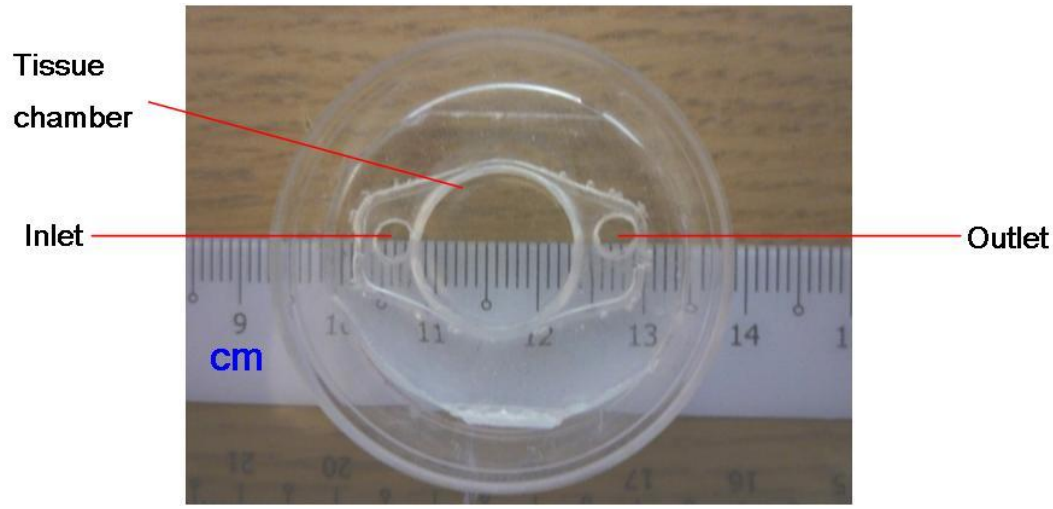

(B)

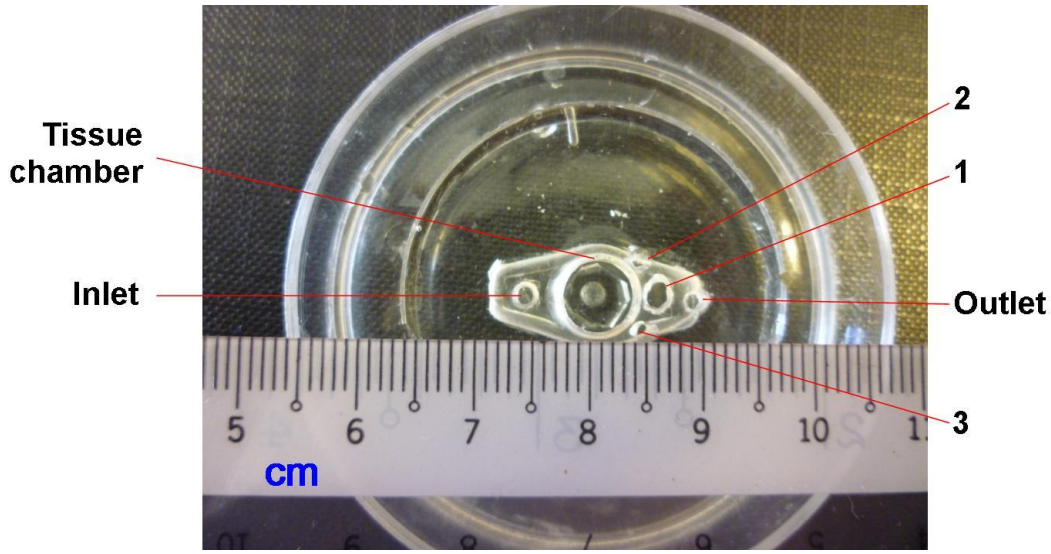

Figure 3.2. Top views of Generation 1 devices with different chamber sizes. The diameters of tissue chambers are 14 mm (A), and 7 mm (B).

1, Working electrode (Pt); 2, Counter electrode (Pt); 3, Reference electrode (AgCl coated Ag wire)

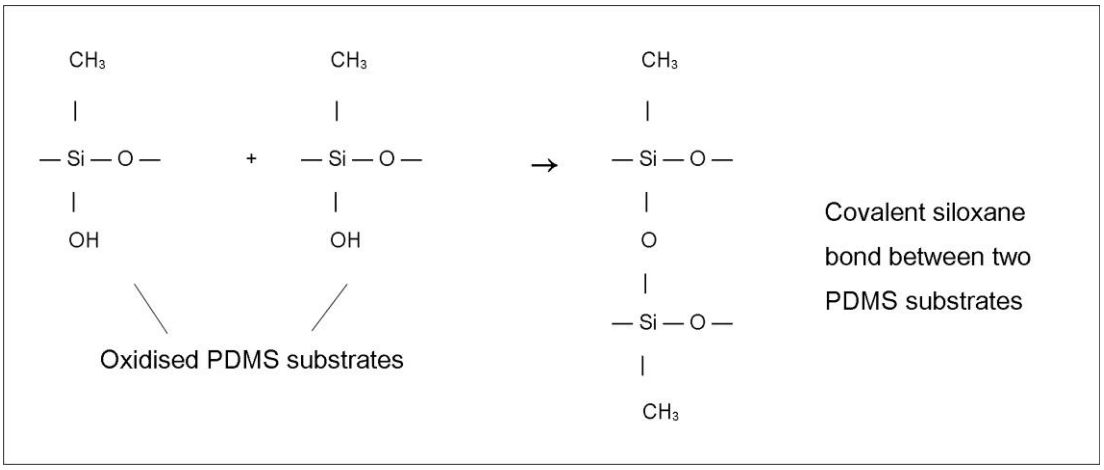

Figure 3.3. Bridging covalent siloxane bond between two PDMS substrates.

3.3. Optimisation of on–chip electrical stimulation, [Ca^{2+}] and flow rate

The tissue was stimulated electrically to mimic the *in vivo* situation. Electrical stimulation (generated via two platinum wired electrodes using a function generator) was initiated at 0.8 V/cm, and incrementally raised until all or part of the tissue commenced beating synchronously as observed visually. Beating was observed at 1 V/cm and above. However, bubbles formed at the electrodes due to electrolysis of water when the electrical field was ≥ 12 V/cm. An electrical field of 3 – 4 V/cm was selected for continued stimulation in this thesis, which is close to that given to isolated cardiomyocytes and whole heart (5 – 6 V/cm; Field *et al*., 2004, Klauke *et al*., 2003, Radisic *et al*., 2004, Klauke *et al.*, 2007). The frequency was kept at 1.5 Hz (90 beats/minute) in order to generate a physiological heart rate.

The normal range of serum Ca^{2+} in human is 1.03 – 1.23 mM (Larsson and Öhman, 1978). However, increased Ca^{2+} has been demonstrated to activate the contractile machinery (Katz, 2001). Therefore two concentrations (1.25 mM and 2.5 mM) of $CaCl_2$ were tested. The contractile function of the tissue in the perfusion chamber was more pronounced visually, and generally lasted longer when the higher [$CaCl_2$] was used. Therefore, 2.5 mM $CaCl_2$ in KHBB was used as standard for all subsequent perfusion experiments, as previously recommended by Riva and Hearse (1991).

An optimal flow rate is the one resulting in adequate nutrient supply and waste products removal, and minimal physical disturbance of the tissue. From a practical point of view, flow rates less than 100 µl/minute led to longer effluent collection time for sufficiently sized aliquots for subsequent biochemical analyses. Conversely, flow rates ≥ 200 µl/minute have been shown to disturb the heart tissue and stimulation probes within the perfusion chamber. A standardized flow rate at 120 µl/minute was chosen for all subsequent experiments.

3.4. Perfusion data

Using cardiac tissue from rats (Section 2.3), effluent samples were collected and LDH analysis was carried out off–chip (Section 2.6). Electrical stimulation was applied throughout the perfusion as previously described. Cell viability was indicated by the cell membrane integrity, assessed by the release of the intracellular enzyme LDH (Racher *et al*., 1990). After an extended period of perfusion during which time viability was assessed, the tissue sample was exposed to an insult of 2 % (w/v) Triton X100 for at least 30 minutes to induce substantial rupture of the membrane and release of LDH.

3.4.1. Control – impact of repeated exposure to Triton X100

Heart tissue was exposed to two, 6 minute, incubations with 2 % (w/v) Triton X100 in KHBB throughout the KHBB perfusion and LDH release was assessed in the effluent samples. From the 270th minute onwards, the heart tissue was perfused continuously with 2 % (w/v) Triton X100 in KHBB.

A LDH ‘spike’ appeared following the short pulses of Triton X100 incubation and during the prolonged exposure with Triton X100, with the first pulse eliciting greater LDH release than the second one (Figure 3.4). LDH appears to act as a good damage indicator, as enzyme activities increased in response to Triton X100 exposure.

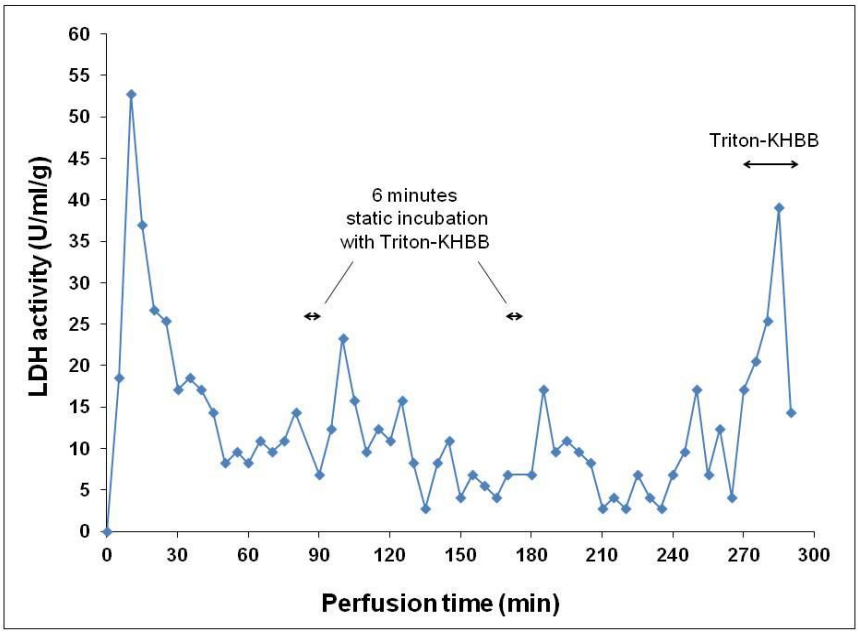

Figure 3.4. A representative study of LDH release from heart tissue following two, 6 minute, incubations with Triton–KHBB, each followed by a 84 minute, oxygenated KHBB perfusion. Tissue sample was finally exposed to continuous Triton–KHBB perfusion (270 – 300 minute). N = 2

3.4.2. Experimental rat model

Cardiac tissues were perfused in the Generation 1 microfluidic system for 5 hours in KHBB, followed by 1 hour of 2 % (w/v) Triton X100 in KHBB and LDH release determined.

Figure 3.5 shows the representative examples of LDH release profile of two separate samples throughout the perfusion. Generally, the trend for the LDH release was similar. The LDH activities were high (~ 320 – 810 U/ml/g) initially, but were maintained at low levels (≤ 100 U/ml/g) after the first hour of perfusion until the cardiac tissue was challenged with 2 % (w/v) Triton X100 at 300th minute. The highest LDH concentrations after the Triton X100 insult were 971.11 U/ml/g and 398.23 U/ml/g (red and blue lines, respectively). The LDH release from the remaining 5 tissues, which were treated in the same way, also demonstrated similar raised enzyme activities at the end of the perfusion.

The tissues perfused in these two experiments were of similar sizes (dimension: ~ 2 x 3 x 3 mm^3; weight: ~ 0.01 – 0.02 g). All samples (N = 7) perfused in this way resulted in the same trend of LDH release. In some instances, the contraction continued until exposed to 2 % (w/v) Triton X100, others ceased beating at an earlier stage of the perfusion. Videos 6 and 7 are two individual examples of tissue contraction recorded during KHBB perfusion (Supplementary DVD). However, the LDH activities remained low, suggesting that despite the loss of ability to contract, the tissue did not lose membrane integrity (Kui *et al*., 2009).

3.4.3. Human model

Human right atrial tissue biopsies were obtained anonymously at the time of CABG surgery, from tissue removed as part of the surgical intervention, supplied by Mr Steve Griffin, a Consultant Cardiothoracic Surgeon. Biopsies were handled as described in Section 2.1.2. These biopsies from patients were investigated and three perfusion durations performed, i.e. 2, 3.5 and 5 hours. Contraction of biopsies within the chamber was recorded using a microscopic camera (Videos 8 and 9; Supplementary DVD).

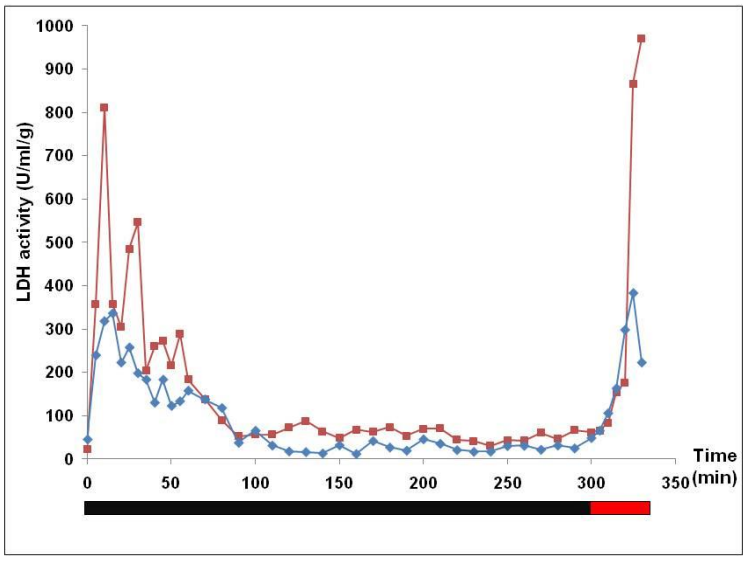

Figure 3.5. LDH release from rat heart tissues perfused for 5 hours with KHBB (black bar), followed by 1 hour with 2 % (w/v) Triton X100 in KHBB (red bar). Blue and red lines are two representative experiments using heart tissues from different rats. N = 7 heart tissues

3.4.3.i. Perfusion protocol: 2 hours KHBB + 30 minutes 2 % (w/v) Triton X100 in KHBB

Cardiac tissue biopsies were perfused for 2 hours in the Generation 1 microfluidic device. Initially, the highest LDH activities in the first 20 minutes were 26.2 U/ml/g and 8.63 U/ml/g and maintained at 3 – 5 U/ml/g until 120th minute (Figure 3.6 blue and red lines, respectively). Insult with 2 % (w/v) Triton X100 after 120th minute increased the LDH activities to 14.17 U/ml/g and 9.11 U/ml/g at 145th and 140th minute, respectively.

In the experiment represented by the blue line (Figure 3.6), the biopsy continued to contract until 8 minutes after Triton X100 insult. The heart tissue biopsy in another experiment did not beat throughout the experiment; however, Triton X100 exposure elicited a rise in LDH levels, again supporting the observations on rat tissue, whereby lack of contraction did not correlate with LDH release.

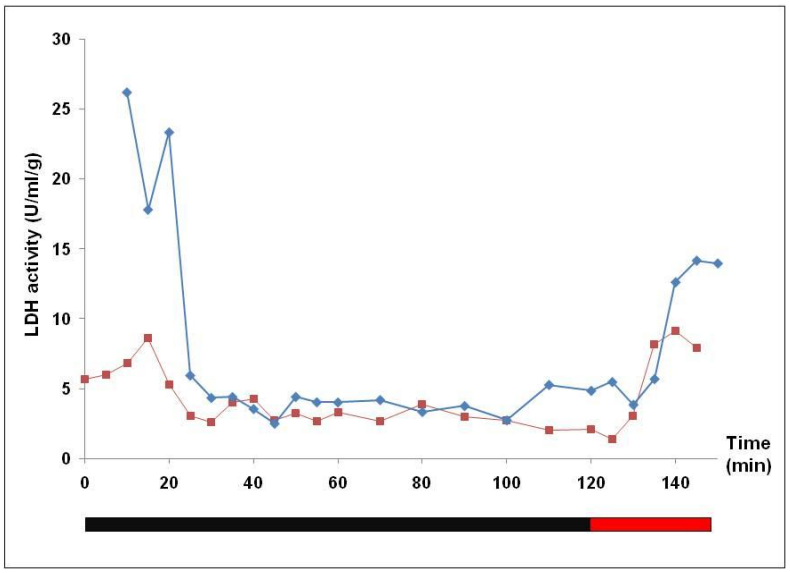

Figure 3.6. LDH release from human heart tissues perfused for 2 hours with KHBB (black bar), followed by 30 minutes with 2 % (w/v) Triton X100 in KHBB (red bar). Blue and red lines are two individual experiments using heart tissues from different patients.

3.4.3.ii. Perfusion protocol: 3.5 hours KHBB + 30 minutes 2 % (w/v) Triton X100 in KHBB

The perfusion period extended to 3.5 hours after the viability of the tissue biopsies for 2 hours in the perfusion system had been demonstrated (Figure 3.7). The tissue in the experiment represented by the red line gave a low level of LDH release (≤ 5 U/ml/g) until Triton X100 exposure, at which point, LDH activities increased gradually, with a highest LDH of 18.69 U/ml/g at 240th minute.

For the other experiment (blue line), the LDH levels fluctuated during the first 90 minutes with the highest LDH peak at 21.56 U/ml/g at 25th minute. LDH activities were low (≤ 5 U/ml/g) between 90th – 210th minutes but were once again raised after the Triton X100 insult (the highest LDH activity being 34.18 U/ml/g at 240th minute).

Furthermore, contraction was not observed in either of these biopsies, although electrical stimulation was applied throughout. A total of 17 independent perfusion experiments were carried out, with 88.2 % (15/17) remaining viable after perfusion for 3.5 hours in the microfluidic chamber.

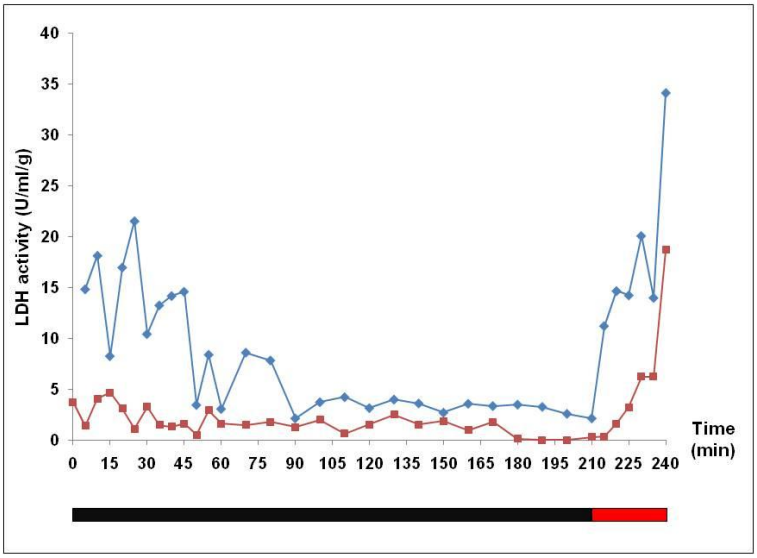

Figure 3.7. LDH release from human heart tissues perfused for 3.5 hours with KHBB (black bar), followed by 40 minutes with 2 % (w/v) Triton X100 in KHBB (red bar). Blue and red lines are two representative experiments using heart tissues from different patients. N = 17 heart tissues

3.4.3.iii. Perfusion protocol: 5 hours KHBB + 30 minutes 2 % (w/v) Triton X100 in KHBB

Two experiments were conducted where human heart tissue was perfused in the microfluidic device for 5 hours. LDH levels fluctuated over the first 80 minutes (Figure 3.8), but were then maintained at ≤ 5 U/ml/g until 300th minute. However, during the Triton X100 insult, the LDH activities were not changed. It would be possible that the majority of the LDH had been released over the first 80 minutes of perfusion. In the meantime, contraction was observed in these samples only over the first 2 hours of perfusion.

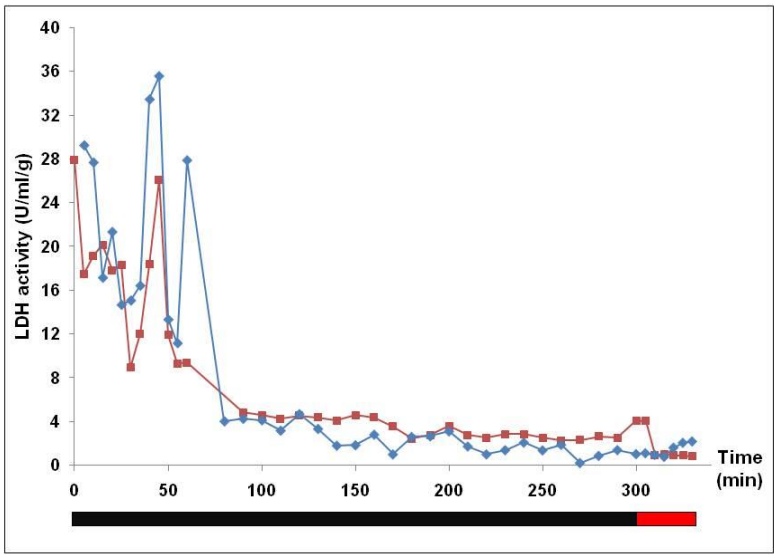

Figure 3.8. LDH release from human heart tissue perfused for 5 hours with KHBB (black bar), followed by 30 minutes with 2 % (w/v) Triton X100 in KHBB (red bar). Blue and red lines are two individual experiments using heart tissues from different patients.

3.4.4. Comparisons of electrochemical data, LDH and H_2O_2 concentrations in a human model

In order to monitor the *in situ* ROS release in real–time, electrochemical probes were integrated with the perfusion chamber. Electrochemical analytical probes were composed of working electrode (Pt), counter electrode (Pt) and reference electrode (AgCl coated Ag wire). The working electrode acted as the transduction element in the biochemical reaction, the counter electrode passed the current through the electrolytic solution, whereas the reference electrode served to provide a stable and well–defined potential (Southampton Electrochemistry Group, 2001). Perfusion experiments as described in Section 3.4.3.ii were repeated and CycV scans were performed on–chip (Section 2.9). During the potential sweep, the potentiostat measured the oxidation and reduction currents, giving a cyclic voltamogram. The oxidation current (I_0) at 0.72 V was chosen because this allows the oxidative detection of total ROS (work done by Dr Y. Dou; Cheah *et al*., 2010). Both LDH and H_2O_2 levels were analysed off–chip in the effluent samples (Sections 2.6 and 2.8, respectively). Changes in I_0 were compared with the LDH and H_2O_2 release during the perfusion.

The I_0 levels corresponded to the changes in LDH release in Figure 3.9, especially at 55^{th} and 220^{th} time points. This indicates that, in addition to the measurement of LDH release, tissue damage can be examined electrochemically by the release of total ROS. Furthermore, Figure 3.10 shows the comparison of off–chip LDH and H_2O_2 measurements and *in situ* electrochemical measurement of total ROS in real–time, using media saturated with N_2 gas to induce ischaemic damage (Webb *et al*., 2004). The I_0 measured was in good agreement with the H_2O_2 assay results in the main. In addition, both the electrochemical measurement of total ROS and H_2O_2 results showed the peaks earlier than LDH peaks, when tissue was deprived of oxygen by N_2 gassed media was introduced from 210^{th} minute onwards.

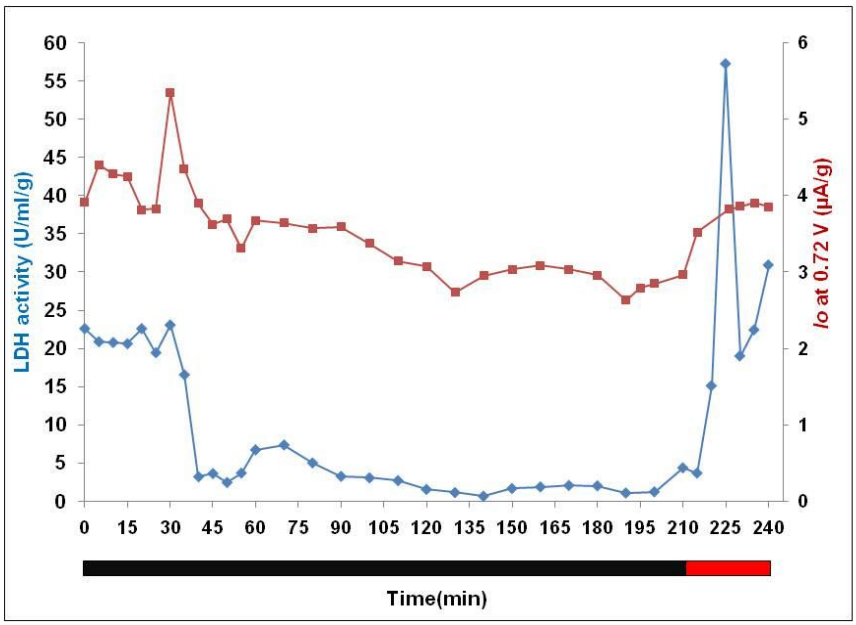

Figure 3.9. LDH release (blue), and oxidation current (I_0; red) at 0.72 V during perfusion. Human cardiac tissue was perfused for 3.5 hours with KHBB (black bar), followed by 30 minutes with 2 % (w/v) Triton X100 in KHBB (red bar).

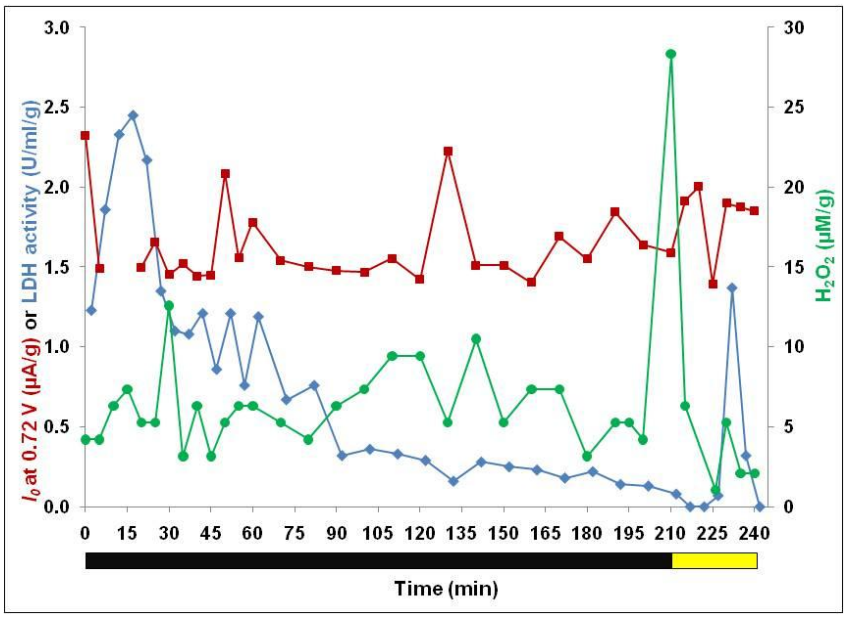

Figure 3.10. LDH release (blue), H_2O_2 release (red), and oxidation current at 0.72 V (green) during perfusion. Human tissue was perfused for 3.5 hours with KHBB (black bar), followed by 30 minutes with KHBB saturated with 95 % N_2 – 5 % CO_2 (yellow bar).

3.5. Discussion

The experiments reported here demonstrate that cardiac tissue from rat can be maintained in a viable state in the Generation 1 perfusion chamber for up to 5 hours, whereas for human tissue, it was up to 3.5 hours. Raised levels of LDH release were used as the marker of damage throughout perfusion. Electrochemical analytical probes were developed and integrated with the perfusion device to measure the real–time release of total ROS. The on–chip data was validated by using an off–chip, conventional, commercial assay for H_2O_2.

LDH concentrations were initially high in all experiments (N = 28), most probably due to cellular damage at the surfaces of the tissue when tissues were harvested. The relatively high initial LDH release in the first hour was also found in other studies reported by Obatomi *et al.* (1998), Hattersley *et al*. (2008), and van Midwoud *et al*. (2010) in kidney and liver tissue perfusions. As perfusion proceeded, this “trauma–associated” LDH was washed out and levels remained relatively low. When the heart tissue was challenged with 2 % (w/v) Triton X100 in KHBB, cell membranes were solubilised and hence LDH release markedly increased. Right ventricular tissues from rats could be maintained viable for up to 5 hours *ex vivo* in the microfluidic device (N = 7), whereas human right atrial tissue could only be maintained reliably for up to 3.5 hours (N = 17).

In this microfluidic perfusion system, although oxygen provision is continuous, oxygen supply to individual cardiomyocytes within the cardiac tissue was not sufficient (Figure 3.1.A). This is mainly determined by the dimension of the tissue sample where the oxygen diffusion distance from the edge to the core of the tissue is large; hence the centre of the sample will not receive adequate oxygen. Even though the confocal images shown in Figure 3.1 were heart tissues which have been exposed to 2 % (w/v) Triton X100, cells on the perimeter were only stained with Calcein AM, suggesting they were viable. It was thought that the plasma membranes of the cells at the outer region have been totally ruptured as a result of the insult with Triton X100, and the DNA contents which were the target of PI could not be

retained but have been released into the perfusion medium and the inner cells were simply taking up the Calcein AM.

In this study, stimulation was generated with electric field strength of 3 – 4 V/cm and a frequency of 1.5 Hz. Some samples contracted continuously under this regimen while perfused with oxygenated media. For comparison, Field *et al.* (1994) conducted a study measuring intracellular Ca^{2+} transients in isolated perfused rat heart stimulated with square monophasic pulses of 5 Hz and 1.5 – 2 V. For individual rat ventricular cardiomyocytes, the frequency applied was between 0.5 – 1 Hz, with field strength of 5 – 6 V/cm (Klauke *et al*., 2003, 2007). In addition, Tandon *et al*. (2011) have recently demonstrated that engineered cardiac tissues stimulated at 3 V/cm had the highest tissue density.

The ways of handling and storing the heart tissue before analysis could affect its viability during the course of perfusion. Rat tissue was placed in the microfluidic device immediately (< 5 minutes) after excision, while human samples were kept in ice cold cardioplegic solution and transported from hospital to the laboratory taking approximately 1 hour. This may explain the difference in the viability maintenance period between rat and human heart tissues. Although some of the heart tissue samples (both rat and human) were not contracting at the start or ceased beating at early stages of the perfusion, they were considered to be viable but quiescent, in order to preserve energy (Casey and Arthur, 2000).

The work demonstrated here is different from tissue engineering in a microfluidic platform, which generates new functional tissues to restore and improve tissue function. However, direct experimentation on the native clinical samples under *in vivo*–like conditions was described in current study. Hattersley *et al.* (2008) have demonstrated similar biological microfluidic work, where liver tissue biopsies could be maintained for over 70 hours in the microfluidic environment. The liver tissue continued to produce albumin and urea during the perfusion, demonstrating viability and functionality within the microfluidic device. Similar work in the group has recently demonstrated, in colorectal tissue, that significant concentrations of vascular endothelial

growth factor were produced in response to hypoxia by malignant but not normal tissue (Webster *et al.*, 2010).

The relationship between ROS and heart injury has been extensively studied. Several electrochemical sensors integrated with microfluidic devices have been developed to measure ROS and other cellular products. Amatore *et al.* (2007) have conducted ROS and reactive nitrogen species assessment amperometrically using a microelectrode within a microfluidic device, where macrophage cells were continually stimulated by microinjection of a Ca^{2+} ionophore. This group also practised the same analytical approach with other cell types, for example lymphocytes (Lachgar *et al*., 1999) and skin cells (Arbault *et al*., 1997). The three microelectrodes used in their electrochemical measurements were similar to this study; the difference was that their their microelectrodes were patterned onto the glass substrate and orthogonal to the flow channel (Figure 3.11). A number of electrochemical biosensors have been established to measure the release of specific reactive species: H_2O_2 (Kasai *et al*., 2009, Yan *et al*., 2011), superoxide anion ($O_2^{\bullet -}$; Chang *et al*., 2005, Cortina-Puig *et al*., 2009, Fujita *et al*., 2009), NO (Boo *et al*., 2011, Quinton *et al*., 2011) and peroxynitrite (Wang and Chen, 2010, Quinton *et al*., 2011). However, these biosensors are different from the probe presented here in which total ROS release was assessed instead of the specific ones.

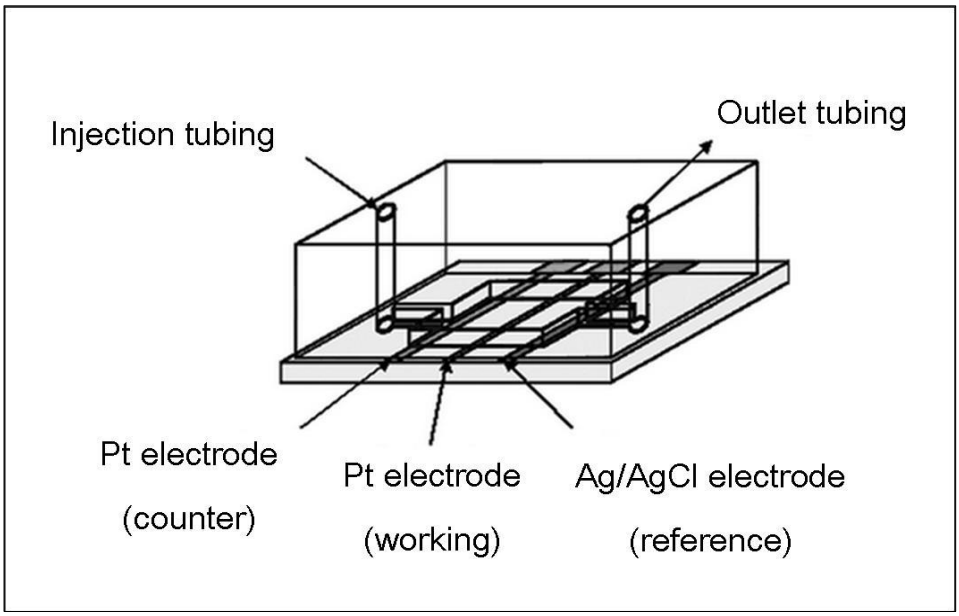

Figure 3.11. Three microelectrodes were patterned onto the glass microfluidic device for use of oxidative stress analysis. (Amatore *et al*., 2007)

In the present study, each electrochemical measurement took 1.5 minutes, whilst it took 2 minutes to collect sufficient effluents for H_2O_2 assay and another 2 minutes to get a sample for LDH analysis. These assays were subsequently performed in batches off–chip for comparison with the real–time electrochemical analysis. Taking these small sampling differences into account, the LDH release matched the H_2O_2 levels, except between 100^{th} – 160^{th} minutes, where there was a raised level of H_2O_2 with only small fluctuations in LDH concentrations (Figure 3.10). [H_2O_2] at 220^{th} minute was 1.18 µM from the off–chip biochemical assay and 3 µM by electrochemical methods (after calibration with standard H_2O_2). This strongly suggests that H_2O_2 does not constitute all the ROS produced by the heart tissues, which would be in agreement with Thannickal and Fanburg (2000). The detection of H_2O_2 release before LDH suggests that oxidative damage occurred prior to membrane damage, although this could simply be an artefact of the timings of sampling.

The amount or rate of H_2O_2 release from the heart tissue indicates the extent of cardiac injury. Two minutes after an IR injury, the rate of H_2O_2 release has previously been reported to be 50 nmol/g/minute (Slezak *et al*., 1995). As the chamber size of the perfusion device used in this study was 400 µl, with a tissue weight of 0.03 g, the H_2O_2 concentration calculated using a release rate of 50 nmol/g/minute would be ~ 3.75 µM/minute. Other research has reported that stimulated human neutrophils released H_2O_2 in a rate of 3×10^{-18} mol/second/cell (Shleev *et al*., 2008). In a ventricle, it is assumed that the average volume of a rat or human cardiomyocyte was approximately 30,000 μm^3; this can vary considerably with gender and age (Campbell *et al.*, 1989). Given that the heart tissue dimensions were 2.5 x 4 x 2 mm^3, the calculated H_2O_2 release rate might be expected to be 0.30 µM/minute. Factors which are not taken into account include cell types, stimulation methods, and diffirences in the nature of tissue samples. Even though the H_2O_2 release rates (3.75 µM/minute and 0.30 µM/minute) were different, they were of a similar order of magnitude. The low H_2O_2 release

rate in this study could be due to the fact that the stress imposed by Triton X100 exposure is less severe than that of IR.

It has been demonstrated that Triton X100 serves as an appropriate damage inducing agent, as LDH release was raised following introduction (Figure 3.4). On the other hand, starving the tissue by using media gassed with 95 % N_2 / 5 % CO_2 was an alternative way of causing cellular damage, with the advantage of reduced effect of gas on the background current during electrochemical CycV measurement. Non–reactive N_2 gas has much less background noise–to–signal ratio which is undesirable for CycV measurement. Nitrogen–induced LDH release peaked 10 minutes earlier than Triton X100 (the 240th minute in Figure 3.7 and the 230th minute in Figure 3.10), but the magnitude of LDH caused by perfusion with N_2 saturated media was lower than that of Triton X100. This is most probably due to the direct cell membrane permeabilisation effect of Triton X100, whilst N_2 limits the oxygen supply to the heart tissue, thereby affecting the cell's energy metabolism. It is hypothesized that longer perfusion with buffer gassed with 95 % N_2 / 5 % CO_2 would produce similar level of cell rupture and LDH release.

In conclusion, the microfluidic system presented here allows the perfusion of clinical samples *in vitro*, whilst retaining *in vivo* microenvironment. Cardiac tissue was maintained viable in the microfluidic chamber for up to 5 hours, whereas it was up to 3.5 hours for human heart biopsies. With the integration of electrochemical probes, sensitive, rapid and real–time measurement of tissue products was achieved.

Chapter 4

Ischaemia Reperfusion in Generation 1 Device

Cardiac surgery often involves an obligatory period of myocardial IR. IR injury has been recognised as a major contributor to heart complications, such as myocardial stunning and arrhythmia. The underlying mechanisms of IR have been extensively investigated (Chi and Karliner, 2004, Baines, 2009). The damage encountered from the disruption of blood flow to the heart during infarction can be salvaged by rapid restoration of coronary blood flow, known as reperfusion (Grech *et al*., 1995). However, depending on the duration and severity of the ischaemic insult, reperfusion itself can lead to deleterious effects, such as the generation of ROS and loss of functioning cardiomyocytes by apoptosis (Masztalerz *et al*., 2006, Buja and Weerasinghe, 2010).

Few myocardial IR studies have been performed using a microfluidic platform. Khanal *et al*. (2011) and Solis-Wever (2011) have studied IR–induced apoptosis in primary porcine cardiomyocytes using a microfluidic device. The earliest phase of apoptosis and mitochondrial depolarization were followed by successfully examining the mitochondrial membrane potential with MitoTracker Red under fluorescent microscopy. However, there have been no studies that adapt the microfluidic technology to probe IR on cardiac tissue biopsies.

In this study, a microfluidic method has been used to simulate episodes of IR on cardiac tissue, providing a better platform to mimic the *in vivo*–like microenvironment for cells and tissues (Bhadriraju and Chen, 2002). Varying durations of ischaemia have been previously studied using a range of different models and techniques (Mehta *et al*., 2000, Hamilton *et al*., 2003, Starnes *et al*., 2005, Kambe *et al*., 2009, Bell *et al*., 2011). The transition from reversible to irreversible injury occurs after approximately 20 minutes of normothermic global ischaemia in the isolated perfused rat heart (Palmer *et al*., 2004). Here, the ischaemic periods of 20 (Ooie *et al*., 2001, Yamanaka *et al*., 2003, Shinohara *et al*., 2007) and 40 minutes (Nie *et al*., 2007, Shackebaei *et al*., 2010a and b) were investigated (Figure 2.19), induced either via no flow (Wambolt *et al*., 2000, Zhu *et al*., 2004, Bentzen *et al*., 2010;

Sections 2.11.1) or anoxia (Matherne *et al*., 1997, Eguchi *et al*., 2003, Horman *et al.*, 2003, Webb *et al*., 2004; Section 2.11.2).

Acute stresses, such as IR, hyperthermia and oxidative stress, can rapidly potentiate the induction of a series of genes (Das *et al*., 1995), including NOS genes and members of HSP family. Altered expression of stress genes (eNOS, iNOS, HSP 72, HSP 73) have been reported following stress or damage encountered by the heart tissue during IR, using a variety of different models (Grilli *et al*., 2003, Di Napoli *et al*., 2007). The aim of the present study was to investigate the expression levels of these stress genes in heart tissue undergoing IR in the novel microfluidic system. The changes in mRNA were assessed off–chip using a conventional semi–quantitative PCR method.

4.1. Primer design

Primer pairs were designed to span or flank an intron, to prevent co–amplification of genomic DNA (gDNA; Figures 4.1 and 4.2).

Sequences of the forward and reverse primers used in this study are given in Table 2.3. eNOS, iNOS, HSP 72 and β–actin primers were taken from published work, whilst neuronal NOS (nNOS), HSP 73 and GAPDH primers were designed using the primer designing tool from NCBI (http://www.ncbi.nlm.nih.gov/tools/primer-blast/). All primers were subjected to a sequence check for their locations within the genome, to see if they were intron–flanking (Figure 4.3). Only HSP 72 did not flank an intron, as the gene is intronless (Silver and Noble, 2011). To prevent gDNA amplification in all samples during RNA extraction, the extract was treated with DNase I.

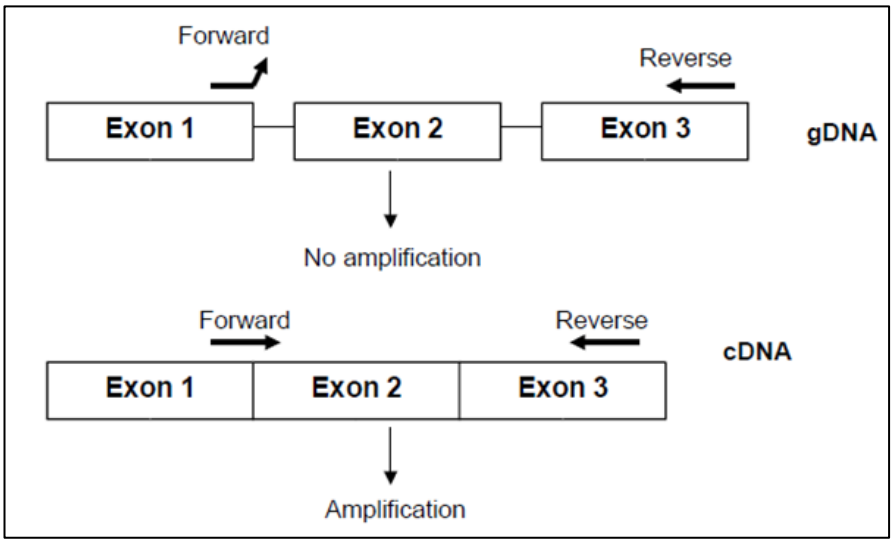

Figure 4.1. Intron–spanning primers work in cDNA but not gDNA (Modified from Wei *et al.*, 2005)

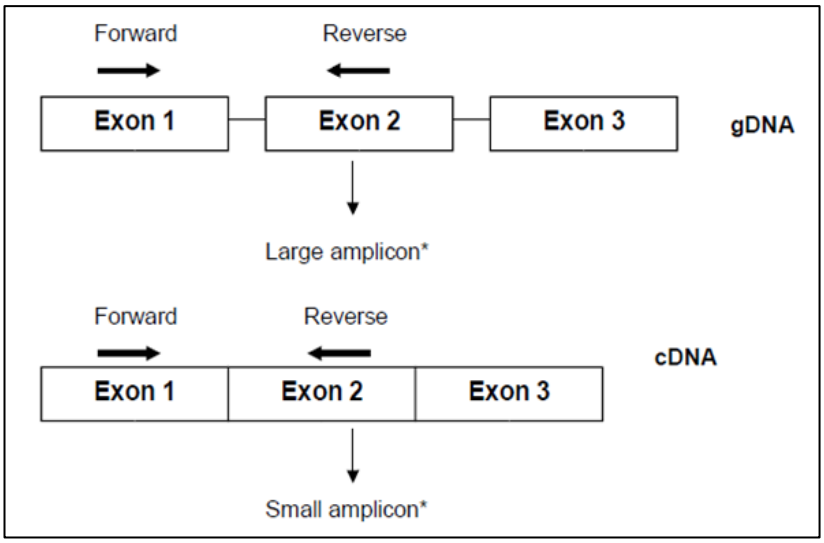

Figure 4.2. Intron–flanking primers distinguish gDNA from cDNA (Modified from Wei *et al.*, 2005)

4.2. Optimisation of PCR conditions

The cDNA from control tissue was used to optimize the PCR conditions for each of the genes. Control tissue was the sample taken at the time of sacrifice.

4.2.1. Amount of cDNA

Following cDNA quantification (Section 2.11.6), differing cDNA amounts (62.5, 125, 250, 500, 1000 ng) were added into each PCR reaction mixture (as listed below). iNOS was then amplified as described in Table 2.4.

PCR reaction mixture:

- *cDNA (62.5, 125, 250, 500, 1000 ng)*
- *12.5 µl of PCR mastermix*
- *2 µl of iNOS forward primers (10 mM)*
- *2 µl of iNOS reverse primers (10 mM)*
- *Make up to 25 µl with sterile nuclease–free water*

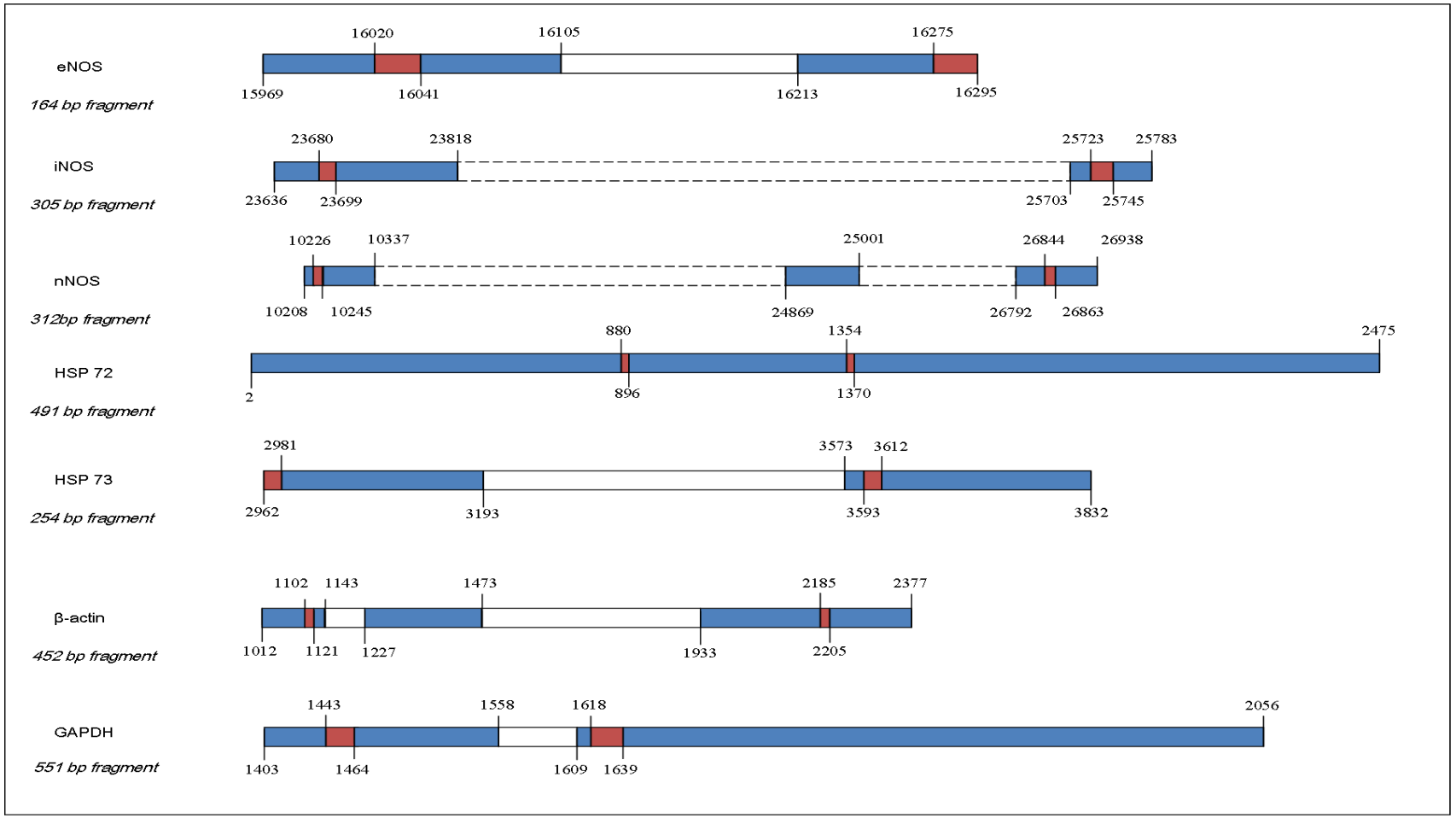

Figure 4.3. Primer location for 7 genes. eNOS, iNOS, nNOS, HSP 73, β–actin and GAPDH each had their forward and reverse primers flanking intron(s). On the contrary, the HSP72 does not contain introns.

(Number: base position from NH_2 terminal, Blue bars: exon, Red bars: primer positions in exon, White bars: intron)

iNOS was detectable irrespective of the amount of cDNA used, however, the intensity of the iNOS bands was greater with increasing amounts of cDNA when viewed visually. The bands were of similar intensity when 500 or 1000 ng cDNA were used (Figure 4.4), hence, a cDNA quantity of 500 ng/PCR mixture was used as the standard amount for the PCR amplifications.

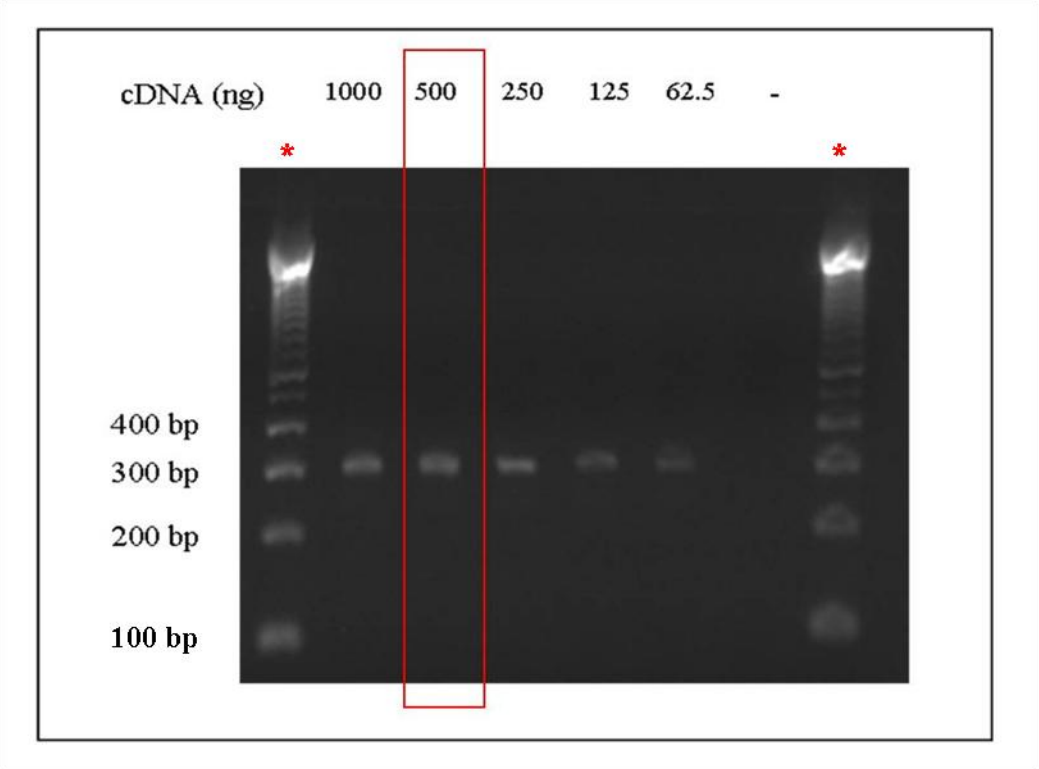

Figure 4.4. Representative 2 % (w/v) gel image showing the iNOS expression with different amount of cDNA. N = 2

* *100 bp DNA ladder*

4.2.2. Optimisation of primers

4.2.2.i. eNOS, iNOS, HSP 72 and HSP 73 primers

Three different volumes (0.5 µl, 1 µl and 2 µl) of the eNOS primers (10 mM) were used in PCR amplification (Figure 4.5.a). eNOS primers of 1 µl were sufficient to give a clear band and hence were used as the optimum volume.

In Figure 4.5.b, iNOS bands were most intense using 2 µl of iNOS primers and thus these were used as the optimum volume. HSP 73 and HSP 72 bands were detectable when any volume of the primers was used (Figures 4.5.c and d). A volume of 1 µl was selected to be the optimum volume for both.

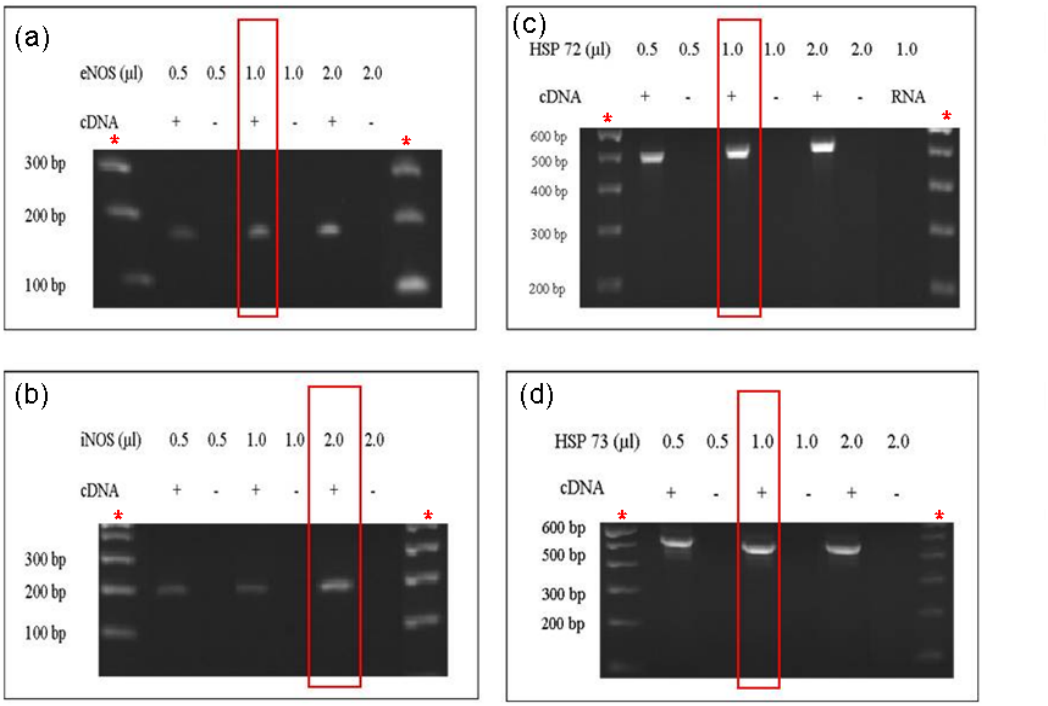

Figure 4.5. Representative gel images comparing the band intensity of (a) eNOS, (b) iNOS, (c) HSP 72 and (d) HSP 73 of different volumes in each PCR mixture. N = 2

* *100 bp DNA ladder*

4.2.2.ii. β–actin and GAPDH primers

β–actin and GAPDH were detectable with all primer volumes used (Figure 4.6). Thus, 1 µl β–actin primers and 0.5 µl GAPDH primers were chosen to be the optimum volumes.

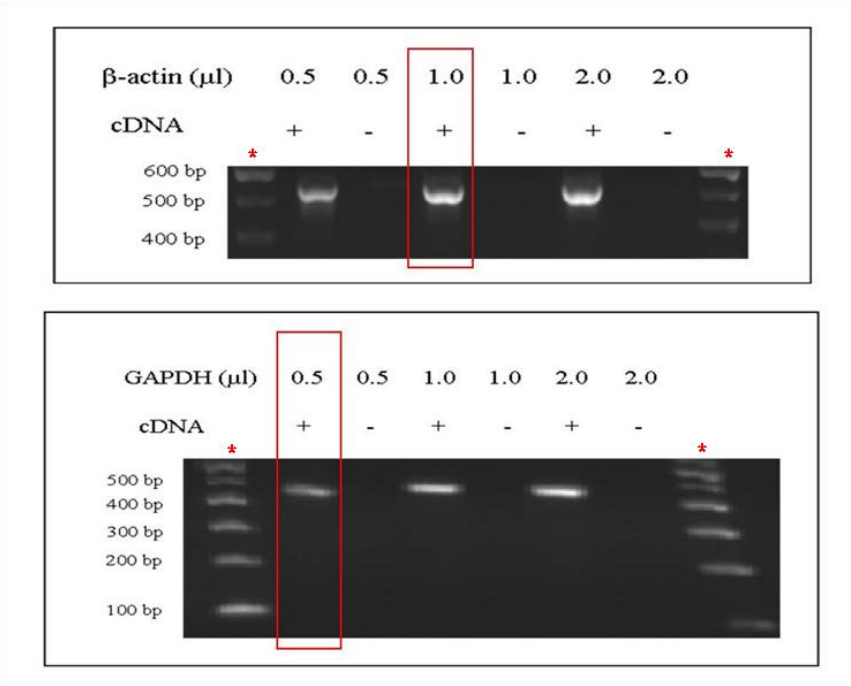

Figure 4.6. Representative gel images comparing the band intensity of β–actin and GAPDH of different volumes in each PCR mixture. N = 2

* *100 bp DNA ladder*

4.2.3. Annealing temperature

Table 4.1 summarizes the annealing temperatures provided by the primer provider (Eurofins), NCBI Primer Blast search and the papers where the primers were referenced. A range of annealing temperatures was tested for each set of primer pairs.

Three annealing temperatures (60 ^{o}C, 55 ^{o}C, and 52 ^{o}C) were tested for eNOS, iNOS and GAPDH with the greatest intensities being observed at 60 ^{o}C (Figure 4.7), which was selected as the optimum temperature for these genes. For HSP 72, 50 ^{o}C gave the optimal expression (Figure 4.8). Since HSP 72 is intronless, reactions with equal amounts of “no–reverse–transcribed (no–RT) RNA” were included as control for amplification of contaminating gDNA (Akçetin *et al*., 1999). The two lanes of no–RT RNA in Figure 4.8 were empty, showing that there was no genomic contamination.

The HSP 73 and β–actin amplified at 60 ^{o}C showed obvious and clear bands; therefore, no other temperature was tested. By considering the annealing temperatures given by Eurofins and NCBI, nNOS was amplified at three annealing temperatures: 65 ^{o}C (data not shown), 63.5 ^{o}C (data not shown) and 60 ^{o}C (Figure 4.8), neither of the higher temperatures showed visible bands. The investigation of nNOS gene was discontinued because of the failure to detect its expression from the samples. It may be due to the primers not working effectively with the cDNA and thus alternative primer pair sequences could be made and tested in the future. Another reason being the presence of nNOS in the heart tissue might be very low or under detectable level

Table 4.1. Annealing temperatures of genes.

Genes	Eurofins A_{temp} (°C)	NCBI A_{temp} (°C)	Reference paper A_{temp} (°C)
eNOS	60.3 59.8	52.57 52.65	60 (Di Napoli *et al.*, 2002)
iNOS	57.3 57.3	52.71 51.66	50 (Grilli *et al.*, 2003)
nNOS	63.5 63.5	60.04 59.98	-
HSP 72	50.4 55.2	45.35 49.06	Not mentioned (Nikaido *et al.*, 2004)
HSP 73	62.1 60.3	57.02 56.17	-
β-actin	65.5 61.8	58.56 55.63	-
GAPDH	59.4 59.4	54.46 55.08	60 (Di Napoli *et al.*, 2002)

A_{temp}, annealing temperature

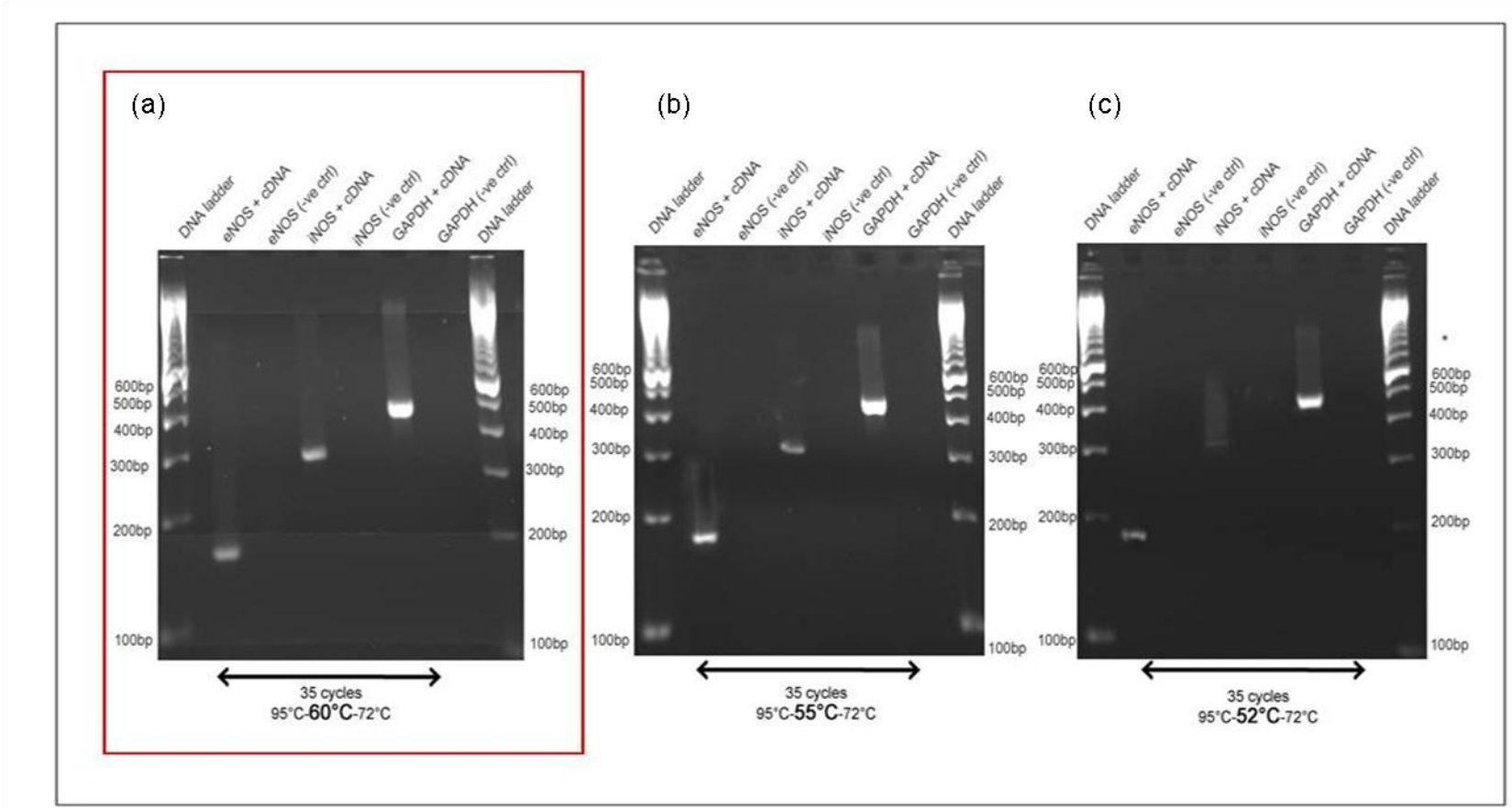

Figure 4.7. Representative gel comparing the intensity of eNOS, iNOS and GAPDH bands with annealing temperatures of (a) 60 ^{o}C, (b) 55 ^{o}C, and (c) 52 ^{o}C. N = 2

-ve ctrl, negative control without primer

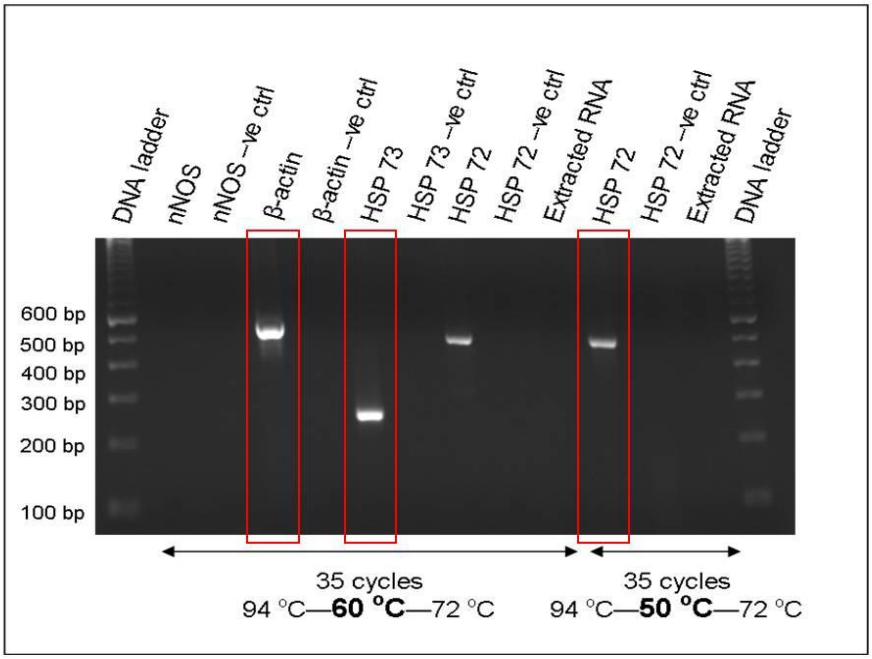

Figure 4.8. Representative gel comparing the intensity of HSP 73, HSP 72, nNOS and β–actin bands. Annealing temperatures of 60 ^{o}C and 50 ^{o}C were tested for HSP 72. N = 2

-ve ctrl, negative control without primer

4.3. House–keeping gene

House–keeping genes such as GAPDH and β–actin are widely used as internal standards for quantitative RNA analysis (Di Napoli *et al*., 2001, Maekawa *et al*., 2002). The expression of these two house–keeping genes during oxygen–deprived IR (20 minutes ischaemic period) was examined as described previously (Sections 2.11.3 – 2.11.8). The intensities of β–actin and GAPDH under different perfusion conditions (Figure 2.19) were quantified by Image J (Section 2.11.9). The density values were normalised to the baseline value (sample taken at the time of sacrifice).

Band intensities for GAPDH under different perfusion conditions had greater variation when compared with β–actin (Figure 4.9), with standard deviations of 0.08 and 0.14, respectively (Table 4.2), even though the same amount of cDNA (500 ng/PCR mixture) was used. As a result, β–actin was chosen to be the house–keeping gene throughout this study.

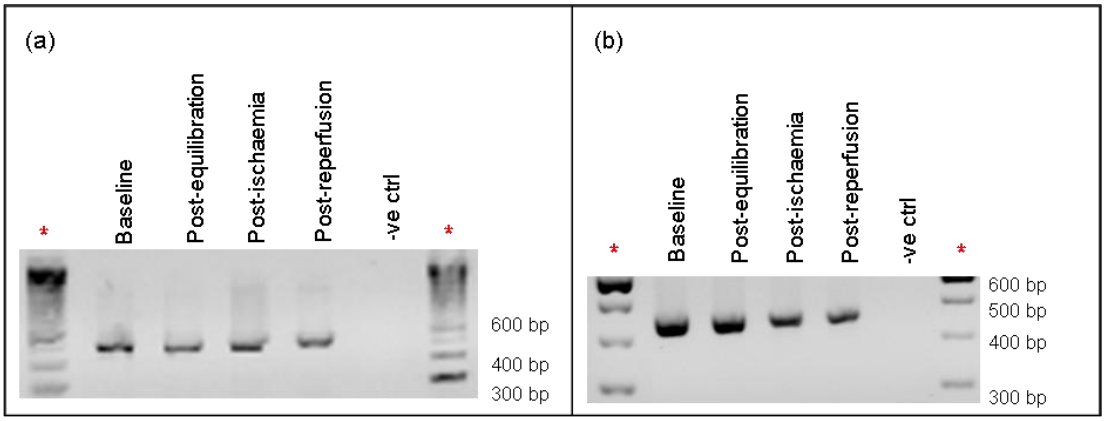

Figure 4.9. Two representative gel images comparing the intensities of (a) β–actin and (b) GAPDH expression following baseline, post–equilibration, post–ischaemia, and post–reperfusion. N = 2

* *100 bp DNA ladder; -ve ctrl, negative control without primer*

Table 4.2. Band intensity quantification of β–actin and GAPDH at different perfusion conditions normalised to baseline value.

Perfusion Stages	β-actin	GAPDH
Baseline	1	1
Post-equilibration	0.84	0.96
Post-ischaemia	0.92	0.78
Post-reperfusion	0.82	0.71
Standard deviation	*0.08*	*0.14*

4.4. PCR

Four tissue samples from the same heart were perfused for different times namely baseline, post–equilibration, post–ischaemia, and post–reperfusion (Figure 2.19). As a control, four separate heart samples were perfused for the same length of time, without any changes in flow or buffer composition. The relevant genes were amplified, quantified and analysed relative to their respective β–actin expression.

4.4.1. Oxygen–deprived IR

4.4.1.i. 20 minutes ischaemia/30 minutes reperfusion

The expression profiles of genes relative to β–actin for oxygen–deprived ischaemia (20 minutes no flow) versus control are demonstrated in Figure 4.10. The statistical analyses are tabulated in Table 4.3. A repeated measure ANOVA design was used because the same parameter was measured under different conditions on tissue samples from the same heart. Sphericity is the assumption of ANOVA where the variances of the differences between all groups are equal (Mauchly, 1940). The assumption of sphericity for all genes was satisfied, i.e. Mauchly's significance, $p > 0.05$ (Table 4.3). There was no significant effect of any perfusion conditions on any of the stress genes expression levels (i.e. $p > 0.05$); however in the case of eNOS the p value is 0.077, so there was a tendancy towards a significant change.

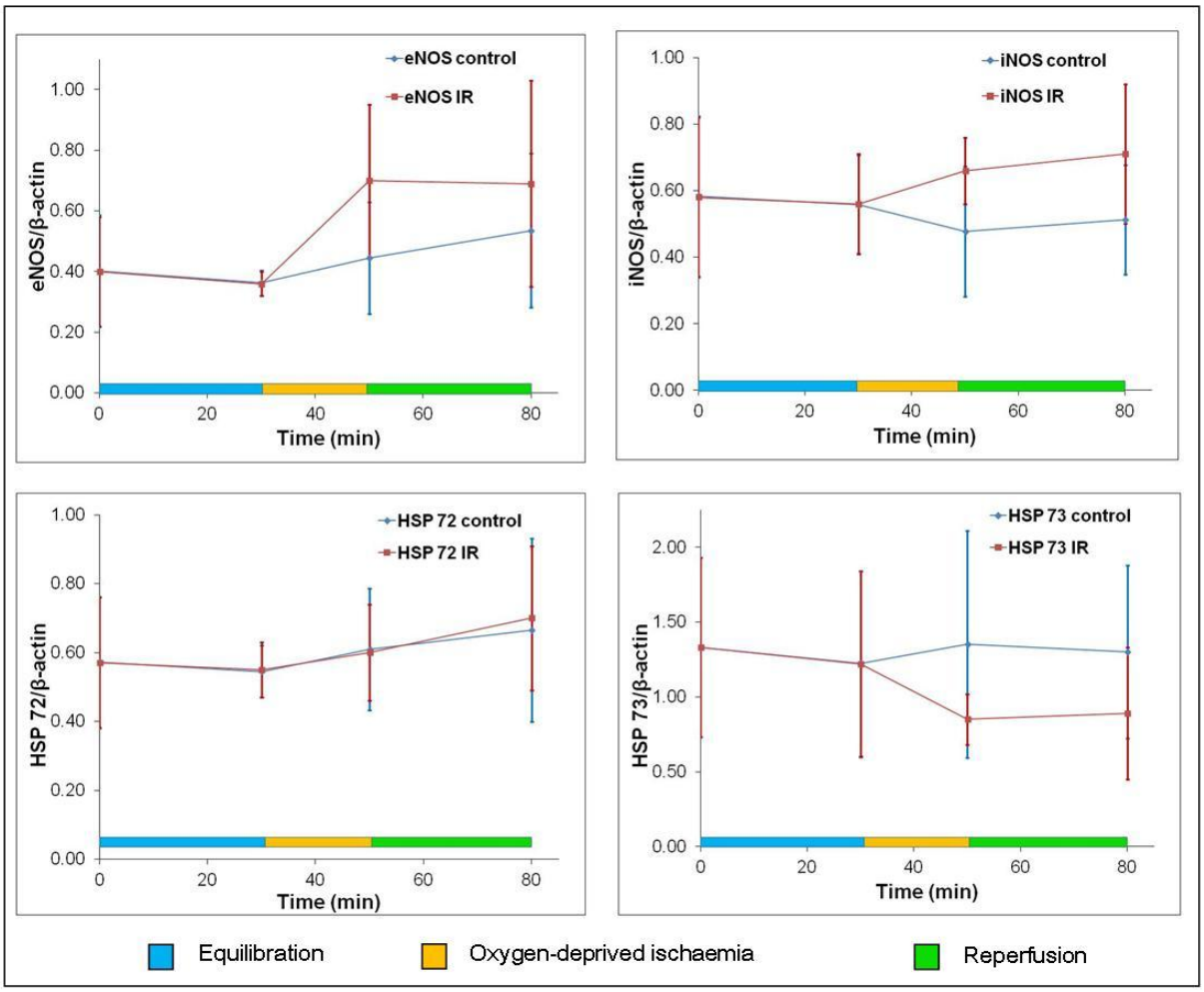

Figure 4.10. Expression profiles of eNOS, iNOS, HSP 72 and HSP 73 relative to β–actin. Data are expressed as mean ± standard deviation. N = 4
IR, ischaemia reperfusion

Table 4.3. Statistical analyses for eNOS, iNOS, HSP 72 and HSP 73.

	Mauchly's significance, *p*	Sphericity assumed significance, *p*
eNOS	0.632	**0.077**
iNOS	0.238	0.858
HSP 72	0.252	0.317
HSP 73	0.497	0.509

Red text represents *p* value that is close to 0.05

4.4.1.ii. 40 minutes ischaemia/30 minutes reperfusion

The expression profiles of the relevant genes following 40 minutes ischaemia (oxygen–deprived, no flow) versus control are showed in Figure 4.11. Data are presented as the expression of gene relative to β–actin. Table 4.4 lists the statistical analyses as shown previously. The expressions of eNOS and iNOS met the sphericity assumption, (i.e. Mauchly's significance, $p > 0.05$). Nevertheless, the assumption of sphericity for HSP 72 and HSP 73 was disregarded (Mauchly's significance, $p < 0.05$), so the Greenhouse–Geisser correction was applied to produce a more accurate significance value. The level of iNOS mRNA expression ($p = 0.012$) was significantly increased, whereas increased eNOS expression tends to be significant.

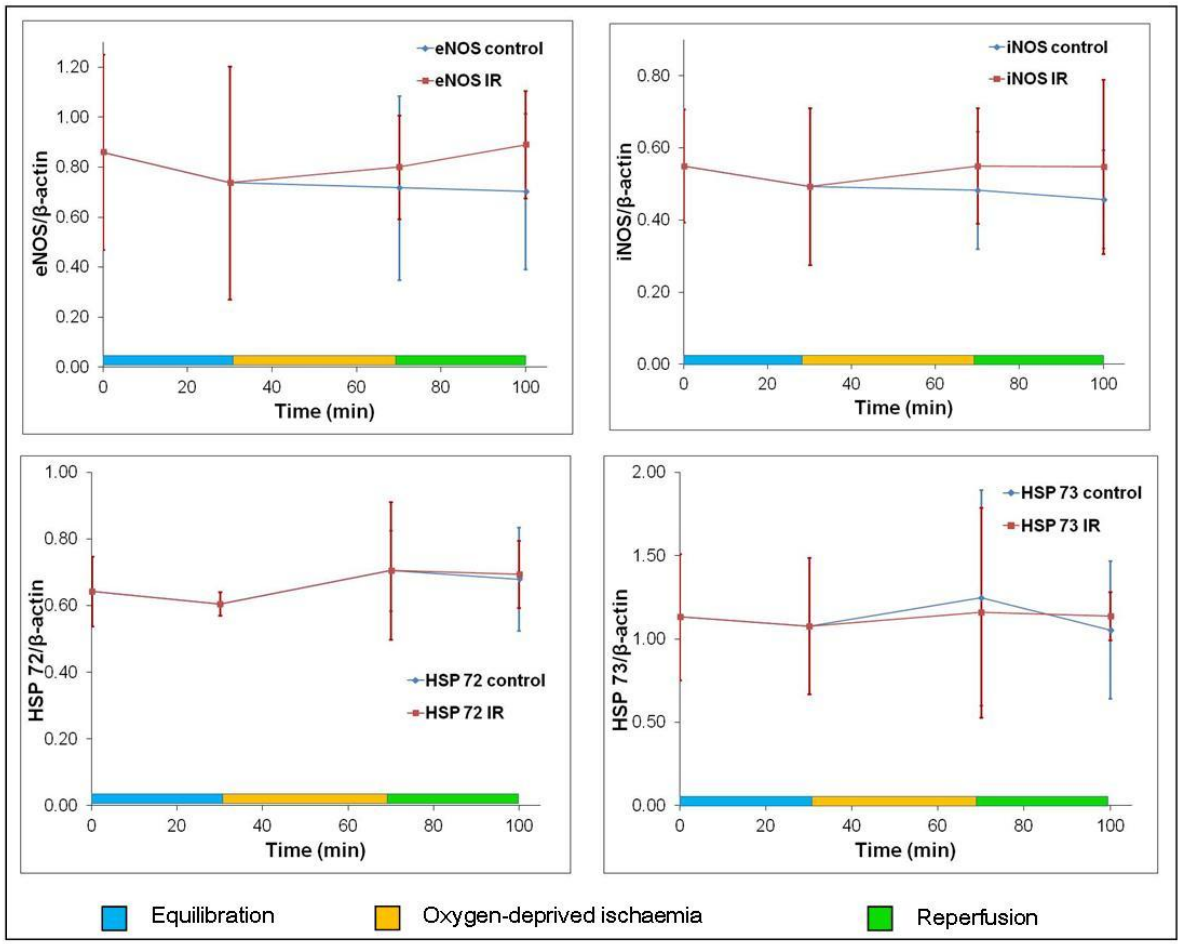

Figure 4.11. Expression profiles for eNOS, iNOS, HSP 72 and HSP 73 relative to β–actin. Data are expressed as mean ± standard deviation. N = 4
IR, ischaemia reperfusion

Table 4.4. Statistical analyses for eNOS, iNOS, HSP 72 and HSP 73.

	Mauchly's significance, *p*	Sphericity assumed significance, *p*	Greenhouse-Geisser significance, *p*
eNOS	0.862	**0.081**	-
iNOS	0.262	**0.012**	-
HSP 72	0.008	-	0.385
HSP 73	0.004	-	0.647

Red text represents *p* value that is close to 0.05

Pink text represents *p* value is significant, i.e. < 0.05

4.4.2. Nitrogen–induced IR

Heart tissue was perfused under different perfusion stages as described in Section 2.11.2. Anoxia was induced in this series of experiments by perfusing with 95 % N_2 / 5 % CO_2–gassed KHBB for 40 minutes. Electrical stimulation was applied during equilibration and reperfusion, but ceased during the ischaemic period. Prolonged reperfusion (2 hours) was carried out to allow greater opportunity for any effects on the gene expression to be realised.

The expression profiles of the stress genes for nitrogen–induced ischaemia (40 minutes) versus control are shown in Figure 4.12 and the statistical analyses given in Table 4.5. Data are presented as the gene expression relative to β–actin. The expressions of eNOS, iNOS and HSP 72 have met the sphericity assumption (i.e. Mauchly's significance, $p > 0.05$). However, the assumption of sphericity for HSP 73 was disregarded, and Greenhouse–Geisser correction was applied. There was no significant effect of perfusion conditions on any of the genes studied (i.e. $p > 0.05$).

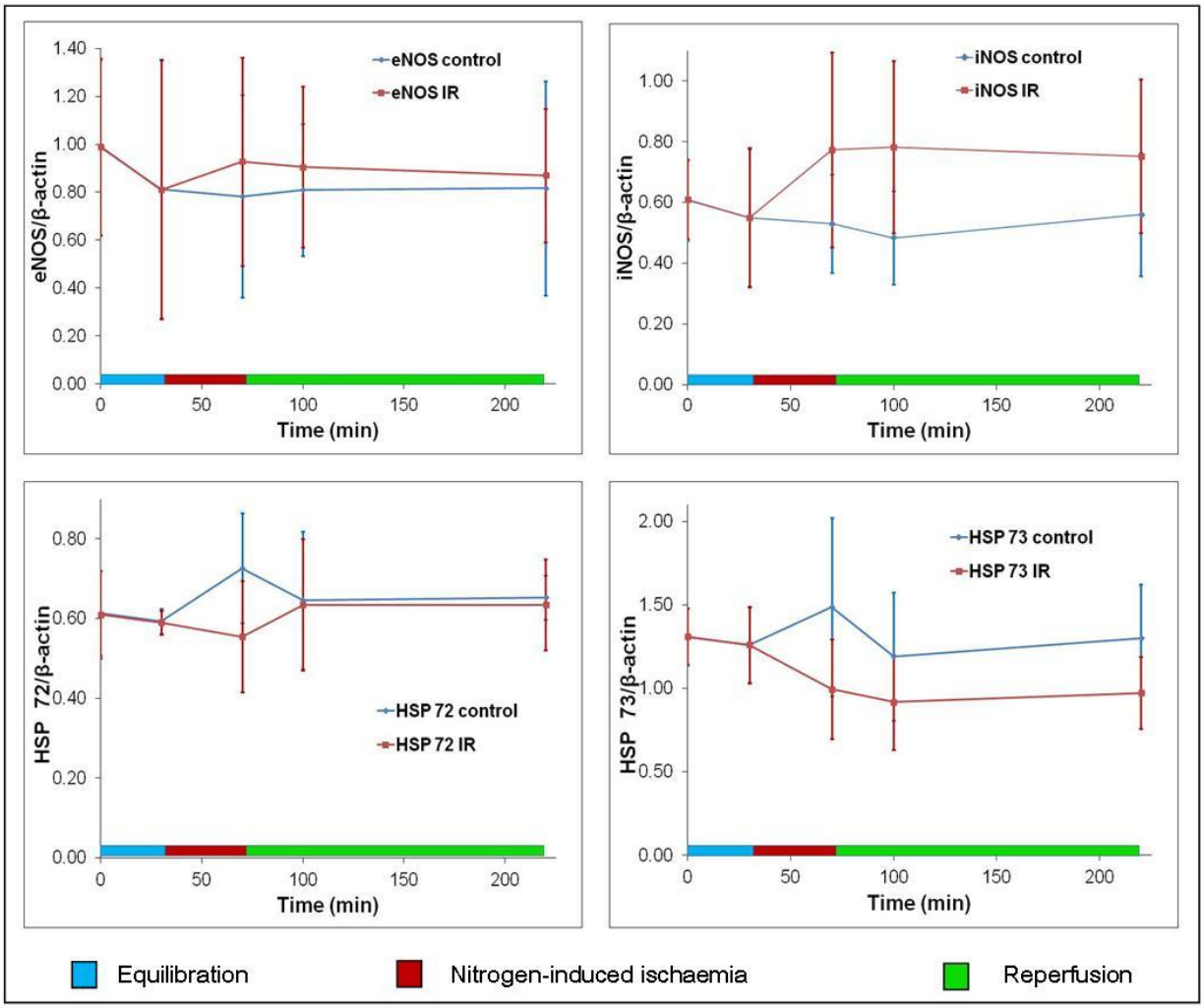

Figure 4.12. Expression profiles for eNOS, iNOS, HSP 72 and HSP 73 relative to β–actin. Data are expressed as mean ± standard deviation. N = 4
IR: ischaemia reperfusion

Table 4.5. Statistical analyses for eNOS, iNOS, HSP 72 and HSP 73.

	Mauchly's significance, *p*	Sphericity assumed significance, *p*	Greenhouse-Geisser significance, *p*
eNOS	0.191	0.933	-
iNOS	0.209	0.739	-
HSP 72	0.452	0.630	-
HSP 73	0.048	-	0.421

4.5. Discussion

Taken together, the data obtained from this investigation revealed that the greater duration of oxygen–deprived ischaemia (40 minutes) was the only condition that induced significant increased expression of iNOS. The increase in eNOS expression was close to significance at both 20 and 40 minutes ischaemia. Anoxia, however, did not generate a marked impact on either iNOS or eNOS. Expression of HSP 72 and HSP 73, however, were not altered under any of the ischaemic conditions.

A whole heart model is generally used to investigate IR (Currie *et al.*, 1993; Liu *et al.*, 1997; Felaco *et al.*, 2000). *In vivo* myocardial IR can be caused by the LAD occlusion where a tubing or needle is placed proximally over the artery and a suture used to occlude blood flow (Matsui *et al.*, 2001, Elrod *et al.*, 2006, Arslan *et al*., 2010). The ligature is released to re–admit blood flow and initiate reperfusion. Alternatively, an *in vitro* myocardial IR model is performed in perfusion system where the heart is perfused in Langendorff mode. Perfusion buffer is delivered in a retrograde direction down the aorta. Global ischaemia is induced by complete cessation of perfusion (Pevni *et al*., 2005, Knight *et al*., 2008, Mohanty *et al*., 2011). In addition, isolated cardiomyocytes have also been used to study simulated IR injury (Ladilov *et al*., 1998, Maddaford *et al*., 1999). However, one of the limitations of isolated cells is that they are essentially quiescent and not performing the level of contractile work normally carried out by the heart.

The properties and structure of the microfluidic chamber may be the reasons why there was no significant alteration observed in the gene expression profiles here. The PDMS microfluidic chamber used in this study was an open to air chamber, thus the perfusion buffer was in contact with the surrounding atmosphere. During the ischaemic phase, although a fresh oxygen supply had been removed from the chamber by cessation of flow and covering the top of the chamber with a glass slide, this might not have been

sufficient to reduce the oxygen content. Alternatively, nitrogen gas was used to replace the oxygen content in the buffer to create anoxic environment. Under these conditions, low oxygen content in the buffer may still increase when reaching the tissue chamber due to diffusion from the atmosphere. Therefore, the control of oxygen content in Generation 1 perfusion system required modification.

More precise control of oxygen within the microfluidic devices could be achieved using integrated oxygen sensing systems in air–tight chambers with cultured cells (Oppegard *et al*., 2010, Sinkala and Eddington, 2010, Khanal *et al*., 2011). One way used previously, is to employ oxygen fluorescent sensors (ruthenium red complexes) to provide spatial and temporal monitoring of oxygen concentration via fluorescence quenching.

House–keeping, or so–called reference, genes are endogenous genes that are essential for normal cell viability and functions (Touchberry *et al*., 2006). An inherent assumption is that expression levels of these genes remain constant between samples and under the experimental conditions (Thellin *et al*., 1999). Normalization to varying or fluctuating internal references can lead to erroneous and inaccurate results (Bustin, 2000). However, house–keeping genes are not exclusively stable, as they are open to variation based upon experimental treatments or environmental influences (Touchberry *et al*., 2006). Therefore, it is very important to validate the constancy of house–keeping genes between different experimental treatments and the time course to be employed.

GAPDH and β–actin are two commonly used house–keeping genes used for comparative gene expression studies. Variations in GAPDH gene expression were observed in heart tissue subjected to different perfusion conditions (Figure 4.9), independent of the amount of cDNA. This finding highlights the fact that GAPDH expression does vary under different conditions, consistent with other studies where GAPDH expression showed significant fluctuations in an *in vitro* cerebral ischaemia model (Gubern *et al*.,

2009). However, IR affects the metabolic processes in the heart and could hence affect the expression of GAPDH. The use of β–actin is suggested in this case as it is a cytoskeletal protein which serves a structural purpose in the cell rather than a metabolic role. Its expression was affected to a lesser extent by ischaemia and reperfusion episodes (Table 4.2).

The small number of experimental repeats (N = 4 for each protocol) resulted in a large standard deviation, limiting the statistical analysis of the results. Larger sample sizes will be needed to achieve sufficient statistical power and increased precision.

Among the NOS genes, only iNOS expression was significantly increased by IR after 40 minutes of oxygen–deprived ischaemia (Table 4.4). Similar results were reported by Grilli *et al.* (2003) in which iNOS activity, mRNA and protein were elevated in hypoxic rat heart tissue *in vivo* (7 – 14 days in 10 % oxygen chamber). Wildhirt *et al.* (1999) revealed that increased iNOS enzyme activity was detected 48 hours after IR in a rabbit heart, examined using both protein assay and immunohistochemistry. Other studies have also showed upregulation of iNOS expression and activity following IR (Table 4.6). However, Barsotti's group (2001) found no significant changes in iNOS but reduced eNOS mRNA expression among IR (30 minutes equilibration, 15 minutes ischaemia, and 180 minutes reperfusion) and control groups.

Table 4.6. IR–induced upregulation of iNOS.

Reference	Method	Equilibration (min)	Ischaemia (min)	Reperfusion (min)	Results
Liu *et al.*, 1997	Left artery occlusion	-	20	120	iNOS activity ↑, tissue NO level ↑
Mehta *et al.*, 2000	Langendorff	20	25	30	iNOS mRNA ↑, SOD mRNA ↓
Di Napoli *et al.*, 2005	Langendorff	20	15	180	iNOS mRNA ↑, eNOS mRNA ↓

iNOS is expressed under certain pathophysiological conditions, including stroke, infection, and a variety of trauma and stress. iNOS can generate relatively large amounts of NO (100 times more than normal) in cardiomyocytes and activated leukocytes which infiltrate the damaged heart (Nathan, 1997, Mungrue *et al*., 2002, Ferdinandy and Schulz, 2003). NO exerts a double–edged effect on the myocardium during IR, it can be both protective and deleterious, depending on the concentration and the source of production (Figure 4.13). NO protects the myocardium by maintaining endothelial function, increasing coronary blood flow, decreasing neutrophil accumulation, maintaining muscle contractility without increasing energy demand, and reducing oxygen consumption in myocardium (Manukhina *et al*., 2006). Bolli (2001) has reviewed a large number of studies examining the impact of NO on IR injury in the myocardium, 73 % of which showed a protective effect of NO whilst only 11 % reported an exert detrimental effect. Long term gene therapy with iNOS in mice has demonstrated a protective effect against MI without inflammation or other adverse functional consequences (Li *et al*., 2005). In addition, administration of NO donors can also limit IR injury (Lefer *et al*., 1993, Beresewicz *et al*., 1995, Mizuno *et al*., 1998).

In contrast to these positive findings, Cui and Zhu (1998) have showed that downregulation of iNOS expression could be cardioprotective. This is because high level of NO may depress myocardial contractility through the formation of peroxynitrite, leading to myocardial damage and dysfunction (Ferdinandy *et al*., 2000, Feng *et al*., 2001). Several mechanisms have been proposed to account for the cytotoxicity caused by peroxynitrite (Hu *et al*., 2006), including causing apoptosis by inducing the opening of mPTP (Brookes and Darley-Usmar, 2004) and the induction of DNA strand breakage (Szabo, 2003).

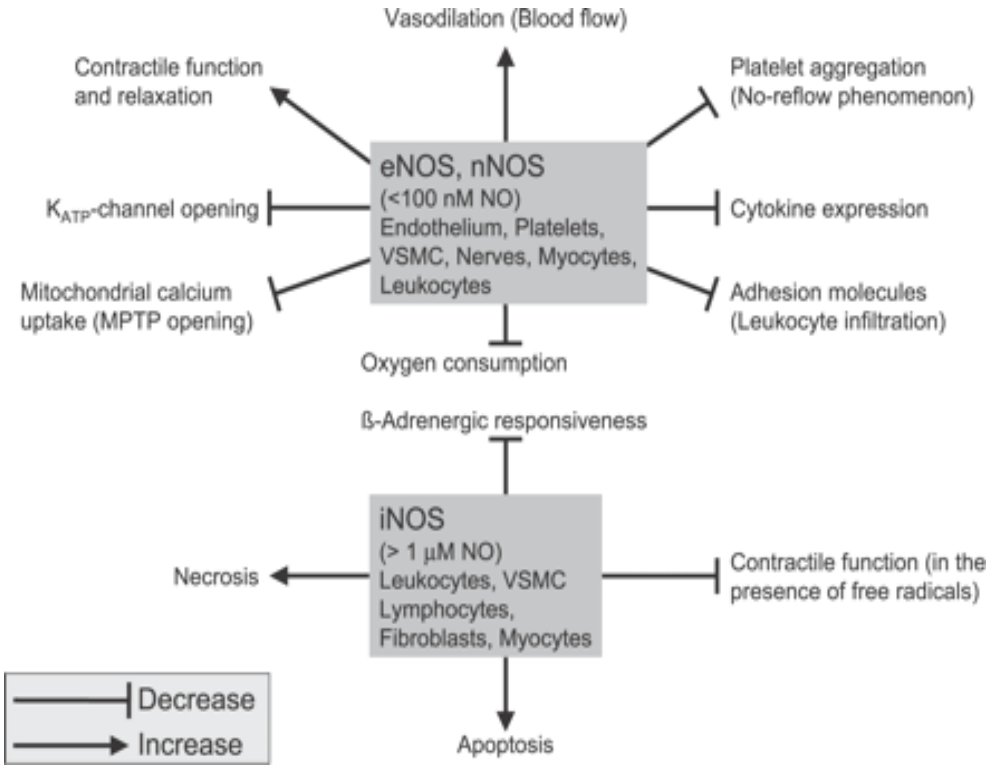

Figure 4.13. Effects of low (eNOS– or nNOS–derived) and high NO (iNOS–derived) concentrations on different cells. (Schulz *et al*., 2004)
MPTP, mitochondrial permeability transition pore; VSMC, vascular smooth muscle cells.

Amongst the IR protocols performed in this investigation, eNOS gene expression was increased as a result of oxygen–deprived IR procedures (both 20– and 40–minute ischaemia; Tables 4.3 and 4.4), with *p* values tending towards significance, but not for the nitrogen–induced IR. This is in contrast to a study conducted by Di Napoli *et al.* (2007) who demonstrated a significant decrease in eNOS mRNA and protein in isolated rat hearts, subjected to 20 minutes equilibration, 15 minutes of global ischaemia and 180 minutes of reperfusion, compared to the non–ischaemic control group. Barsotti *et al*. (2001) have shown that angiotensin receptor blocker treatment (1 mM Losartan) before ischaemia and during reperfusion induced overexpression of eNOS, leading to the reduction of reperfusion injury as evidenced by decreased mechanical and microcirculatory dysfunction, reduced necrotic cell death, and protected endothelium. The increased eNOS expression found in this study were different from others may be due to the

differences in the IR procedures and the severity of the ischaemia. Treatment with 3–hydroxy–3–methylglutaryl–coenzyme A (HMG–CoA) reductase inhibitor (2 mg/kg/day Rosuvastatin for 3 weeks prior to IR) have been shown to increase eNOS and decrease iNOS mRNA after IR (20 minutes equilibration, 15 minutes of global ischaemia and 180 minutes of reperfusion), reducing IR injury and preventing endothelial cell and cardiomyocytes damage (Di Napoli *et al*., 2005). There are many other pharmacological alternatives which can upregulate eNOS expression and consequently limit myocardial IR injury, for example simvastatin and lovastatin (Laufs *et al*., 1998), cerivastatin (Wolfrum *et al*., 2003), AVE 9488 (Frantz *et al*., 2009), and North American ginseng (Wu *et al*., 2011). Hence, the trend towards an increase in eNOS expression observed in this investigation may be indicative of a protective mechanism in cardiac tissue against IR.

Although nNOS investigation was discontinued in this study, its importance in regulating myocardial contractility in normal and failing heart has previously been well documented (Casadei, 2006). nNOS is expressed in the SR, sarcolemma and mitochondria of cardiomyocytes (Xu *et al*., 1999, Kanai *et al*., 2001, Takimoto *et al*., 2002). Increased nNOS protein expression delays the transition to heart failure as a result of pressure overload (Loyer *et al*., 2008), protects the heart from functional deterioration (Dawson *et al*., 2005) and reduces mortality following MI (Saraiva *et al*., 2005). Conditional nNOS overexpression in transgenic mice conferred cardioprotection after IR injury with reduced ROS production (Burkard *et al*., 2010). In contrast, nNOS inhibition was demonstrated to reduce myocardial ischaemic/reoxygenation induced injury (Barua *et al*., 2010), as nNOS exacerbated injury by increasing oxidative/nitrative stress (Lu *et al*., 2009). However, infarct size and myocardial injury in nNOS knockout mice were not augmented by ischaemia/reoxygenation (Sumeray *et al*., 2000, Takimoto *et al*., 2000). This literature would suggest that nNOS expression by cardiac biopsies required further investigation with new nNOS primers.

HSPs are molecular chaperones that aid proper folding, conformation and transport of proteins into different cellular compartments (Parcellier *et al*., 2003). They are induced under hyperthermia, as well as a variety of stressful conditions, e.g. IR stress (Latchman *et al*., 2001, Lepore *et al*., 2001, Lanneau *et al.*, 2007; Figure 4.14), and play an important role in cardioprotection. Two isoforms of 70 kDalton HSPs, HSP 72 and HSP 73, exist in mammalian tissues (Garrido *et al.*, 2003, Erbse *et al*., 2004). HSP 72 is the inducible form, whereas HSP 73 is consititutively expressed (Giffard and Yenari, 2004). Although there is a relatively high conservation of the gene sequences between HSP 72 and HSP 73 suggesting similar roles, the different expression profiles under normal and stress conditions indicate that they are differentially regulated (Ikeda *et al*., 1999). Expression profiles of HSP 72 and HSP 73 following IR injury were investigated; however, this study did not demonstrate any conclusive trend in expression for either type.

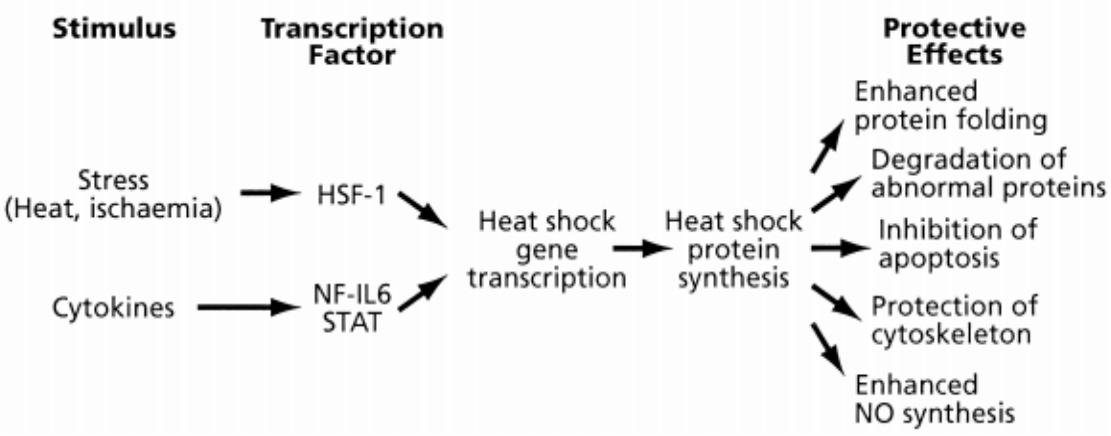

Figure 4.14. Induction of HSPs by specific stimuli and their protective effect. (Latchman, 2001)
HSF–1, heat shock factor protein–1; NF–IL6, nuclear factor for interleukin 6; STAT, signal transducer and activator of transcription.

Most of the studies of HSP 72 have focused on stressed hearts, such as treatment of hyperthermia, exercise or hypoxia prior to IR (Staib *et al*., 2007, Wakisaka *et al*., 2007, Staib *et al*., 2009). It was first reported that HSP induction by hyperthermia confers cardioprotection from ischaemia; this phenomenon is known as cross–tolerance (Currie *et al*., 1988). Hyperthermic

treatment improved functional recovery and reduced CK release following global IR. Ischaemic preconditioning has shown cardioprotection with elevated HSP 72 expression. Knowlton *et al*. (1991) demonstrated that a single 5 minutes coronary occlusion doubled HSP 72 expression, whilst 4 cycles of 5 minutes of IR increased it by 3 – fold. Marber *et al*. (1993) also reported reduction in infarct size and induction of HSP 72 as a result of pre–treatment of 4 repetitive cycles of 5 minutes ischaemia and 5 minutes of reperfusion, 24 hours before the hearts were subjected to 30 minutes of occlusion and 120 minutes of reperfusion.

Apart from the chaperone function, HSP 72–induced cardioprotection during IR injury was proposed to associate with enhanced MnSOD activity (Suzuki *et al*., 2002). MnSOD limits mitochondria–related apoptosis by scavenging superoxide produced within the organelle. HSP 72 overexpression also retards IR–induced apoptosis via caspase–dependent and –independent pathways, by binding with apoptosis protease–inducing factor, inhibiting subsequent activation of caspase–9 and caspase–3 (Ravagnan *et al*., 2001). Furthermore, expression of HSP 72 in transgenic mice protects against post–ischaemic myocardial dysfunction as shown by preserved ventricular peak systolic pressure (Trost *et al*., 1998).

There have been few investigations of HSP 72 expression in heart in the native state. One of the few studies conducted by Yu *et al.* (1999) demonstrated that 30 minutes of LAD occlusion followed by 4 hours of reperfusion induced higher levels of HSP 72 expression compared with either 24 hours or 7 days of reperfusion. Here, regardless of the durations of ischaemia or methods of induction, the expression of HSP 72 was not significantly altered, when compared to the control group. Previously a correlation between the degree of stress, the amount of HSP 72 induced and the level of cardioprotection was reported (Donnelly *et al*., 1992), thus a critical amount of HSP 72 may be necessary to confer protection from ischaemic injury (Knowlton *et al*., 1991, Marber *et al*., 1993). Donnelly *et al*. (1992) were able to demonstrate a significant reduction in infarct size after whole body heat stress treatment, whereas ischaemic pre–treatment with a

single 20 minutes coronary occlusion failed to decrease the infarct size or alter HSP 72 to the level seen after heat stress. Therefore, this suggests that the stress induced by the three IR conditions in this study may have been insufficient to cause differential HSP 72 levels.

Despite no significant changes being found in HSP 73 expression in this study, its expression in 7–day neonatal rat hearts doubled following 4 hours of hypoxia, but with no change in HSP 72 mRNA (Ikeda *et al*., 1999), in contrast to the observations described above. It has been reported that HSP 73 overexpression (Chong *et al*., 1998), and activation by stress (Su *et al*., 1999) in H9c2 cardiac myoblasts confer protection against oxidative injury.

In conclusion, the microfluidic approach described here is a simple method for induction of IR injury in small heart biopsies, which is applicable for analysing clinical samples from patients undergoing CABG. While expression of other genes was not altered as a result of both IR procedures, eNOS expression demonstrated a rise that tended towards significance following 40 minutes of oxygen–deprived ischaemia, similarly at 20 minutes, whereas iNOS expressions were significantly increased in 40 minutes of ischaemia. Nitrogen–induced ischaemia did not exert as strong an IR injury effect as the oxygen–deprived ischaemia. Despite small experimental repeat and insufficient IR stress, this microfluidic platform offers the opportunity to understand the molecular mechanisms involved in myocardial protection during IR injury, thus providing the translation into clinically relevant therapeutic or preventive strategies.

Chapter 5

Generation 2
Perfusion System

To generate a comprehensive understanding of cells or tissues, the ability in performing multiple studies under a controllable microenvironment within a chip is essential. The number of integrated microfluidic device for multiple cell or tissue manipulations and assays on–chip is increasing in the past few years. For example, an integrated microfluidic device for intestinal tissue maintenance and monitoring has been described; with its polarized transport activity being measured using on–line optical fiber detection system (Kimura *et al*., 2008). Another multifunctional microfluidic cell culture platform was proposed for endothelial cells perfusion and on–chip analysis, where cell morphology and permeability were analyzed in response to pulsatile and oscillatory shear stress (Shao *et al*., 2009).

A Generation 2 glass device has been fabricated, where microchannels were etched on a glass layer for media flow, resembling blood vessels. Two different methods of assembly of components onto the glass chip (namely Generations 2.1 and 2.2) were tested. Unidirectional perfusion media delivery was achieved using a syringe pump, constantly supplying the tissue sample with nutrients and removing waste products. In addition, an incubator box was designed to contain all relevant equipment and maintain the internal temperature (Figure 2.10).

Generation 2 perfusion system was characterized for optimal control of temperature, fluid flow and gas compositions, prior to perfusion experiments. With the optimised parameters established using the Generation 1 perfusion system, viability of rat heart tissue was again tested within the sealed glass chip. LDH activities measured in the effluent samples were used as before as the marker of tissue damage during the perfusion period.

The main objective of this study was to establish an optimised glass microfluidic device for heart tissue perfusion which allowed monitoring of its viability and responsiveness simultaneously.

5.1. Glass chip design, assembly and optimisation

A glass microfluidic chip was designed (Figure 2.7) and manufactured by Dr Steve Clark in the Microfabrication Laboratory (Department of Chemistry, University of Hull). The chip was composed of two layers of glass; with an upper layer (3 mm thick) containing holes of specific diameters, and a bottom layer (1 mm thick) in which channels (cross–sectional diameter = 150 µm) were etched. A nanoport reservoir assembly (Kinesis, UK) was bonded on top of the tissue chamber aperture according to the company instructions (Figures 2.8 A and B). The tissue chamber had a volume of 21.2 µl in which a tissue sample of approximate dimensions of 2.5 x 4 x 2 mm^3 could be contained.

Two different Generation 2 glass chips have been assembled, named Generations 2.1 and 2.2 (Figure 2.8). Ferrules (GC Supplies, Australia) and Araldite adhesive (Bostik Findley Ltd, UK) were used to connect PEEK tubings to ports A – E in Generation 2.1 (Figure 2.8.A). For Generation 2.2, however, headless 6 – 32” coned nanoport assemblies (Kinesis, UK) were used to hold tubings in ports A – E and stimulation electrodes, according to company instructions (Figure 2.8.B).

Electrical stimulation electrodes in Generation 2.1 consisted of platinum wire fused to glass capillary as shown in Figure 2.9. They were bonded onto the glass chip by using Araldite adhesive. Furthermore, in Generation 2.2, the stimulation electrodes were platinum wires fed through the nanoport nut and held in place with Araldite adhesive. This allowed reuse of the electrodes.

One of the potential problems in using Araldite adhesive for bonding was the possibility of fluid leakage through the glass apertures and/or blocking the channels. With the current microfabrication technique, however, the apertures were not a perfect fit for the PEEK tubing, and hence increased the risk of leakage and subsequent channel blockage. Leakage of perfusion

media from underneath the Araldite adhesive was observed in some glass chips after long term (~ 24 hours) use at 37 ^{o}C, despite the claims of Chang *et al*. (2010) who used it to prevent leakage around the microfluidic device. Nanoports were used to replace Araldite adhesive in Generation 2.2 because (i) PEEK tubings could be exchanged and recycled, (ii) risk of channel blockage due to adhesive and leakage was markedly reduced, and (iii) amount of PEEK tubing required for each chip was reduced since gauge plugs could replace the nanoport nut at unused ports

5.1.1. Fluid flow

Fluid flow is a crucial element in all microfluidic systems. The fluid flow in this study was pressure–driven, as fluid was pumped through the microfluidic device via a syringe pump (Harvard Apparatus, UK). The fluid flow pattern in the Generation 2.1 device was examined, in which two streams of fluid: deionised water and red food colouring (Silver Spoon; diluted 1:10 in deionised water) were pumped through Generation 2.1 chip from left and right inlets, at a flow rate of 120 µl/minute.

It can be observed that the two streams of fluid flow laterally and the width (W) of diluted red food colouring was halved when two streams meet, even though the channels were not clearly defined in Figure 5.1.

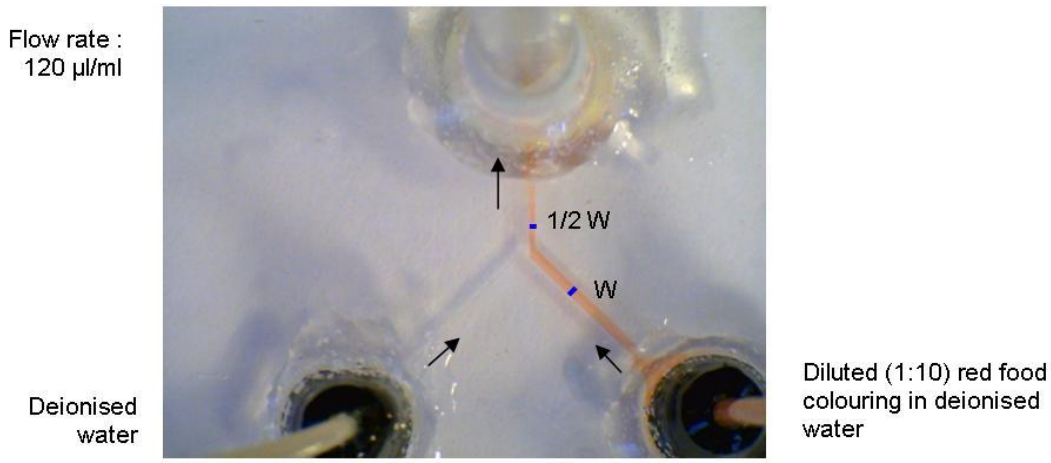

Figure 5.1. Laminar flow generated in the Generation 2.1 chip.
W, width; ↑,direction of flow.

The cross–sectional diameter of the channel in the device was 150 µm, viscosity and density of water were 8.9 x 10^{-4} Pa·s, and 1 kg/L, whereas the fluid velocity was 1.132 m/second (flow rate/cross–sectional area). The Re was 191, according to the Reynolds equation (Equation 2; Osborne, 1883). This Re corresponded to the laminar flow regime in the microfluidic device.

5.1.2. Incubator box design

An incubator box constructed in polycarbonate (trademarked name Lexan) was designed and manufactured in the Mechanical Workshop (Department of Engineering, University of Hull; Figure 2.10). Polycarbonate was the chosen material because of its high transparency, resistance to fracture, thermal insulation and ease of machining and bonding.

The dimensions of the incubator box and positioning of the access doors and ports were carefully designed, so that all necessary equipment could fit within sufficient space for sample manipulation. The incubator box had two access doors at the front, for transferring media–contained glass syringe and collecting effluent samples. The top panel of the incubator box could be lifted to place equipment (i.e. syringe pump, two heat mats, retort stand, hotplate) into the box. The cables of equipment were fed through the designated ports, and secured with individual cable glants. Furthermore, adhesive spongy tape sealed the gap between the sliding pane and the incubator box. The cable glants and adhesive spongy tape were used to minimise any heat lost.

5.1.3. Temperature control

A glass chip was put on the hotplate (Linkam Scientific Instruments, UK) and a type K thermocouple wire (TC Direct, UK) was placed on top (Figure 2.11), connected to a multi thermocouple type indicator (TC Direct, UK) to monitor chip temperature. The variation of the hotplate reading and the temperature of glass chip were monitored (Figure 5.2). In order to maintain the glass chip at 37 ^{o}C, the hotplate was set at 38.8 ^{o}C.

Two heat mats (52 cm x 28 cm, 28 W; Pennine Industries, UK) were placed at the bottom of the incubator box, and connected to two thermostats (Komodo, UK), to regulate the temperature within the incubator box. Thermostats were turned to maximum (30 ^{o}C), and the variation of the temperatures of glass chip and incubator box internal environment was monitored. The incubator box internal temperature measured by a digital thermometer suspended in the centre of the incubator box ceiling. The internal atmosphere gradually increased and maintained at 28.7 ± 0.12 ^{o}C by the thermostats (30 ^{o}C). The glass chip heated directly by the hotplate was maintained at 37 ± 0.16 ^{o}C throughout the experiment when the hotplate was set at 38.8 ^{o}C (Figure 5.3).

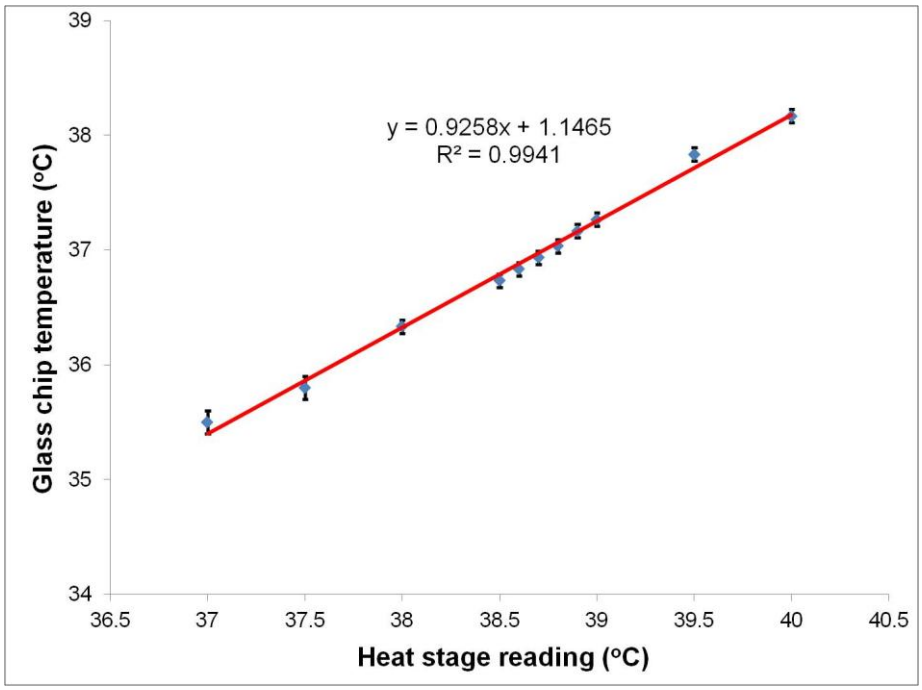

Figure 5.2. Variation of hotplate reading and glass chip temperature. Error bars indicate the standard deviation of 3 repeats.

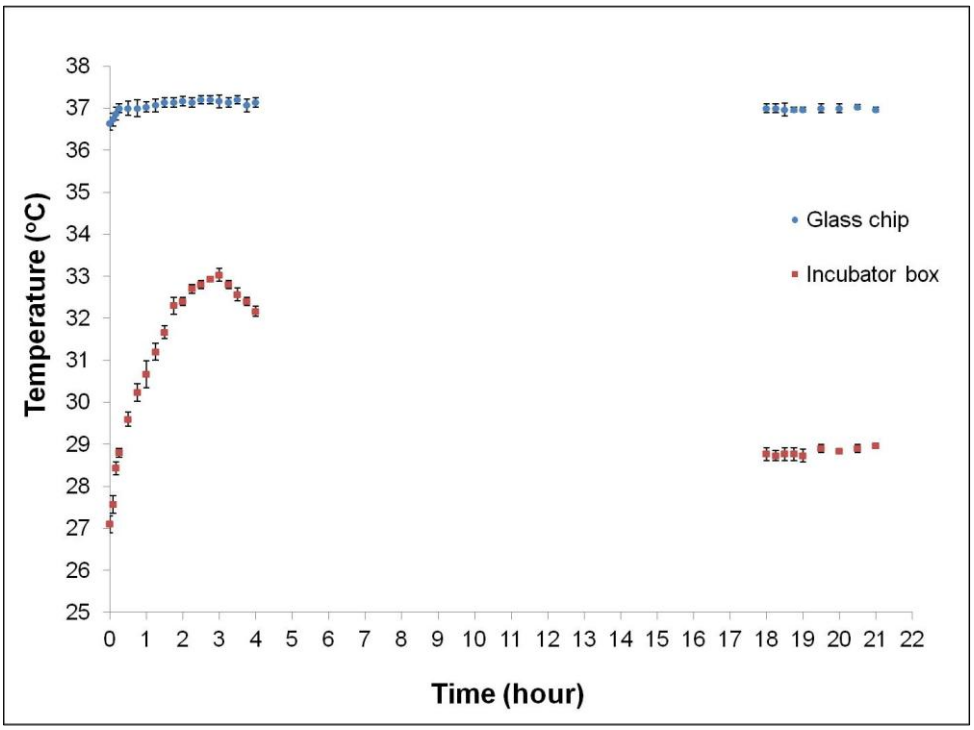

Figure 5.3. Variation of the temperatures of glass chip and incubator box internal environment with time. Measurements were not taken between 4 – 18 hours during which the setup was left overnight. Error bars indicate the standard deviation of 3 repeats.

5.1.4. Oxygen content

Oxygen is a critical factor in maintaining the viability of heart tissue. Thus, a series of tests were performed to ensure that the heart tissue had sufficient oxygen supply within the sealed glass chip.

Perfusion media, KHBB, was gassed with 95 % O_2 / 5 % CO_2 for various time intervals in the water bath at 37 ^{o}C and 200 µl aliquots were taken from the reservoir for partial pressure of oxygen (pO_2) measurements; pO_2 of KHBB was achieved in the range of 580 – 620 mmHg after oxygenation for at least 15 minutes (Figure 5.4). However, a standardized 30 minutes of KHBB oxygenation was performed before commencing an experiment.

Oxygenated KHBB was transferred into a glass syringe and the syringe was connected to the glass chip via adaptors and PEEK tubing. KHBB was perfused through the glass chip (without heart tissue sample) and its pO_2 checked. Effluent samples (200 µl) were collected at the end of the chip over 10 hours for pO_2 measurement. A 20 ml glass syringe was used for short perfusion experiments (e.g 2.5 hours); whereas 100 ml glass syringe was mainly used for long period perfusion study, up to 13 hours. After being oxygenated for 30 minutes at 37 ^{o}C, the pO_2 of KHBB was 635.7 ± 17.6 mmHg and 668.3 ± 11.2 mmHg from two separate experiments, before being delivered into a 20 ml and 100 ml glass syringes, respectively (Figure 5.5). The initial *p*O2 measurements were 268.7 ± 96.5 mmHg and 448.5 ± 9.19 mmHg in 20 ml and 100 ml glass syringes, respectively. This may be due to the lost of oxygen to the environment during the procedure of handling and connecting glass syringe contained media to the perfusion system.

After 20 minutes of perfusion, pO_2 levels were maintained in a range of 400 – 450 mmHg and 520 – 580 mmHg until the 20 ml and 100 ml glass syringes were emptied, respectively. This highlighted the need for priming the system for at least 20 minutes, before introducing a tissue sample into the tissue chamber to get to a steady state level.

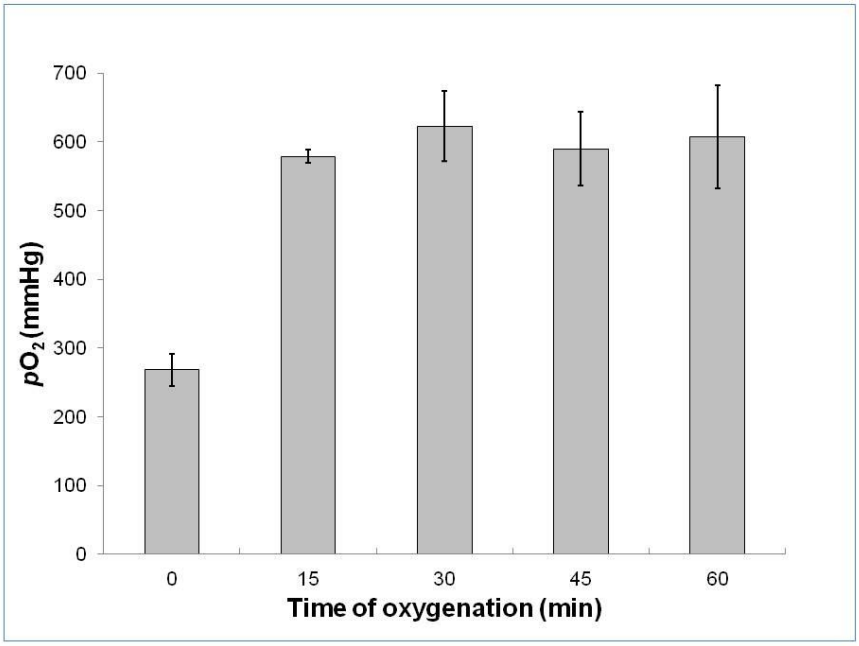

Figure 5.4. pO_2 in KHBB after being gassed with 95 % O_2 / 5 % CO_2 for various periods. Error bars indicate the standard deviation of 4 repeats.

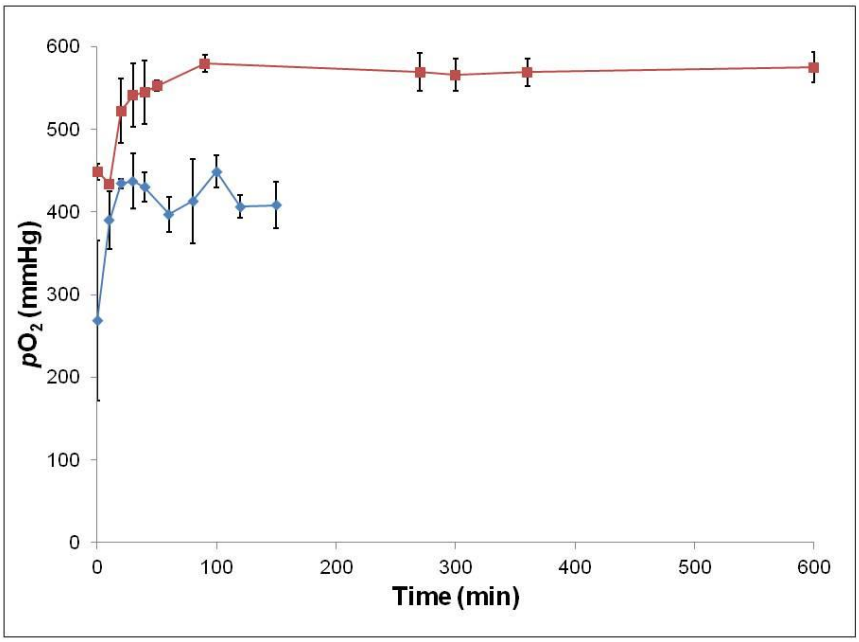

Figure 5.5. pO_2 in KHBB perfused through a glass chip without heart tissue sample, using 20 ml (blue) and 100 ml (red) glass syringes. Error bars indicate the standard deviation of 3 repeat experiments.

5.2. Perfusion data

Right ventricular rat tissue was perfused within the glass chip (Section 2.4) to determine its viability and stability in the Generation 2 perfusion system. Effluent samples (240 µl) were collected every 5 minutes for the first 60 minutes and during Triton X100 perfusion and every 10 minutes thereafter, and stored at –20 ^{o}C for LDH analysis (Section 2.6). The system was primed for 20 minutes prior to introduction of tissue. Then the syringe pump was paused whilst transferring a tissue sample into the tissue chamber.

LDH release from three separate rat heart tissues (A, B, and C) is shown in Figure 5.6. The initial high level of LDH due to excision of tissue samples were observed as expected. These were 'washed out' in the first 15 – 30 minutes and maintained at a low level (below 20 U/ml/g) for sample B and C. The time taken for LDH of sample A to come to steady level was 70 minutes. The LDH released from sample A was about 3 times higher than that of B and C at 10th minute (A: 86.16 U/ml/g, B: 15.22 U/ml/g, C: 13.16 U/ml/g), but all samples showed gradual LDH decrease with time. However only sample A was maintained viable in this perfusion system, releasing 159.75 U/ml/g of LDH during Triton X100 perfusion. In contrast, LDH activities for samples B and C were not elevated when they were exposed to Triton X100.

In both experiments A and B, a bubble was found trapped in the tissue chamber when introducing tissue sample into the system when the perfusion flow was paused, probably due to the atmospheric pressure (Figure 5.7). To prevent this circumstance, the syringe pump was kept turned on for subsequent tissue loading when the gauge plug of the tissue chamber was taken off for tissue sample introduction. Perfusion media was allowed to overfill the tissue chamber before the gauge plug was screwed and sealed the tissue chamber. The precaution ensured that no bubbles formed in the chamber.

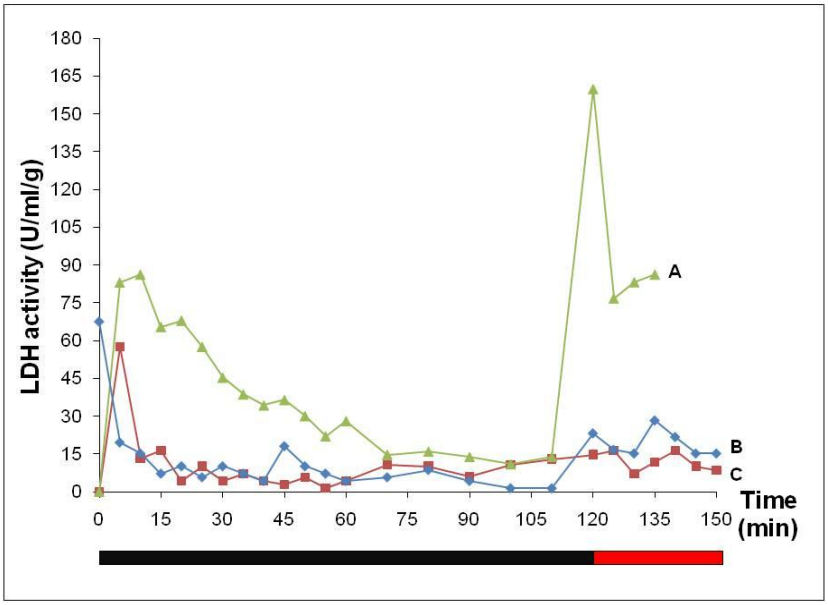

Figure 5.6. LDH release from rat right ventricular tissues perfused for 2 hours with KHBB (black bar), followed by 30 minutes with 2 % (w/v) Triton X100 in KHBB (red bar). A, B and C were individual heart tissue samples from different rats.

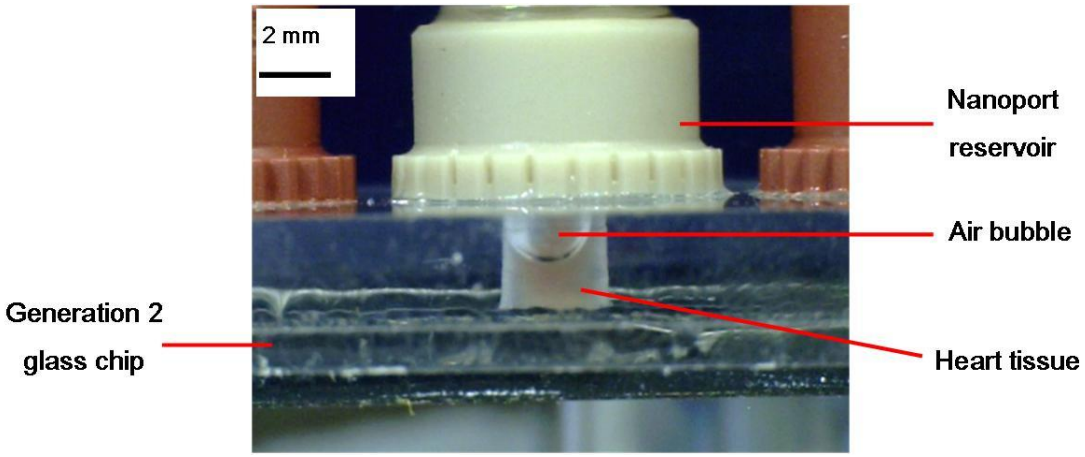

Figure 5.7. Bubble trapped in the tissue chamber (horizontal view).

5.2.1. Directions of media flow

Flow was introduced either: (I) from the top (Figure 5.8 A); or (II) from the side (Figure 5.8 B). Heart tissue was perfused for 2 hours with oxygenated KHBB, and then exposed to 2 % (w/v) Triton X100 in KHBB for 30 minutes. Effluent collection and LDH assay were done as described in Section 5.2.

Upon Triton X100 perfusion, increases in LDH activities were elicited as shown in both Figures 5.8.A and B (137.76 U/ml/g and 254.35 U/ml/g, respectively), indicating that tissue viability was unaffected by either flow directions. In both cases, the sample was introduced into the tissue chamber while the syringe pump was running, allowing overfilling of the tissue chamber. Perfusion medium was pumped in the direction as in Figure 5.8.B for the subsequent experiments as this was most similar to the fluid flow from the Generation 1 device.

5.2.2. Electrical stimulation

The impact of electrical stimulation on LDH release was investigated. Heart tissue samples were electrically stimulated using platinum wires connected to a programmable function generator (Thurlby Thandar Instruments, UK) at 3 – 4 V/cm, 1.5 Hz. An episode of 30 minutes 2 % (w/v) Triton X100 in KHBB perfusion was induced following 2 hours of oxygenated KHBB perfusion. Effluent samples (~ 240 µl) were collected as previously described and stored at –20 ^{o}C for LDH analysis (Section 2.6).

In the absence or presence of electrical stimulation, heart tissue released an increased LDH activity following Triton X100 addition and the general profile of damage pattern was similar (Figure 5.9). Nevertheless, LDH activity was significantly greater in the absence of electrical stimulation after 2 hours (341.74 U/ml/g versus 197.16 U/ml/g). Electrical stimulation was maintained throughout the perfusion in the following experiments, as this best mimicked the *in vivo* situation.

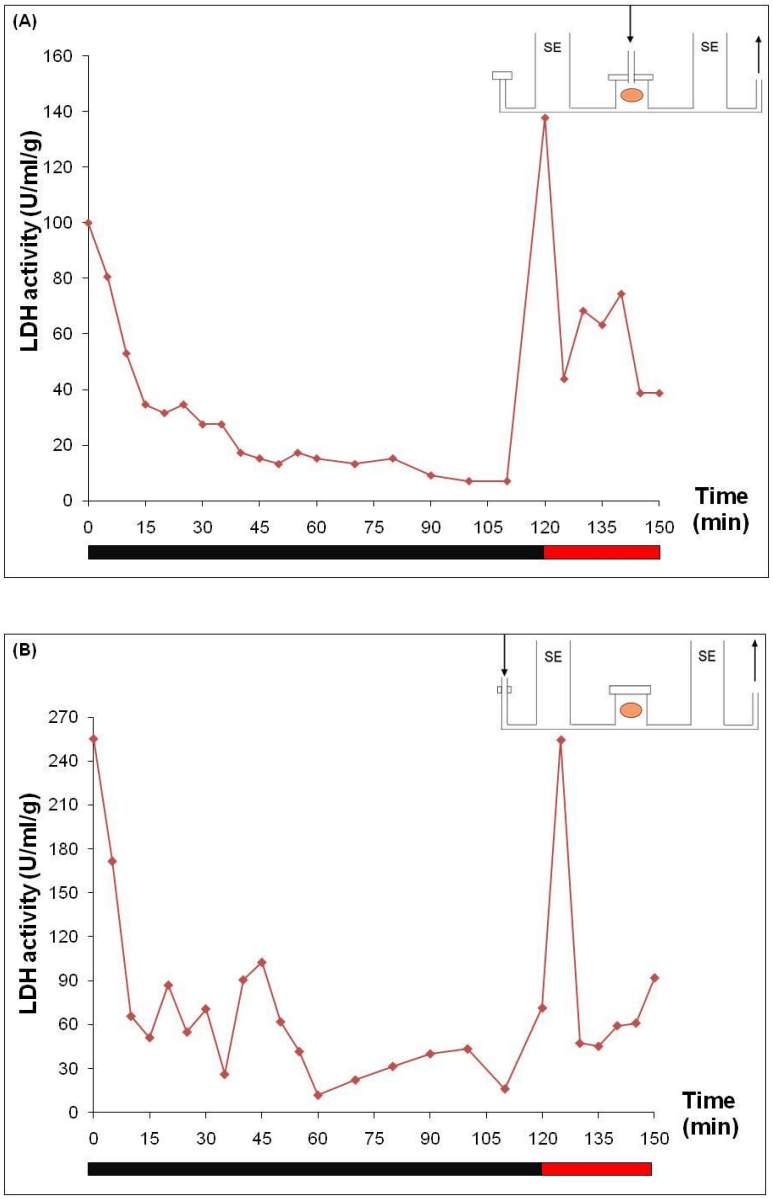

Figure 5.8. LDH release from rat right ventricular tissues perfused for 2 hours with KHBB (black bar), followed by 30 minutes with 2 % (w/v) Triton X100 in KHBB (red bar). Heart tissue samples (orange oval) were perfused from the top (A), and from the side (B), respectively, as shown in the sketches on top right corners. N = 3 for each condition.

SE, stimulation electrode

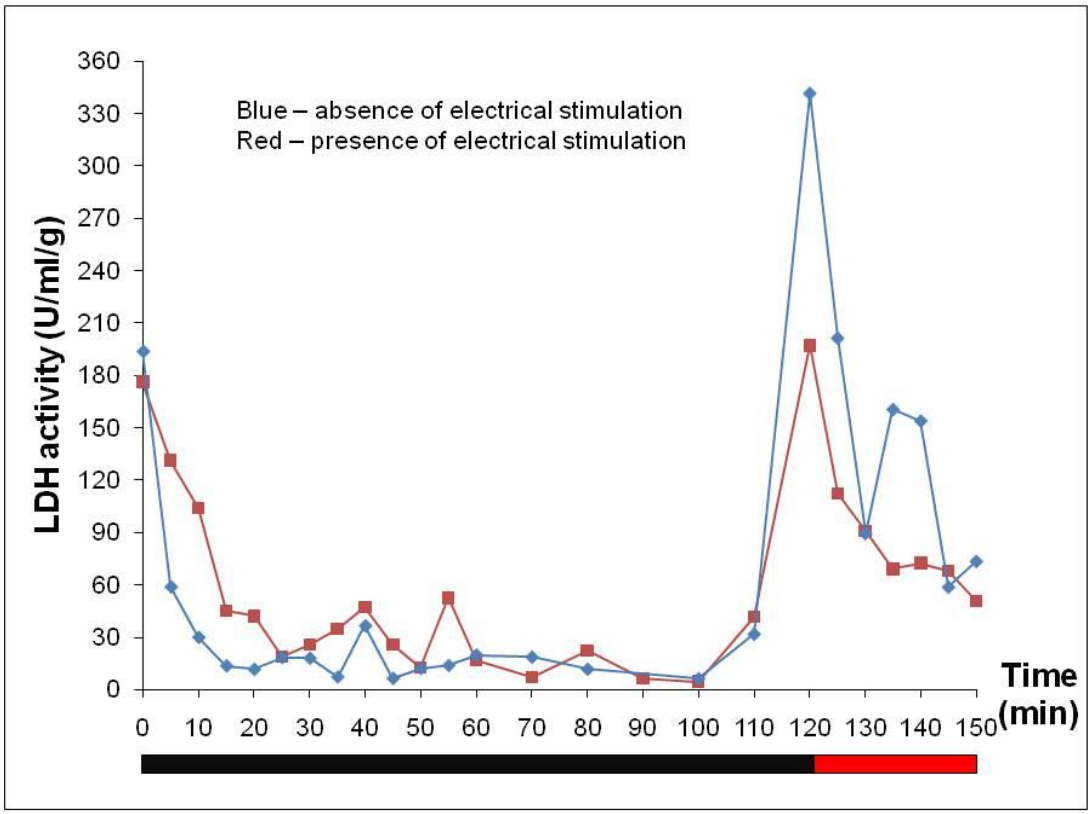

Figure 5.9. LDH release during 2 hours KHBB perfusion of rat right ventricular tissues (black bar), followed by 30 minutes with 2 % (w/v) Triton X100 in KHBB (red bar). Blue and red lines represent the absence and presence of electrical stimulation during the entire perfusion, respectively. N = 2 for each condition.

5.2.3. Length of perfusion period

The optimised parameters were used in the studies of tissue viability using the Generation 2 perfusion system. The perfusion period was extended to 5 hours and finally to 24 hours. The sample was then exposed to Triton X100 for 30 minutes. Effluent samples were collected and stored as previously described for LDH analysis.

Similarly to profiles previously observed, the LDH activity declined within the first hour and then maintained at low level as perfusion went on until Triton X100 was introduced (Figures 5.10.A and B). The LDH peaks were 128.24 U/ml/g and 355.85 U/ml/g for 5–hour and 24–hour perfusion, respectively.

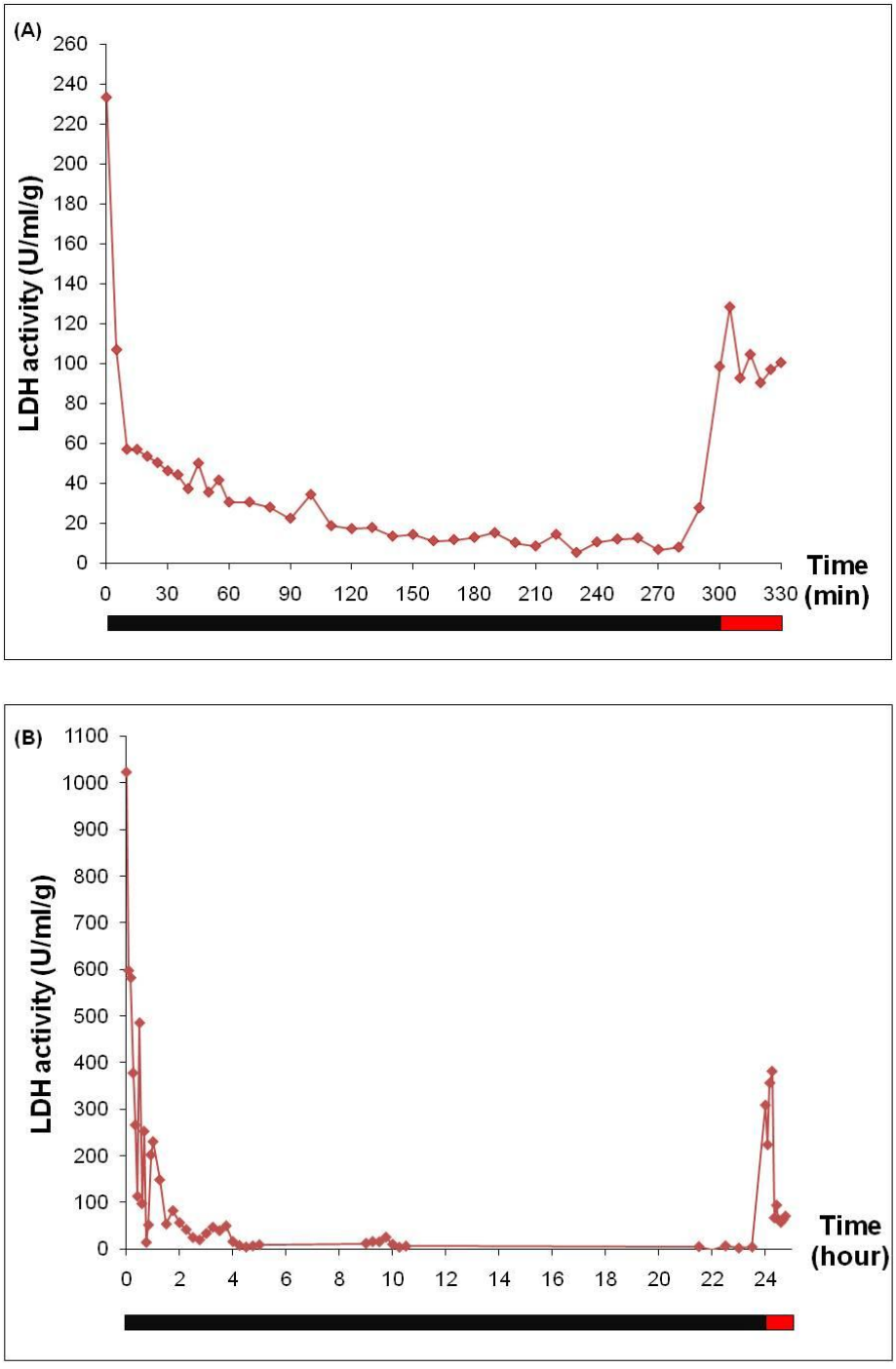

Figure 5.10. LDH release from rat right ventricular tissues perfused for (A) 5 hours and (B) 24 hours with KHBB (black bar), followed by 30 minutes with 2 % (w/v) Triton X100 in KHBB (red bar). Electrical stimulation was maintained throughout the experiment. A and B are individual representative experiments. N = 2 (5 hours); N = 4 (24 hours)

5.3. Discussion

A sealed Generation 2 glass chip has been developed for maintenance of heart tissue. Optimised parameters that have been used previously in Generation 1 system including tissue size and electrical pacing were applied. An incubator box was built to contain all equipment and a syringe pump was used to flow the perfusion media. This glass chip (Generation 2.2) was able to maintain rat right ventricular tissue viable for up to 24 hours in contrast with 5 hours in the Generation 1 perfusion system (Chapter 3).

The Generation 2 perfusion system was designed and manufactured taking into account the following variables: the choice of materials of tubing, syringe type, incubator box design. Capillary PEEK tubing was used to deliver buffer from the glass syringe to the glass chip because it is least permeable to gas compared with other polymer tubings. PEEK tubing is opaque, so it is not possible to see bubbles within the tubing, nevertheless, the flexibility of PEEK tubing makes it a good choice for use as it can withstand being bent to fit into the connectors of the chip. For example, PEEK tubing that connected the glass chip and led to the eppendorf tube was bent to 90 degrees for effluent sample collection (Figure 2.11).

In addition, glass syringes were used instead of plastic ones because of the lack of permeability to oxygen (Scott *et al.*, 1971, Wiwanitkit, 2006). Oxygen in blood or water samples stored in syringes made of polypropylene or polystyrene exchanges rapidly with the environment (Scott *et al.*, 1971). Glass syringes are better than plastic in preserving arterial blood gas for pO_2 examination based on nanomaterial composition (Wiwanitkit, 2006). The size of the oxygen molecule was calculated based on the chemical bonding principle, and the relative pore sizes and densities of the glass and plastic were estimated. Under controlled temperatures and other environmental factors, oxygen has a ~ 150 times greater probability of diffusion across

plastic than glass, owing to the greater overall porous nature of plastic. Therefore glass syringes were chosen in this study.

The incubator box was designed for ease of use. The temperature of the glass chip was mainly controlled by the hotplate temperature, instead of the internal temperature of the incubator box (Figure 5.3). The tissue sample was kept at the optimal temperature, to reflect the *in vivo* condition. The buffer contained in the glass syringe was maintained at 30 ^{o}C during the perfusion, but the buffer temperature was raised and equilibrated to 37 ^{o}C at the glass chip as demonstrated in Figure 5.3. The conduction from the hotplate to the tissue chamber is mainly determined by the material of which the microfluidic device consisted. Compared with the Generation 1 microfluidic device, glass had higher heat conduction than PDMS, determined by thermal conductivities (Shin *et al*., 2003). The thermal conductivities for glass and PDMS are 1.13 W/mK and 0.17 W/mK, respectively. Accordingly, the Generation 2 glass chip offers a better temperature control for heart tissue maintenance.

The rate of perfusion media delivered from the glass syringe to the glass chip was controlled by the syringe pump. Compared with the Generation 1 perfusion system which used two peristaltic pumps to transfer fluid in and out from the microfluidic device, only one syringe pump was used in this enclosed perfusion system. Overheating of the peristaltic tubing by friction of the pump rollers modified the physical properties of the plastic and led to variations of flow rate (Ba *et al*., 2001). However, Ba's group prevented this inconsistency in flow rates by using computer–controlled syringe pumps. In the present study, the risk of uneven flow due to inconsistency of two independent pumps was eliminated in the Generation 2 perfusion system. This is particularly important especially for long–duration experiments where heart tissue can be perfused continuously without frequent monitoring.

In microfluidics, it is often necessary to interface the chip using tubings. Araldite adhesive has been commonly used to secure tubings on glass chips (Wang *et al*., 2007, Lanigan *et al*., 2009), as in Generation 2.1 glass chip. However, this caused a number of problems as the tubing was not always a

perfect match for the reservoir hole. Thus when using Araldite adhesive to attach tubing, the glue can seep into the aperture and clog the microchannel. Commercially available nanoport assemblies were used in Generation 2.2 glass chip to offer reliable fluid connections via preformed adhesive rings, with no additional volume added to the fluidic path. These nanoports have also been used by other microfluidic researchers to interface microfluidic devices (Li and Lee, 2004, Abbyad *et al*., 2010, Morshed *et al*., 2011).

Unwanted bubbles introduced into a microfluidic perfusion system can markedly affect the device operation and experimental outcome (Cheng and Jiang, 2009). During the course of perfusion, the system may be interrupted, disconnected and reconnected for glass syringe replacement; this increases the possibility of air bubbles accumulation in the device. The opaque PEEK tubing prevents the observation of bubbles trapped in the fluidic line. If air bubbles are present in the device, they may obstruct the fluidic line, distort the laminar flow, and damage the cells at the liquid–gas interface (Kim *et al*., 2007). The heart tissue was not fully immersed in perfusion media due to the presence of air bubbles; therefore it received insufficient oxygen, nutrients, and electrical stimulation (Figure 5.6.B and C). Several studies have shown that air bubble formation within the chip could be prevented by incorporating a bubble trap before the main system (Leclerc *et al*., 2003, Sung and Shuler, 2009), or integrating bubble trap and debubbler (Skelley and Voldman, 2008, Cheng and Jiang, 2009).

Maintenance studies and interrogations on various types of tissue samples within microfluidic devices, or tissue–on–a–chip, for different lengths of time have been reported. For instances, liver tissues [24 hours (van Midwoud *et al.*, 2010) and 70 hours (Hattersley *et al*., 2008)], human colorectal tissues [70 hours (Webster *et al.*, 2010)], head and neck tumour tissue [8 days (Sylvester *et al*., 2010)] and brain hippocampal slices [4 weeks (Berdichevsky *et al*., 2009)]. However, studies on intact heart tissue section in microfluidic perfusion system have not yet been documented. This is the first study demonstrating that heart tissue was successfully maintained viable

in a glass microfluidic device for 24 hours, with controlled oxygen level, temperature, nutrients supply and waste removal.

Interrogation of the functionalities of various tissue samples in microfluidic devices has been reported. Albumin and urea syntheses (Hattersley *et al*., 2008) as well as 7–ethoxycoumarin metabolism (van Midwoud *et al.*, 2010) have been investigated in liver biopsies. Albumin is the most abundant protein produced by hepatocytes, and urea production only occurs in liver. Hence albumin and urea serve as markers of liver function (Peters *et al*., 2008). 7–ethoxycoumarin also acts as a positive control compound to demonstrate metabolic capacity in hepatocytes (Hamilton *et al*., 2001). In this investigation, tissue viability was determined by the release of LDH into the perfusion media. Functionality or contractility, however, has not yet been examined. The release of cardiac damage marker, CK will be measured electrochemically (See Chapter 8). In addition, contractile force and action potential investigations on the heart tissue will be performed in the future, where miniaturised, ultrasensitive, force transducer systems and optical devices are integrated with the current perfusion system.

In conclusion, a Generation 2 glass microfluidic device and a more controllable perfusion setup have been developed for heart tissue maintenance for up to 24 hours. Although only rat heart tissue was investigated in this study, it offers, like Generation 1 system, the opportunity for monitoring clinical biopsies where sample size is usually small. Not only does this device have the benefit that clinical samples can be analysed, there should also be reduction in animal experimentations, contributable to the UK government's aim of Reduction, Refinement, and Replacement (3Rs) of animal work.

Chapter 6

Ischaemia Reperfusion

in

Generation 2 Device

Understanding the genetic changes in response to the energetic crisis arising from limitation of oxygen supply during myocardial IR is essential for the new development of therapies. In addition to the stress genes described and discussed in Chapter 4, a series of additional gene products were examined here. These include BNP, CK–M, CKmito and TnT.

BNP, first isolated from porcine brain (Sudoh *et al*., 1988), is released in response to enhanced tension in the ventricular wall that usually accompanies MI (Schrier and Abraham, 1999, Boomsma and van den Meiracker, 2001). Generally, a normal level of plasma BNP level is 17.3 ± 8.1 pg/ml (Günes *et al*., 2008). It has been well established that BNP plasma levels are increased after MI and associated with LV dysfunction (Maisel, 2001, Cowie and Mendez, 2002). BNP levels with different heart failure classes are listed in Table 1.3. Goetze *et al.* (2003) have reported that myocardial hypoxic ventricular biopsies from patients undergoing CABG surgery had elevated BNP mRNA expression which was positively associated with augmented plasma concentrations of BNP.

CK is the key enzyme in the phosphocreatine shuttle that transfers a high energy phosphate bond from ATP and creatine to generate phosphocreatine (Figure 1.5; Bessman and Geiger, 1981). The myofibrillar–bound M isoenzyme (CK–M) predominates in the heart and is localized at the thick filaments of contractile apparatus, whereas CKmito is the isoform located on the outer surface of the mitochondrial inner membrane, where it is functionally coupled with ANT (Khuchua *et al*., 1998). CK–MB mass of ≥ 7 ng/ml in plasma is the diagnostic standard for patients with MI (Zimmermann *et al*., 1999). The majority of the IR studies measured CK activity and protein expression, but only a few have examined the CK–M and CKmito gene expressions following IR (Mehta *et al*., 1988, Hoang *et al*., 1997, Neubauer *et al*., 1998).

The presence of circulating TnT in bloodstream also serves as a specific indicator of myocardial damage; plasma TnT ≥ 0.03 µg/l is now routinely

used to diagnose MI (McCann *et al*., 2008). Generally, plasma concentration and/or protein expression of TnT were measured in myocardial IR models, whilst its mRNA expression was not investigated (Chen and Ogut, 2006, Haubner *et al*., 2010, Jan *et al*., 2010).

The expressions of BNP, CK–M and CKmito genes have been shown to be altered as a result of IR in clinical and experimental studies (Hoang *et al*., 1997, Neubauer *et al*., 1998, Goetze *et al*., 2003, Goetze *et al*., 2004, Ramos *et al*., 2009, Möllmann *et al*., 2010). Although TnT expression was changed during muscle adaptation to stress or functional demands in a rat hindlimb suspension model (Yu *et al*., 2007), its expression following myocardial IR has not been previously investigated. Following the IR simulation using the Generation 1 device (Chapter 4), a more controllable and defined Generation 2 microfluidic system in terms of temperature and oxygen content (Sections 5.1.3 and 5.1.4) was used in this study. Delivery of media was from the glass syringe via PEEK tubing, which is minimally permeable to oxygen, and ultimately transferred to the glass chip using a syringe pump. There is limited or no diffusion from the environment to the media which created a better ischaemic insult within the chip. The aim of this chapter was to investigate the effect of IR on gene expression markers of injury in rat heart tissue using the Generation 2 perfusion system.

6.1. Optimisation of primers

In addition to the stress genes (eNOS, iNOS, HSP 72 and HSP 73) optimised in Chapter 4, PCR conditions for a further four more genes were optimised to provide a more comprehensive study of IR, they are BNP, CK–M, CKmito and TnT. Primer sequences for these genes are listed in Table 2.3. Three sequences were taken from published work and TnT primers were designed using the Primer Designing Tool from NCBI (http://www.ncbi.nlm.nih.gov/tools/primer-blast/). The primers were all subjected to a sequence check for their locations within the genome (Figure 6.1). CK–M and CKmito primer pairs span an intron, whereas the rest do not span or flank an intron. In order to ensure there was no gDNA contamination in the samples, a no–reverse–transcribed (no–RT) control (extracted RNA without RT reaction) for each sample was also subjected to PCR.

6.1.1. Volumes of BNP, CK–M, CKmito and TnT

Figures 6.2 and 6.3 show the optimisation of primers volume. Optimum volumes for BNP at 2 µl and the other primers at 1 µl were chosen.

6.1.2. Annealing temperature

Annealing temperatures of 60 ^{o}C, and 63.5 ^{o}C were tested for TnT; 59 ^{o}C, and 60 ^{o}C for CK–M and CKmito, all the bands produced were of similar intensities (Table 6.1 and Figure 6.3), and hence 60 ^{o}C was selected for subsequent PCR. In addition, BNP was amplified with annealing temperatures of 56 ^{o}C, and 60 ^{o}C, with greater intensities observed at 56 ^{o}C (Figure 6.2). No–RT controls showed no visible bands for BNP and TnT (data not shown), indicating minimal contamination with gDNA in any of the samples.

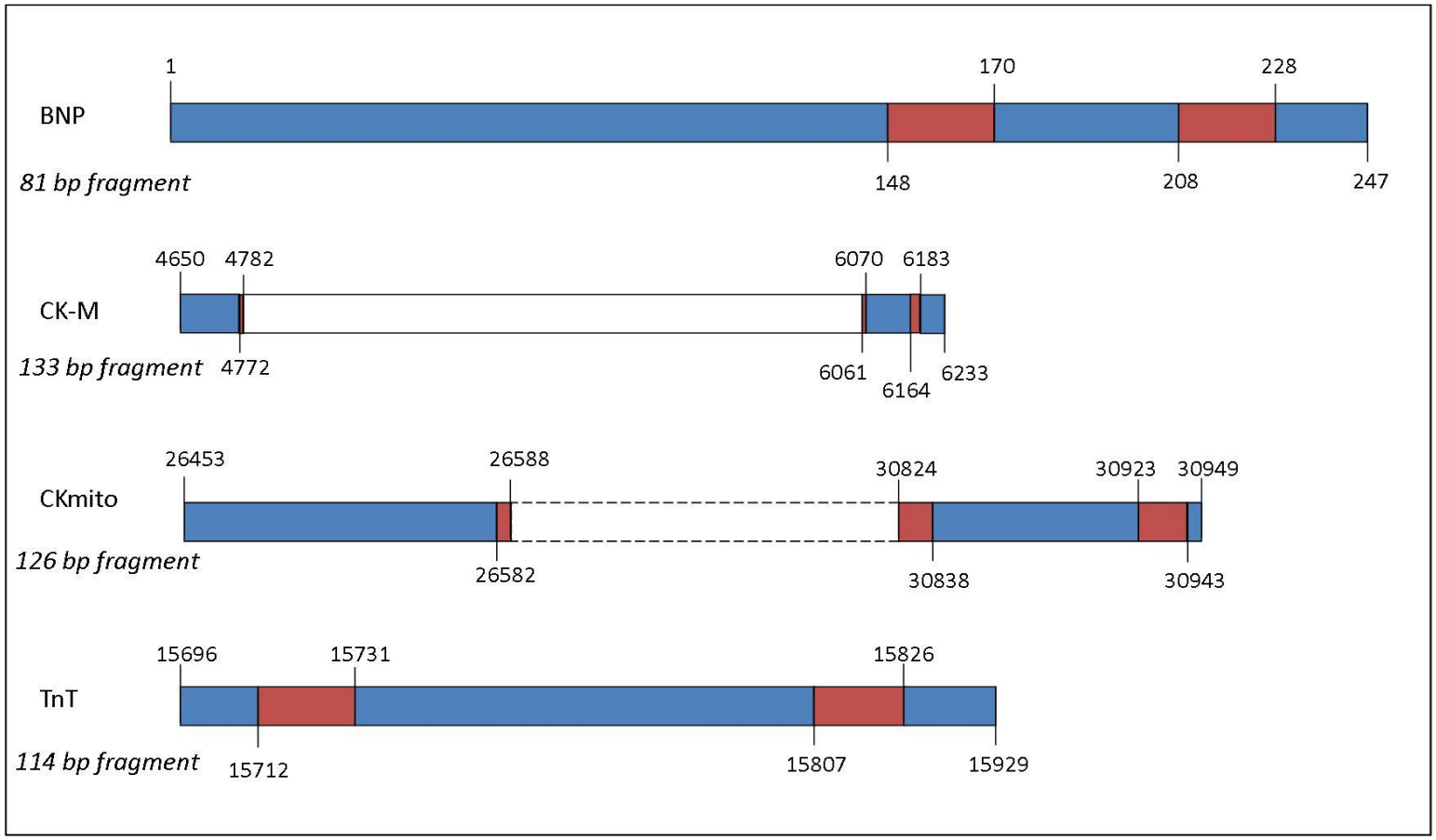

Figure 6.1. Primer locations for individual genes. Forward primers for CK–M and CKmito flank an intron, whereas BNP and TnT do not span/flank any intron.

(Number: base position from NH_2 terminal; Blue bars: exon; Red bars: primer positions in exon; White bar: intron)

Table 6.1. Annealing temperatures of genes.

Genes	Product length (bp)	Eurofins A_{temp} (°C)	NCBI A_{temp} (°C)	Reference paper A_{temp} (°C)
BNP	81	60.6 63.7	54.1 55.4	56
CK-M	133	61.8 61.4	55.2 56.6	59
CKmito	126	57.9 55.9	47.6 42.7	59
TnT	114	63.5 63.5	59.9 60.1	-

A_{temp}, annealing temperature

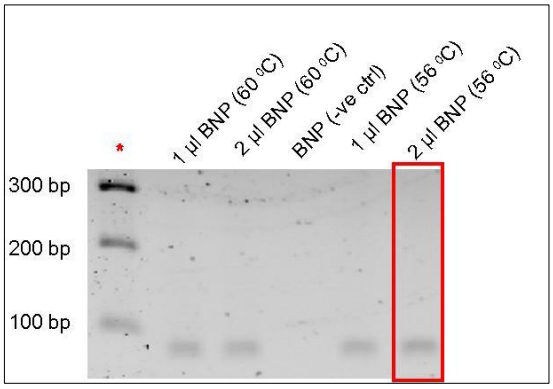

Figure 6.2. Representative gel comparing the intensity of BNP bands with different primer volumes and annealing temperatures.

*, *100 bp DNA ladder; -ve ctrl, negative control without primer*

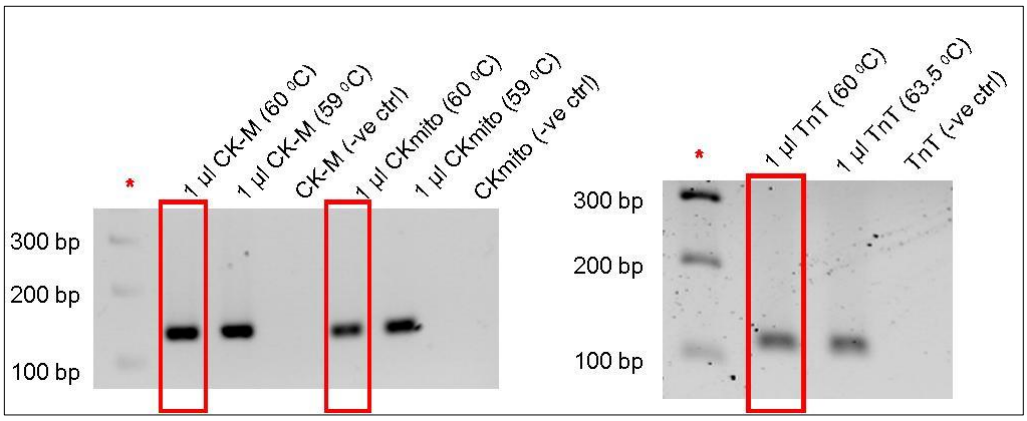

Figure 6.3. Representative gel comparing the intensity of CK–M, CKmito and TnT bands with different annealing temperatures**.**

*****, *100 bp DNA ladder; -ve ctrl, negative control without primer*

6.2. Oxygen levels in perfusion media

Many studies using IR protocols do not specify the oxygen content of the media used. In an isolated rat heart perfusion, the pO_2 during normoxia and hypoxia were 660 mmHg and 220 mmHg, respectively (Poizat *et al*., 1993). However, the arterial pO_2 of perfusion medium in the isolated hypoxic rat heart in another study were 70 – 90 mmHg, but the pO_2 during normoxia was not mentioned (Lin *et al*., 1997). Here, the pO_2 of the perfusion medium within the glass microfluidic device (without tissue sample) was measured prior to IR simulation, using the two types of IR regimes as described previously in Chapter 4.

Initially, KHBB was gassed with nitrogen for various time intervals at 37 ^{o}C and 200 µl aliquots were analysed for pO_2 measurements. The pO_2 of KHBB was maintained in the range of 35 – 38 mmHg after being gassed with nitrogen for at least 15 minutes (Figure 6.4). KHBB was gassed for a standardized 30 minutes before transferring into a glass syringe for use in a nitrogen–induced ischaemia episode. In addition, oxygenated KHBB was used during equilibration and reperfusion, whilst non-oxygenated KHBB was used to generate an oxygen-deprived ischaemia episode.

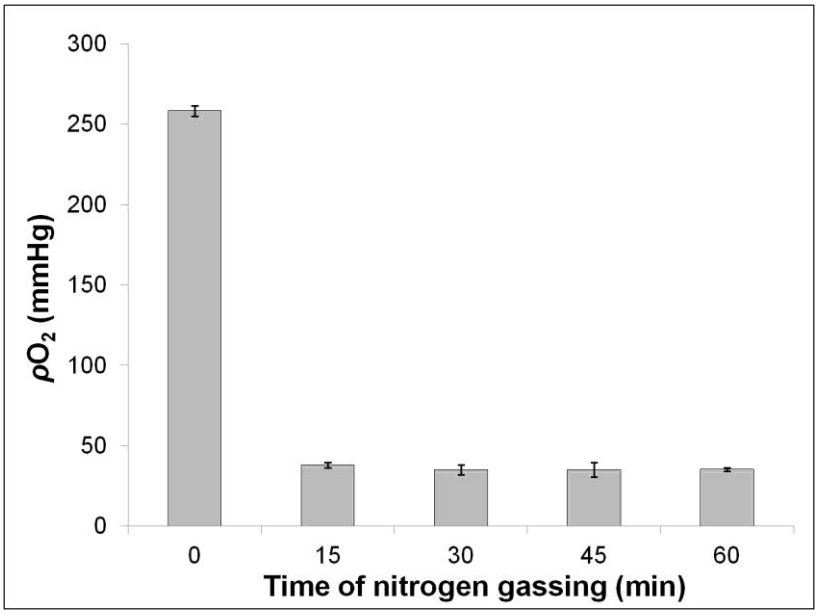

Figure 6.4. pO_2 in KHBB after being gassed with 95 % N_2 / 5 % CO_2 for various periods. Error bars indicate the standard deviation of 3 repeats.

For both regimes, effluent aliquots (200 µl) were taken from the outlet at 5 minute intervals for pO_2 measurements. The pO_2 of the KHBB during equilibration and reperfusion in the Generation 2 glass chip was greater than 300 mmHg, whereas the average of pO_2 were 214.53 ± 14.32 and 102.13 ± 4.03 mmHg during oxygen–deprived and nitrogen–induced ischaemia, respectively (Figure 6.5). These values are consistent with those determined in other hypoxic studies using isolated rat heart models (Poizat *et al*., 1993, Lin *et al*., 1997). The KHBB pO_2 in the glass syringe (102.13 ± 4.03 mmHg) was higher than the buffer reservoir after gassing with nitrogen for 30 minutes (35 ± 3 mmHg) because of the procedure of transferring gassed media from the reservoir to the glass syringes.

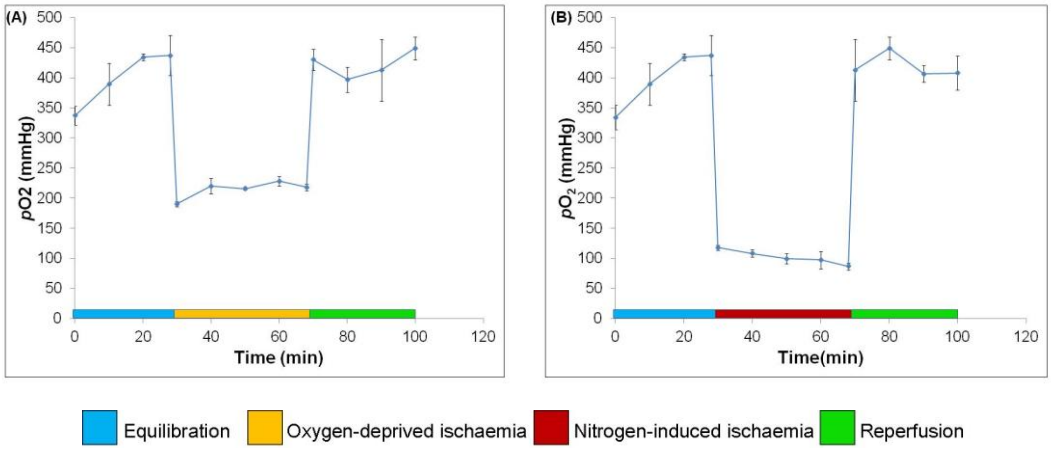

Figure 6.5. pO_2 in KHBB during the oxygen–deprived (A) and nitrogen–induced (B) IR procedures. Data are expressed as mean ± standard deviation. N = 3

6.3. PCR

Rat ventricular samples (N = 4 for each protocol) were subjected to the protocols as described in Figure 2.19. Control samples were perfused for the same length of time with oxygenated KHBB. A total of 8 genes were amplified, quantified and expressed relative to β–actin expression (Sections 2.11.7 – 2.11.9).

6.3.1. Oxygen–deprived IR (20 minutes ischaemia / 30 minutes reperfusion)

The expression profiles of genes relative to β–actin are shown in Figure 6.6, while statistical analyses listed in Table 6.2. The IR group showed increased CKmito, and decreased iNOS, BNP and TnT expression levels, compared to controls. The expressions of other genes tested were comparable to controls. Greenhouse–Geisser correction test was used for TnT as its assumption of sphericity was not met (Mauchly's significance, $p < 0.05$). It has been demonstrated that this IR perfusion condition had no significant effect on any of the genes tested.

Table 6.2. Statistical analyses for all genes.

	Mauchly's significance, *p*	Sphericity assumed significance, p	Greenhouse-Geisser significance, *p*
eNOS	0.183	0.951	-
iNOS	0.347	0.873	-
HSP 72	0.536	0.979	-
HSP 73	0.635	0.924	-
BNP	0.149	0.757	-
CK-M	0.354	0.816	-
CKmito	0.351	0.708	-
TnT	0.003	-	0.595

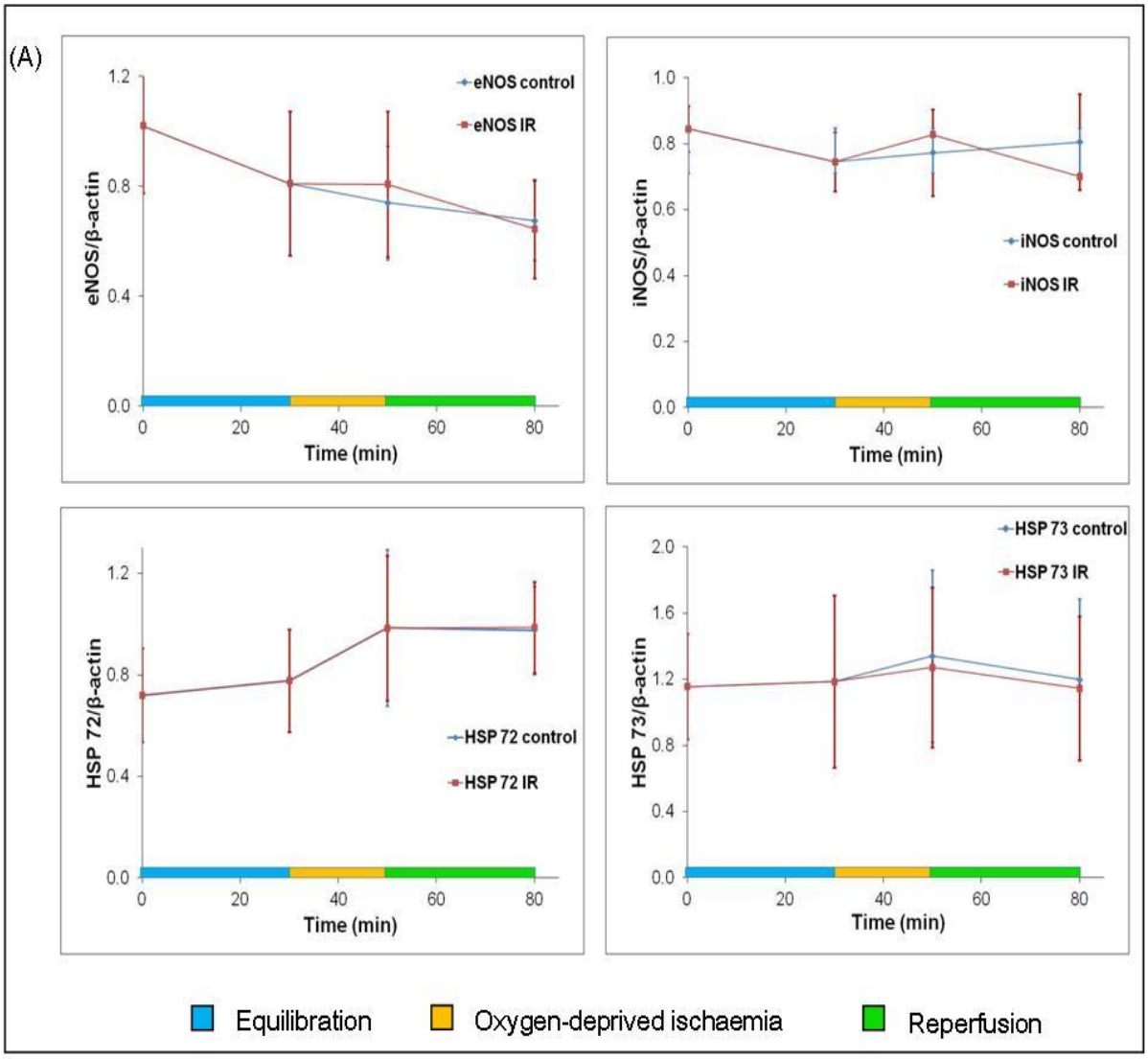

Figure 6.6. (a) Expression profiles of genes relative to β–actin. Data are expressed as mean ± standard deviation. N = 4

IR, ischaemia reperfusion.

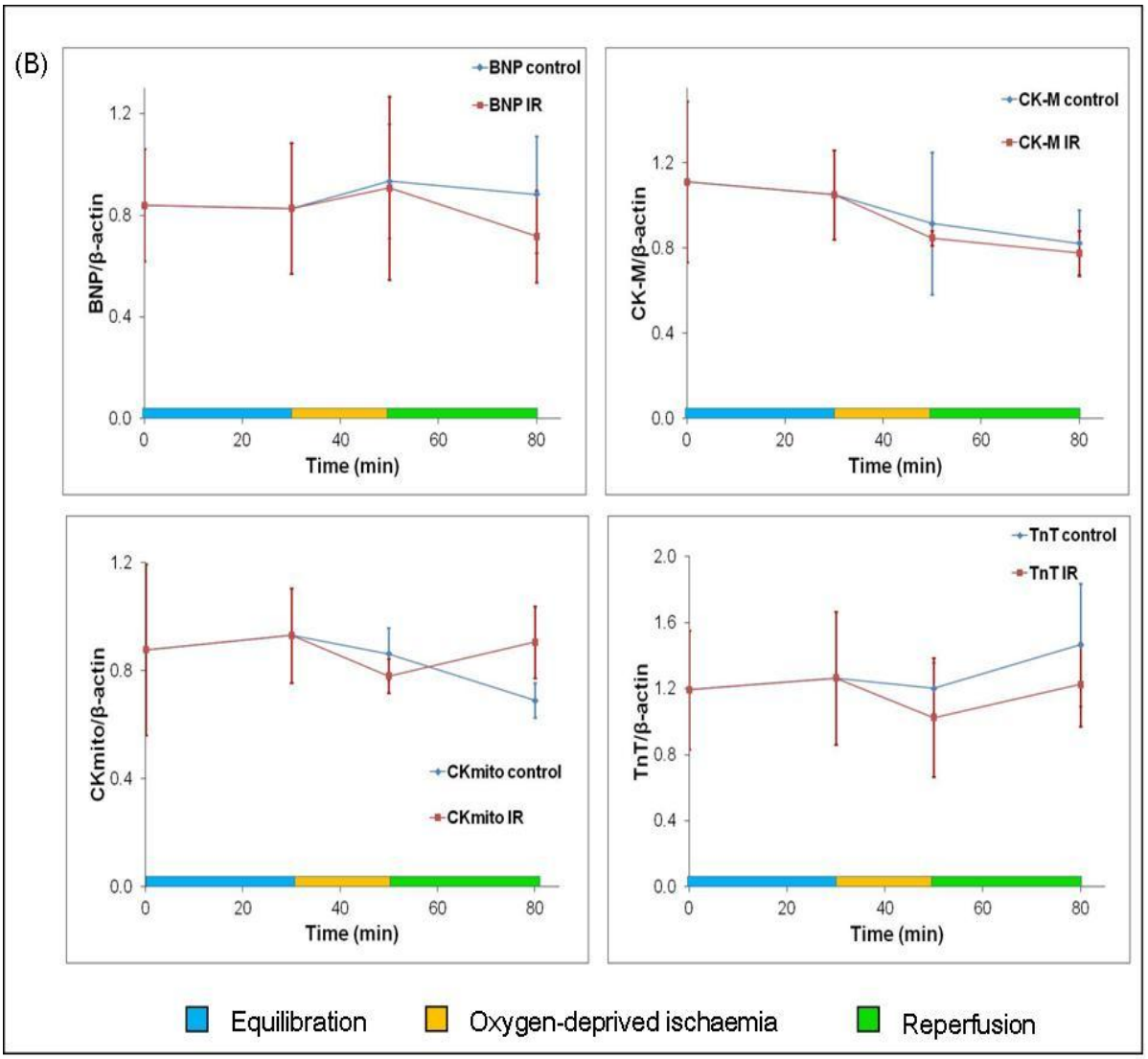

Figure 6.6. (b) Expression profiles of genes relative to β–actin. Data are expressed as mean ± standard deviation. N = 4

IR, ischaemia reperfusion.

6.3.2. Oxygen–deprived IR (40 minutes ischaemia / 30 minutes reperfusion)

Figure 6.7 shows the expression profiles of genes relative to β–actin during 30 minutes of equilibration, 40 minutes of ischaemia and 30 minutes of reperfusion, with statistical analyses in Table 6.3. Greenhouse–Geisser correction test was applied to eNOS as its assumption of sphericity was not met (Mauchly's significance, $p < 0.05$). HSP 72 was the only gene which was significantly decreased by prolonged oxygen–deprived ischaemia ($p = 0.008$).

Table 6.3. Statistical analyses for all genes.

	Mauchly's significance, *p*	Sphericity assumed significance, *p*	Greenhouse-Geisser significance, *p*
eNOS	0.021	-	0.774
iNOS	0.361	0.362	-
HSP 72	0.403	**0.008**	-
HSP 73	0.184	0.996	-
BNP	0.551	0.310	-
CK-M	0.01	-	0.476
CKmito	0.362	0.742	-
TnT	0.087	0.856	-

Pink text represents *p* value is significant, i.e. < 0.05

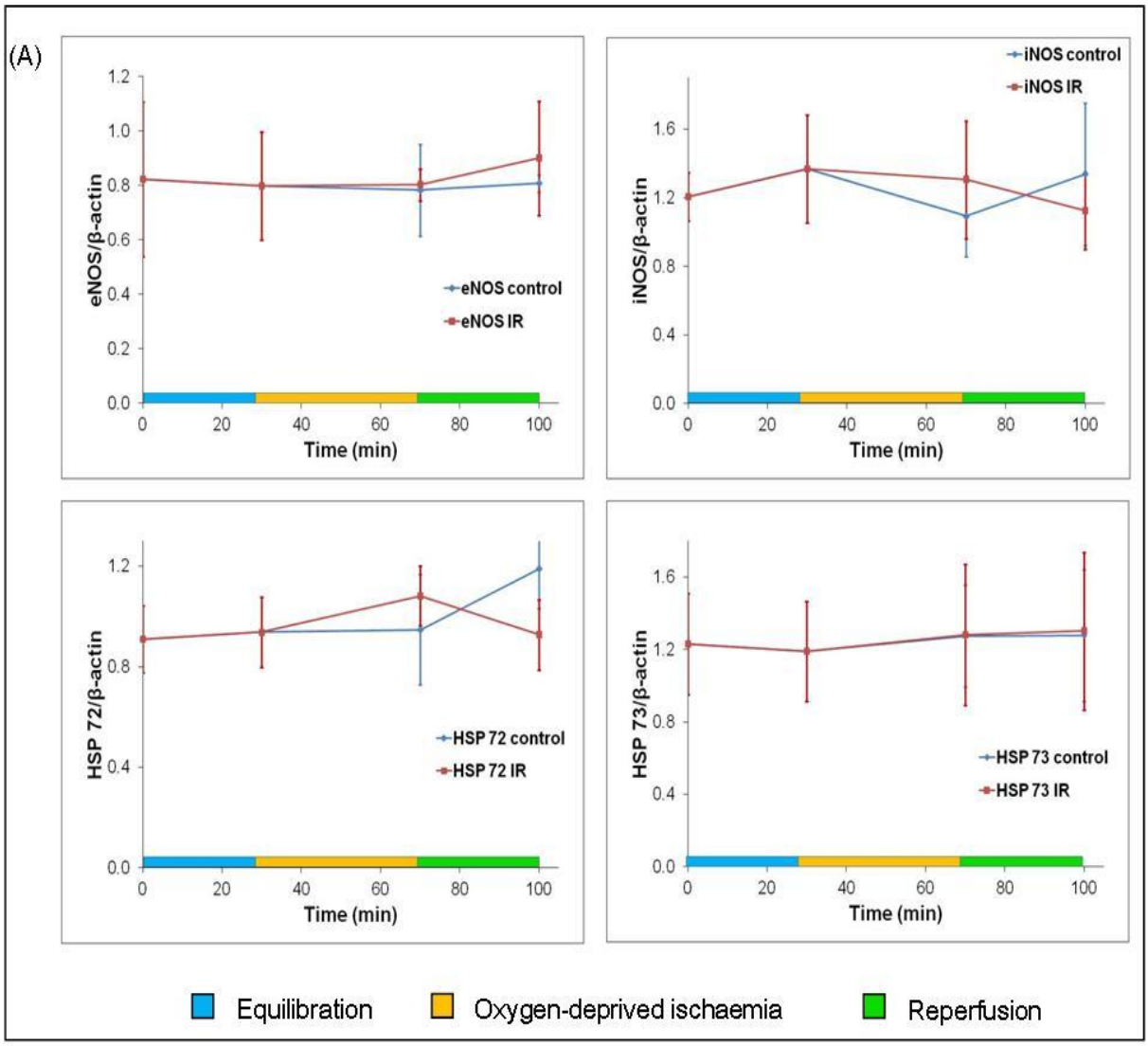

Figure 6.7. (a) Expression profiles for genes relative to β–actin. Data are expressed as mean ± standard deviation. N = 4

IR, ischaemia reperfusion.

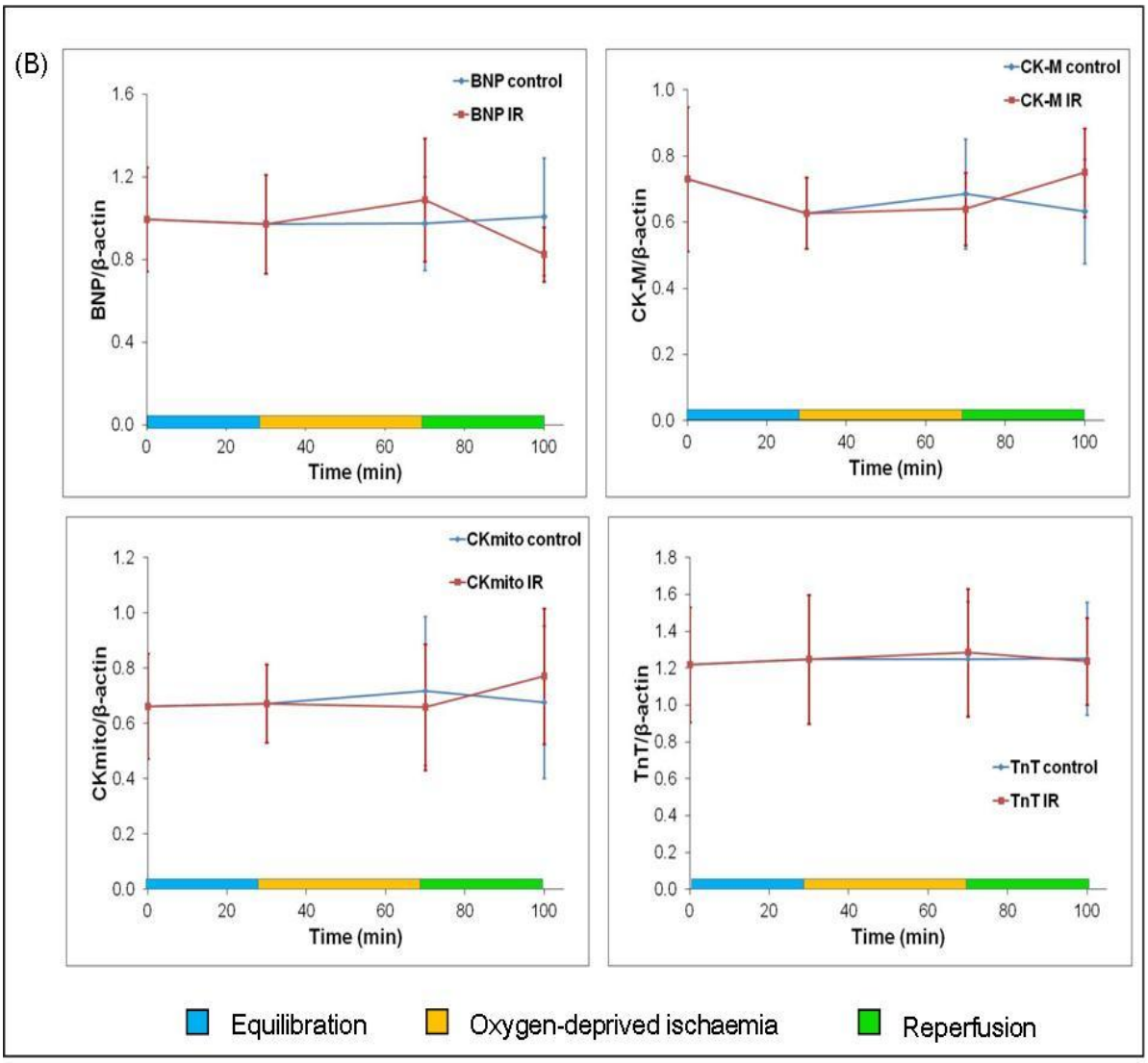

Figure 6.7. (b) Expression profiles for genes relative to β–actin. Data are expressed as mean ± standard deviation. N = 4

IR, ischaemia reperfusion.

6.3.3. Nitrogen–induced IR (40 minutes ischaemia / 30 or 120 minutes reperfusion)

The impact of nitrogen–induced IR regime on NOS and HSP genes expression levels was tested in rat heart samples exposed to 40 minutes of ischaemia and either 30 or 120 minutes of reperfusion.

The mRNA expression profiles for these genes in IR were markedly higher than the control group, except for HSP 73 (Figure 6.8). Greenhouse–Geisser correction test was used in the case where Mauchly's significance is less than 0.05. Expression was not altered as a result of 40 minutes nitrogen–induced ischaemia followed by 30 minutes of reperfusion (Table 6.4). However, when the reperfusion period was extended to 120 minutes, iNOS mRNA level was significantly increased (p = 0.011, Table 6.5).

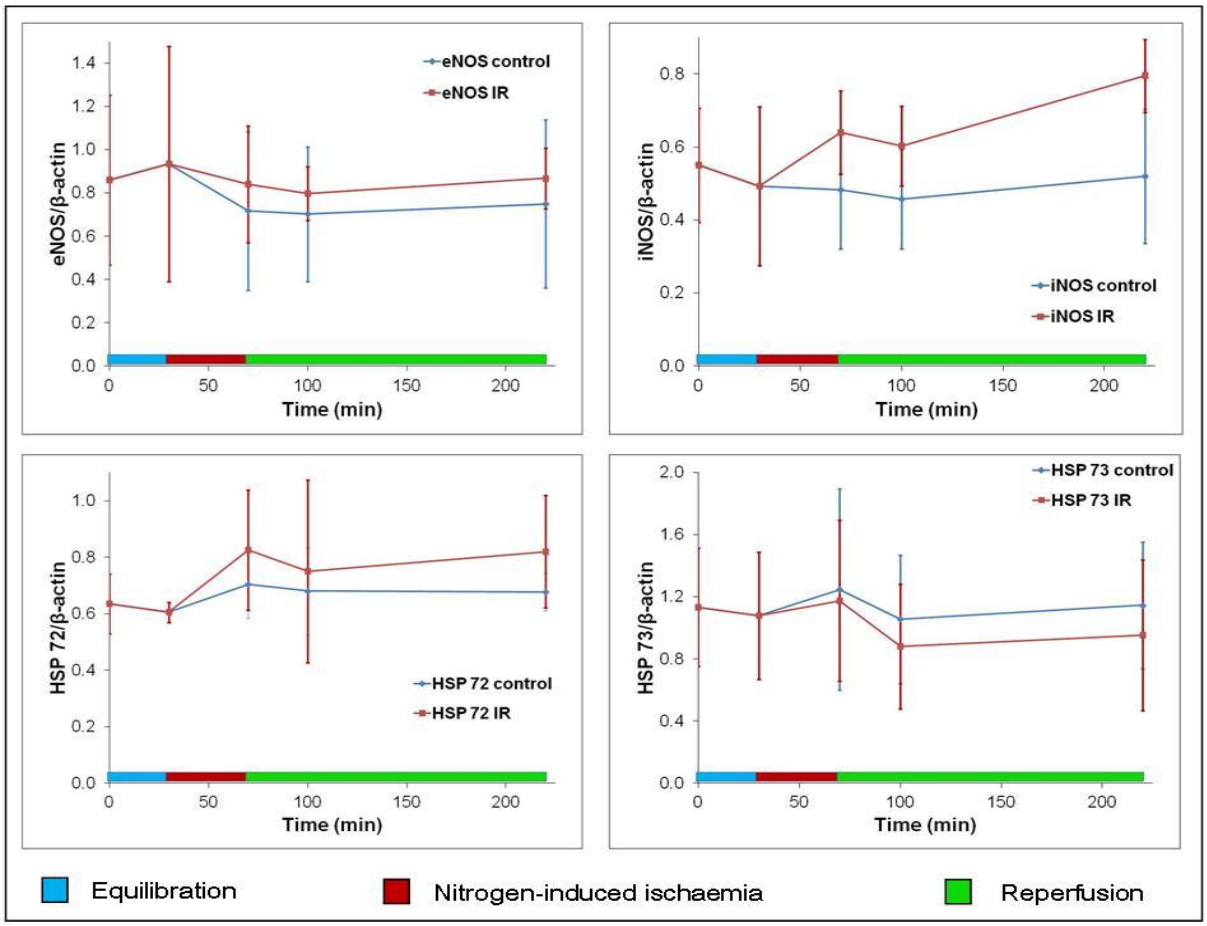

Figure 6.8. Expression profiles for NOS and HSP genes relative to β–actin. Data are expressed as mean ± standard deviation. N = 4

IR, ischaemia reperfusion.

Table 6.4. Statistical analyses for NOS and HSP genes after 40/30 minutes of IR.

	Mauchly's significance, *p*	Greenhouse-Geisser significance, *p*
eNOS	0.024	0.931
iNOS	0.043	0.141
HSP 72	0.002	0.757
HSP 73	0.016	0.847

Table 6.5. Statistical analyses for NOS and HSP genes after 40/120 minutes of IR.

	Mauchly's significance, *p*	Sphericity assumed significance, *p*	Greenhouse-Geisser significance, *p*
eNOS	0.015	-	0.791
iNOS	0.274	**0.011**	-
HSP 72	0.289	0.668	-
HSP 73	0.000	-	0.820

Pink text represents *p* value is significant, i.e. < 0.05

6.4. Discussion

Episodes of myocardial IR were performed on rat ventricular samples in this Generation 2 perfusion platform and gene expression profile analysis was examined under these conditions. In the present study, HSP 72 mRNA expression was significantly altered by 40 minutes (but not 20 minutes) of oxygen–deprived ischaemia, followed by 30 minutes of reperfusion in constrast to the HSP 72 expression observed in Chapter 4. In nitrogen–induced IR, however, only iNOS was upregulated after 120 minutes reperfusion,as well as 30 minutes of reperfusion within the Generation 1 device (Chapter 4).

Khanal *et al*. (2011) have performed research on IR injury in primary porcine cardiomyocytes in a polydimethylsiloxane (PDMS) microfluidic device; this study was the first investigation of IR on cardiac tissue within a microfluidic chip. Khanal's group used nitrogen flow to generate ischaemia and oxygen content was monitored and controlled on–chip by injecting a fluorescent dye, Tris(4,7–diphenyl–1,10–phenanthroline) –ruthenium(II) dichloride, into the upper layer of the chip, in contrast to the study here in which perfusion media were prepared off–chip.

In the current study, even though only iNOS and HSP 72 expression profiles were affected by certain IR procedures, the standard deviation was largely due to small number of experimental repeats (N = 4 for each IR regime). Therefore, further replicates are necessary to fully realise the statistical profile.

BNP gene expression was unaffected by oxygen–deprived IR procedures similar to observations from Luo *et al*. (2006). However, these findings are in contrast to Möllmann *et al*., (2010) who demonstrated significantly increased BNP expression in hypoxic human myocardium. A surgical reduction of blood flow to anterior ventricular wall in pig for 2.2 ± 0.2 hour also caused 3.5 fold

increased myocardial BNP mRNA expression (Goetze *et al*., 2004). In addition, Ramos *et al.* (2009) showed that 15 minutes of ischaemia and 15 minutes reperfusion in rat hearts has increased BNP mRNA content compared to non–ischaemic regions.

Exogenous administration of BNP exerts protective effects against myocardial IR injury, and limiting infarct size (D'Souza *et al*., 2003b). The protective mechanism is reported to be associated with mitochondrial K_{ATP} channel opening. There is evidence that opening of this channel decreases ROS generation at reperfusion (Ozcan *et al*., 2002) and blunts mitochondrial Ca^{2+} accumulation during ischaemia (Murata *et al*., 2001). Interestingly, the addition of L–NAME, the NOS inhibitor abrogated the cardioprotective effect of BNP in rat heart *in vivo* (D'Souza *et al*., 2003a, Ren *et al*., 2007), but not iNOS inhibitor, S-methyl-isothiourea (Ren *et al*., 2007). Ren *et al*. (2007) also showed that the beneficial effects of BNP were associated with increased eNOS expression, enhancing NO concentrations.

Although CK–M mRNA expression was not altered in any of the IR regimes in this study, several studies have demonstrated reduced CK–M gene expression using different IR models. Previously, Mehta *et al*. (1988) showed that CK–M mRNA levels were at least 40 % lower in ischaemic dog and rabbit hearts occluded for 90 minutes, compared to normal myocardium. In addition, MI has significantly reduced CK–M mRNA levels (38 % reduction) compared to control (Neubauer *et al*., 1998). The finding obtained here was agreed with Hoang *et al*., (1997), who also reported unchanged CK–M mRNA expression in a remodelled left ventricular post–MI pig model.

An explanation for the reduction in CK–M gene expression in other IR studies is the adaptive mechanisms accompanying LV hypertrophy, i.e. re–appearance of the foetal CK pattern with an isoenzyme switch from CK–M to CK–B in failing human (Nascimben *et al*., 1996) or dog (Ye *et al*., 2001) hearts. Energy transduction via CK–B is more efficient (Ingwall, 1993) as a result of higher affinity of CK–B to ADP compared to CK–M. Conflicting

results have been obtained by Saupe *et al*. (2000), where the shift in CK isoenzyme toward foetal pattern conferred no obvious kinetic advantage.

In a remodelled LV post–MI pig model, Hoang *et al.* (1997) demonstrated 46 % decreased CKmito mRNA expression, compared with the controls. Mitochondrial oxidative phosphorylation via CKmito is essential in ATP production in the heart during high workload; therefore the decreased expression may ultimately compromise energy metabolism and contribute to heart failure. Additionally, CKmito is part of the protein complex involved in the mPTP (Dolder *et al*., 2003, Kroemer *et al*., 2007). CKmito octamer–substrate complexes possess a protective and stabilizing effect against mPTP opening (Andrienko *et al*., 2003, Speer et *al*., 2005). Hence, reduced CKmito gene expression post–MI may exacerbate mPTP opening and induce subsequent apoptosis. However, CKmito gene expression was not observed to change in the present study, indicating that mitochondrial oxidative phosphorylation may not be affected by acute IR protocols, and hence the cardioprotective effect from CKmito against opening of the mPTP may be retained. In support of this, Neubauer *et al*. (1998) also detected unchanged CKmito mRNA expression in rat heart post MI.

The current study has shown that TnT mRNA expression of rat heart was not influenced by IR stress. Although post–translational modification of TnT has not been evaluated in this study, its role in myocardial IR was determined by others. The NH_2–terminal region of TnT is hypervariable and can be selectively removed during myocardial IR by μ–calpain proteolysis whereas conserved regions of TnT are preserved. Zhang *et al*. (2006) have showed that global IR in *ex vivo* bovine working heart preparations generated a 1 – 71 truncated NH_2–terminal peptide of TnT. These NH_2–terminal alterations affected the overall protein conformation and subsequent Ca^{2+}–regulation of muscle contraction (Jin *et al*., 2000, Jin and Root, 2000), can possibly serve as an adaptation mechanism in the myocardium under stress conditions (Feng *et al*., 2008).

In this study, the oxygen content of KHBB was determined in effluent samples. A less labour intensive method can be applied in the future where electrochemical modules would be integrated onto the device to detect *in situ* pO_2 throughout the perfusion. In addition, multiple analytical modules can be integrated with the current device to examine the kinetics of cardiomyocyte injury and damage throughout IR. Furthermore, the present perfusion device can also be modified via connection to a PCR on–chip platform, giving a continuous and online read–out of gene expression.

In conclusion, a proof–of–concept microfluidic device has been established for investigation of heart tissue, which can be adopted or modified for experimentation of various tissue types. Only iNOS and HSP 72 were affected by the IR regimes but not the biomarkers BNP, CK–M, CKmito and TnT and other stress genes tested in this investigation, suggesting that the myocardial stress was insufficiently great to cause extensive IR injuries. Other IR–induced stress models remain to be tested in this microfluidic perfusion system for the analysis of contractile dysfunction, myocardial injuries and cell death.

Chapter 7

Use of Magnetohydrodynamics in Generation 1 Perfusion System

The diameter of channels in microfluidic devices is normally in the order of 100 μm, and the Reynolds numbers (Re) associated in these devices are small (Re < 1; Sia and Whitesides, 2003, Lam *et al*., 2009), indicating laminar flow with little mixing exists between two or more streams of fluids (Choban *et al*., 2004, Ong *et al*., 2008), as shown in Figure 5.1. In biological processes, efficient mixing is particularly critical to ensure even distribution of interacting particles; hence there is often a need to integrate extra components such as micromixers and microstirrers within microfluidic devices, when they are used to study biological systems (Miyake *et al*., 1993, Voldman *et al*., 2000, Wong *et al*., 2004).

Magnetohydrodynamics (MHD) provides an elegant and flexible solution to existing mixers, as it does not require any mechanical components. MHD offers the potential to control fluid flow or fluid mixing locally by using an ion current within a magnetic field (Qian and Bau, 2009, Weston *et al*., 2010). The cross product of ion flux and the magnetic field gives rise to a magnetic force, thus causing the fluid to rotate around the electrodes (Anderson *et al*., 2010). Electroactive redox species can be added into the buffer solution to enhance fluid convection in the presence of magnetic field, termed redox–MHD.

In a number of redox–MHD studies, fluid flow was imaged using coloured redox species generated *in situ*, for example orange–red radical nitrobenzene anion (Pullins *et al*., 2001, Grant *et al*., 2002, Leventis and Dass, 2005), or with dye tracers (Bau *et al.*, 2003, Qian and Bau, 2005). However, monitoring the microscopic convective paths within these dyes is difficult. In addition, the effect of these dyes on the tissue was unclear. To overcome the limitations of dyes, polystyrene latex microbeads (10 μm) were used to track and follow fluid flow under inverted microscope, following the method of Anderson *et al*. (2010).

In this chapter, the application of redox–MHD in the microfluidic system for heart tissue maintenance was described. The effect of redox–MHD on heart tissue viability in the modified Generation 1 perfusion system was

examined using LDH assay. Parallel tissue samples were analysed simultaneously to allow comparison between treated and control groups. In addition, a single tissue sample was interrogated repeatedly within one experiment, to eliminate inter–sample variations due to excision artefacts, or the region from which the tissue was sampled. Three redox species (Ruhex, hydroquinone, and potassium ferricyanide/ferrocyanide) were considered to improve MHD–induced mixing but there remains concern for the reactivity and interference of redox species with biological samples and the LDH assay. Therefore, redox species with minimal impact on the LDH assay was selected before the impact of redox species and redox–MHD on tissue viability was investigated. Qualitative microscopy of redox–MHD was also examined using polystyrene microbeads.

The main aim of this chapter was to determine the effect of redox–MHD on fluid mixing around the heart tissue within the modified Generation 1 perfusion system.

7.1. Multiple experiments with single tissue sample

The feasibility of performing multiple experiments on a single tissue sample was first examined in the absence of MHD. A perfusion system as described in Section 2.10.1 was set up and all buffer solutions were prepared as described in Section 2.10.4. A series of cardiac tissue biopsies were perfused with KHBB for 84 minutes, followed by 6 minutes incubation with Triton–KHBB, and a further 84 minutes of KHBB perfusion. Subsequently the tissue was exposed to a second 6 minutes Triton–KHBB incubation, and a final 90 minutes of KHBB perfusion, and lastly 30 minutes of Triton–KHBB perfusion (Section 2.10.5). A recovery period of 84 minutes was chosen because it has been shown in previous studies (Chapter 3) that LDH release resulting from an insult has returned to minimal within this time frame. During the perfusion, effluent samples (240 µl) were collected every 5 minutes and stored at –20 ^{o}C until LDH analysis (Section 2.6). Electrical stimulation at 3 – 4 V/cm, 1.5 Hz was applied throughout the perfusion as previously described.

LDH activity increased at 100th minute after the brief Triton–KHBB incubation, but subsequently decreased with time (Figure 7.1). The delay after the Triton–KHBB incubation period and the LDH peak is most likely attributable to a combination of chamber–emptying time (approximately 4 minutes) and time of travel of solution from the chamber to collection tube (6.9 minutes). The second Triton–KHBB incubation (174 – 180th minute) produced a similar LDH response, with a spike at 185th minute. A final Triton–KHBB perfusion (≥ 270th minute) elicited the greatest LDH release.

Cardiac tissue remained viable after two pulses of 6 minutes incubation with Triton–KHBB, suggesting that multiple experiments can be performed on the same tissue sample.

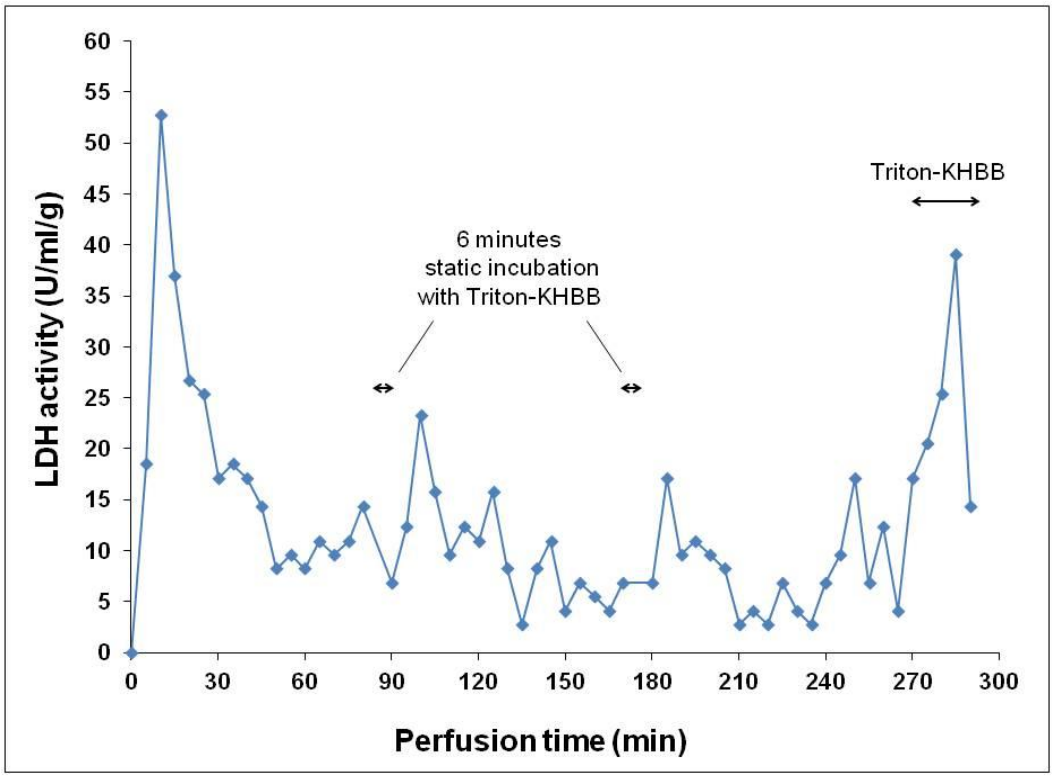

Figure 7.1. A representative study of LDH release from heart tissue following two 6 minute incubations with Triton–KHBB without MHD, each followed by a 84 minute oxygenated KHBB perfusion. The tissue sample was exposed to continuous Triton–KHBB perfusion after 270th minute. N = 2

7.2. Choices of redox species

It was important that redox species used to generate MHD did not interfere with the measurement of LDH. Three redox species (5 mM Ruhex, 5 mM hydroquinone, or a mixture of 2.5 mM potassium ferricyanide and 2.5 mM potassium ferrocyanide) were individually added into the perfusion media, to check its effect on the sensitivity of assay. The colours of each redox species are given in Table 7.1. Figure 7.2. shows the comparison of prepared and calculated LDH activities in the presence of redox species, showing the impact of the redox species in the LDH assay. The calculated LDH activities were derived as described in Section 2.10.3.

Table 7.1. Colour and absorbance of redox species.

Redox species	Colour (solid form)	Absorbance at 490 nm
Ruhex	Pale yellow	0.04
Hydroquinone	White	0.04
Potassium ferro/ferricyanide	Red/Pale yellow	0.35
KHBB alone	-	0.04

In the presence of 5 mM Ruhex, the calculated LDH activity increased linearly with the prepared LDH activity, but it was about 43.2 ± 7.6 % of the prepared LDH (Figure 7.2.Blue). The calculated LDH activities were very low in the presence of 5 mM hydroquinone, i.e. 7.4 ± 1.9 % of expected, but an approximately linear calibration curve for LDH was produced (Figure 7.2.Green). With the mixture of potassium ferri– and ferrocyanide (2.5 mM each), a curve instead of linear line was produced (Figure 7.2.Red), and the LDH activities were unable to be detected when LDH activities below 0.15 U/ml were prepared.

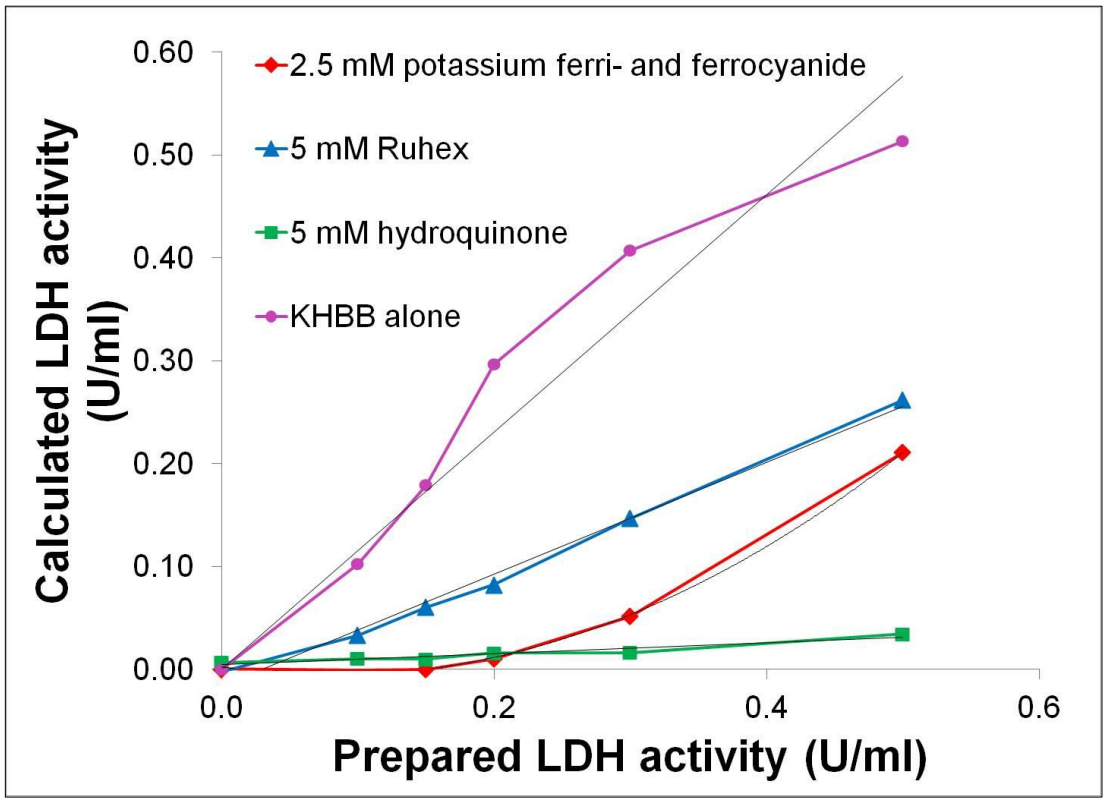

Figure 7.2. The influence of the presence of redox species on measurement of LDH activity. N = 2

In conclusion, 5 mM Ruhex was selected for the redox–MHD study despite the reduction in levels of LDH detection, as these effects were consistent across the range of detectable value and did not substantially alter the sensitivity.

7.3. Impact of Ruhex and Ruhex–MHD on tissue viability

Before Ruhex–MHD was investigated, the effect of 5 mM Ruhex on heart tissue viability was investigated. A parallel perfusion system (Figure 2.17) was set up where two heart tissues were perfused according to the protocol described in Section 2.10.5, with Ruhex–KHBB present in the 6 minutes incubation for **one** sample (Figure 7.3.Red). Similar LDH release trends were observed, with LDH activity peaks at 95^{th} and 100^{th} minutes, for tissue exposed to KHBB alone and Ruhex–KHBB during the 6 minutes incubation, respectively. The LDH activities remained low after the Ruhex–KHBB or KHBB exposure. LDH activities increased at the end of the incubation period following Triton–KHBB perfusion in both samples, which confirmed that both samples remained viable following a brief exposure to Ruhex–KHBB or KHBB alone.

The impact of Ruhex–MHD on cardiac tissue was examined subsequently, where a steel U–shape magnet was inserted across **one** of the tissue chambers in the parallel perfusion setup (Figure 2.17.b). The magnet was present only during the 6 minutes incubation period for **one** sample. An increase in LDH activity in both samples was observed at 95^{th} minute, followed by a decline with time (Figure 7.4). This is in contrast to previous investigations where the decline in LDH release took a longer period (90^{th} – 130^{th} minutes in Figure 7.4 versus 90^{th} – 100^{th} minutes in Figure 7.3). However, since this observation was seen in both samples, it may not be due to alterations in the chemistry of the samples, but rather the behaviour of the flow system. The final perfusion with Triton–KHBB elicited a marked rise in LDH activity, showing that both samples were viable throughout the perfusion. This study demonstrated that the magnetic field had no noticeable effect on the release of LDH.

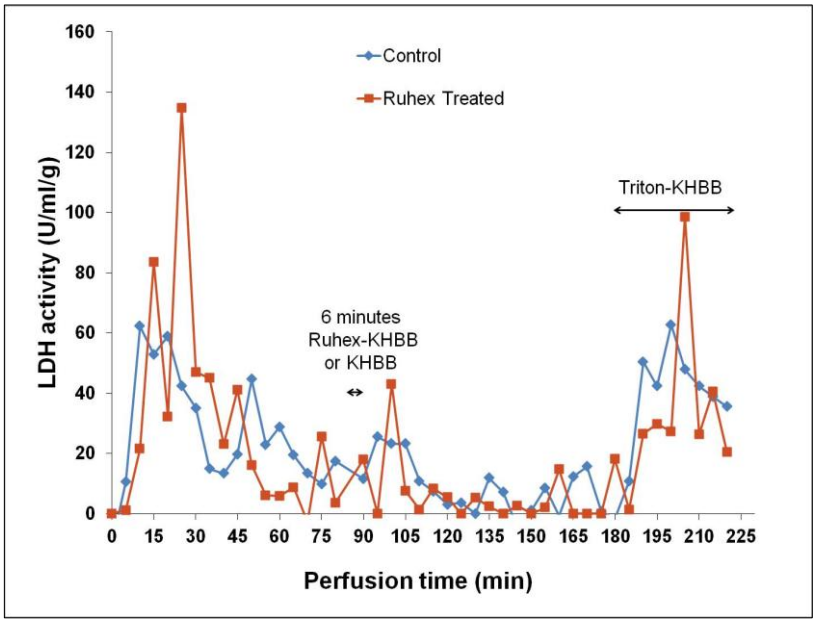

Figure 7.3. A representative study of the effect of Ruhex on LDH release from cardiac samples during parallel perfusion. Ruhex–KHBB was only present in treated sample for 6 minutes (84^{th} – 90^{th}), the remaining time both tissues were perfused with oxygenated KHBB until 180^{th} minute, and then perfused with Triton–KHBB. N = 2 for each condition

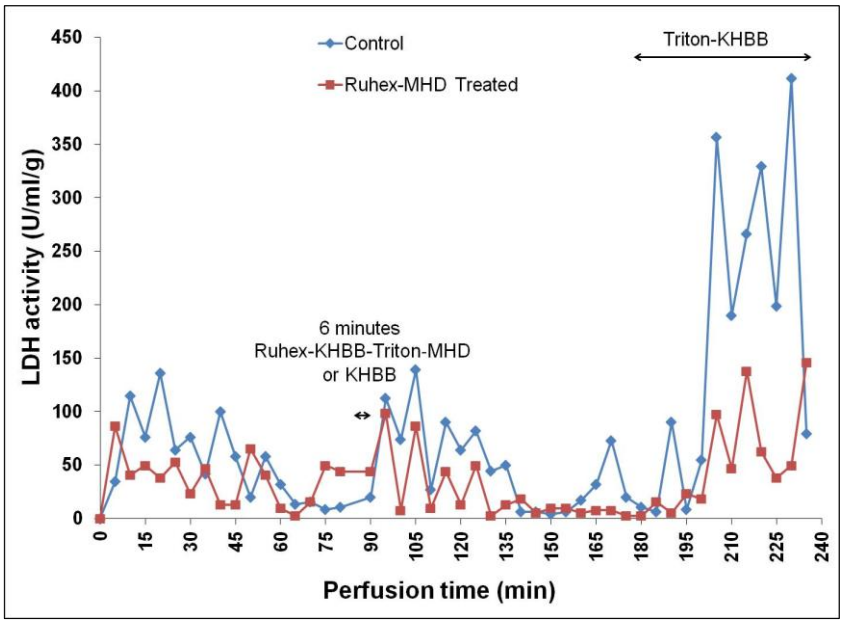

Figure 7.4. A representative study of the effect of Ruhex–MHD on LDH release from biopsies during parallel perfusion. Ruhex–KHBB–Triton–MHD was only present in the treated sample for 6 minutes (84^{th} – 90^{th}), the remaining time both tissues were perfused with oxygenated KHBB in the absence of magnet until 180^{th} minute, and then perfused with Triton–KHBB. N = 3 for each condition

7.4. Observation of MHD–fluid flow

Qualitative determination of MHD was carried out by placing the tissue chamber on a hotplate attached to the stage of an inverted microscope (Section 2.10.1). Microbeads (10 μm diameter) were diluted in the perfusion buffer (1:30 dilution) to track the flow of fluid. Videos were recorded under different perfusion conditions (static/perfusion, presence/absence of electrical stimulation, presence/absence of magnet, different buffer compositions) Supplementary videos (1 – 5) are provided in the DVD attached with this thesis.

Agitation during Triton–KHBB incubation was observed, before switching on the stimulating electrodes (Video 1). This was most likely due to the thermal gradients from the hotplate under the tissue chamber. When the electrical stimulation was switched on at 4 seconds, in the absence of magnet, there was no significant change in fluid flow. However, the combination of stimulation and the magnet showed that MHD flow was superimposed on the thermal convection as shown in Video 2. This demonstrated MHD–induced fluid flow (pulsating motion of microbeads) superimposed on the thermal convection. It was difficult to monitor the MHD flow motion when the perfusion was initiated (Video 3). Instead, a relatively slower pulsating movement was noticed consistent with frequency of the peristaltic pump roller (~ 0.18 Hz).

When 5 mM Ruhex was added to the Triton–KHBB in the presence of magnet, MHD flow movement was more noticeable (Video 4) than previously. The direction of flow motion due to thermal convection was changed when electrical stimulation was activated at 3 seconds when magnet was present. In addition, the MHD flow was approximately 1.5 – 2 fold greater compared with that in the absence of Ruhex (Video 2). This was determined by the net displacement of microbead over a fixed time from the recordings. However, the MHD flow remained visible in addition to thermal convection effects. Even during perfusion, a surge of Ruhex–MHD was noticeable when electrical

stimulation was switched on at 2 seconds, in the presence of magnet (Video 5). Bead movement slowed after the initial surge and Ruhex–MHD flow was indistinguishable from the highly variable convection due to perfusion.

7.5. Discussion

Since a laminar flow regime dominates in microfluidic devices, mixing is largely relied on diffusion. Here, redox–MHD was applied to the Generation 1 perfusion system to enhance mixing in a controlled manner. A parallel perfusion setup was established to study two samples from the same heart simultaneously, maintained for the same period prior to analysis. Ruhex (5 mM) was chosen for redox–MHD study (among other redox species) because it allows LDH activity to be measured, with a correction in the effluent samples contained Ruhex based on Figure 7.2. The presence of Ruhex and Ruhex–MHD in the perfusion system had little detrimental effect on the sample viability, and the videos of MHD and Ruhex–MHD showed alterations in flow. Furthermore, mechanical contraction was observed in some tissue samples but this ceased at the early stages of perfusion.

This study has demonstrated that a single biopsy can be interrogated repeatedly within one experiment by transient exposure to Triton–KHBB incubation, eliciting appropriate LDH release. Hence multiple experiments can be performed on the same tissue sample, eliminating inherent variation due to sample excision and handling procedures. Furthermore, the parallel perfusion setup increased the experiment efficiency in term of time and number of samples required. Hattersley *et al.* (2008) reported a similar approach where a rat liver sample in a microfluidic device was exposed repeatedly but transiently to lysis buffer, followed by Williams Media E (typical media for liver tissue maintenance) perfusion. LDH release and DNA levels were showed to diminish with repeated exposure to lysis buffer. Hattersley's study differed from the current work in which the liver sample was not exposed to longer lysis buffer perfusion at the end of the experiment. The increased LDH release from the tissue samples due to continuous Triton–KHBB perfusion indicated that these samples were not adversely affected by the previous incubation with Triton.

Among the three redox species tested, it was assumed that the interference of hydroquinone and a mixture of potassium ferri– and ferrocyanide with the LDH assay were much more intense than that of Ruhex. However, the reason for the effect was unclear. Furthermore, it has been demonstrated that the tissue viability was unaffected by the presence of 5 mM Ruhex. Ruhex has been used previously in cardiac research by Schoenfisch and colleagues (2005), where 1 – 5 mM Ruhex was used in rat heart perfusion, in order to carry out *in situ* electrochemical measurements. The tissue was considered to be 'living' based on the criterion that the heart was still metabolizing nutrients and hence able to generate a heartbeat.

Although the final Triton–KHBB perfusion caused a marked increase in LDH release, demonstrating that the samples remained viable during perfusion; LDH release following the static incubation of Ruhex – Triton – KHBB in the presence of magnet was relatively high (Figure 7.4), indicating a considerable degree of cellular damage. It may be due to the effect of the magnetic field on heart tissue, or Ruhex – MHD induced stirring of Triton, causing greater tissue lysis.

In the existing Generation 1 perfusion system, two platinum electrodes were used for stimulation of heart tissue and source of ion flux for MHD. In the future, this setup can be modified as electrodes can be easily patterned on the microfluidic chips to generate ion flux at desired locations and to create different flow patterns (Qian and Bau, 2005, Weston *et al*., 2006, Anderson *et al.*, 2010, Weston *et al*., 2010), within confined volumes, channels, and reservoirs e.g. Figure 7.5. The flow direction can be simply reversed, by (i) changing the potential at one electrode or the direction of the current flux, or (ii) changing the direction of magnetic field. The device can operate as a pump for continuous flow, or to induce chaotic advection (Qian and Bau, 2005), by activating microelectrodes patterned differently on the chip. The fluid flow around the tissue can also be fine–tuned, and used to modify the concentration gradient at the tissue surface, and hence, facilitating the tissue uptake and release of chemical species.

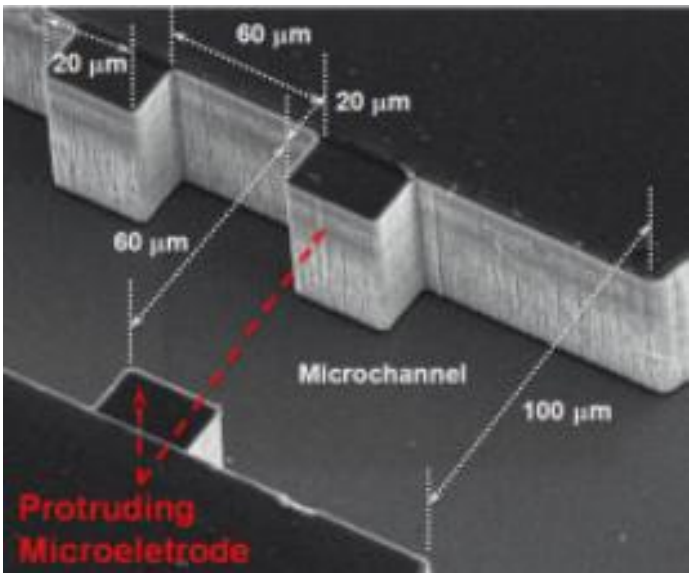

Figure 7.5. A schematic diagram of microelectrodes patterned along the microchannel. (Hu *et al.*, 2011)

In conclusion, the application of Ruhex–MHD in the modified Generation 1 perfusion system showed no deleterious effect on tissue viability, as determined by LDH release. This application could be of particular importance when the tissue sample is exposed to certain drugs or therapeutic agents during the perfusion, to test the responsiveness of cardiac tissue to treatment. Efficient mixing around the tissue will allow effective and reproducible uptake of drugs and release of chemical species in response to the therapeutic treatment. Hence, a better understanding of the biological response of heart to different relevant therapeutic strategies could be investigated in the future.

Chapter 8

Development

of

Creatine Kinase MB Microsensor

Cardiac markers play an important role in the diagnosis, prognosis, monitoring, and risk stratification of suspected heart attack patients (Marrow *et al.*, 2007, Thygesen *et al.*, 2007). Assessment of the presence of cardiac marker is critical for clinician's evaluation of acute coronary syndromes, in addition to electrocardiographic changes. CK–MB is one of the cardiac markers which is widely used for the clinical diagnosis of AMI (Collinson, 1998), even though reports received in recent years have shown that TnI is superior as a diagnostic marker (Kontos *et al*., 2003, Basu *et al*., 2009). CK–MB is an intracellular enzyme present primarily in cardiac muscle. Injuries to the heart and to a lesser extent to skeletal muscle; or a period of intensive exercise may lead to CK–MB release into the blood serum. After the onset of AMI, CK–MB level is elevated markedly for up to 6 hours, peaking after 24 hours and returning to normal within 48 – 72 hours (Singh *et al*., 2011).

A normal serum CK–MB in the range of 0 – 6 ng/ml was reported (Knight, 2001, Mercuro *et al*., 2007). However, these results have to be interpreted relative to the total CK in serum (reported in IU); the ratio is termed a CK–MB index. Generally, an index ≥ 3 is associated with myocardial injury. Table 8.1 demonstrates the diagnosis of AMI based on the CK–MB concentration and its index. In the microfluidic perfusion system described previously (Chapters 3 and 5), the release of a much lower amount of CK–MB would be expected as the biopsies of heart tissue are small (~ 10 mg). Therefore, development of a sensitive, robust and accurate CK–MB methodology is needed for use with these perfusion systems.

Table 8.1. CK–MB diagnosis of AMI.

CK-MB concentration	CK-MB index	Indication of AMI
≥ 10 ng/ml	≥ 10	Probable
4 – 10 ng/ml	4 – 10	Positive
≤ 4 ng/ml	≤ 4	Negative

(Knight, 2001)

The use of a specific antibody to capture cardiac biomarkers in immunoassays has been a well known clinical diagnostic methodology. Recently, a variety of biosensors have been established using immunoassay techniques, where the targeted antigen is efficiently captured and information is relayed into a detectable signal via a label on a secondary reaction antibody. These labels include fluorescent moieties (Gervais and Delmarche, 2009, Zimmermann *et al*., 2009), enzymes (Bhattacharyya and Klapperich, 2009, Hatakeyama *et al*., 2009), or paramagnetic particles (Kiely *et al*., 2007, Eveness *et al*., 2009). Electrochemical immunoassays (ECIA), however, are promising alternatives to the existing immunochemical tests (Fowler *et al*., 2008), due to their robustness, simplicity and inexpensive fabrication, sensitivity and accuracy. The basis of electrochemical biosensors utilises a measurable electric current signal when the target antigen binds to the antibody pre–attached on the electrode surface.

Microelectrodes are widely used in ECIA, where their applications are developing due to the increasing demands for *in situ* electroanalytical measurements from living cells. Carbon fibre microelectrodes (outer diameter = 8 µm) were first used by Pujol and colleagues to measure the oxidation of several neurotransmitters *in vitro* (Ponchon *et al*., 1979) and in neostriatum of rat *in vivo* (Gonon *et al*., 1978). The benefits of carbon fibres are primarily owing to their biological compatibility, non–toxic and good electrochemical properties, as well as their well–characterized electrochemistry (Michael and Wightman, 1996). In addition, carbon fibres are cheap and readily available and the small physical dimensions cause less tissue damage, compared with larger conventional electrodes.

The aim of this chapter was to develop a novel CK–MB microsensor, using ferrocene–carboaldehyde (Fc–CHO)–conjugated CK–MB antibody linked to the surface of the carbon fibre microelectrode. The concentration of CK–MB could then be determined by electrochemical means, via the oxidation of ferrocene tethered on the CK–MB antibody.

8.1. Fabrication of carbon fibre microelectrode

Carbon fibre microelectrodes were fabricated and prepared as described in Section 2.12.1 (Figure 2.21). Due to the brittleness of the carbon fibre, separation of an individual full length of fibre from a fibre bundle can be a challenging task. Only 50 % of the glass capillaries made contained a carbon fibre after being pulled using a micropipette puller, the reason being that not all the aspirated carbon fibres were sufficiently long to cover the full length of capillary, and the carbon fibre was sometimes pulled out from the glass capillary. Moreover, fragility of the glass housing material posed great difficulty in handling and manipulation of the microelectrodes. The fine–end of the microelectrode was very delicate and could be easily broken; all electrodes were handled with great care.

CycV and SWV scans were run in PBS for all the microelectrode prior to each experiment (Section 2.12.4). Current was able to pass through the microelectrodes, indicating that there was a good connection between carbon fibre, graphite powder and the wire. A microelectrode can be used repeatedly by transecting the carbon fibre tip, exposing new surface for CK–MB antibody attachment (Bruns, 2004).

8.2. Serial measurement of CK–MB

Fc–CHO was attached to CK–MB antibody as previously described in Section 2.12.2 (Okochi *et al*., 2005) and immobilized onto the microelectrode surface via 18 hours incubation at 4 ^{o}C (Section 2.12.3). Subsequently, the microelectrode was washed with 0.1 % Tween 20 in PBS before incubating in PBS (pH 7.4) for 10 minutes and CycV as well as SWV scans were performed (Section 2.12.4). Incubation (10 minutes) and washing steps were repeated for a series of CK–MB protein solutions with increasing concentrations. The SWV scans obtained are shown in Figures 8.1. A and B. A single current peak is present at potential of 0.25 V, corresponding to the oxidation of antibody–tethered ferrocene into the ferrocenium cation. The difference between the peak at 0.25 V and baseline current (ΔI) were gradually decreasing with increasing CK–MB protein concentrations. A total of 18 microelectrodes were tested of which 12 gave good responses (e.g. Figure 8.1), two microelectrodes broke in the middle of experiments, and 4 only gave weak signals against CK–MB incubations.

The microelectrode in Figure 8.1.B was incubated in CK–MB protein, 100 – fold more diluted compared to Figure 8.1.A, however it was interesting to note that the current signal detected was 10 – fold greater. The antibody binding sites on these microelectrodes were saturated at 1 and 0.01 ng/ml CK–MB proteins in Figures 8.1.A and B, respectively, where their current peaks diminished. Hence the experiments were stopped at these concentrations.

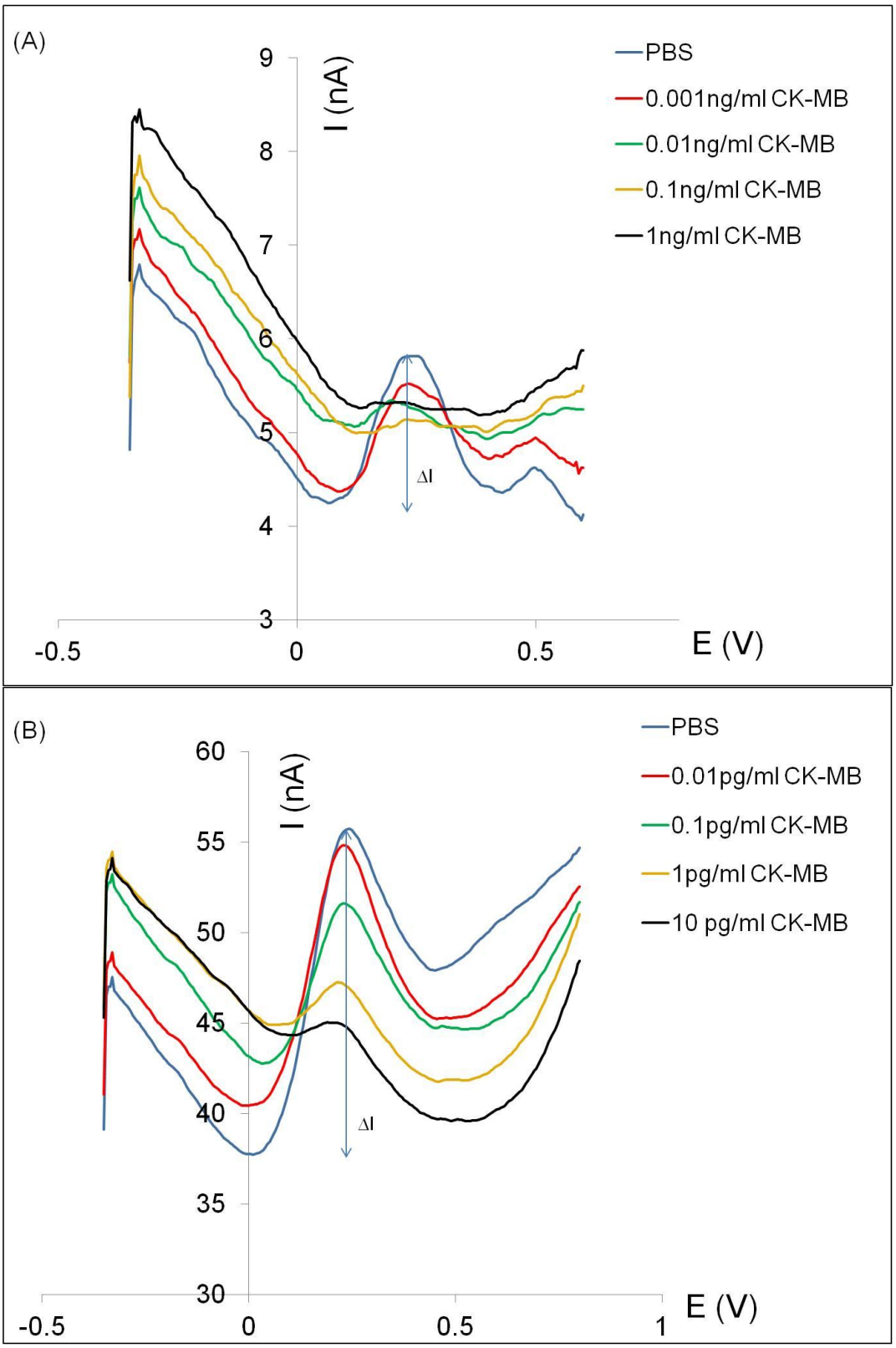

Figure 8.1. SWV scans of Fc–CHO–labelled microelectrode after incubation in PBS (pH 7.4) and increasing CK–MB protein (0.001 – 1 ng/ml for (A), 0.01 – 10 pg/ml for (B)). A and B represent data from two individual microelectrodes. N = 14

The ΔI was calculated and plotted against the log of CK–MB protein (Figure 8.2). Three individual calibration curves (C1, C2 and C3) were plotted and their profiles greatly differed from each other. The difference observed is due, most probably to the difference in the surface area of each microelectrode labelled with Fc–CHO. The peak current disappeared at 10 ng/ml CK–MB for C1 and 0.1 ng/ml for C2 and C3, indicating that C1 had a greater surface area labelled with Fc–CHO-conjugated antibody, compared to C2 and C3.

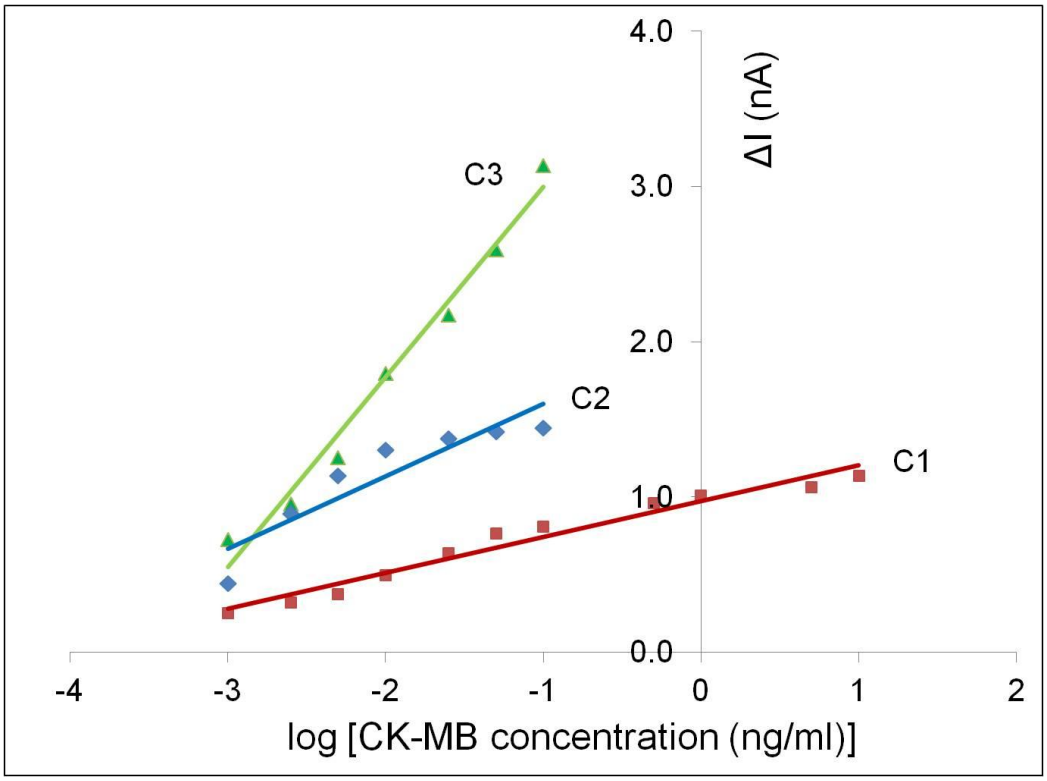

Figure 8.2. Three independent CK–MB protein calibration curves based on SWV. C1, C2 and C3 represent three different microelectrodes following serial incubation in CK–MB protein (from 1 pg/ml to 10 ng/ml).

8.3. Microelectrode surface area determination

The surface area of each microelectrode was determined using the Randles–Sevcik equation (Equation 5; Zanello, 2003). Three microelectrodes of similar surface area were chosen for this experiment: C4 = 1.55, C5 = 1.91, C6 = 1.37 cm^2. Following SWV scans, ΔIs obtained from each experiment were then normalised relative to their surface areas and plotted against the log of CK–MB protein (Figure 8.3). The peak currents diminished at the same point, i.e. 2.5 pg/ml of CK–MB as expected given that the surface areas of these microelectrodes for antibody adherence were similar. However, these calibration curves still greatly deviated because the current differed largely in each microelectrode, despite normalization of surface area. Therefore, one microelectrode can only test one sample using an extrapolation method (described in next section), in order to eliminate the differences between electrodes.

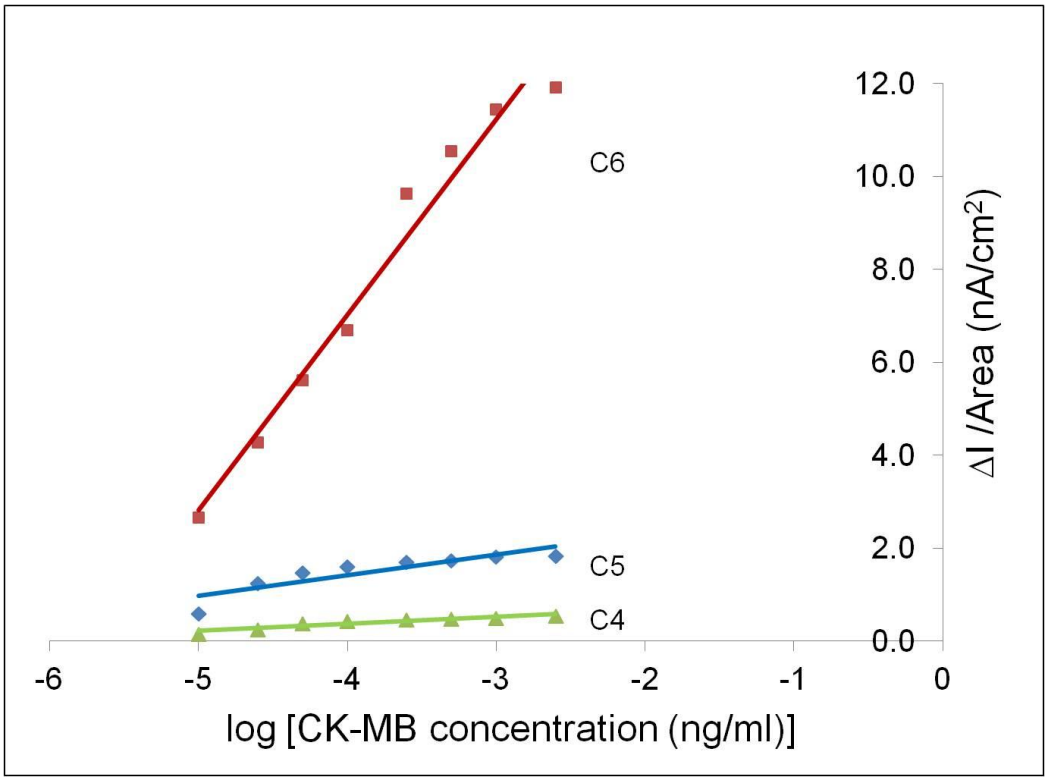

Figure 8.3. CK–MB protein calibration curves with surface area normalisation. C4, C5 and C6 represent three individual microelectrodes following serial incubation in CK–MB protein (from 0.01 to 2.5 pg/ml).

8.4. Testing sample of known CK–MB concentration by extrapolation

A series of solutions with known CK–MB concentrations were tested as a proof–of–concept. The CK–MB concentration of test sample was prepared at 1.5 pg/ml. After the Fc–CHO–labelled microelectrode was incubated in the PBS, it was washed 0.1 % Tween 20 in 10 mM PBS and incubated in test solution for 10 minutes, followed by addition of a small quantity (0.5 pg/ml) of CK–MB protein to the test solution (Section 2.12.4). CycV and SWV scans were then performed.

Five microelectrodes were prepared, of which only two produced a responsive signal where the SWV scans and the peak showed the same pattern as demonstrated in Figure 8.1. Figures 8.4.A and B are the two independent calibration curves of CK–MB concentration against ΔI. The best–fit trendline and equation were displayed in each graph, and used for calculation of the unknown concentration.

By applying the respective Y (ΔI) into the quadratic equations displayed in each graph (electrode A: 0.4593 nA; electrode B: 2.601 nA); the X (or CK–MB concentration) can be calculated. Both the calculated Xs were close to the actual X, i.e. 1.5 pg/ml (Table 8.2), indicating that this extrapolation method gave acceptable data. These two microelectrodes represent preliminary experiments to demonstrate the feasibility of the overall experimental approach.

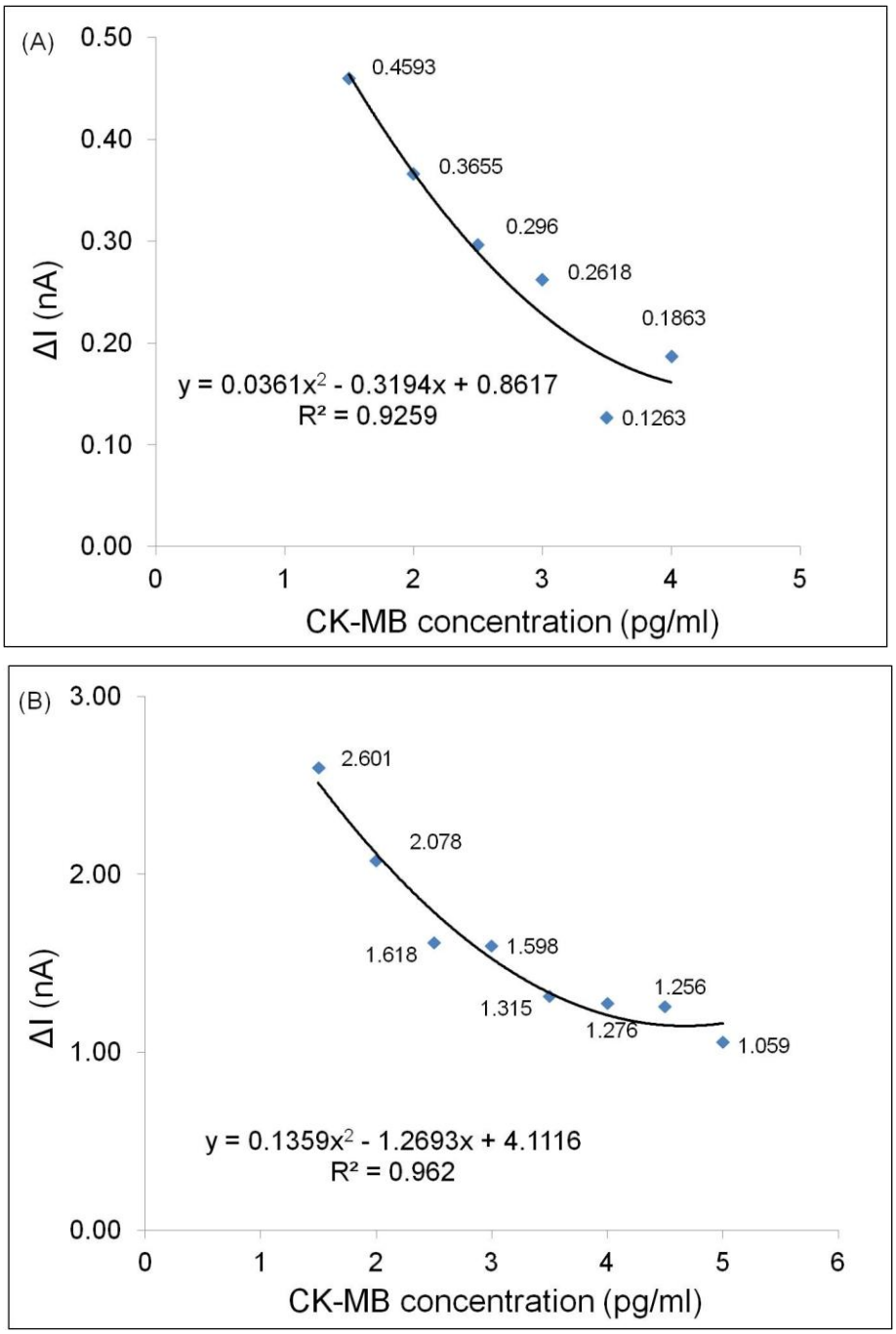

Figure 8.4. CK–MB measurement of test sample of known concentration. Data for A and B are from two independent microelectrodes.

Table 8.2. Comparison of actual and calculated CK–MB concentrations.

Figure 8.4	Equation	Y	Calculated X (pg/ml)	Actual X (pg/ml)
A	$Y = 0.0361\ X^2 - 0.3194\ X + 0.8617$	0.4593	1.522	1.5
B	$Y = 0.1359\ X^2 - 1.2693\ X + 4.1116$	2.601	1.399	

8.5. Testing sample of unknown CK–MB concentration by extrapolation

This CK–MB measurement protocol was applied to test an effluent sample collected during heart tissue perfusion in a Generation 2 device at the 10th minute. After incubation in the test sample, increments of 0.5 pg/ml CK–MB were added to the test sample. A total of 3 microelectrodes were prepared, but data was only obtained from two of these due to technical reasons. Data in Figures 8.5.A and B were collected from two separate microelectrodes, measuring the same test sample. The current peak diminished at different point after the 4th and 8th measurements in Figures 8.5.A and B, respectively, because these values were not normalized to their respective surface areas. Table 8.3 shows the calculation of the CK–MB concentration according to their respective quadratic equations. The heart tissue released an average CK–MB of 0.83 pg/ml at the 10th minute during the perfusion.

Table 8.3. Calculation of the CK–MB concentration.

Figure 8.5	Equation	Y	Calculated X (pg/ml)	Average X (pg/ml)
A	$Y = 0.0273\ X^2 - 0.2438\ X + 0.638$	0.423	0.992	0.831
B	$Y = 0.0018\ X^2 - 0.0617\ X + 0.5141$	0.474	0.670	

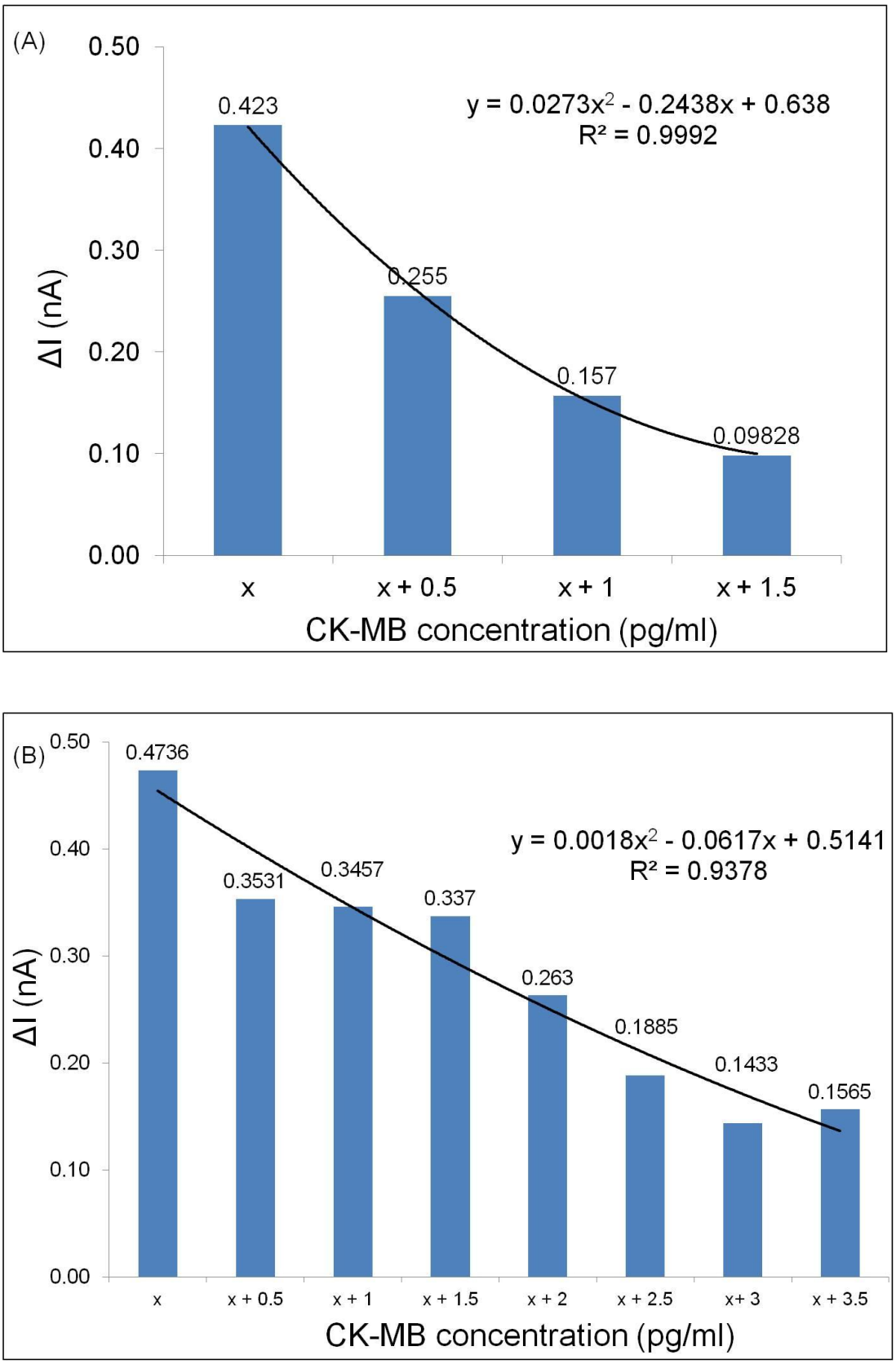

Figure 8.5. CK–MB concentration measurement of effluent sample. A and B are data obtained from two independent microelectrodes.

8.6. CK isoenzymes measurement using commercial electrophoretic kit

Measurement of CK isoenzyme protein was performed using a commercial electrophoretic kit (Section 2.12.6). Initially, serial dilutions of CK–MB protein ranged from 0 to 1 ng/ml were prepared and loaded into the gel. No band was visualised at any of these concentrations (data not shown).

A second run was performed for CK–MB concentrations ranging from 0 to 1000 ng/ml, and a duplicate rat serum samples. CK bands were only observed in the rat serum samples (Figure 8.6), indicative of a lack of sensitivity of the electrophoretic kit. The serum CK activity of rat was approximately 280 IU/L (Kim and Chae, 2006). The sensitivity of the kit is 8 IU/L per band, but the conversion of IU/L to ng/ml was not specified in the kit.

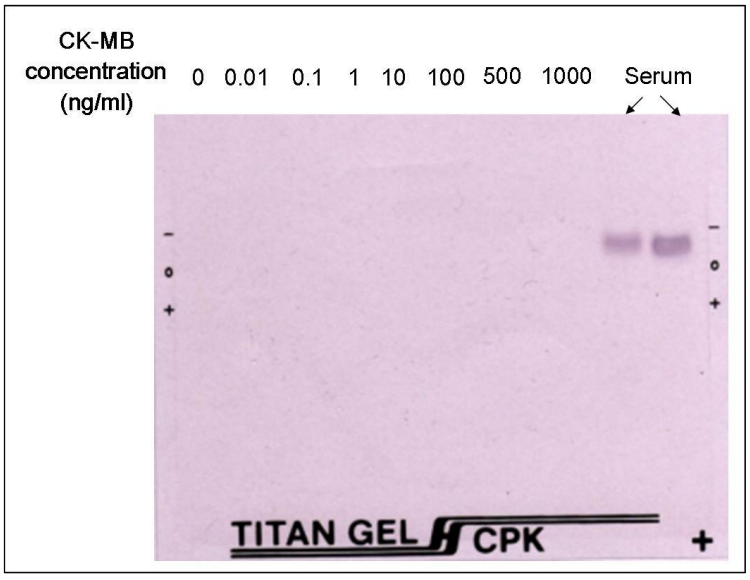

Figure 8.6. CK–MB concentration determination by electrophoretic kit.

8.7. Discussion

A novel CK–MB microsensor made up of carbon fibre housed in a borosilicate capillary tube was constructed for this study. CK–MB antibody was adhered onto the microelectrode electrodeposited with poly(oxyphenylene) insulating layer via a mediator, Fc–CHO. This microsensor was able to detect decreasing current signal in response to increasing CK–MB protein concentrations. Although the limit of detection (LOD) and the range of linear calibration were not determined in this study, the microsensor was able to detect the current change when the CK–MB protein concentration was as little as 0.01 pg/ml in the PBS solution. The CK–MB mass of an unknown sample was determined by incubating the microsensor in the test sample prior to the addition of a series of small amounts (0.5 pg/ml) of CK–MB protein addition in the test sample, using an extrapolation method.

Clinically, although CK–MB is a highly sensitive marker of myocardial injury, its diagnostic specificity can be compromised when trauma of skeletal muscle or extreme exercise is involved. In the microfluidic setting described in previous chapters, a cardiac biopsy was excised from the body and rinsed before placing into the perfusion device; hence the CK–MB release detected by the microsensor would solely determine the damage of the heart biopsy. Construction of this sensitive CK–MB microsensor will therefore assist in the diagnosis of myocardial injury *ex vivo*.

In the microfluidic setting that uses a small biopsy size, a much lower concentration of CK–MB is expected than *in vivo* under oxidative stress or injury and possibly exceeds the LOD of most commercial kits. The sensitivity of the electrophoretic kit used in this study can reach 8 IU/L per band, but it is clear that the kit is insensitive in measuring CK–MB ≤ 1 µg/ml, although the conversion of IU/L to ng/ml was not clear. Additionally, the LODs for CK–MB enzyme–linked immunoassays (ELISA) kits from Percipio Biosciences and Tosoh Bioscience are 2.5 and 0.5 ng/ml, respectively. The effluent sample taken at 10 minutes of perfusion had a mean CK–MB concentration of 0.83 pg/ml, which is below the LOD of these kits. Furthermore, it has been shown

in Chapter 5 that the release of LDH from tissue sample was initially high but the tissue injury was decreased to low level after the first hour of perfusion (Figure 5.6.A), therefore CK–MB concentrations are expected to be lower than 0.83 pg/ml as perfusion continues. Hence, the commercial ELISA kits from Percipio Biosciences and Tosoh Bioscience were not be suitable for use in the current study.

One of the benefits of current electrochemical detection methodology is the speed and robustness in measurement compared with ELISA kits which require more than an hour to generate results. In this study, the procedure time involved 10 minutes of test sample incubation followed by < 1 minute of SWV scans. Although one microelectrode was only able to measure one test sample, the microelectrode can be used repeatedly by transecting the carbon fibre tip, exposing new disk for CK–MB antibody attachment. The antigen binding sites were fully occupied when the peak current at 0.25 V diminished.

Despite normalization of surface area, the calibration curves were greatly varied. This is due, most likely to the fact that each microelectrode has unique properties, such as the length of exposed carbon fibre and the efficiency of insulation coating of the microelectrode. The thickness and integrity of the insulating layer on the microelectrode are critical in the production of a suitable microelectrode for applications in small environment (El-Giar and Wipf, 2006). This can be controlled by standardizing the deposition voltage and time. Deposition potentials below +4 V have been shown to generate thin, non–homogeneous and non–protective insulating layers, whereas potentials greater than +7 V produced thick, non–uniform but protective insulation (El-Giar and Wipf, 2006). In addition, deposition times of less than 3 minutes produced porous and non–insulating layers, when the deposition potential was held at +4.3 V. The thickness of poly(oxyphenylene) coating was approximately 2 µm after 3 minutes of electropolymerization. In this study, deposition was accomplished by applying potential of +4 V for 3 minutes versus a graphite rod (Amatore *et al.*, 2008). At +4 V, the phenolic

group on the 2–allylphenol was oxidized via a one electron and one proton transfer, generating a phenoxy radical (Mengoli and Musiani, 1994). This free radical then induced a step–growth polymerization, forming the poly(oxyphenylene) film around the microelectrode. Subsequent studies will determine the optimum deposition potential and time for carbon fibre microelectrode, thereby enhancing the reproducibility in microsensor construction.

Electrochemical signal is generated via the transfer of electrons at the electrode. The redox centre of the enzyme (i.e. CK-MB) is usually shielded by a thick protein shell, therefore the direct electron transfer between the enzyme and electrode is very slow (Okawa *et al*., 1999). This limitation can be overcome by using a redox mediator which assists in direct shuttling of electrons between the microelectrode and a redox enzyme. There are many redox mediators reported in the biosensor preparation, for example ferrocene derivatives (Frasconi *et al*., 2009) and enzymes, such as HRP (Cai *et al*., 2007, Lee *et al*., 2008), glucose oxidase (Wang *et al*., 2009, Chirizzi *et al*., 2011) and alkaline phosphatase (Fanjul-Bolado *et al.,* 2007, Centi *et al*., 2010). HRP is the most commonly used electrochemical immunoassay mediator. Although a CK–MB antibody conjugated with HRP pre–made by the antibody supplier exists, the release of H_2O_2 from the tissue as a result of oxidative stress may lead to the interference in the redox processes of HRP, giving inaccurate measurement of CK–MB.

In this study, Fc–CHO was used as mediator and attached to the IgG antibody through Schiff–base reaction as described previously (Okochi *et al*., 2005). The antibody–immobilization protocols performed in this study are also applicable to any antibody on different types of carbon electrodes. Similar protocols have been employed in the laboratory, where dual Fc–tagged, FITC–labelled antibodies (mouse anti human CD 14 and anti human interleukin 10) were immobilized on a gold–film electrode surface. Fluorescence signals were exhibited, showing that the antibodies were successfully immobilised onto the electrode surface and the crosslinking

procedures were not interfering with the FITC–tag that was already present on the antibodies (unpublished results by Dr Y. Dou).

A number of electrochemical biosensors have been fabricated to detect total CK activity using different mediators and methods of enzyme immobilization (Nagy *et al*., 1998 a and b, Cai *et al*., 2007, Liu *et al*., 2007). An amperometric microcell used for total CK activity measurement was established (Nagy *et al*., 1998a). The working electrode was made up of gold plate electrode electroplated with a platinum layer, and reference electrode was the Ag/AgCl. In their studies, two different reactions were investigated for CK activity determination. In the catalytic action of CK at pH 6.7 (PCr + ADP ⇌ creatine + ATP), the ATP produced reacts with glycerol under glycerol kinase (GK) catalysis (ATP + glycerol ⇌ ADP + glycerol–3–P). Then glycerol–3–phosphate (glycerol–3–P) was oxidised and yielded H_2O_2, under catalytic action of glycerophosphate oxidase (GPO; Glycerol–3–P + O_2 ⇌ dihydroxyacetone + H_2O_2). In the second reaction, the creatine produced was hydrolyzed by creatinase, liberating sarcosine (Creatine + H_2O ⇌ sarconine + urea). Subsequently, sarcosine was oxidized under the catalytic action of sarcosine oxidase, generating H_2O_2 (Sarcosine + H_2O + O_2 ⇌ glycine + HCHO + H_2O_2). The H_2O_2 production from these reactions was followed by amperometric electrochemical microelectrode and the rate of the production was proportional to the total CK activity. The biosensor with the GK catalytic principle was more sensitive than that of the creatinase, with a higher current–time transient after 2 µl serum sample was added.

A three–gold–electrode system was also developed for total CK examination, fabricated by polyvinylpyridine–osmium–wired horseradish peroxidase (PVP–Os–HRP) redox polymer film (Cai *et al*., 2007). The HRP catalyzed the reduction of H_2O_2 to water, and itself reduced by osmium (II) that was converted to osmium (III) (H_2O_2 + osmium (II) ⇌ H_2O + osmium (III)). The working electrode donates electrons to osmium (III), regenerating

osmium (II) and hence producing a measurable electrical current (Yigzaw *et al*., 2002). The amount of current generated at the electrode was proportional to the CK activity. The same principle was also employed by Liu *et al*. (2007) to produce a disposable biosensor where a highly active redox polymer containing osmium (II/III) was modified onto the working electrode, and subsequently a trienzyme (HRP, GPO, and GK) complex was immobilized on the biosensor.

Cai *et al*. (2007) have used ferricyanide ($Fe(CN)_6^{3-}$] as the mediator, in comparison to PVP–Os–HRP. The glycerol–3–P was oxidised by GPO, while $Fe(CN)_6^{3-}$ was reduced to ferrocyanide ($Fe(CN)_6^{4-}$; Glycerol–3–P + $Fe(CN)_6^{3-}$ ⇌ dihydroxyaceone + $Fe(CN)_6^{4-}$). Electron donation from the working electrode regenerated $Fe(CN)_6^{3-}$ and generated an electrical current. The current flow occurred when $Fe(CN)_6^{3-}$ was oxidised on the working electrode and the rate of current was proportional to the CK activity. They have reported that the CK biosensor modified with $Fe(CN)_6^{3-}$ had a higher LOD (100 U/L versus 10 U/L) than the one modified with PVP–Os–HRP.

However, the limitation of these previous biosensors was attributed to the lack of specificity, which was different to the biosensor developed in current study, specifically measuring CK–MB protein concentration. To date, no one has employed 7 µm carbon fibres as the working electrode; hence this study presents a novel CK–MB carbon fibre microsensor, which allows its application and integration with the microfluidic platform in the future. The fine tip of microsensor can be positioned adjacent to the heart tissue surface, causing no physical tissue damage, to measure the CK–MB released from cardiac biopsies.

In summary, a preliminary study for the rapid and sensitive ECIA measurement of CK–MB concentration has shown that this microsensor was able to detect the current changes with CK–MB protein concentration as little as 0.01 pg/ml. Although additional work is still required to produce a reliable, integrated sensing system, it has provided proof–of–concept in capturing protein biomarkers and determination of concentration by electrochemistry.

Chapter 9

Conclusion

The work presented in this thesis described the heart tissue maintenance and interrogation in two different microfluidic devices. A prototype PDMS microfluidic device was first designed and fabricated followed by the production of a more controllable and defined glass microfluidic chip. These PDMS and glass devices were able to keep biopsies viable for 5 and 24 hours, respectively, which was considered sufficient as clinical heart biopsies are usually preserved *ex vivo* for no longer than 4 – 6 hours (Ozeki *et al*., 2007). Furthermore, these devices were subsequently used to study the effect of myocardial IR injury on a series of stress and injury marker genes. Since the biopsy perfused in the system was millimetres in dimension, it allows direct *in vitro* analysis of primary clinical tissue. This proof of concept device can be adopted for many types of tissue experimentation, potentially leading to significant reduction and even replacement of animal experimentations.

Cardiac remodelling against acute and chronic stress signalling is thought to be due to the activation or repression of certain genes that encode proteins which modulate cardiac contractility and structure (van Rooij *et al*., 2006). Therefore, patients with different cardiac complications or disease stages exhibit different patterns of gene expression, known as the gene signature. Despite large–scale analysis giving huge amounts of information; this is costly and involves significant investment in equipment. Simple, easy to perform and cost effective methods for generating relevant gene signatures are lacking, however, microfluidic devices could be an alternative to identify and validate gene signatures, in an automated, real–time and routine manner, either for diagnostic use, or in treatment monitoring during the course of cardiac disease.

A novel CK–MB microsensor has also been described here, where CK–MB protein concentration changes as little as 0.01 pg/ml could be detected by electrochemical means. Further work is currently under investigation in the laboratory to optimise the microsensor and further integrate with the existing

Generation 2 glass chip, giving a real–time and sensitive on–chip CK–MB measurement during the perfusion. Additionally, antibodies of other cardiac markers or metabolites could be adhered onto microelectrodes via the same method so that the response of the cardiac biopsy under stress and/or pharmacological treatments can be assessed simultaneously, by placing a number of these in series.

Mice and rats are the popular animal models in cardiovascular studies, because they are cheap and relatively easy for creating transgenic models. However, results obtained in these animals might not transfer to the human system. For instance, large numbers of therapeutic drugs in clinical trials have given disappointing results, even though successes have been found in animal studies, e.g. vitamin E (Lassnigg *et al*., 2003, Vivekananthan *et al*., 2003), and angiogenic cytokine protein (Zachary and Morgan, 2011) treatments. The need for cardiac research on human biopsies can be addressed by experimenting using these devices, with reduced reliance on animal models. The application of these devices could be used in the clinical setting for POC diagnostics. The enclosed Generation 2 perfusion system can be set up near the cardiac operating theatre and the heart tissue biopsy obtained from patients undergoing CABG surgery subjected to perfusion in this system immediately following surgical resection, reducing the biopsy transportation time and increasing the speed of analysis.

Increases in NHS expenditure appear to be a great concern. According to the Department of Health–Spending Review 2010, total NHS spending was £103.8 billion in 2010/11, £ 105.9 billion in 2011/12 and expected to increase to £ 114.4 by 2014/15 (HM Treasury, 2010). However, the quality of service remains ineffective and does not necessarily correlate with the total spending. Patients with cardiac complications are often given different prescribed drugs to control the course of disease, depending on the nature of their heart problem and the presence of concomitant diseases (Muntwyler *et al.*, 2004). This is different for every patient. If the drug does not work or has unpleasant side effects, other dosage or new drugs will be given. Such cycle may be repeated until a suitable treatement is discovered. Apart from diagnosis,

microfluidics is capable of aiding clinicians in treatment decision making. Microfluidic devices could be used to determine the best medications (in term of combination and dosage), with most beneficial effects and least detrimental injury or side effects, tailored specifically for each patient, hence offering an opportunity for individualized patient treatment (Higgins *et al*., 2007). Raising national healthcare service (NHS) quality through the practice of individualised or personalised treatment can generate savings in the long term (Eddy *et al*., 2011), via early and effective treatment, substantial reduction in the length of in–patient stays, and the number of clinic visits required.

The long term vision of the current work is to carry out multiple, parallel analyses on a single device (Figure 9.1), so that huge amounts of information can be obtained from a single sample. The very first step, i.e. tissue maintenance in an optimised device has been demonstrated here. While continuously paced, the contraction of the tissue can be measured using a miniaturised ultrasensitive force transducer. The release of cardiac biomarkers or other metabolites can be captured by the relevant electrochemical probes. In addition, cell lysis (Lu *et al*., 2005) and sorting (Kang *et al*., 2008), on–chip DNA analysis (Ottesen *et al*., 2006), fluorescence study (Huang *et al.*, 2007) and flow cell analysis (Wang *et al*., 2008) modules are available and these could be coupled with the current microfluidic device, generating as much information as possible from a small tissue biopsy. Miniaturization or downscaling of medical technologies has the potential to take over the conventional methods by which patients are diagnosed. Current POC diagnostic systems available in the market only allow cardiac biomarkers measurement in blood or serum. However, the idea proposed in Figure 9.1 would be particularly valuable and useful in assessing clinical samples to generate large amounts of data and aid the clinician in making the best therapeutic decision on patients, through a greater insight of the biological basis of heart diseases. This will hopefully serve as a novel platform technology for future cardiac research over the forthcoming decade.

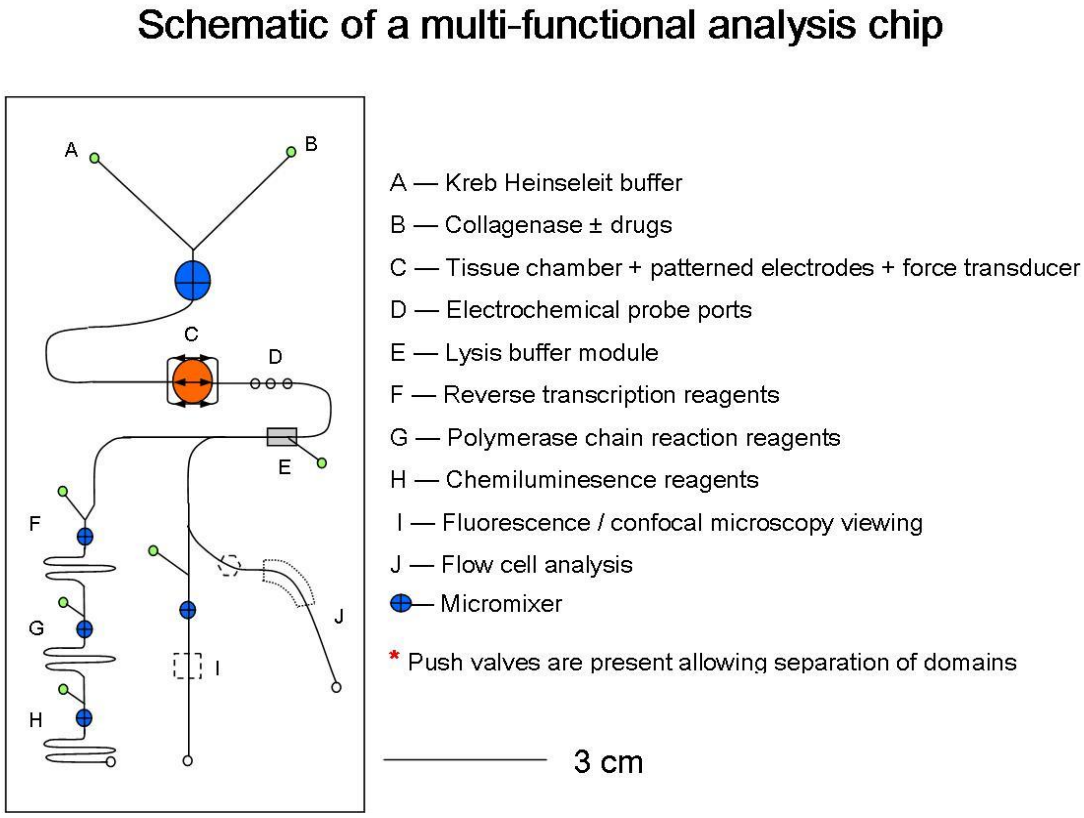

Figure 9.1. A proposed multi–functional analysis chip for heart tissue.

Publications and Presentations

Papers

Cheah, L. T., Dou, Y. H., Seymour, A. M. L., Dyer, C. E., Haswell, S. J., Wadhawan, J. D. and Greenman, J. (2010) Microfluidic perfusion system for maintaining viable heart tissue with real–time electrochemical monitoring of reactive oxygen species. *Lab on a Chip* **10**: 2720 – 2726.

Cheah, L. T., Fritsch, I., Haswell, S. J. and Greenman, J. (2011) Evaluation of heart tissue viability under redox–magnetohydrodynamics conditions: toward fine–tuning flow in biological microfluidic applications. *Biotechnology and Bioengineering* (DOI 10.1002/bit.24426).

Oral Presentations

Development of a miniaturized perfusion device for maintaining viable heart tissue biopsies. **Cheah, L. T.** and Dou, Y. H., Northern Cardiovascular Research Group Meeting, Leeds (2009)

Poster Presentations

Lab on a chip: the way forward in myocardial diagnostics? **Cheah, L. T.**, Riaz, I., Dou, Y. H., Seymour, A. M. L., Dyer, C. E., Haswell, S. J., Wadhawan, J. D. and Greenman, J., European Society of Cardiology Congress, Berlin (2010)

Microfluidic perfusion system for maintaining viable heart tissue with real–time electrochemical monitoring of reactive oxygen species. Dou, Y. H., **Cheah, L. T.**, Seymour, A. M., Dyer, C. E., Haswell, S. J., Wadhawan, J. D. and Greenman, J., Northern Cardiovascular Research Group Meeting, Manchester (2010)

Miniaturized perfusion devices for heart tissue. **Cheah, L. T.**, Seymour, A. M. L., Haswell, S. J. and Greenman, J., Northern Cardiovascular Research Group Meeting, Hull (2011)

Suppliers of chemicals, materials and equipment

Suppliers	Products
Abcam (UK)	• Creatine kinase–M/B protein (ab73649)
Alfa Aesar (UK)	• Polystyrene latex microspheres
AlfaLab (US)	• Direct current magnetometer
Bibby Sterilin (UK)	• Borosilicate capillary tubes
Bioanalytical Systems (UK)	• Ag/AgCl reference electrode
Bio–Rad Laboratories (US)	• Ethidium bromide (161–0433)
BioTek Instruments (US)	• Microplate reader
BOC (UK)	• Gaseous 95 % O_2, 5 % CO_2
Bostik Findley (UK)	• Araldite adhesive
Charles River Laboratories International (UK)	• Male sprague dawley rats
Creativematerials (US)	• Silver paste
Dow Corning Corporation (US)	• SYLGARD®184 silicone elastomer kit
Edwards High Vacuum (UK)	• SPEEDIVAC coating unit (Model 12E6/1405)
Energas (UK)	• Gaseous N_2
Eurofins MWG Operon (Germany)	• PCR primers
GE Healthcare (Sweden)	• Vivaspin concentrators
Gilson (France)	• Minipuls3 peristaltic pumps
Grant Instruments (UK)	• Water bath
Harvard Apparatus (UK)	• Syringe pump (PHD 22/2000 series)
Helena Biosciences (UK)	• SAS–MX CK VIS–10 isoenzyme kit
Hopkin and Williams (UK)	• Graphite powder

Suppliers	Products
Invitrogen (UK)	• Amplex red hydrogen peroxide assay kit (A22188) • Calcein, acetoxymethyl ester (C3100MP) • DNA ladder (15628–019) • dNTP mix (18427–088) • Moloney murine leukemia virus reverse transcriptase kit (28025–013) • Oligo $(dT)_{15}$ primer (18418–012) • Pluronic F–127 (P6866) • RNaseOUT™ recombinant ribonuclease inhibitor (10777–019) • UltraPure™ agarose 1000 (10975–035)
Kemet International (UK)	• Polishing pads
Kinesis (UK)	• Ferrule (072655) • Micro tight gauge plug 6–32” (P553) • Nanoport assemblies headless 6–32” coned (N–126H) • Nanoport nut (F–126H) • Nanoport reservoir assembly (N–131) • PEEK tubings (1568)
Komodo (UK)	• Thermostat
Linkam Scientific Instruments (UK)	• Hotplate • MC 60 controller
Loctite (UK)	• Instant adhesive (Loctite 4850)
Martindale Pharmaceuticals (UK)	• Cardioplegia infusion
Milipore Corporation (US)	• 0.22 µm syringe driven filters
Nikon	• Inverted confocal microscope (TE2000–E)
Norland Products (US)	• Norland optical adhesive
Omni International (US)	• Omni mixer homogenizer
PalmSens Instruments BV (Netherland)	• Potentiostat
Pennine Industries (UK)	• Heat mat
Permabond Engineering Adhesives (UK)	• Adhesive
Pharmacia Biotech (US)	• GeneQuant II RNA/DNA calculator

Suppliers	Products
Promega (UK)	• PCR mastermix (M7502)
QIAgen (UK)	• RNeasy fibrous tissue mini kit (74704)
Roche Diagnostics (UK)	• Cytotoxicity detection kit ^{Plus} (LDH)
Santa Cruz Biotechnology (Germany)	• Creatine kinase–M/B rabbit polyclonal IgG (sc–28898)
Sigma–Aldrich (UK)	• Dimethylformamide • Ethyl(dimethylaminopropyl) carbodiimide • Ferrocene–carboaldehyde • L–lactic dehydrogenase, from rabbit muscle (L1254) • Penicillin–Streptomycin solution (P0781) • Propidium iodide (P4864) • Ruhex (III) • N–hydroxysulphosuccinimide • Miscellaneous chemicals
Silver Spoon (UK)	• Red food colouring
Spectroline Spectronics Corporations (US)	• UV source
Sutter Instrument (US)	• Micropipette puller (Model P–97)
Syngene (US)	• Gene flash bio imaging system
TC Direct (UK)	• Dual input multi thermocouple type indicator • Type K thermocouple wire
SLS (UK)	• DNA thermal cycler
Thurlby Thandar Instruments (UK)	• Programmable function generator
Veho (UK)	• VMS–001 USB microscope camera
World Precision Instruments (UK)	• Hotplate
Link Pharmaceuticals (UK)	• Sodium thiopentone
Zeiss	• Inverted microscope (Axiovert S100)

Supplementary Videos

Short video clips are provided in the CD, showing the microbead movement due to thermal convection and MHD (Videos 1 – 5; Chapter 7) and contraction of tissues during perfusion within Generation 1 system (Videos 6 – 9; Chapter 3). The conditions of each video are given below:

Conditions	Perfusion/ Static	Electrical stimulation	Presence of Ruhex	Presence of magnet
Video 1	Static	From 4 seconds	–	–
Video 2	Static	√	–	√
Video 3	Perfusion	√	–	√
Video 4	Static	From 3 seconds	√	√
Video 5	Perfusion	From 2 seconds	√	√
Video 6	Rat heart tissue perfused within Generation 1 system (Example 1)			
Video 7	Rat heart tissue perfused within Generation 1 system (Example 2)			
Video 8	Human heart tissue perfused within Generation 1 system (Example 1)			
Video 9	Human heart tissue perfused within Generation 1 system (Example 2)			

References

Abbate, A., Bussani, R., Sinagra, G., Barresi, E., Pivetta, A., Perkan, A., Hoke, N. H., Salloum, F. N., Kontos, M. C., Biondi-Zoccai, G. G. L., Vetrovec, G. W., Sabbadini, G., Baldi, F., Silvestri, F., Kukreja, R. C. and Baldi, A. (2008) Right ventricular cardiomyocyte apoptosis in patients with acute myocardial infarction of the left ventricular wall. *The American Journal of Cardiology* **102** (6): 658 – 662.

Abbyad, P., Tharaux, P., Martin, J., Baroud, C. N. And Alexandrou, A. (2010) Sickling of red blood cells through rapid oxygen exchange in microfluidic drops. *Lab on a Chip* **10**: 2505 – 2512.

Adluri, R. S., Thirunavukkarasu, M., Zhan, L., Maulik, N., Svennevig, K. and Maulik, M. B. G. (2011) Cardioprotective efficacy of a novel antioxidant mix VitaePro against *ex vivo* myocardial ischaemia–reperfusion injury. *Cell Biochemistry and Biophysics*: Epub.

Akçetin, Z., Pregla, R., Darmer, D., Heynemann, H., Haerting, J., Brömme, H. J. and Holtz, J. (1999) Differential expression of heat shock proteins 70–1 and 70–2 mRNA after ischaemia–reperfusion injury of rat kidney. *Urological Research* **27**: 306 – 311.

Akki, A., Smith, K. and Seymour, A. L. (2008) Compensated cardiac hypertrophy is characterised by a decline in palmitate oxidation. *Molecular and Celular Biochemistry* **311**: 215 – 224.

Alcalá, S., Klee, M., Fernández, J., Fleischer, A. and Pimentel-Muiños, F. X. (2008) A high–throughput screening for mammalian cell death effectors identifies the mitochondrial phosphate carrier as a regulator of cytochrome *c* release. *Oncogene* **27**: 44 – 54.

Aldakkak, M., Stowe, D. F., Chen, Q., Lesnefsky, E. J. and Camara, A. K. (2008) Inhibited mitochondrial respiration by amobarbital during cardiac ischaemia improves redox state and reduces matrix Ca^{2+} overload and ROS release. *Cardiovascular Research* **77** (2): 406 – 415.

Aleyassine, H., Tonks, D. B. and Kaye, M. (1978) Natural fluorescence in serum of patients with chronic renal failure not to be confused with creatine kinase–BB isoenzyme. *Clinical Chemistry* **24**: 492 – 493.

Alloatti, G., Arnoletti, E., Bassino, E., Penna, C., Perrelli, M. G., Ghé, C. and Muccioli, G. (2010) Obestatin affords cardioprotection to the ischaemic–reperfused isolated rat heart and inhibits apoptosis in cultures of similarly stressed cardiomyocytes. *American Journal of Physiology – Heart and Circulatory Physiology* **299** (2): H470 – H481.

Alpert, J. S., Thygesen, K., Antman, E. and Bassand, J. P. (2000) Myocardial infarction redefined–a consensus document of The Joint European Society of Cardiology/American College of Cardiology Committee for the redefinition of myocardial infarction. *Journal of The American College of Cardiology* **36**: 959 – 969.

Amatore, C., Arbault, S., Chen, Y., Crozatier, C. and Tapsoba, I. (2007) Electrochemical detection in a microfluidic device of oxidative stress generated by macrophage cells. *Lab on a Chip* **7**: 233 – 238.

Amatore, C., Arbault, S., Ferreira, D. C. M., Tapsoba, I. and Verchier, Y. (2008) Vitamin C stimulates or attenuates reactive oxygen and nitrogen species (ROS, RNS) production depending on cell state: Quantitative amperometric measurements of oxidative bursts at PLB–985 and RAW 264.7 cells at the single cell level. *Journal of Electroanalytical Chemistry* **615**: 34 – 44.

Anderson, E. C., Weston, M. C. and Fritsch, I. (2010) Investigations of redox magnetohydrodynamic fluid flow at microelectrode arrays using microbeads. *Analytical Chemistry* **82**: 2643 – 2651.

Anderson, J. L., Adams, C. D., Antman, E. M., Bridges, C. R., Califf, R. M., Casey Jr, D. E., Chavey II, W. E., Fesmire, F. M., Hochman, J. S., Levin, T. N., Lincoff, A. M., Peterson, E. D., Theroux, P., Wenger, N. K. and Wright, R. S. (2011) 2011 ACCF/AHA focused update incorporated into the ACC/AHA 2007 guidelines for the management of patients with unstable angina/non–ST–elevation myocardial infarction. A report of the american college of cardiology foundation/american heart association task force on practice guidelines. *Circulation* **123**: e426 – e579.

Andrienko, T., Kuznetsov, A. V., Kaambre, T., Usson, Y., Orosco, A., Appaix, F., Tiivel, T., Sikk, P., Vendelin, M., Margreiter, R. and Saks, V. A. (2003) Metabolic consequences of functional complexes of mitochondria, myofibrils and sarcoplasmic reticulum in muscle cells. *The Journal of Experimental Biology* **206**: 2059 – 2072.

Apple, F. S., Jesse, R. L., Newby, L. K., Wu, A. H. B. and Christenson, R. H. (2007) National academy of clinical biochemistry and IFCC committee for standardization of markers of cardiac damage laboratory medicine practice guidelines: analytical issues for biochemical markers of acute coronary syndromes. *Clinical Chemistry* **53** (4): 547 – 551.

Apple, F. S., Falahati, A., Paulsen, P. R., Miller, E. A., Sharkey, S. W. (1997) Improved detection of minor ischaemic myocardial injury with measurement of serum cardiac troponin I. *Clinical Chemistry* **43** (11): 2047– 2051.

Arbault, S., Edeas, M., Legrand-Poels, S., Sojic, N., Amatore, C., Piette, J., Best-Belpomme, M., Lindenbaum, A. and Vuillaume, M. (1997) Phenylarsine oxide inhibits *ex vivo* HIV–1 expression. *Biomedicine and Pharmacother*apy **51** (10): 430 – 438.

Arbustini, E. and Narula, J. (2010) Cyclosporin A in reperfusion injury: not opening to cell death knocking at the door? *The Annals of Thoracic Surgery* **89**: 1349 – 1351.

Arslan, F., Smeets, M. B., O'Neill, L. A. J., Keogh, B., McGuirk, P., Timmers, L., Tersteeg, C., Hoefer, I. M., Doevendans, P. A., Pasterkamp, G. and de Kleijn, D. P. V. (2010) Myocardial ischaemia/reperfusion injury is mediated by leukocytic toll–like receptor–2 and reduced by systemic administration of a novel anti–toll–like receptor–2 antibody. *Circulation* **121**: 80 – 90.

Avkiran, M., Cook, A. R. and Cuello, F. (2008) Targeting Na^+/H^+ exchanger regulation for cardiac protection: a RSKy approach? *Current Opinion in Pharmacology* **8** (2): 133 – 140.

Ba, B. B., Bernard, A., Iliadis, A., Quentin, C., Ducint, D., Etienne, R., Fourtillan, M., Macchi-Guillot, I. and Saux, M. (2001) New approach for accurate simulation of human pharmacokinetics in an *in vitro* pharmacodynamic model: application to ciprofloxacin. *Journal of Antimicrobial Chemotherapy* **47**: 223 – 227.

Babuin, L. and Jaffe, A.S. (2005) Troponin: the biomarker of choice for the detection of myocardial injury. *Canadian Medical Association Journal* **173**: 1191– 1202.

Baines, C. P. (2009) The mitochondrial permeability transition pore and ischaemia–reperfusion injury. *Basic Research in Cardiology* **104** (2): 181 – 188.

Baines, C. P. (2009) The molecular composition of the mitochondrial permeability transition pore. *Journal of Molecular and Cellular Cardiology* **46** (6): 850 – 857.

Baines, C. P., Kaiser, R. A., Purcell, N. H., Blair, N. S., Osinska, H., Hambleton, M. A., Brunskill, E. W., Richard Sayen, M., Gottlieb, R. A., Dorn II, G. W., Robbins, J. and Molkentin, J. D. (2005) Loss of cyclophilin D reveals a critical role for mitochondrial permeability transition in cell death. *Nature* **434**: 658 – 662.

Baines, C. P., Kaiser, R. A., Sheiko, T., Craigen, W. J. and Molkentin, J. D. (2007) Voltage dependent anion channels are dispensable for mitochondrial–dependent cell death. *Nature Cell Biology* **9**: 550 – 555.

Baker, D. R. (1995) *Capillary electrophoresis*. New York: John Wiley & Sons.

Bär, F. W., Tzivoni, D., Dirksen, M. T., Fernández-Ortiz, A., Heyndrickz, G. R., Brachmann, J., Reiber, J. H. C., Avasthy, N., Tatsuno, J., Davies, M., Hibberd, M. G. and Krucoff, M. W. (2006) Results of the first clinical study of adjunctive CAldaret (MCC–135) in patients undergoing primary percutaneous

coronary intervention for ST–Elevation Myocardial Infarction: the randomized multicentre CASTEMI study. *European Heart Journal* **27**: 2516 – 2523.

Barsotti, A., Di Napoli, P., Taccardi, A. A., Spina, R., Stuppia, L., Palka, G., Barbacane, R. C., De Caterina, R. and Conti, P. (2001) MK–954 (losartan potassium) exerts endothelial protective effects against reperfusion injury: evidence of an e–NOS mRNA overexpression after global ischaemia. *Atherosclerosis* **155**: 53 – 59.

Barua, A., Standen, N. B. and Galinanes, M. (2010) Dual role of nNOS in ischaemic injury and preconditioning. *BioMed Central Physiology* **10**: 15.

Bassani, J. W. M., Bassani, R. A. and Bers, D. M. (1994) Relaxation in rabbit and rat cardiac cells: species dependent differences in cellular mechanisms. *The Journal of Physiology* **476**: 279 – 293.

Bassani, J. W. M., Yuan, W. and Bers, D. M. (1995) Fractional SR Ca release is regulated by trigger Ca and SR Ca content in cardiac myocytes. *Americal Journal of Physiology Cellular Physiology* **268**: C1313 – C1319.

Bassenge, E., Sommer, O., Schwemmer, M. and Bünger, R. (2000) Antioxidant pyruvate inhibits cardiac formation of reactive oxygen species through changes in redox state. *American Journal of Physiology – Heart and Circulatory Physiology* **279** (5): H2431 – H2438.

Basso, E., Fante, L., Fowlkes, J., Petronilli, V., Forte, M. A. and Bernardi, P. (2005) Properties of permeability transition pore in mitochondria devoid of cyclophilin D. *Journal of Biological Chemistry* **280** (19): 18558 – 18561.

Basu, S., Uma Rani, P. and Srinivasan, A. R. (2009) Association of Creatine kinase (MB) and troponin (I) with electrocardiographic changes, in acute myocardial infarction. *Biomedical Research* **20** (2): 84 – 86.

Bau, H. H., Zhu, J., Qian, S. and Xiang, Y. (2003) A magneto–hydrodynamically controlled fluidic network. *Sensors and Actuators B* **88**: 205 – 216.

Belikova, N. A., Vladimirov, Y. A., Osipov, A. N., Kapralov, A. A., Tyurin, V. A., Potappovich, M. V., Basova, L. V., Peterson, J., Kurnikov, I. V. and Kagan, V. E. (2006) Peroxidase activity and structural transitions of cytochrome c bound to cardiolipin–containing membranes. *Biochemistry* **45** (15): 4998 – 5009.

Bell, R. M., Mocanu, M. M. and Yellon, D. M. (2011) Retrograde heart perfusion: the Langendorff technique of isolated heart perfusion. *Journal of Molecular and Cellular Cardiology* **50**: 940 – 950.

Bentzen, B. H., Andersen, R. W., Olesen, S. P., Grunnet, M. and Nardi, A. (2010) Synthesis and characterisation of NS13558: a new important tool for

addressing KCa1.1 channel function *ex vivo*. *Naunyn–Schmiedeberg's Archives of Pharmacology* **381**: 271 – 283.

Berdichevsky, Y., Sabolek, H., Levine, J. B., Staley, K. J. and Yarmush, M. L. (2009) Microfluidics and multielectrodes array–compatible organotypic slice culture method. *Journal of Neuroscience Methods* **178**: 59 – 64.

Beresewicz, A., Karwatowska-Prokopczuk, E., Lewartowski, B. and Cedro-Ceremuåzyńska, K. (1995) A protective role of nitric oxide in isolated ischaemic/reperfused rat heart. *Cardiovascular Research* **30** (6): 1001 – 1008.

Bernardi, P., Krauskopf, A., Basso, E., Petronilli, V., Blachly-Dyson, E., Di Lisa, F. and Forte, M. A. (2006) The mitochondrial permeability transition from *in vitro* artefact to disease target*. FEBS Journal* **273**: 2077 – 2099.

Berry, G. J. and Billingham, M. E. (2007) Heart. In: S. E. Mills, ed. 2007. *Histology for pathologists*. 3rd ed. US: Lippincott Williams & Wilkins.

Bers, D. M. (2002) Cardiac excitation–contraction coupling. *Nature* **415**: 198 – 205.

Bers, D. M. (2008) *Excitation–contraction coupling and cardiac contractile force*. 2nd ed. Netherland: Springer.

Bessman, S. P. and Geiger, P. J. (1981) Transport of energy in muscle: the phosphorylcreatine shuttle. *Science* **211** (4481): 448 – 452.

Beuerle, J. R., Azzazy, H. M. E., Styba, G., Duh, S. H. and Christenson, R. H. (2000) Characteristics of myoglobin, carbonic anhydrase III and the myoglobin/carbonic anhydrase III ratio in trauma, exercise, and myocardial infarction patients. *Clinica Chimica Acta* **294** (1 – 2): 115 – 128.

Bhadriraju, K. and Chen, C. S. (2002) Engineering cellular microenvironments to improve cell–based drug testing. *Drug Discovery and Therapeutics* **7** (11):612 – 620.

Bhakuni, P., Chandra, M. and Misra, M. K. (2005) Oxidative stress parameters in erythrocytes of post reperfused patients with myocardial infarction. *Journal of Enzyme Inhibition and Medicinal Chemistry* **20**: 377 – 381.

Bhattacharyya, A. and Klapperich, C. M. (2007) Design and testing of a disposable microfluidic chemiluminescent immunoassay for disease biomarkers in human serum samples. *Biomedical Microdevices* **9** (2): 245 – 251.

Bissell, M. (2003) Biology's new dimension. *Nature* **424**: 870 – 872.

Bolli, R. (2001) Cardioprotective function of inducible nitric oxide synthase and role of nitric oxide in myocardial ischaemia and preconditioning: an overview of a decade of research. *Journal of Molecular and Cellular Cardiology* **33**: 1897 – 1918.

Boo, Y. C., Mun, G. I., Tressel, S. L. and Jo, H. (2011) Detection of low levels of nitric oxide using an electrochemical sensor. *Methods in Molecular Biology* **704**: 81 – 89.

Boomsma, F. and van den Meiracker, A. H. (2001) Plasma A– and B–type natriuretic peptides: physiology, methodology and clinical use. *Cardiovascular Research* **51**: 442 – 449.

Borutaite, V. and Brown, G. C. (2003) Mitochondria in apoptosis of ischaemic heart. *Federation of European Biochemical Societies* **541**: 1 – 5.

Borutaite, V., Morkuniene, R., Arandarcikaite, O., Jekabsone, A., Barauskaite, J. and Brown, G. C. (2009) Nitric oxide protects the heart from ischaemia–induced apoptosis and mitochondrial damage via protein kinase G mediated blockage of permeability transition and cytochrome c release. *Journal of Biomedical Science* **16**: 70.

Boyce, S. W., Bartels, C., Bolli, R., Chaitman, B., Chen, J. C., Chi, E., Jessel, A., Kereiakes, D., Knight, J., Thulin, L., Theroux, P. and GUARDIAN study investigators. (2003) Impact of sodium–hydrogen exchange inhibition by cariporide on death or myocardial infarction in high–risk CABG surgery patients: results of the CABG surgery cohort of the GUARDIAN study. *The Journal of Thoracic and Cardiovascular Surgery* **126** (2): 420 – 427.

Brand, M. D. (2005) The efficiency and plasticity of mitochondrial energy transduction. *Biochemical Society Transactions* 33: 897 – 904.

Brand, M. D. and Nicholls, D. G. (2011) Assessing mitochondrial dysfunction in cells. *Biochemical Journal* **435**: 297 – 312.

Braunwald, E., Antman, E. M., Beasley, J. W., Califf, R. M., Cheitlin, M. D., Hochman, J. S., Jones, R. H., Kereiakes, D., Kupersmith, J., Levin, T. N., Pepine, C. J., Schaeffer, J. W., Smith III, E. E., Steward, D. E. and Theroux, P. (2000) ACC/AHA guidelines for the management of patients with unstable angina and non–ST segment elevation myocardial infarction: a report of the american college of cardiology/american heart association task force on practice guidelines (Committee on the Management of Patients With Unstable Angina). *Circulation* **102** (10): 1193 – 1209.

Breeuwer, P. and Abee, Tjakko (2004) *Assessment of the membrane potential, intracellular pH and respiration of bacteria employing fluorescence techniques. Molecular Microbial Ecology Manual.* 2nd ed. Netherland: Kluwer Academic Publishers.

Brette, F. and Orchard, C. (2003) T–tubule function in mammalian cardiac myocytes. *Circulation Research* **92**: 1182 – 1192.

Brookes, P. S. and Darley-Usmar, V. M. (2004) Role of calcium and superoxide dismutase in sensitizing mitochondria to peroxynitrite–induced permeability transition. *American Journal of Physiology Heart and Circulatory Physiology* **286**: H39 – H46.

Bruns, D. (2004) Detection of transmitter release with carbon fiber electrodes. *Methods* **33** (4): 312 – 321.

Bruus, H. (2008) *Theoretical microfluidics*. US: Oxford University Press.

Buchakjian, M. R. and Kornbluth, S. (2010) The engine driving the ship: metabolic steering of cell proliferation and death. *Nature Reviews Molecular Cell Biology* **11**: 715 – 727.

Buffon, A., Rigattieri, S., Santini, S. A., Ramazzotti, V., Crea, F., Giardina, B. and Maseri, A. (2000) Myocardial ischaemia–reperfusion damage after pacing–induced tachycardia in patients with cardiac syndrome X. *American Journal of Physiology – Heart and Circulatory Physiology* **279** (6): H2627 – H2633.

Buja, L. M. and Weerasinghe, P. (2010) Unresolved issues in myocardial reperfusion injury. *Cardiovascular Pathology* **19** (1): 29 – 35.

Burkard, N., Williams, T., Czolbe, M., Blömer, N., Panther, F., Link, M., Fraccarollo, D., Widder, J. D., Hu, K., Han, H., Hofmann, U., Frantz, S., Nordbeck, P., Bulla, J., Schuh, K. and Ritter, O. (2010) Conditional overexpression of neuronal nitric oxide synthase is cardioprotective in ischaemia/reperfusion. *Circulation* **122**: 1588 – 1603.

Cai, X., Liu, C., Liu, H., Guo, Z. and Liu, J. (2007) Optimization of electrochemical total creatine kinase biosensors based on three–Au–electrode. *Electroanalysis* **19** (6): 1689 – 1694.

Campbell, S. E., Rakusan, K. and Gerdes, A. M. (1989) Change in cardiac myocyte size distribution in aortic–constricted neonatal rats. *Basic Research in Cardiology* **84**: 247 – 258.

Cao, Z., Xu, X., Que, L., Chen, Q. and Li, Y. (2009) Dephosphorylation of cardiomyocyte Cx 43 is associated with myocardial ischaemia and reperfusion injury. *Journal of Nanjing Medical University* **23** (3): 163 – 167.

Casadei, B. and Sears, C. E. (2003) Nitric–oxide–mediated regulation of cardiac contractility and stretch responses. *Progress in Biophysics and Molecular Biology* **82**: 67 – 80.

Casey, T. M. and Arthur, P. G. (2000) Hibernation in noncontracting mammalian cardiomyocytes. *Circulation* **102**: 3124 – 3129.

Centi, S., Tombelli, S., Palchetti, I. and Mascini, M. (2010) Development of an aptamer–based electrochemical sandwich assay for the detection of a clinical biomarker. *Sensors and Microsystems – Lecture Notes in Electrical Engineering* **54**: 207 – 210.

Cesura, A. M., Pinard, E., Schubenel, R., Goetschy, V., Friedlein, A., Langen, H., Polcic, P., Forte, M. A., Bernardi, P. and Kemp, J. A. (2003) The voltage–dependent anion channel is the target for a new class of inhibitors of the mitochondrial permeability transition pore. *The Journal of Biological Chemistry* **278**: 49812 – 49818.

Chang, H., Khan, R., Rong, Z., Sapelkin, A. and Vadgama, P. (2010) Study of albumin and fibrinogen membranes formed by interfacial crosslinking using microfluidic flow. *Biofabrication* **2** (3): 035002.

Chang, S. C., Pereira Rodrigues, N. P., Zurgil, N., Henderson, J. R., Bedioui, F., McNeil, C. J. and Deutsch, M. (2005) Simultaneous intra– and extracellular superoxide monitoring using an integrated optical and electrochemical sensor system. *Biochemical and Biophysical Research Communications* **327** (4): 979 – 984.

Chaudhury, M. K. and Whitesides, G. M. (1992) Correlation between surface free energy and surface constitution. *Science* **255**: 1230 – 1232.

Cheah, L. T., Dou, Y. H., Seymour, A. M. L., Dyer, C. E., Haswell, S. J., Wadhawan, J. D. and Greenman, J. (2010) Microfluidic perfusion system for maintaining viable heart tissue with real–time electrochemical monitoring of reactive oxygen species. *Lab on a Chip* **10**: 2720 – 2726.

Chen, F. C. and Ogut, O. (2006) Decline of contractility during ischaemia–reperfusion injury: actin glutathionylation and its effect on allosteric interaction with tropomyosin. *American Journal of Physiology – Cell Physiology* **290** (3): C719 – C727.

Chen, Q., Hoppel, C. L. and Lesnefsky, E. J. (2006) Blockade of electron transport before cardiac ischaemia with the reversible inhibitor amobarbital protects rat heart mitochondria. *Journal of Pharmacology and Experimental Therapeutics* **316**: 200 – 207.

Chen, Q., Vazquez, E. J., Moghaddas, S., Hoppel, C. L. and Lesnefsky, E. J. (2003) Production of reactive oxygen species by mitochondria: central role of complex III. *The Journal of Biological Chemistry* **278**: 36027 – 36031.

Cheng, D. and Jiang, H. (2009) A debubbler for microfluidics utilizing air–liquid interfaces. *Applied Physics Letters* **95**: 214103.

Cheng, W., Klauke, N., Sedgwick, H., Smith, G. L. and Cooper, J. M. (2006) Metabolic monitoring of the electrically stimulated single heart cell within a microfluidic platform. *Lab on a Chip* **6**: 1424 – 1431.

Chi, N. C. and Karliner, J. S. (2004) Molecular determinants of responses to myocardial ischaemia/reperfusion injury: focus on hypoxia–inducible and heat shock factors. *Cardiovascular Research* **61**: 437 – 447.

Chirizzi, D., Guascito, M. R., Malitesta, C. and Mazzotta, E. (2011) Electrochemical and spectroscopic characterization of glucose oxidase immobilized in polyvinyl alcohol and applications in glucose detection. *Sensors and Microsystems – Lecture Notes in Electrical Engineering* **91**: 339 – 343.

Choban, E. R., Markoski, L. J., Wieckowski, A. and Kenis, P. J. A. (2004) Microfluidic fuel cell based on laminar flow. *Journal of Power Sources* **128**: 54 – 60.

Chong, K. Y., Lai, C. C., Lille, S., Chang, C. and Su, C. Y. *(*1998*)* Stable overexpression of the consistutive form of heat shock protein 70 confers oxidative protection*. Journal of Molecular and Cellular Cardiology* **30***:* 599 – 608*.*

Christenson, R. H. and Azzazy, H. M. E. (1998) Biochemical markers of the acute coronary syndromes. *Clinical Chemistry* **44**: 1855 – 1864.

Christenson, R. H. and Azzazy, H. M. E, (2009) Cardiac point of care testing: A focused review of current National Academy of Clinical Biochemistry guidelines and measurement platforms. *Clinical Biochemistry* **42** (3): 150 – 157.

Cohen, M. V., Yang, X. M. and Downey, J. M. (2007) The pH hypothesis of postconditioning–staccato reperfusion reintroduces oxygen and perpetuates myocardial acidosis. *Circulation* **115**: 1895 – 1903.

Collinson, P. O. (1998) Troponin T or troponin I or CK–MB (or none?) *European Heart Journal* **19**: 16 – 24.

Collinson, P. O., John, C., Lynch, S., Rao, A., Canepa-Anson, R., Carson, E. and Cramp, D. (2004) A prospective ramdomized controlled trial of point–of–care testing on the coronary care unit. *Annals of Clinical Biochemistry* **41** (5): 397 – 404.

Cortina-Puig, M., Munoz-Berbel, X., Calas-Blanchard, C. and Marty, J. L. (2009) Electrochemical characterization of a superoxide biosensor based on the co–immobilization of cytochrome c and XOD on SAM–modified gold electrodes and application to garlic samples. *Talanta* **79** (2): 289 – 294.

Cowie, M. R. and Mendez, G. F. (2002) BNP and congestive heart failure. *Progress in Cardiovascular Diseases* **44**: 293 – 321.

Crompton, M. (2000) Mitochondrial intermembrane junctional complexes and their role in cell death. *The Journal of Physiology* **529**: 11 – 21.

Crompton, M., Barksby, E., Johnson, N. and Capano, M. (2002) Mitochondrial intermembrane junctional complexes and their involvement in cell death. *Biochimie* **84** (2 – 3): 143 – 152.

Cross, H. R., Clarke, K., Opie, L. H. and Radda, G. K. (1995) Is lactate–induced myocardial ischaemic injury mediated by decreased pH or increased intracellular lactate? *Journal of Molecular and Cellular Cardiology* **27** (7): 1369 – 1381.

Cui, S. and Zhu, H. (1998) Myocardial ischaemic reperfusion injury affected by the isozymes of nitric oxide synthase and their gene expression: experimental study. *Zhonghua Yi Xue Za Zhi* **78**: 327 – 330.

Currie, R. W., Karmazyn, M. and Kloc, M. (1988) Heat–shock response is associated with enhanced postischaemic ventricular recovery. *Circulation Research* **63**: 543 – 549.

Currie, R. W., Tanguay, R. M. and Kingma Jr. J. G. (1993) Heat–shock response and limitation of tissue necrosis during occlusion/reperfusion in rabbit hearts. *Circulation* **87**: 963 – 971.

Daniels, L. B. and Maisel, A. S. (2007) Natriuretic peptides. *Journal of the American College of Cardiology* **50** (25): 18 – 25.

Daniels, L. B. and Maisel, A. S. (2010) Multiple marker approach to risk stratification in patients with stable coronary artery disease: to have or have not. *European Heart Journal* **31** (24): 2980 – 2983.

Darwish, I. A. (2006) Immunoassay methods and their applications in pharmaceutical analysis: basic methodology and recent advances. *International Journal of Biomedical Science* **2** (3): 217 – 235.

Das, D. K., Maulik, N. and Moraru, I. I. (1995) Gene expression in acute myocardial stress. Induction by hypoxia, ischaemia, reperfusion, hyperthermia and oxidative stress. *Journal of Molecular and Cellular Cardiology* **27**: 181 – 193.

Dawson, D., Lygate, C. A., Zhang, M. H., Hulbert, K., Neubauer, S. and Casadei, B. (2005) nNOS gene deletion exacerbates pathological left ventricular remodeling and functional deterioration after myocardial infarction*. Circulation* **112***:* 3729 – 3737*.*

Day, B. J. (2009) Catalase and glutathione peroxidase mimics. *Biochemical Pharmacology* **77** (3): 285 – 296.

Delanghe, J. R., Chapelle, J. P. and Van derschueren, S. C. (1990) Quantitative nephelornetric assay for determining myoglobin evaluated. *Clinical Chemistry* **36**: 1675 – 1678.

Derveaux, S., Stubbe, B. G., Braeckmans, K., Roelant, C., Sato, K., Demeester, J. and De Smedt, S. C. (2008) Synergism between particle–based multiplexing and microfluidics technologies may bring diagnostics closer to the patient. *Analytical and Bioanalytical Chemistry* **391**: 2453 – 2467.

Dhalla, N. S., Temsah, R. M. and Netticadan, T. (2000) Role of oxidative stress in cardiovascular diseases. *Journal of Hypertension* **18**: 655 – 673.

Di Lisa, F., Carpi, B., Giorgio, V. and Bernardi, P. (2011) The mitochondrial permeability transition pore and cyclophilin D in cardioprotection. *Biochimica et Biophysica Acta – Molecular Cell Research* **1813** (7): 1316 – 1322.

Di Napoli P., Taccardi A. A., Grilli A., Felaco M., Caterina R. D. and Barsotti A. (2002) Hypertonic reperfusion preserves endothelial nitric oxide synthase expression after ischaemia–reperfusion in isolated working rat hearts. *Italian Heart Journal* **3**: 40 – 45.

Di Napoli, P., Chierchia, S., Taccardi, A. A., Grilli, A., Felaco, M., De Caterina, R. and Barsotti, A. (2007) Trimetazidine improves post–ischaemic recovery by preserving endothelial nitric oxide synthase expression in isolated working rat hearts. *Nitric Oxide* **16**: 228 – 236.

Di Napoli, P., Taccardi, A. A., Grilli, A., De Lutiis, M. A., Barsotti, A., Felaco, M. and De Caterina, R. (2005) Chronic treatment with rosuvastatin modulates nitric oxide synthase expression and reduces ischaemia–reperfusion injury in rat hearts. *Cardiovascular Research* **66** (3): 462 – 471.

Di Napoli, P., Taccardi, A. A., Grilli, A., Spina, R., Felaco, M., Barsotti, A. and De Caterina, R. (2001) Simvastatin reduces reperfusion injury by modulating nitric oxide synthase expression: an *ex vivo* study in isolated working rat hearts. *Cardiovascular Research* **51**: 283 – 293.

Dizdaroglu, M., Jaruga, P., Birincioglu, M. and Rodriguez, H. (2002) Free radical–induced damage to DNA: mechanisms and measurement. *Free Radical Biology and Medicine* **32**: 1102 – 1115.

Dolder, M., Walzel, B., Speer, O., Schlattner, U. and Wallimann, T. (2003) Inhibition of the mitochondrial permeability transition by creatine kinase substrates. Requirement for microcompartmentation. *The Journal of Biological Chemistry* **278**: 17760 – 17766.

Dong, L., Fan, Y., Shao, X. and Chen, Z. (2011) Vitexin protects against myocardial ischaemia/reperfusion injury in langendorff–perfused rat hearts by attenuating inflammatory response and apoptosis. *Food and Chemical Toxicology* **49** (12): 3211 – 3216.

Donnelly, T. J., Sievers, R. E., Vissern, F. L., Welch, W. J. and Wolfe, C. L. (1992) Heat shock protein induction in rat hearts. A role for improved myocardial salvage after ischaemia and reperfusion? *Circulation* **85**: 769 – 778.

Downey, J. M., Davis, A. M. and Cohen, M. V. (2007) Signalling pathways in ischaemic preconditioning. *Heart Failure Reviews* **12**: 181 – 188.

Droge, W. (2002) Free radicals in the physiological control of cell function. *Physiological Reviews* **82**: 47 – 95.

D'Souza, S. P., Yellon, D. M. and Baxter, G. F. (2003a) Cardioprotective action of B–type natriuretic peptide is NO–dependent. *British Journal of Pharmacology* **138**: 21.

D'Souza, S. P., Yellon, D. M., Martin, C., Schulz, R., Heusch, G., Onody, A., Ferdinandy, P. and Baxter, G. F. (2003b) B–type natriuretic peptide limits infarct size in rat isolated hearts via KATP channel opening. *American Journal of Physiology – Heart and Circulatory Physiol*ogy **284**: H1592 – H1600.

Dunlop, M. (2000) Aldose reductase and the role of the polyol pathway in diabetic nephropathy. *Kidney International* **58**: S3 – S12.

Eddy, D. M., Adler, J., Patterson, B., Lucas, D., Smith, K. A. and Morris, M. (2011) Individualized guidelines: the potential for increasing quality and reducing costs. *Annals of Internal Medicine* **154** (9): 627 – 634.

Eguchi, M., Fujiwara, M., Mizukami, Y. and Miwa, N. (2003) Cytoprotection by pro–vitamin C against ischaemic injuries in perfused rat heart together with differential activation of MAP kinase family. *Journal of Cellular Biochemistry* **89**: 863 – 867.

El-Giar, E. E. M. and Wipf, D. O. (2006) Preparation of tip–protected poly (oxyphenylene) coated carbon–fiber ultramicroelectrodes. *Electroanalysis* **18** (23): 2281 – 2289.

Elmore, S. (2007) Apoptosis: A review of programmed cell death. *Toxicologic Pathology* **35** (4): 495 – 516.

Elrod, J. W., Greer, J. J., Bryan, N. S., Langston, W., Szot, J. F., Gebregzlabher, H., Janssens, S., Feelisch, M. and Lefer, D. J. (2006) Cardiomyocyte–specific overexpression of NO synthase–3 protects against myocardial ischaemia–reperfusion injury. *Arteriosclerosis, Thrombosis, and Vascular Biology* **26**: 1517 – 1523.

Erbse, A., Mayer, M. P. and Bukau, B. (2004) Mechanism of substrate recognition by Hsp70 chaperones. *Biochemical Society Transactions* **32**: 617 – 621.

Eveness, J., Kiely, J., Hawkins, P., Wraith, P. and Luxton, R. (2009) Evaluation of paramagnetic particles for use in a resonant coil magnetometer based magneto–immunoassay. *Sensors and Actuators B: Chemical* **139** (2): 538 – 542.

Fabiato, A. (1983) Calcium–induced release of calcium from the cardiac sarcoplasmic reticulum. *American Journal of Physiology Cellular Physiology* **245**:C1 – C14.

Fang, Q., Sun, M. and Huang, Y. Z. (2009) Capillary–based microfluidic analysis systems. *Analytical and Bioanalytical Chemistry* **393** (1): 63 – 66.

Fanjul-Bolado, P., Hernández-Santos, D., González-García, M. B. and Costa-García, A. (2007) Alkaline phosphatase–catalyzed silver deposition for electrochemical detection. *Analytical Chemistry* **79** (14): 5272 – 5277.

Fantinelli, J. C., Schinella, G., Cingolani, H. E. and Mosca, S. M. (2005) Effects of different fractions of a red wine non–alcoholic extract on ischaemia–reperfusion injury. *Life Science* **76**: 2721 – 2733.

Felaco, M., Grilli, A., Gorbunov, N., Di Napoli, P., Lutiis, M. A. D., Giulio, C. D., Taccardi, A. A., Barsotti, A., Barbacane, R. C., Reale, M. and Conti, P. (2000) Endothelial NOS expression and ischaemia–reperfusion in isolated working rat heart from hypoxic and hyperoxic conditions. *Biochimica et Biophysica Acta* **1524** (2 – 3): 203 – 211.

Feng, H. Z., Biesiadecki, B. J., Yu, Z. B., Hossain, M. M. and Jin, J. P. (2008) Restricted N–terminal truncation of cardiac troponin T: a novel mechanism for functional adaptation to energetic crisis. *The Journal of Physiology* **586**: 3537 – 3550.

Feng, Q., Lu, X., Jones, D. L., Shen, J. and Arnold, J. M., O. (2001) Increased inducible nitric oxide synthase expression contributes to myocardial dysfunction and higher mortality after myocardial infarction in mice. *Circulation* **104**: 700 – 704.

Ferdinandy, P. and Schulz, R. (2003) Nitric oxide, superoxide and peroxynitrite in myocardial ischaemia–reperfusion injury and preconditioning. *British Journal of Pharmacology* **138**: 532 – 543.

Ferdinandy, P., Danial, H., Ambrus, I., Rothery, R. A. and Schulz, R. (2000) Peroxynitrite is a major contributor to cytokine–induced myocardial contractile failure. *Circulation Research* **87**: 241 – 247.

Ferguson, G. S., Chaudhury, M. K., Biebuyck, H. A. and Whitesides, G. M. (1993) Monolayers on disordered substrates: self–assembly of alkyltrichlorosilanes on surface–modified polyethylene and poly (dimethylsiloxane). *Macromolecules* **26**: 5870 – 5875.

Ferrari, R. (2001) Pathophysiological vs biochemical ischaemia: a key to transition from reversible to irreversible damage. *European Heart Journal Supplements* **3**: C2 – C10.

Field, M. L., Azzawi, A., Styles, P., Henderson, C., Seymour, A. M. and Radda, G. K. (1994) Intracellular Ca^{2+} transients in isolated perfused rat heart: measurement using the fluorescent indicator Fura–2/AM. *Cell Calcium* **16** (2): 87 – 100.

Foo, R. S. Y., Mani, K. and Kitsis, R. N. (2005) Death begets failure in the heart. *The Journal of Clinical Investigation* **115** (3): 565 – 571.

Fowler, J. M., Wong, D. K. Y., Halsall, H. B. and Heineman, W. R. (2008) Recent developments in electrochemical immunoassays and immunosensors. *Electrochemical Sensors, Biosensors and their Biomedical Applications* **2008**: 115 – 143.

Frantz, S., Adamek, A., Fraccarollo, D., Tillmanns, J., Widder, J. D., Dienesch, C., Schäfer, A., Podolskaya, A., Held, M., Ruetten, H., Ertl, G. and Bauersachs, J. (2009) The eNOS enhancer AVE 9488: a novel cardioprotectant against ischaemia reperfusion injury. *Basic Research in Cardiology* **104**: 773 – 779.

Frasconi, M., Deriu, D., D'Annibale, A. and Mazzei, F. (2009) Nanostructured materials based on the integration of ferrocenyl–tethered dendrimer and redox proteins on self–assembled monolayers: an efficient biosensor interface. *Nanotechnology* **20** (50): 505501.

Frey, N., Muller-Bardor, V. M. and Katus, H. A. (1998) Myocardial damage: the role of troponin T. In: J. C. Kaski and D. W. Holt, eds. *Myocardial damage. Early detection by novel biochemical markers.* New York: Kluwer Academic Publishers.

Fujita, M., Tsuruta, R., Kasaoka, S., Fujimoto, K., Tanaka, R., Oda, Y., Nanba, M., Igarashi, M., Yuasa, M., Yoshikawa, T. and MAekawa, T. (2009) *In vivo* real–time measurement of superoxide anion radical with a novel electrochemical sensor. *Free Radical Biology and Medicine* **47** (7): 1039 – 1048.

Fuller, W., Parmar, V., Eaton, P., Bell, J. R. and Shattock, M. J. (2003) Cardiac ischaemia causes inhibition of the Na/K ATPase by a labile cytosolic compound whose production is linked to oxidant stress. *Cardiovascular Research* **57** (4):1044 – 1051.

Gao, H. K., Yin, Z., Zhou, N.,Feng, X. Y., Gao, F. and Wang, H. C. (2008) Glycogen synthase kinase 3 inhibition protects the heart from acute ischaemia–reperfusion injury via inhibition of inflammation and apoptosis. *Journal of Cardiovascular Pharmacology* **52** (3): 286 – 292.

García-Dorado, D. and Piper, H. M. (2006) Postconditioning: reperfusion of "reperfusion injury" after hibernation. *Cardiovascular Research* **69** (1): 1 – 3.

García-Dorado, D., Inserte, J., Ruiz-Meana, M., Gonzalez, M. A., Solares, J., Julia, M., Barrabes, J. A. and Soler-Soler, J. (1997) Gap junction uncoupler

heptanol prevents cell–to–cell progression of hypercontracture and limits necrosis during myocardial reperfusion. *Circulation* **96**: 3579 – 3586.

Garrido, C., Schmitt, E., Cande, C., Vahsen, N., Parcellier, A. and Kroemer, G. (2003) HSP27 and HSP70: potentially oncogenic apoptosis inhibitors. *Cell Cycle* **2**: 579 – 584.

Gervais, L. and Delmarche, E. (2009) Toward one–step point–of–care immunodiagnostics using capillary–driven microfluidics and PDMS substrates. *Lab on a Chip* **9** (23): 3330 – 3337.

Ges, I. A., Dzhura, I. A. and Baudenbacher, F. J. (2008) On–chip acidification rate measurements from single cardiac cells confined in sub–nanoliter volumes. *Biomedical Microdevices* **10**: 347 – 354.

Gibler, W. B., Runyon, J. P., Levy, R. C., Sayre, M. R., Kacich, R., Hattemer, C. R., Hamilton, C., Gerlach, J. W. and Walsh, R. A. (1995) A rapid diagnostic and treatment center for patients with chest pain in the emergency department. *Annals of Emergency Medicine* **25** (1): 1 – 8.

Giffard, R. G. and Yenari, M. A. (2004) Many mechanisms for hsp70 protection from cerebral ischaemia. *Journal of Neurosurgical Anesthesiology* **16**: 53 – 61.

Goetze, J. P., Christoffersen, C., Perko, M., Arendrup, H., Rehfeld, J. F., Kastrup, J. and Nielsen, L. B. (2003) Increased cardiac BNP expression associated with myocardial ischaemia J. P. *The FASEB Journal* **17**: 1105 – 1107.

Goetze, J. P., Gore, A., Møller, C. H., Steinbrüchel, D. A., Rehfeld, J. F. and Nielsen, L. B. (2004) Acute myocardial hypoxia increases BNP gene expression. *The FASEB Journal* **18** (15): 1928 – 1930.

Gohil, V. M., Sheth, S. A., Nilsson, R., Wojtovich, A. P., Lee, J. H., Perocchi, F., Chen, W., Clish, C. B., Ayata, C., Brookes, P. S . and Mootha, V. K. (2010) Discovery and therapeutic potential of drugs that shift energy metabolism from mitochondrial repiration to glycolysis. *Nature Biotechnology* **28** (3): 249 – 255.

Goldsmith, E. C. (2002) The dynamic interaction of the extraceelular matrix in cardiac remodeling. *Journal of Cardiac Failure* **8** (6): S314 – S318.

Gomez, L., Li, B., Mewton, N., Sanchez, I., Piot, C., Elbaz, M. and Ovize, M. (2009) Inhibition of mitochondrial permeability transition pore opening: translation to patients. *Cardiovascular Research* **83** (2): 226 – 233.

Gonon, F., Cespuglio, R., Ponchon, J. L., Buda, M., Jowet, M., Adams, R. N. and Pujd, J. F. (1978) *In vivo* continuous electrochemical determination of dopamine release in rat neostriatum. *Comptes Rendus Hebdomadaires des Séances de l'Academie des Sciences* **286**: 1203 – 1206.

Gonzalez, F. M., Shiva, S., Vincent, P. S., Ringwood, L. A., Hsu, L. Y., Hon, Y. Y., Aletras, A. H., Cannon III, R. O., Gladwin, M. T. and Arai, A. E. (2008) Nitrite anion provides potent cytoprotective and antiapoptotic effects as adjunctive therapy to reperfusion for acute myocardial infarction. *Circulation* **117**: 2986 – 2994.

Grant, K. M., Hemmert, J. W. and White, H. S. (2001) Magnetic field–controlled microfluidic transport. *Journal of the Americal Chemical Society* **124**: 462 – 467.

Grech, E. D., Jackson, M. J. and Ramsdale, D. R. (1995) Reperfusion injury after acute myocardial infarction. *British Medical Journal* **310**: 477 – 478.

Griffiths, J. and Handschuh, G. (1977) Creatine kinase isoenzyme MB in myocardial infarction: methods compared. *Clinical Chemistry* **23**: 567 – 570.

Grilli, A., Lutiis, M. A. D., Patruno, A., Speranza, L., Cataldi, A., Centurione, L., Taccardi, A. A., Di Napoli, P., Caterina, R. D., Barbacane, R., Conti, P. and Felaco, M. (2003) Effect of chronic hypoxia on inducible nitric oxide synthase expression in rat myocardial tissue. *Experimental Biology and Medicine* **228**: 935 – 942.

Gubern, C., Hurtado, O., RodrÍguez, R., Morales, J. R., Romera, V. G., Moro, M. A., Lizasoain, I., Serena, J. and Mallolas, J. (2009) Validation of housekeeping genes for quantitative real–time PCR in *in vivo* and *in vitro* models of cerebral ischaemia. *BioMed Central Molecular Biology* **10**: 57.

Günes, Y., Okcün, B., Kavlakm E., Erbas, C. and Karcier, S. (2008) Value of brain natriuretic peptide after acute myocardial infarction. *Anadolu Kardiyoloji Dergisi* **8** (3): 182 – 187.

Halestrap, A. P. (2002) The mitochondrial permeability transition – a pore way for the heart to die. *Journal of Clinical and Basic Cardiology* **5**: 29 – 41.

Halestrap, A. P. (2006) Calcium, mitochondria and reperfusion injury: a pore way to die. *Biochemical Society Transactions* **34**: 232 – 237.

Halestrap, A. P. (2009) What is the mitochondrial permeability transition pore? *Journal of Molecular and Cellular Cardiol*ogy **46**: 821 – 831.

Halestrap, A. P., Doran, E., Gillespie, J. P. and O'Toole, A. (2000) Mitochondria and cell death. *Biochemical Society Transactions* **28**: 170 – 177.

Halestrap, A. P., McStay, G. P. and Clarke, S. J. (2002) The permeability transition pore complex: another view*. Biochimie* **84**: 153 – 166.

Hamilton, G. A., Westmoreland, C. and George, E. (2001) Effects of medium composition on the morphology and function of rat hepatocytes cultured as

spheroids and monolayers. *In Vitro Cellular and Developmental Biology – Animal* **37**: 656 – 667.

Hamilton, K. L., Staib, J. L., Phillips, T., Hess, A., Lennon, S. L. and Powers, S. K. (2003) Exercise, antioxidants, and HSP 72: protection against myocardial ischaemia/reperfusion. *Free Radical Biology and Medicine* **34**: 800 – 809.

Harrison, D. J., Fluri, K., Seiler, K., Fan, Z. H., Effenhauser, C. S. and Manz, A. (1993) Micromachining a miniaturized capillary electrophoresis–based chemical analysis system on a chip. *Science* **261**: 895 – 897.

Hatakeyama, K., Tanaka, T., Sawaguchi, M., Iwadate, A., Mizutani, Y., Sasaki, K., Tateishi N. and Matsunaga, T. (2009) Microfluidic device using chemiluminescence and a DNA–arrayed thin film transistor photosensor for single nucleotide polymorphism genotyping of PCR amplicons from whole blood. *Lab on a Chip* **9**: 1052 – 1058.

Hattersley, S. M., Dyer, C. E., Greenman, J. and Haswell, S. J. (2008) Development of a microfluidic device for the maintenance and interrogation of viable tissue biopsies. *Lab on a Chip* **8**: 1842 – 1846.

Haubner, B. J., Neely, G. G., Voelkl, J. G. J., Damilano, F., Kuba, K., Imai, Y., Komnenovic, V., Mayr, A., Pachinger, O., Hirsch, E., Penninger, J. M. and Metzler, B. (2010) PI3Kγ protects from myocardial ischaemia and reperfusion injury through a kinase–independent pathway. *PLoS ONE* **5** (2): e9350.

Haugland, R. P., MacCoubrey, I. C. and Moore, P. L. (1994) Dual–fluorescence cell viability assay using ethidium homodimer and calcein AM. *United States Patent* **5314805**: 1 – 4.

Hausenloy, D. J., Baxter, G., Bell, R., Bøtker, H. E., Davidson, S. M., Downey, J., Heusch, G., Kitakaze, M., Lecour, S., Mentzer, R., Mocanu, M. M., Ovize, M., Schulz, R., Shannon, R., Walker, M., Walkinshaw, G. and Yellon, D. M. (2010) Translating novel strategies for cardioprotection: the Hatter Workshop Recommendations. *Basic Research in Cardiology* **105**: 677 – 686.

Hayashida, K., Sano, M., Ohsawa, I., Shinmura, K., Tamaki, K., Kimura, K., Endo, J., Katayama, T., Kawamura, A., Kohsaka, S., Makino, S., Ohta, S., Ogawa, S. and Fukuda, K. (2008) Inhalation of hydrogen gas reduces infarct size in the rat model of myocardial ischaemia–reperfusion injury. *Biochemical and Biophysical Research Communications* **373** (1): 30 – 35.

Heart Protection Study Collaborative Group (2002) MRC/BHF heart protection study of antioxidant vitamin supplementation in 20536 high–risk individuals: a randomised placebo–controlled trial. *The Lancet* **360** (9326): 23 – 33.

Higgins, J. M., Eddington, D. T., Bhatia, S. N. And Mahadevan, L. (2007) Sickle cell vasoocclusion and rescue in a microfluidic device. *Proceedings of*

the National Academy of Sciences of the United States of America **104** (51): 20496 – 20500.

Hinkle, P. C. (2005) P/O ratios of mitochondrial oxidative phosphorylation. *Biochimica et Biophysica Acta* **1706**: 1 – 11.

Hirai, M., Hotta, Y., Ishikawa, N., Wakida, Y., Fukuzawa, Y., Isobe, F., Nakano, A., Chiba, T. and Kawamura, N. (2007) Protective effects of EGCg or GCg, a green tea catechin epimer, against postischaemic myocardial dysfunction in guinea–pig hearts. *Life Science* **80**: 1020 – 1032.

HM Treasury (2010) *Spending review 2010* (Cm 7942) London: The Stationery Office Limited.

Hoang, C. D., Zhang, J., Payne, R. M. and Apple, F. S. (1997) Post–infarction left ventricular remodelling induces changes in creatine kinase mRNA and protein subunit levels in porcine myocardium. *The American Journal of Pathology* **151** (1): 257 – 264.

Horman, S., Beauloye, C., Vertommen, D., Vanoverschelde, J., Hue, L. and Rider, M. H. (2003) Myocardial ischaemia and increased heart work modulate the phosphorylation state of eukaryotic elongation factor–2. *The Journal of Biological Chemistry* **278**: 41970 – 41976.

Hu, A., Jiao, X., Gao, E., Koch, W. J., Sharifi-Azad, S., Grunwald, Z., Ma, X. L. and Sun, J. (2006) Chronic β–adrenergic receptor stimulation induces cardiac apoptosis and aggravates myocardial ischaemia/reperfusion injury by provoking inducible nitric–oxide synthase–mediated nitrative stress. *The Journal of Pharmacology and Experimental Therapeutis* **318**: 469 – 475.

Hu, N., Yang, J., Yin, Z. Q., Ai, Y., Qian, S., Svir, I. B., Xia, B., Yan, J. W., Hou, W. S. and Zheng, X. L. (2011) A high–throughput dielectrophoresis–based cell electrofusion microfluidic device. *Electrophoresis* **32**: 2488 – 2495.

Hu, R., Guille, M., Arbault, S., Lin, C. J. and Amatore, C. (2010) *In situ* electrochemical monitoring of reactive oxygen and nitrogen species released by single MG63 osteosarcoma cell submitted to a mechanical stress. *Physical Chemistry Chemical Physics* **12**: 10048 – 10054.

Hu, S., Ren, X., Bachman, M., Sims, C. E., Li, G. P. and Allbritton, N. L. (2004) Tailoring the surface properties of poly(dimethylsiloxane) microfluidic devices. *Langmuir* **20**: 5569 – 5574.

Huang, B., Wu, H., Bhaya, D., Grossman, A., Granier, S., Kobilka, B. K. And Zare, R. N. (2007) Counting low–copy number proteins in a single cell. *Science* **315** (5808): 81 – 84.

Huang, Z., Li, H., Guo, F., Jia, Q., Zhang, Y., Liu, X. and Shi, G. (2009) Egr–1, the potential target of calcium channel blockers in cardioprotection with

ischaemia/reperfusion injury in rats. *Cellular Physiology and Biochemistry* **24**: 17 – 24.

Hung, P. J., Lee, P. J., Sabounchi, P. Lin, R. and Lee, L. P. (2005) Continuous perfusion microfluidic cell culture array for high–throughput cell–based assays. *Biotechnology and Bioengineering* **89** (1): 1 – 8.

Huxley, A. F. (1957) Muscle structure and theories of contraction. *Progress in Biophysics and Biophysical Chemistry* **7**: 255 – 318.

Ibanez, B., Fuster, V., Jiménez-Borreguero, J. and Badimon, J. J. (2011) Lethal myocardial reperfusion injury: A necessary evil? *Interational Journal of Cardiology* **151** (1): 3 – 11.

Ichai, C., Leverve, X. and Orban, J. C. (2008) Lactate and acute heart failure syndrome. *Acute Heart Failure* **2**: 768 – 780.

Ikeda, T., Abe, K., Ota, A. and Ikenoue, T. (1999) Heat shock protein 70 and heat shock cognate protein 70 messenger acid induction in the brains, hearts, and livers of neonatal rats after hypoxic stress*. American Journal of Obstertric and Gynecology* **180** (2): 457 – 461.

Imahashi, K., Schneider, M. D., Steenbergen, C. and Murphy, E. (2004) Transgenic expression of Bcl–2 modulates energy metabolism, prevents cytosolic acidification during ischaemia, reduces ischaemia/reperfusion injury. *Circulation Research* **95**: 734 – 741.

Ingle, J. D. and Crouch, S. R. (1988) *Spectrochemical Analysis*. New Jersey: Prentice Hall.

Ingwall, J. S. (1993) Is cardiac failure a consequence of decreased energy reserve? *Circulation* **87**: 58 – 62.

Ingwall, J. S. (2002) *ATP and the heart.* Boston, MA: Kluwer Academic Publishers.

Ingwall, J. S. (2009) Energy metabolism in heart failure and remodelling. *Cardiovascular Research* **81**: 412 – 419.

Inserte, J., Barba, I., Hernando, V., Abellán, A., Ruiz-Meana, M., Rodríguez-Sinovas, A. and García-Dorado, D. (2008) Effect of acidic reperfusion on prolongation of intracellular acidosis and myocardial salvage. *Cardiovascular Research* **77** (4): 782 – 790.

Iqbal, M. P., Kazmi, K. A., Mehboobali, N. and Rahbar, A. (2004) Myoglobin – a marker of reperfusion and a prognostic indicator in patients with acute myocardial infarction. *Clinical Cardiology* **27** (3): 144 – 150.

Ito, T., Suzuki, T., Tamura, K., Nezu, T., Honda, K. and Kobayashi, T. (2008) Examination of mRNA expression in rat hearts and lungs for analysis of

effects of exposure to concentrated ambient particles on cardiovascular function. *Toxicology* **243**: 271 – 283.

Jan, M., Reinhard, B., Paula, Z., Nguyen, T., Alexander, K., Kazuma, I., Stefanie, D., Tiago, G., Olaf, B., William C, C. and Kai, Z. (2010) Preconditioning by toll–like receptor 2 agonist Pam3CSK4 reduces CXCL1–dependent leukocyte recruitment in murine myocardial ischaemia/reperfusion injury. *Critical Care Medicine* **38** (3): 903 – 909.

Jang, I. K., Weissman, N. J., Picard, M. H., Zile, M. R., Pettigrew, V., Shen, S., Tatsuno, J., Hibberd, M. G., Tzivoni, D., Wackers, F. J. T. and EVOLVE investigators. (2008) A randomized, double–blind, placebo–controlled study of the safety and efficacy of intravenous MCC–135 as an adjunct to primary percutaneous coronary intervention in patients with acute myocardial infarction: evaluation of MCC–135 for left ventricular salvage in acute myocardial infarction (EVOLVE). *American Heart Journal* **155**: 113e1 – e8.

Jeyaraman, M., Tanguy, S., Fandrich, R. R., Lukas, A. and Kardami, E. (2003) Ischaemia–induced dephosphorylation of cardiomyocyte connexion–43 is reduced by okadaic acid and calyculin A but not fostriecin. *Molecular and Cellular Biochemistry* **242**: 129 – 134.

Ji, L., Fu, F., Zhang, L., Liu, W., Cai, X., Zhang, L., Zheng, Q., Zhang, H. and Gao, F. (2010) Insulin attenuates myocardial ischaemia/reperfusion injury via reducing oxidative/nitrative stress. *American Journal of Physiology – Endocrinology and Metabolism* **298** (4): E871 – E880.

Jin, J. P. and Root, D. D. (2000) Modulation of troponin T molecular conformation and flexibility by metal ion binding to the NH2–terminal variable region. *Biochemistry* **39**: 11702 – 11713.

Jin, J. P., Chen, A., Ogut, O. and Huang, Q. Q. (2000) Conformational modulation of slow skeletal muscle troponin T by an NH2–terminal metal–binding extension. *American Journal of Physiology – Cell Physiology* **279**: C1067 – C1077.

Kaji, H., Nishizawa, M. and Matsue, T. (2003) Localized chemical stimulation to micropatterned cells using multiple laminar fluid flows. *Lab on a Chip* **3**: 208 – 211.

Kambe, M., Bessho, R., Fujii, M., Ochi, M. and Shimizu, K. (2009) Sivelestat reduces myocardial ischaemia and reperfusion injury in rat hearts even when administered after onset of myocardial ischaemia. *Interactive CardioVascular and Thoracic Surgery* **8**: 629 – 634.

Kanai, A. J., Pearce, L. L., Clemens, P. R., Birder, L. A., VanBibber, M. M., Choi, S., de Groat, W. C. and Peterson, J. (2001) Identification of a neuronal nitric oxide synthase in isolated cardiac mitochondria using electrochemical detection. *Proceedings of the National Academy of Sciences of the United States of America* **98**: 14126 – 14131.

Kang, Y., Wu, X., Wang, Y. and Li, D. (2008) On–chip fluorescence–activated particle counting and sorting system. *Analytical Chimica Acta* **626** (1): 97 – 103.

Kasai, N., Shimada, A., Nyberg, T. and Torimitsu, K. (2009) An electrochemical sensor array and its application to real–time brain slice imaging. *Electronics and Communications in Japan* **92** (9): 217 – 221.

Katz, A. M. (2001) A growth of ideas: role of calcium as activator of cardiac contraction.*Cardiovascular Research* **52**: 8 – 13.

Keeley, E. C., Boura, J. A. and Grines, C. L. (2003) Primary angioplasty versus intravenous thrombolytic therapy for acute myocardial infarction: a quantitative review of 23 randomised trials. *Lancet* **361**: 13 – 20.

Kempf, T., Eden, M., Strelau, J., Naguib, M., Willenbockel, C., Tongers, J., Heineke, J., Kotlarz,D., Xu, J., Molkentin, J. D., Niessen, H. W., Drexler, H. and Wollert, K. C. (2006) The transforming growth factor–β superfamily member growth–differentiation factor–15 protects the heart from ischaemia/reperfusion injury. *Circulation Research* **98**: 351 – 360.

Kevin, L. G., Novalija, E. and Stowe, D. F. (2005) Reactive oxygen species as mediators of cardiac injury and protection: the relevance to anesthesia practice. *Anaesthesia and Analgesia* **101** (5): 1275 – 1287.

Khademhosseini, A., Langer, R., Borenstein, J. and Vacanti, J. P. (2005) Microscale technologies for tissue engineering and biology. *Proceedings of the National Academy of Sciences of the United States of America* **103** (8): 2480 – 2487.

Khanal, G., Chung, K., Solis-Wever, X., Johnson, B. and Pappas, D. (2011) Ischaemia/reperfusion injury of primary porcine cardiomyocytes in a low–shear microfluidic culture and analysis device. *Analyst* **136**: 3519 – 3526.

Khuchua, Z. A., Qin, W., Boero, J., Cheng, J., Payne, R. M., Saks, V. A. and Strauss, A. W. (1998) Octamer formation and coupling of cardiac sarcomeric mitochondrial creatine kinase are mediated by charged N–terminal residues. *The Journal of Biological Chemistry* **273**: 22990 – 22996.

Kiely, J., Hawkins, P., Wraith, P. and Luxton, R. (2007) Paramagnetic particle detection for use with an immunoassay based biosensor. *Science, Measurement and Technology* **1** (5): 270 – 275.

Kim, H. T. and Chae, C. H. (2006) Effect of exercise and α–lipoic acid supplementation on oxidative stress in rats. *Biology of Sport* **23** (2): 143 – 155.

Kim, L., Toh, Y., Voldman, J. and Yu, H. (2007) A practical guide to microfluidic perfusion culture of adherent mammalian cells. *Lab on a Chip* **7**: 681 – 694.

Kim, M. S., Yeon, J. H. and Park, J. (2007) A microfluidic platform for 3–dimensional cell culture and cell–based assays. *Biomedical Microdevices* **9**: 25 – 34.

Kimura, H., Yamamoto, T., Sakai, H., Sakai, Y. And Fujii, T. (2008) An integrated microfluidic system for long–term perfusion culture and on–line monitoring of intestinal tissue models. *Lab on a Chip* **8**: 741 – 746.

Klauke, N., Smith, G. and Cooper, J. M. (2003) Stimulation of single isolated adult ventricular myocytes within a low volume using a planar microelectrode array. *Biophysical Journal* **85** (3): 1766 – 1774.

Klauke, N., Smith, G. and Cooper, J. M. (2007) Microfluidic systems to examine intercellular coupling of pairs of cardiac myocytes. *Lab on a Chip* **7**: 731 – 739.

Klauke, N., Smith, G. L. and Cooper, J. (2006) Extracellular recordings of field potentials from single cardiomyocytes. *Biophysical Journal* **91** (7): 2543 – 2551.

Klein, H. H., Pich, S., Bohle, R. M., Lindert-Heimberg, S. and Nebendahl, K. (2000) Na^+/H^+ exchange inhibitor cariporide attenuates cell injury predominantly during ischaemia and not at onset of reperfusion in porcine hearts with low residual blood flow. *Circulation* **102** (16): 1977 – 1982.

Klocke, F. J., Copley, D. P., Krawczyk, J. A. and Reichlin, M. (1982) Rapid renal clearance of immunoreactive canine plasma myoglobin. *Circulation* **65** (7):1522 – 1528.

Knight, J. A. (2001) Serum enzymes. In: Jones, S. L. ed. *Clinical laboratory pearls* Philadelphia, USA: Lippincott Williams and Wilkins.

Knight, R. A., Chen-Scarabelli, C., Yuan, Z., McCauley, R. B., Di Rezze, J., Scarabelli, G. M., Townsend, P. A., Latchman, D., Saravolatz, L., Faggian, G., Mazzucco, A., Chowdrey, H. S., Stephanou, A. and Scarabelli, T. M. (2008) Cardiac release of urocortin precedes the occurrence of irreversible myocardial damage in the rat heart exposed to ischaemia/reperfusion injury. *FEBS Letters* **582** (6): 984 – 990.

Knowlton, A. A., Brecher, P. and Apstein, C. S. (1991) Rapid expression of heat shock protein in the rabbit after brief cardiac ischaemia. *The Journal of Clinical Investigation* **87**: 139 – 147.

Kokoszka, J. E., Waymire, K. G., Levy, S. E., Sligh, J. E., Cal, J. Y., Jones, D. P., MacGregor, G. R. and Wallace, D. C. (2004) The ADP/ATP translocator is

not essential for the mitochondrial permeability transition pore. *Nature* **427**: 461 – 465.

Kontos, M. C., Fritz, L. M., Anderson, F. P., Tatum, J. L., Ornato, J. P. and Jesse, R. L. (2003) Impact of troponin I standard on the prevalence of acute myocardial infarction. *American Heart Journal* **146**: 446 – 452.

Kost, G. J., Kirk, D. and Omand, K. (1998) A strategy for the use of cardiac injury markers (troponin I and T, creatine kinase–MB mass and isoforms, and myoglobin) in the diagnosis of acute myocardial infarction. *Archives of Pathology and Laboratory Medicine* **122**: 245 – 251.

Krauskopf, A., Eriksson, O., Craigen, W. J., Forte, M. A. and Bernardi, P. (2006) Properties of the permeability transition in VDAC1 (–/–) mitochondria. *Biochimica et Biophysica Acta* **1757**: 590 – 595.

Kroemer, G., Galluzzi, L. and Brenner, C. (2007) Mitochondrial membrane permeabilization in cell death. *Physiological Reviews* **87**: 99 – 163.
Kumar, A. and Cannon, C. P. (2009) Acute coronary syndromes: diagnosis and management, part I. *Mayo Clinic Proceedings* **84**: 917 – 938.

Kui, L., Weiwei, Zhang, Ling, L., Daikun, H., Guoming, Z., Linuo, Z. and Renming, H. (2009) Ghrelin inhibits apoptosis induced by high glucose and sodium palmitate in adult rat cardiomyocytes through the PI3K–Akt signalling pathway. *Regulatory Peptides* **155** (1 – 3):62 – 69.

Labiche, L. A. and Grotta, J. C. (2004) Clinical trials for cytoprotection in stroke. *NeuroRx* **1**: 46 – 70.

Lachgar, A., Sojic, N., Arbault, S., Bruce, D., Sarasin, A., Amatore, C., Bizzini, B., Zagury, D. and Vuillaume, M. (1999) Amplification of the inflammatory cellular redox state by human immunodeficiency virus type 1–immunosuppressive Tat and gp 160 proteins. *The Journal of Virology* **73** (2): 1447 – 1452.

Ladilov, Y. V., Balser, C. and Piper, H. M. (1998) Protection of rat cardiomyocytes against simulated ischaemia and reoxygenation by treatment with protein kinase c activator. *Circulation Research* **82**: 451 – 457.

Lam, Y. C., Gan, H. Y., Nguyen, N. T. and Lie, H. (2009) Micromixer based on viscoelastic flow instability at low Reynolds number. *Biomicrofluidics* **3**: 014106.

Lanigan, P. M. P., Ninkovic, T., Chan, K., de Mello, A. J., Willison, K. R., Klug, D. R., Templer, R. H., Neil, M. A. A. and Ces, O. (2009) A microfluidic platform for probing single cell plasma membranes using optically trapped Smart Droplet Microtools (SDMs). *Lab on a Chip* **9**: 1096 – 1101.

Lanneau, D., Thonel, A. D., Maurel, S., Didelot, C. and Garrido, C. (2007) Apoptosis versus cell differentiation: Role of heat shock protein HSP90, HSP70 and HSP27. *Prion* **1** (1): 53 – 60.

Larsson, L. and Öhman, S. (1978) Serum ionized calcium and corrected total calcium in borderline hyperparathyroidism. *Clinical Chemistry* **24** (11): 1962 – 1965.

Lassnigg, A., Punz, A., Barker, R., Keznickl, P., Manhart, N., Roth, E. and Hiesmayr, M. (2003) Influence of intravenous vitamin E supplementation in cardiac surgery on oxidative stress: a double–blinded, randomized, controlled study. *British Journal of Anaesthesia* **90**: 148 – 154.

Latchman, D. S. (2001) Heat shock proteins and cardiac protection. *Cardiovascular Research* **51**: 637 – 646

Laufs, U., La Fata, V., Plutzky, J. and Liao, J. K. (1998) Upregulation of endothelial nitric oxide synthase by HMG CoA reductase inhibitors. *Circulation* **97**: 1129 – 1135.

Lavrik, I. N. (2010) Systems biology of apoptosis signalling networks. *Current Opinion in Biotechnology* **21** (4): 551 – 555.

Leclerc, E., Sakai, Y. and Fujii, T. (2003) Cell culture in 3–dimensional microfluidic structure of PDMS (polydimethylsiloxane). *Biomedical Microdevices* **5**: 109 – 114.

Lee, A. C., Liu, G., Heng, C. K., Tan, S. N. and Lim, T. M. (2008) Sensitive electrochemical detection of horseradish peroxidase at disposable screen–printed carbon electrode. *Electroanalysis* **20** (1): 2040 – 2046.

Lefer, D. J., Nakanishi, K., Johnston, W. E. and Vinten-Johansen, J. (1993) Antineutrophil and myocardial protecting actions of a novel nitric oxide donor after acute myocardial ischaemia and reperfusion of dogs. *Circulation* **88**: 2337 – 2350.

Lepore, D. A., Knight, K. R., Anderson, R. L. and Morrison, W. A. (2001) Role of priming stresses and Hsp70 in protection from ischaemia–reperfusion injury in cardiac and skeletal muscle. *Cell Stress Chaperones* **6**: 93 – 96.

Leroux, M. L., Rabson, J. and Desjardins, P. R. E. (1984) Clinical effectiveness of the Du Pont *aca* measurement of creatine kinase MB in serum from patients in the coronary–care unit. *Clinical Chemistry* **30** (9): 1552 – 1554.

Lesnefsky, E. J., Chen, Q., Moghaddas, S., Hassan, M. O., Tandler, B. and Hoppel, C. L. (2004) Blockade of electron transport during ischaemia protects cardiac mitochondria. *The Journal of Biological Chemistry* **279**: 47961 – 47967.

Lesnefsky, E. J., Moghaddas, S., Tandler, B., Kerner, J. and Hoppel, C. L. (2001) Mitochondrial dysfunction in cardiac disease: ischaemia–reperfusion, aging, and heart failure. *Journal of Molecular and Cellular Cardiology* **33** (6): 1065 – 1089.

Leung, A. W. C. and Halestrap, A. P. (2008) Recent progress in elucidating the molecular mechanism of the mitochondrial permeability transition pore. *Biochimica et Biophysica Acta – Bioenergetics* **1777** (7 – 8): 946 – 952.

Leung, A. W., Varanyuwatana, P. and Halestrap, A. P. (2008) The mitochondrial phosphate carrier interacts with cyclophilin D and may play a key role in the permeability transition. *The Journal of Biological Chemistry* **283**: 26312 – 26323.

Leventis, N. and Dass, A. (2005) Demonstration of the elusive concentration–gradient paramagnetic force. *Journal of the American Chemical Society* **127**: 4988 – 4989.

Levraut, J., Iwase, H., Shao, Z. H., Vanden Hoek, T. L. and Schumacker, P. T. (2003) Cell death during ischaemia: relationship to mitochondrial depolarization and ROS generation. *American Journal of Physiology – Heart and Circulatory Physiology* **284**: H549 – H558.

Lewandrowski K. (2009) Point–of–care testing for cardiac markers in acute coronary syndromes and heart failure. *Clinics in Laboratory Medicine* **29** (3): 561 – 572.

Lewandrowski, K., Chen, A. and Januzzi, J. (2002) Cardiac markers for myocardial infarction. *American Journal of Clinical Pathology* **118**: S93 – S99.

Li, C. and Lee, K. H. (2004) Affinity depletion of albumin from human cerebrospinal fluid using Cibacron–blue–3G–A–derivatized photopatterned copolymer in a microfluidic device. *Analytical Biochemistry* **333**: 381 – 388.

Li, Q., Guo, Y., Tan, W., Stein, A. B., Dawn, B., Wu, W., Zhu, X., Lu, X., Xu, X., Siddiqui, T., Tiwari, S. and Bolli, R. (2005) Gene therapy with iNOS provides long–term protection against myocardial infarction without adverse functional consequences. *American Journal of Physiology – Heart and Circulatory Physiology* **290** (2): H584 – H589.

Li, X. and Li, P. C. H. (2005) Microfluidic selection and retention of a single cardiac myocyte, on–chip dye loading, cell contraction by chemical stimulation, and quantitative fluorescent analysis of intracellular calcium. *Analytical Chemistry* **77** (14): 4315 – 4322.

Lim, S. Y., Davidson, S. M., Hausenloy, D. J. and Yellon, D. M. (2007) Preconditioning and postconditioning: The essential role of the mitochondrial permeability transition pore. *Cardiovascular Research* **75** (3): 530 – 535.

Limoges. B., Savéant, J. M. and Yazidi, D. (2003) Quantitative analysis of catalysis and inhibition at horseradish peroxidase monolayers immobilized on an electrode surface. *Journal of the American Chemical Society* **125** (30): 9192 – 9203.

Lin, Z., Richards, S. M., Rosenfeldt, F. L. and Pepe, S. (1997) Uridine preserves ATP during hypoxic perfusion of the rat heart. *Asia Pacific Heart Journal* **6** (3): 190 – 196.

Liu, C. X., Jiang, L. Y., Wang, H., Guo, Z. H. and Cai, X. X. (2007) A novel disposable amperometric biosensor based on trienzyme electrode for the determination of total creatine kinase. *Sensors and Actuators B: Chemical* **122** (1): 295 – 300.

Liu, P., Hock, C. E., Nagele, R. and Wong, P. Y. (1997) Formation of nitric oxide, superoxide, and peroxynitrite in myocardial ischaemia–reperfusion injury in rats. *American Journal of Physiology – Heart and Circulatory Physiology* **272**: 2327 – 2336.

Liu, P., Xiang, J., Zhao, L., Yang, L., Hu, B. and Fu, Q. (2008) Effect of β2–adrenergic agonist clenbuterol on ischaemia/reperfusion injury in isolated rat hearts and cardiomyocyte apoptosis induced by hydrogen peroxide. *Acta Pharmacologica Sinica* **29** (6): 661 – 669.

Liu, R., Liu, J., Xie, L., Wang, M., Luo, J. and Cai, X. (2010) A fast and sensitive enzyme immunoassay for brain natriuretic peptide based on micro–magnetic probes strategy. *Talanta* **81** (3): 1016 – 1021.

Li-Weber, M. (2010) Targeting apoptosis pathways in cancer by Chinese medicine. *Cancer Letters:* In Press.

Ljungdahl, L. and Gerhardt, W. (1978) Creatine kinase enzyme variants in human serum. *Clinical Chemistry* **24**: 832 – 834.

Lopaschuk, G. D., Ussher, J. R., Folmes, C. D., Jaswal, J. S. and Stanley, W. C. (2010) Myocardial fatty acid metabolism in health and disease. *Physiological Reviews* **90**: 207 – 258.

Loyer, X., Gomez, A. M., Milliez, P., Fernandez-Velasco, M., Vangheluwe, P., Vinet, L., Charue, D., Vaudin, E., Zhang, W., Sainte-Marie, Y., Robidel, E., Marty, I., Mayer, B., Jaisser, F., Mercadier, J. J., Richard, S., Shah, A. M., Bénitah, J. P., Samuel, J. L. and Heymes, C. (2008) Cardiomyocyte overexpression of neuronal nitric oxide synthase delays transition toward heart failure in response to pressure overload by preserving calcium cycling. *Circulation* **117***:* 3187 – 3198*.*

Lu, H., Schmidt, M. A. and Jensen, K. F. (2005) A microfluidic electroporation device for cell lysis. *Lab on a Chip* **5**: 23 – 29.

Lu, X. M., Zhang, G. X., Yu, Y. Q., Kimura, S., Nishiyama, A., Matsuyoshi, H., Shimizu, J. and Takaki, M. (2009) The opposite roles of nNOS in cardiac ischaemia–reperfusion–induced injury and in ischaemia preconditioning–induced cardioprotection in mice. *The Journal of Physiological Sciences* **59** (4): 253 – 262.

Luo, Y., Jiang, C., Belanger, A., Akita, G., Wadsworth, S., Gregory, R. and Vincent, K. (2006) A constitutively active HIF–1α/VP16 hybrid factor activates expression of the human B–type natriuretic peptide gene. *Molecular Pharmacology* **69**: 1953 – 1962.

Lv, X., Wan, J., Yang, J., Cheng, H., Li, Y., Ao, Y. and Peng, R. (2008) Cytochrome P450 ω–hydroxylase inhibition reduces cardiomyocyte apoptosis via activation of ERK1/2 signaling in rat myocardial ischaemia–reperfusion. *European Journal of Pharmacology* **596** (1 – 3): 118 – 126.

Ma, X., Zhang, X., Li, C. and Luo, M. (2006) Effect of postconditioning on coronary blood flow velocity and endothelial function and LV recovery after myocardial infarction. *The Journal of Interventional Cardiology* **19**: 367 – 375.

Maddaford, T. G., Hurtado, C., Sobrattee, S., Czubryt, M. P. and Pierce, G. N. (1999) A model of low–flow ischaemia and reperfusion in single, beating adult cardiomyocytes. *American Journal of Physiology Heart and Circulatory Physiology* **277**: H788 – H798.

Maeda, K., Tsutamoto, T., Wada, A., Hisanaga, T. and Kinoshita, M. (1998) Plasma brain natriuretic peptide as a biochemical marker of high left ventricular end–diastolic pressure in patients with symptomatic left ventricular dysfunction. *American Heart Journal* **135**: 825 – 832.

Maekawa, N., Wada, H., Kanda, T., Niwa, T., Yamada, Y., Saito, K., Fujiwara, H., Sekikawa, K. and Seishima, M. (2002) Improved myocardial ischaemia/reperfusion injury in mice lacking tumor necrosis factor–α. *Journal of the American College of Cardiology* **39**: 1229 – 1235.

Maisel, A. (2001) B–type natriuretic peptide in the diagnosis and management of congestive heart failure. *Cardiology Clinics* **19**: 557 – 571.

Maisel, A. S., Krishnaswamy, P., Nowak, R. M., McCord, J., Hollander, J. E., Duc, P., Omland, T., Storrow, A. B., Abraham, W. T., Wu, A. H., Clopton, P., Steg, P. G., Westheim, A., Knudsen, C. W., Perez, A., Kazanegra, R., Herrmann, H. C. and McCullough, P. A. (2002) Rapid measurement of B–type natriuretic peptide in the emergency diagnosis of heart failure. *The New England Journal of Medicine* **347**: 161 – 167.

Makazan, Z., Saini, H. K. and Dhalla, N. S. (2007) Role of oxidative stress in alterations of mitochondrial function in ischaemic–reperfused hearts. *American Journal of Physiology – Heart and Circulatory Physiology* **292** (4): H1986 – H1994.

Manukhina, E. B., Downey, H. F. and Mallet, R. T. (2006) Role of nitric oxide in cardiovascular adaptation to intermittent hypoxia. *Experimental Biology and Medicine* **231**: 343 – 365.

Manz, A., Harrison, D. J., Verpoorte, E. M. J., Fettinger, J. C., Paulus, A., Ludi, H. and Widmer, H. M. (1992) Planar chips technology for miniaturization and integration of separation techniques into monitoring systems: Capillary electrophoresis on a chip. *Journal of Chromatogaphy A* **59**: 253 – 258.

Marber, M. S., Latchman, D. S., Walker, J. M. and Yellon, D. M. (1993) Cardiac stress protein elevation 24 hours after brief ischaemia or heat stress is associated with resistance to myocardial infarction. *Circulation Research* **88**: 1264 – 1272.

Mark, J. E., Allcock, H. and West, R. (2005) *Inorganic Polymers*. Cary, NC, USA:Oxford University Press, Inc.

Marnett, L. J. (1999) Lipid peroxidation – DNA damage by malondialdehyde. *Mutation Research – Fundamental and Molecular Mechanisms of Mutagenesis* **424**: 83 – 95.

Marnett, L. J. (1999) Lipid peroxidation – DNA damage by malondialdehyde. *Mutation Research* **424** (1 – 2): 83 – 95.

Martini, F. H. and Bartholomew, E. F. (2010) *Essentials of anatomy and physiology*. 5th ed. San Francisco: Pearson Education, Inc.

Martini, F. H. and Nath, J. L. (2009) *Fundamentals of anatomy and physiology*. 8th ed. New York: Pearson Benjamin Cummings.

Maruyama, K., Mishima, Y., Minagawa, K. and Motonaka, J. (2002) DNA sensor with a dipyridophenazine complex of osmium (II) as an electrochemical probe. *Analytical Chemistry* **74**: 3698 – 3703.

Masztalerz, M., Wlodarczyk, Z., Czuczejko, J., Slupski, M. and Kedziora, J. (2006) Superoxide anion as a marker of ischaemia–reperfusion injury of the transplanted kidney. *Transplantation Proceedings* **38** (1): 46 – 48.

Matherne, G. P., Linden, J., Byford, A. M., Gauthier, N. S. and Headrick, J. P. (1997) Transgenic A1 adenoside receptor overexpression increases myocardial resistance to ischaemia. *Proceedings of the National Academy of Sciences of the United States of America* **94**: 6541 – 6546.

Matsui, T., Tao, J., Monte, F., Lee, K. H., Li, L., Picard, M., Force, T. L., Franke, T.F., Hajjar, R. J. and Rosenzweig, A. (2001) *Akt* activation preserves cardiac function and prevents injury after transient cardiac ischaemia *in vivo*. *Circulation* **104**: 330 – 335.

Matsuki, A., Igawa, A., Nozawa, T., Nakadate, T., Igarashi, N., Nonomura, M. and Inoue, H. (2006) Early administration of fluvastatin, but not at the onset of ischaemia or reperfusion, attenuates myocardial ischaemia–reperfusion injury through the nitric oxide pathway rather than its antioxidant property. *Circulation Journal* **70**: 1643 – 1649.

Mauchly, J. W. (1940) Significance test for sphericity of a normal n–variate distribution. *The Annals of Mathematical Statistics* **11** (2): 204 – 209.

McCann, C. J., Glover, B. M., Menown, I. B. A., Moore, M. J., McEneny, J., Owens, C. G., Smith, B., Sharpe, P. C., Young, I. S. and Adgey, J. A. (2008) Novel biomarkers in early diagnosis of acute myocardial infarction compared with cardiac troponin T. *European Heart Journal* **29**: 2843 – 2850.

McCord, J., Nowak, R. M., McCullough, P. A., Foreback, C., Borzak, S., Tokarski, G., Tomlanovich, M. C., Jacobsen, G. and Weaver, D. (2001) Ninety–minute exclusion of acute myocardial infarction by use of quantitative point–of–care testing of myoglobin and troponin I. *Circulation* **104**: 1483 – 1488.

McCullough, P. A. and Sandberg, K. R. (2003) Sorting out the evidence on natriuretic peptides. *Reviews in Cardiovascular Medicine* **4**: S13 – S19.

McDonald, J. C. and Whitesides, G. M. (2002) Poly (dimethylsiloxane) as a material for fabricating microfluidic devices. *Accounts of Chemical Research* **35**: 491 – 499.

McDonald, J. C., Duffy, D. C., Anderson, J. R., Chiu, D. T., Wu, H., Schueller, O. J. A. and Whitesides, G. M. (2000) Fabrication of microfluidic systems in poly(dimethylsiloxane). *Electrophoresis* **21**: 27 – 40.

McDonnell, B., Hearty, S., Leonard, P. and O'Kennedy, R. (2009) Cardiac biomarkers and the case for point–of–care testing. *Clinical Biochemistry* **42**: 549 – 561.

McLean, A. S., Huang, S. J. and Salter, M. (2008) Bench–to–bedside review: The value of cardiac biomarkers in the intensive care patient. *Critical Care* **12** (3): 215.

McLean, A. S., Tang, B., Nalos, M., Huang, S. J. and Stewart, D. E. (2003) Increased B–type natriuretic peptide (BNP) level is a strong predictor for cardiac dysfunction in intensive care unit patients. *Anaesthesia and Intensive Care Journal* **31** (1): 21 – 27.

McNeil, C. J. and Manning, P. (2002) Sensor–based measurements of the role and interactions of free radicals in cellular systems. *Reviews in Molecular Biotechnology* **82** (4): 443 – 455.

Mehta, H. B., Popovich, B. K. and Dillmann, W. H. (1988) Ischaemia induces changes in the level of mRNAs coding for stress protein 71 and creatine kinase M. *Circulation Research* **63**: 512 – 517.

Mehta, J. L., Chen, H., Li, D. and Phillips, M. I. (2000) Modulation of myocardial SOD and iNOS during ischaemia–reperfusion by antisense directed at ACE mRNA. *Journal of Molecular and Cellular Cardiology* **32**: 2259 – 2268.

Mengoli, G. and Musiani, M. M. (1994) Phenol electropolymerization: a straight route from monomers to polymer coatings. *Progress in Organic Coatings* **24**: 237 – 251.

Mentzer Jr, R. M., Bartels, C., Bolli, R., Boyce, S., Buckberg, G. D., Chaitman, B., Haverich, A., Knight, J., Menasché, P., Myers, M. L., Nicolau, J., Simoons, M., Thulin, L., Weisel, R. D. and EXPEDITION study investigators (2008) Sodium–hydrogen exchange inhibition by cariporide to reduce the risk of ischaemic cardiac events in patients undergoing coronary artery bypass grafting: results of the EXPEDITION study. *The Annals of Thoracic Surgery* **85** (4): 1261 – 1270.

Mercuro, G., Cadeddu, C., Piras, A., Dessi, M., Madeddu, C., Deidda, M., Serpe, R., Massa, E. and Mantovani, G. (2007) Early epirubicin–induced myocardial dysfunction revealed by serial tissue Doppler echocardiography: correlation with inflammatory and oxidative stress markers. *The Oncologist* **12** (9): 1124 – 1133.

Michael, A. C. and Wightman, R. M. (1996) Microelectrodes. In: P. Kissinger and W. R. Heineman, eds. *Laboratory Techniques in Electroanalytical Chemistry*. New York: Marcel Dekker, Inc.

Miguelez, C., Aristieta, A., Cenci, M. A. and Ugedo, L. (2011) The locus coeruleus is directly implicated in L–DOPA–induced dyskinesia in parkinsonian rats: an electrophysiological and behavioural study. *PLoS ONE* **6** (9): e24679.

Mitchell, P. (1972) Chemiosmotic coupling in energy transduction: a logical development of biochemical knowledge. *Bioenergetics* **3**: 5 – 24.

Mizuno, M., Takeba, Y., Matsumoto, N., Tsuzuki, Y., Asoh, K., Takagi, M., Kobayashi, S. and Yamamoto, H. (2010) Antenatal glucocorticoid therapy accelerates ATP production with creatine kinase increase in the growth–enhanced fetal rat heart. *Circulation Journal* **74**: 171 – 180.

Mizuno, R., Watanabe, M., Sakamoto, T. and Sunamori, M. (1998) L–arginine, a nitric oxide precursor, attenuates ischaemia–reperfusion injury by inhibiting inositol–1,4,5–triphosphate. *The Journal of Thoracic and Cardiovascular Surgery* **115** (4): 931 – 936.

Moens, A. L., Champion, H. C., Claeys, M. J., Tavazzi, B., Kaminski, P. M., Wolin, M. S., Borgonjon, D. J., Nassauw, L. V., Haile, A., Zviman, M., Bedja, D., Wuyts, F. L., Elsaesser, R. S., Cos, P., Gabrielson, K. L., Lazzarino, G., Paolocci, N., Timmermans, J. P., Vrint, C. J. and Kass, D. A. (2008) High–dose folic acid pretreatment blunts cardiac dysfunction during ischaemia coupled to maintenance of high–energy phosphates and reduces postreperfusion injury. *Circulation* **117**: 1810 – 1819.

Moens, A. L., Claeys, M. J., Timmermans, J. P. and Vrints, C. J. (2005) Myocardial ischaemia/reperfusion–injury, a clinical view on a complex pathophysiological process. *International Journal of Cardiology* **100**: 179 – 190.

Mohanty, I. R., Maheshwari, U., Joseph, D. and Deshmukh, Y. (2011) Tribulus teresstris modulates heat shock protein and key anti–apoptotic proteins in the Langendorff model of myocardial ischaemia and reperfusion injury. *African Journal of Pharmacy and Pharmacology* **5**: 165 – 174.

Molho, J. M., Herr, A. E., Desphande, M., Gilbert, J. R., Garguilo, M. G., Paul, P. H., John, P. M., Woudenberg, T. M. And Connel, C. (1998) Fluid transport mechanisms in micro fluidic devices. Micro–electro–mechanical–systems (MEMS), *1998 ASME International Mechanical Engineering Congress and Exposition* (DSC–Vol.66).

Möllmann, H., Nef, H. M., Kostin, S., Dragu, A., Maack, C., Weber, M., Troidl, C., Rolf, A., Elsässer, A., Böhm, M., Branter, R., Hamm, C. W. and Halubarsch, C. J. F. (2010) Ischaemia triggers BNP expression in the human myocardium independent from mechanical stress. *International Journal of Cardiology* **143** (3): 289 – 297.

Monahan, J., Gewirth, A. A. and Nuzzo, R. G. (2002) Indirect fluorescence detection of simple sugars via high–pH electrohpresis in poly(dimethylsiloxane) microfluidic chips. *Electrophoresis* **23**: 2347 – 2354.

Moncada, S. and Erusalimsky, J. D. (2002) Does nitric oxide modulate mitochondrial energy generation and apoptosis? *Nature Reviews Molecular Cell Biology* **3**: 214 – 220.

Morrison, L. K., Harrison, A., Krishnaswamy, P., Kazanegra, R., Clopton, P. and Maisel, A. (2002) Utility of a rapid B–natriuretic peptide assay in differentiating congestive heart failure from lung disease in patients presenting with dyspnea. *Journal of the American College of Cardiology* **39**: 202 – 209.

Morrow, D. A., Cannon, C. P., Jesse, R. L., Newby, L. K., Ravkilde, J., Storrow, A. B., Wu, A. H. B. and Christenson, R. H. (2007) National academy of clinical biochemistry laboratory medicine practice guidelines: clinical characteristics and utilization of biochemical markers in acute coronary syndromes. *Clinical Chemistry* **53**: 552 – 574.

Morshed, B. I., Shams, M. and Mussivand, T. (2011) Identifying severity of electroporation through quantitative image analysis. *Applied Physics Letters* **98**: 143704.

Mukherjee, S., Lekli, I., Das, M., Azzi, A. and Das, D. K. (2008) Cardioprotection with α–tocopheryl phosphate: amelioration of myocardial ischaemia reperfusion injury is linked with its ability to generate a survival signal through Akt activation. *Biochimica et Biophysica Acta – Molecular Basis of Disease* **1782** (9): 498 – 503.

Mungrue, I. N., Gros, R., You, X., Pirani, A., Azad, A., Csont, T., Schulz, R., Butany, J., Stewart, D. J. and Hussain, M. (2002) Cardiomyocyte overexpression of iNOS in mice results in peroxynitrite generation, heart block and sudden death. *The Journal of Clinical Investigation* **109**: 735 – 743.

Muntwyler, J., Cohen-Solal, A., Freemantle, N., Eastaugh, J., Cleland, J., G. and Follath, F. (2004) Relation of sex, age and concomitant diseases to drug prescription for heart failure in primary care in Europe. *European Journal of Heart Failure* **6** (5): 663 – 668.

Murata, M., Akao, M., O'Rourke, B. and Marban, E. (2001) Mitochondrial ATP–sensitive potassium channels attenuate matrix Ca^{2+} overload during simulated ischaemia and reperfusion: possible mechanism of cardioprotection. *Circulation Research* **89**: 891 – 898.

Murphy, E. and Steenbergen, C. (2008) Ion transport and energetics during cell death and protection. *Physiology* **23**: 115 – 123.

Murthy, S. K., Sethu, P., Vunjak-Novakovic, G., Toner, M. and Radisic, M. (2006) Size–based microfluidic enrichment of neonatal rat cardiac cell populations. *Biomedical Microdevices* **8**: 231 – 237.

Nag, A. C. (1980) Study of non–muscle cells of the adult mammalian heart: a fine structural analysis and distribution. *Cytobios* **28**: 41 – 61.

Nagy, G., Xu, C. X., Buck, R. P., Lindner, E. and Neuman, M. R. (1998a) Amperometric microcell for enzyme activity measurements. *Analytical Chemistry* **70** (10): 2156 – 2162.

Nagy, G., Xu, C. X., Buck, R. P., Lindner, E., Neuman, M. R. and Sprinkle, R. H. (1998b) Wet and dry chemistry kits for total creatine kinase activity using a microfabricated, planar, small–volume, amperometric cell. *Analytica Chimica Acta* **377** (1): 1 – 12.

Nakagawa, T., Shimizu, S., Watanabe, T., Yamaguchi, O., Otsu, K., Yamagata, H., Inohara, H., Kubo, T. and Tsujimoto, Y. (2005) Cyclophilin D–dependent mitochondrial permeability transition regulates some necrotic but not apoptotic cell death. *Nature* **434**: 652 – 658.

Nascimben, L., Ingwall, J. S., Pauletto, P., Friedrich, J., Gwathmey, J. K., Saks, V., Pessina, A. C. and Allen, P. D. (1996) Creatine kinase system in failing and nonfailing human myocardium. *Circulation* **94** (8): 1894 – 1901.

Nathan, C. (1997) Inducible nitric oxide synthase: what difference does it make? *The Journal of Clinical Investigation* **100**: 2417 – 2423.

Neubauer, S. (2007) The failing heart – an engine out of fuel. *The New England Journal of Medicine* **356**: 1140 – 1151.

Neubauer, S., Frank, M., Hu, K., Remkes, H., Laser, A., Horn, M., Ertl, G. and Lohse, M. J. (1998) Changes of creatine kinase expression in rat heart post–myocardial infarction. *Journal of Molecular and Cellular Cardiology* **30** (4): 803 – 810.

Nguyen, M. D., Giridharan, G., Prabhu, S. D. and Sethu, P. (2009) Microfluidic cardiac circulation model (microCCM) for functional cardiomyocyte studies. *Conference Proceedings: IEEE Engineering in Medicine and Biology Society* **2009**: 1060 – 1063.

Nie, R., Xia, R., Zhong, X. and Xia, Z. (2007) Salvia miltiorrhiza treatment during early reperfusion reduced postischaemic myocardial injury in the rat. *Canadian Journal of Physiology ad Pharmacology* **85** (10): 1012 – 1019.

Nikaido, H., Tsunoda, H., Nishimura, Y., Kirino, T. and Tanaka, T. (2004) Potential role for heat shock protein 72 in antagonizing cerebral vasopasm after rat subarachnoid hemorrhage. *Circulation* **110**: 1839 – 1846.

Obatomi, D. K., Brant, S., Anthonypillai, V., Early, D. A. and Bach, P. H. (1998) Optimizing perincubation conditions for precision–cut kidney and liver tissue slices: Effect of culture media and antioxidants. *Toxicology in Vitro* **12**: 725 – 737.

Occhiello, E., Morra, M., Cinquina, P. and Garbassi, F. (1992) Hydrophobic recovery of oxygen–plasma–treated polystyrene. *Polymer* **33** (14): 3007 – 3015.

Ohlin, K. E., Francardo, V., Lindgren, H. S., Sillivan, S. E., O'Sullivan, S. S., Luksik, A. S., Vassoler, F. M., Lees, A. J., Konradi, C. and Cenci, M. A. (2011) Vascular endothelial growth factor is upregulated by L–dopa in the parkinsonian brain: implications for the development of dyskinesia. *Brain* DOI: 10.1093/brain/awr165.

Okawa, Y., Nagano, M., Hirota, S., Kobayashi, H., Ohno, T. and Watanabe, M. (1999) Tethered mediator biosensor. Mediated electron transfer between redox enzyme and electrode via ferrocene anchored to electrode surface with long poly(oxyethylene) chain. *Biosensors and Bioelectronics* **14** (2): 229 – 235.

Okochi, M., Ohta, H., Tanaka, T. and Matsunaga, T. (2005) Electrochemical probe for on–chip type flow immunoassay: immunoglobulin G labelled with ferrocenecarboaldehyde. *Biotechnology and Bioengineering* **90**: 14 – 19.

Ong, S. E., Zhang, S., Du, H. and Fu, Y. (2008) Fundamental principles and applications of microfluidic systems. *Frontiers in Bioscience* **13**: 2757 – 2773.

Onogi, H., Minatoguchi, S., Chen, X. H., Bao, N., Kobayashi, H., Misao, Y., Yasuda, S, Yamaki, T., Maruyama, R., Uno, Y., Arai, M., Takemura, G. and Fujiwara, H. (2006) Edaravone reduces myocardial infarct size and improves cardiac function and remodelling in rabbits. *Clinical and Experimental Pharmacology and Physiology* **33** (11): 1035 – 1041.

Ooie, T., Takahashi, N., Saikawa, T., Nawata, T., Arikawa, M., Yamanaka, K., Hara, M., Shimada, T. and Sakata, T. (2001) Single oral dose of geranylgeranylacetone induces heat–shock protein 72 and renders protection against ischaemia/reperfusion injury in rat heart. *Circulation* **104**: 1837 – 1843.

Opie, L. H. (2004) *Heart physiology: from cell to circulation*, 4th ed. Philadephia: Lippincott Williams & Wilkins.

Oppegard, S. C., Blake, A. J., Williams, J. C. and Eddington, D. T. (2010) Precise control over the oxygen conditions within the Boyden chamber using a microfabricated insert. *Lab on a Chip* **10**: 2366 – 2373.

Osbourne, R. (1883) An experimental investigation of the circumstances which determine whether the motion of water shall be direct or sinuous, and of the law resistance in parallel channels. *Philosophical Transactions of the Royal Society* **174**: 935 – 982.

Ottesen, E. A., Hong, J. W., Quake, S. R. and Leadbetter, J. R. (2006) Microfluidic digital PCR enables multigene analysis of individual environmental bacteria. *Science* **314** (5804): 1464 – 1467.

Owen, M. J. and Smith, P. J. (1994) Plasma treatment of polydimethylsiloxane. *Journal of Adhesion Science and Technology* **8:** 1063 – 1075.

Ozcan, C., Bienengraeber, M., Dzeja, P. P. and Terzic, A. (2002) Potassium channel openers protect cardiac mitochondria by attenuating oxidant stress at reoxygenation. *American Journal of Physiology – Heart and Circulatory Physiology* **282**: H531 – H539.

Ozeki, T., Kwon, M. H., Gu, J., Collins, M. J., Brassil, J. M., Miller, M. B., Gullapalli, R. P., Zhuo, J., Pierson, R. N., Griffith, B. P. and Poston, R. S. (2007) Heart preservation using continuous *ex vivo* perfusion improves viability and functional recovery. *Circulation Journal* **71**: 153 – 159.

Palmer, B. S., Hadziahmetovic, M., Veci, T. and Angelos, M. G. (2004) Global ischaemic duration and reperfusion function in the isolated perfused rat heart. *Resuscitation* **62**: 97 – 106.

Pandey, N. R., Kaur, G., Chandra, M., Sanwal, G. G. and Misra, M. K. (2000) Enzymatic oxidant and antioxidants of human blood platelets in unstable angina and myocardial infarction. *International Journal of Cardiology* **76**: 33 – 38.

Panic, S., Loebbecke, S., Tuercke, T., Antes, J. and Boškovic, D. (2004) Experimental approaches to a better understanding of mixing performance of microfluidic devices. *Chemical Engineering Journal* **101**: 409 – 419.

Paradies, G., Petrosillo, G., Pistolese, M., Di Venosa, N., Serena, D. and Ruggiero, F. M. (1999) Lipid peroxidation and alterations to oxidative metabolism in mitochondria isolated from rat heart subjected to ischaemia and reperfusion. *Free Radical Biology and Medicine* **27**: 42 – 50.

Paradies, G., Petrosillo, G., Paradies, V. and Ruggiero, F. M. (2009) Role of cardiolipin peroxidation and Ca^{2+} in mitochondrial dysfunction and disease. *Cell Calcium* **45** (6): 643 – 650.

Parcellier, A., Gurbuxani, S., Schmitt, E., Solary, E. and Garrido, C.(2003) Heat shock proteins, cellular chaperones that modulate mitochondrial cell death pathways. *Biochemical and Biophysical Research Communications* **304**: 505 – 512.

Park, J. L. and Lucchesi, B. R. (1999) Mechanisms of myocardial reperfusion injury. *The Annals of Thoracic Surgery* **68**: 1905 – 1912.

Park, S. J., Kim, J. K., Park, J., Chung, S., Chung, C. and Chang, J.K. (2004) Rapid three–dimensional passive rotation micromixer using the breakup process. *Journal of Micromechanics and Microengineering* **14**: 6 – 14.

Patolsky, F., Lichtenstein, A. and Willner, I. (2001) Detection of single–base DNA mutations by enzyme–amplified electronic transduction. *Nature Biotechnology* **19**: 253 – 257.

Peela, J. R., Jarari, A. M., Hai, A., Rawal, A. K., Kolla, S. D., Sreekumar, S., Khurana, L. and Sidhanathi, N. R. (2010) Cardiac biomarkers: the troponins and CK–MB. *Ibnosina Journal of Medicine and Biomedical Sciences* **2** (5): 190 – 197.

Peters, S. J. A. C., Haagsman, H. P. and van Norren, K. (2008) Arginase release by primary hepatocytes and liver slices results in rapid conversion of arginine to urea in cell culture media. *Toxicology in Vitro* **22**: 1094 – 1098.

Pevni, D., Frolkis, I., Shapira, I., Schwartz, D., Schwartz, I.F., Chernichovski, T., Lev-Ran, O., Sharony, R. and Uretzky, G. (2005) Ischaemia or reperfusion: which is a main trigger for changes in nitric oxide mRNA

synthase expression? *European Journal of Clinical Investigation* **35**: 546 – 550.

Piot, C., Croisille, P., Staat, P., Thibault, H., Rioufol, G., Mewton, N., Elbelghiti, R., Cung, T. T., Bonnefoy, E., Angoulvant, D., Macia, C., Raczka, F., Sportouch, C., Gahide, G., Finet, G., André-Fouët, X., Revel, D., Kirkorian, G., Monassier, J. P., Derumeaux, G. and Ovize, M. (2008) Effect of cyclosporine on reperfusion injury in acute myocardial infarction. *The New England Journal of Medicine* **359**: 473 – 481.

Piper, H. M., Abdallah, Y. and Schäfer, C. (2004) The first minutes of reperfusion: a window of opportunity for cardioprotection. *Cardiovascular Research* **61**: 365 – 371.

Piper, H. M., Kasseckert, S. and Abdallah, Y. (2006) The sarcoplasmic reticulum as the primary target of reperfusion protection. *Cardiovascular Research* **70** (2): 170 – 173.

Plebani, M. and Zaninotto, M. (1998) Diagnostic strategies using myoglobin measurement in myocardial infarction. *Clinica Chimica Acta* **272** (1): 69 – 77.

Poirey, S., Polge, A., Bertinchant, J. P., Bancel, E., Boyer, J. C., Fabbro-Peray, P., de Bornier, B. M., Ledermann, B., Bonnier, M. and Bali, J. P. (2000) CK–MB mass test in ischaemic myocardial injury. Comparison of two tests: BioMerieux Vidas and sanofi access immunoassays. *Journal of Clinical Laboratory Analysis* **14** (2): 43 – 47.

Poizat, C., Keriel, C., Garner, A., Dubois, F., Cand, F. and Cuchet, P. (1993) An experimental model of hypoxia on isolated rat heart in recirculating system: study of fatty acid metabolism with an iodinated fatty acid. *Archives of Physiology and Biochemistry* **101** (6): 347 – 356.

Ponchon, J. L., Cespuglio, R., Gonon, F., Jouvet, M. and Pujol, J. F. (1979) Normal pulse polarography with carbon fiber electrodes for *in vitro* and *in vivo* determination of catecholamines. *Analytical Chemistry* **51** (9): 1483 – 1486.

Pongnimitprasert, N. (2009) Atheroscelosis and NADPH oxidase. *Silpakorn University Science and Technology Journal* **3** (1): 13 – 24.

Pullins, M. D., Grant, K. M. and White, H. S. (2001) Microscale confinement of paramagnetic molecules in magnetic field gradients surrounding ferromagnetic microelectrodes. *The Journal of Physical Chemistry B* **105**: 8989 – 8994.

Qi, L., Pan, H., Li, D., Fang, F., Chen, D. and Sun, H. (2011) Luteolin improves contractile function and attenuates apoptosis following ischaemia–reperfusion in adult rat cardiomyocytes. *European Journal of Pharmacology* **668** (1 – 2): 201 – 207.

Qian, S. and Bau, H. H. (2005) Magneto–hydrodynamic stirrer for stationary and moving fluids. *Sensors and Actuators B* **106**: 859 – 870.

Qian, S. and Bau, H. H. (2008) Magneto–hydrodynamics based microfluidics. *Mechanics Research Communications* **36**: 10 – 21.

Quinton, D., Girard, A., Kim, L. T. T., Raimbault, V., Griscom, L., Razan, F., Griveau, S. and Bedioui, F. (2011) On–chip multi–electrochemical sensor array platform for simultaneous screening of nitric oxide and peroxynitrite. *Lab on a Chip* **11**: 1342 – 1350.

Racher, A. J., Looby, D. and Griffiths, J. B. (1990) Use of lactate dehydrogenase release to assess changes in culture viability. *Cytotechnology* **3**: 301 – 307.

Radisic, M., Park, H., Shing, H., Consi, T., Schoen, F. J., Langer, R., Freed, L. E. and Vunjack-Novakovic, G. (2004) Functional assembly of engineered myocardium by electrical stimulation of cardiac myocytes cultured on scaffolds. *Proceedings of the National Academy of Sciences of the United States of America* **101** (52): 18129 – 18134.

Raghuvanshi, R., Chandra, M., Misra, P. C. and Misra, M. K. (2005) Effect of vitamin E on the platelet xanthine oxidase and lipid peroxidation in the patients of myocardial infarction. *Indian Journal of Clinical Biochemistry* **20**: 26 – 29.

Raghuvanshi, R., Kaul, A., Bhakuni, P., Mishra, A. and Misra, M. K. (2007) Xanthine oxidase as a marker of myocardial infarction. *Indian Journal of Clinical Biochemistry* **22** (2): 90 – 92.

Rajesh, Sharma, V., Tanwar, V. K., Mishra, S. K. and Biradar, A. M. (2010) Electrochemical impedance immunosensor for the detection of cardiac biomarker Myogobin (Mb) in aqueous solution. *Thin Solid Films* **519** (3): 1167 – 1170.

Ramasamy, R., Oates, P. J. and Schaefer, S. (1997) Aldose reductase inhibition protects diabetic and nondiabetic rat hearts from ischaemic injury. *Diabetes* **46** (2): 292 – 300.

Ramirez, J. M., Folkow, L. P. and Blix, A. S. (2007) Hypoxia tolerance in mammals and birds: from the wilderness to the clinic. *Annual Review of Physiology* **69**: 113 – 143.

Ramos, L. W. F., Murad, N., Goto, E., Antônio, E. L., Silva, J., Tucci, P. F. and Carvalho, A. C. (2009) Ischaemia/reperfusion is an independent trigger for increasing myocardial content of mRNA B–type natriuretic peptide. *Heart and Vessels* **24** (6): 454 – 459.

Ravagnan, L., Gurbuxani, S., Susin, S. A., Maisse, C., Daugas, E., Zamzami, N., Mak, T., Jaattela, M., Penninger, J. M., Garrido, C. and Kroemer,

G. Heat–shock protein 70 antagonizes apoptosis–inducing factor. *Nature Cell Biology* **3**: 839 – 843.

Regehr, K. J., Domenech, M., Koepsel, J. T., Carver, K. C., Ellison-Zelski, S. J., Murphy, W. L., Schuler, L. A., Alarid, E. T. and Beebe, D. J. (2009) Biological implications of polydimethylsiloxane–based microfluidic cell culture. *Lab on a Chip* **9**: 2132 – 2139.

Ren, B., Shen, Y., Shao, H., Qian, J., Wu, H. and Jing, H. (2007) Brain natriuretic peptide limits myocardial infarct size dependent of nitric oxide synthase in rats. *Clinica Chimica Acta* **377**(1 – 2): 83 – 87.

Riva, E. and Hearse, D. J. (1991) Isolated, perfused neonatal rat heart preparation for studies of calcium and functional stability. *The Annals of Thoracic Surgery* **52**: 987 – 992.

Rodríguez-Sinovas, A., Abdallah, Y., Piper, H. M. and García-Dorado, D. (2007) Reperfusion injury as a therapeutic challenge in patients with acute myocardial infarction. *Heart Failure Reviews* **12**: 207 – 216.

Roncaglioni, M. C. and Collaborative Group of the Primary Prevention Project. Low–dose aspirin and vitamin E in people at cardiovascular risk: a randomised trial in general practice. *The Lancet* **357** (9250): 89 – 95.

Rott, N. (1990) Note on the history of the Reynolds number. *Annual Review of Fluid Mechanics* **22***: 1 – 2.*

Ruiz-Meana, M., Abellan, A., Miró-Casas, E. and García-Dorado, D. (2007) Opening of mitocondrial permeability transition pore induces hypercontracture in Ca^{2+} overloaded cardiac myocytes. *Basic Research in Cardiology* **102**: 542 – 552.

Ruiz-Meana, M. and García-Dorado, D. (2009) Pathophysiology of ischaemia–reperfusion injury: New therapeutic options for acute myocardial infarction. *Revista Espanola de Cardiología* **62** (2): 199 – 209.

Ruiz-Meana, M., García-Dorado, D., Hofstaetter, B., Piper, H. M. and Soler-Soler, J. (1999) Propagation of cardiomyocyte hypercontracture by passage of Na^{+} through gap junctions. *Circulation Research* **85**: 280 – 287.

Saleh Ahammad, A. J., Choi, Y. H., Koh, K., Kim, J. H., Lee, J. J. and Lee, M. (2011) Electrochemical detection of cardiac biomarker troponin I at gold nanoparticle–modified ITO electrode by using open circuit potential. *International Journal of Electrochemical Science* **6**: 1906 – 1916.

Salem, J. E., Saidel, G. M., Stanley, W. C. and Cabrera, M. E. (2002) Mechanistic model of myocardial energy metabolism under normal and ischaemic conditions. *Annals of Biomedical Engineering* **30** (2): 202 – 216.

Sambandam, N. and Lopaschuk, G. D. (2003) AMP–activated protein kinase (AMPK) control of fatty acid and glucose metabolism in the ischaemic heart. *Progress in Lipid Research* **42**: 238 – 256.

Saraiva, R. M., Minhas, K. M., Raju, S. V., Barouch, L. A., Pitz, E., Schuleri, K. H., Vandegaer, K., Li, D. and Hare, J. M. (2005). Deficiency of neuronal nitric oxide synthase increases mortality and cardiac remodeling after myocardial infarction: role of nitroso–redox equilibrium. *Circulation* **112**: 3415 – 3422.

Sasaki, D. T., Dumas, S. E. and Engleman, B. G. (1987) Discrimination of viable and non–viable cells using propidium iodide in two color immunofluorescence. *Cytometry* **8**: 413.

Saupe, K. W., Spindler, M., Hopkins, J. C., Shen, W. and Ingwall, J. S. (2000) Kinetic, thermodynamic, and developmental consequences of deleting creatine kinase isoenzymes from the heart. Reaction kinetics of the creatine kinase isoenzymes in the intact heart. *The Journal of Biological Chemistry* **275**: 19742 – 19746.

Schinzel, A. C., Takeuchi, O., Huang, Z., Fisher, J. K., Zhou, Z., Rubens, J., Hetz, C., Danial, N. N., Moskowitz, M. A. and Korsmeyer, S. J. (2005) Cyclophilin D is a component of mitochondrial permeability transition and mediates neuronal cell death after focal cerebral ischaemia. *Proceedings of the National Academy of Sciences of the United States of America* **102**: 12005 – 12010.

Schlattner, U., Tokarska-Schlattner, M. and Wallimann. T. (2006) Mitochondrial creatine kinase in human health and disease. *Biochimica et Biophysica Acta – Molecular Basis of Disease* **1762** (2): 164 – 180.

Schlattner, U., Tokarska-Schlattner, M., Ramirez, S., Brückner, A., Kay, L., Polge, C., Epand, R,. F., Lee, R. M., Lacombe, M. L. and Epand, R. M. (2009) Mitochondrial kinases and their molecular interaction with cardiolipin. *Biochimica et Biophysica Acta – Biomembranes* **1788** (10): 2032 – 2047.

Schoenfisch, M. H., Pemberton, J. E., Ovadia, M. and Levy, M. (2005) *In situ* electrochemistry of $Ru(NH_3)_6^{3+}$ in a perfused rat heart. *Electroanalysis* **9**: 135 – 140.

Scholz, F., López de Lara González, G., Machado de Carvalho, L., Hilgemann, M., Brainina, K., Kahlert, H., Jack, R. and Minh, D. (2007), Indirect electrochemical sensing of radicals and radical scavengers in biological matrices. *Angewandte Chemie International Edition* **46**: 8079 – 8081.

Schrier, R. W. and Abraham, W. T. (1999) Hormones and hemodynamics in heart failure. *The New England Journal of Medicine* **341**: 577 – 585.

Schulz, R., Boengler, K., Totzeck, A., Luo, Y., García-Dorado, D., and Heusch, G. (2007) Connexin 43 in ischaemic pre– and postconditioning. *Heart Failure Reviews* **12**: 261 – 266.

Schulz, R., Kelm, M. and Heusch, G. (2004) Nitric oxide in myocardial ischaemia/reperfusion injury. *Cardiovascular Research* **61**: 402 – 413.

Schulz, R., Gres, P., Skyschally, A., Duschin, A., Belosjorow, S., Konietzka, I. and Heusch, G. (2003) Ischaemic preconditioning preserves connexin 43 phosphorylation during sustained ischaemia in pig hearts *in vivo*. *The FASEB Journal* **17**: 1355 –1357.

Scolletta, S., Biagioli, B. and Giomarelli, P. (2011) Cardiac mitochondria and heart failure: the chicken or the egg? In: J. L. Vincent ed. *Annual update in intensive care and emergency medicine 2011*. New York: Springer.

Scott, P. V., Horton, J. N. and Mapleson, W. W. (1971) Leakage of oxygen from blood and water samples stored in plastic and glass syringes. *British Medical Journal* **3**: 512 – 516.

Seidman, J. G. and Seidman, C. (2001) The genetic basis for cardiomyopathy: from mutation identification to mechanistic paradigms. *Cell* **104** (4): 557 – 567.

Shackebaei, D., Ghazvineh, S., Godini, A., Pilehvarian, A. and Reshadat, S. (2010a) Cardioprotective effect of garlic juice on the isolated rat heart in ischaemia–reperfusion. *Journal of Medicinal Plants* **9** (35): 7.

Shackebaei, D., Godini, A. A., Abolghazi, M., Majnouni, M. B. and Hesari, M. (2010b) Protection of ischaemic and reperfused rat heart by aqueous extract of urtica dioica. *Iranian Cardiovascular Research Journal* **4** (3): 107 – 111.

Shan, X., Xu, X., Cao, B., Wang, Y., Guo, L., Zhu, Q., Li, J., Que, L., Chen, Q., Ha, T., Li, C. and Yuehua Li, Y. (2009) Transcription factor GATA–4 is involved in erythropoietin–induced cardioprotection against myocardial ischaemia/reperfusion injury. *International Journal of Cardiology* **134** (3): 384 – 392.

Shao, J., Wu, L., Wu, J., Zheng, Y., Zhao, H., Jin, Q. And Zhao, J. (2009) Integrated microfluidic chip for endothelial cells culture and analysis exposed to a pulsatile and oscillatory shear stress. *Lab on a Chip* **9**: 3118 – 3125.

Shin, Y. S., Cho, K., Lim, S. H., Chung, S., Park, S., Chung, C., Han, D. and Chang, J. K. (2003) PDMS–based micro PCR chip with parylene coating. *Journal of Micromechanics and Microengineering* **13**: 768 – 774.

Shinohara, T., Takahashi, N., Kohno, H., Yamanaka, K., Ooie, T., Wakisaka, O., Murozono, Y., Taniguchi, Y., Torigoe, Y., Hara, M., Shimada, T., Saikawa, T. and Yoshimatsu, H. (2007) Mitochondria are targets for geranylgeranylacetone–induced cardioprotection against ischaemia–

reperfusion in the rat heart. *American Journal of Physiology Heart and Circulatory Physiology* **293**: H1892 – H1899.

Shintani-Ishida, K. and Yoshida, K. (2011) Ischaemia induces phospholamban dephosphorylation via activation of calcineurin, PKC–α, and protein phosphatise 1, thereby inducing calcium overload in reperfusion. *Biochimica et Biophysica Acta – Molecular Basis of Disease* **1812** (7): 743 – 751.

Shleev, S., Wetterö, J., Magnusson, K. E. and Ruzgas, T. (2008) Simultaneous use of electrochemistry and chemiluminescence to detect reactive oxygen species produced by human neutrophils. *Cell Biology International* **32**(12): 1486 – 1496.

Sia, S. K. and Whitesides, G. M. (2003) Microfluidic devices fabricated in poly(dimethylsiloxane) for biological studies. *Electrophoresis* **24**: 3563 – 3576.

Sileikyte, J., Petronilli, V., Zulian, A., Dabbeni-Sala, F., Tognon, G., Nikolov, P., Bernardi, P. and Ricchelli, F. (2011) Regulation of the inner membrane mitochondrial permeability transition by the outer membrane translocator protein (peripheral benzodiazepine receptor. *The Journal of Biological Chemistry* **286**: 1046 – 1053.

Silver, J. T. and Noble, E. G. (2011) Regulation of survival gene hsp70. *Cell Stress and Chaperones*: DOI: 10.1007/s12192–011–0290–6.

Singh, T. P., Nigam, A. K., Gupta, A. K. and Singh, B. (2011) Cardiac biomarkers: When to test? – Physician perspective. *Journal, Indian Academy of Clinical Medicine* **12** (2): 117 – 121.

Sinha Roy, S., Madesh, M., Davies, E., Antonsson, B., Danial, N. and Hajnóczky, G. (2009) Bad targets the permeability transition pore independent of Bax or Bak to switch between Ca^{2+}–dependent cell survival and death. *Molecular Cell* **33**: 377 – 388.

Sinkala, E. and Eddington, D. T. (2010) Oxygen sensitive microwells. *Lab on a Chip* **10**: 3291 – 3295.

Skelley, A. M. and Voldman, J. (2009) An active bubble trap and debubbler for microfluidic systems. *Lab on a Chip* **8**: 1733 – 1737.

Slezak, J., Tribulova, N., Pristacova, J., Uhrik, B., Thomas, T., Khaper, N., Kaul, N. and Singalt, P. K. (1995) Hydrogen peroxide changes in ischaemic and reperfused heart. Cytochemistry and biochemical and X–ray microanalysis. *The American Journal of Pathology* **147**: 772 – 781.

Slyvester, D. C., Hattersley, S. M., Haswell, S. J., Stafford, N. D. and Greenman, J. (2010) Development of microfluidic based devices for studying tumour biology and evaluating treatment response in head and neck cancer biopsies. In: The Chemical and Biological Miniaturisation Society, *14th*

International Conference on Miniaturized systems for Chemistry and Life Sciences. Groningen, The Netherlands 3 – 7 October 2010.

Sodha, N. R., Clements, R. T., Feng, J., Liu, Y., Bianchi, C., Horvath, E. M., Szabo, C. and Sellke, F. W. (2008) The effects of therapeutic sulfide on myocardial apoptosis in response to ischaemia–reperfusion injury. *European Journal of Cardio – Thoracic Surgery* **33** (5): 906 – 913.

Solis-Wever, M. X. (2011) *Microfluidic investigations of cardiomyocyte hypoxia*. Highest Honors. University Honors College.

Sood, R. (2006) *Textbook of Medical Laboratory Technology*. Delhi: Jaypee Brothers Medical Publishers (P) Ltd.

Southampton Electrochemistry Group, University of Southampton (2001) *Instrumental methods in electrochemistry*. West Sussex, UK: Horwood Publishing.

Speer, O., Back, N., Buerklen, T., Brdiczka, D., Koretsky, A., Wallimann, T. and Eriksson, O. (2005) Octameric mitochondrial creatine kinase induces and stabilizes contact sites between the inner and outer membrane. *Biochemical Journal* **385**: 445 – 450.

Staat, P., Rioufol, G., Piot, C, Cottin, Y. Cung, T. T., L'Huillier, I., Aupetit, J. F., Bonnefoy, E., Finet, G., André-Fouët, X. and Ovize, M. (2005) Postconditioning the human heart. *Circulation* **112**: 2143 – 2148.

Stadtman, E. R. (2004) Role of oxidant species in aging. *Current Medicinal Chemistry* **11**: 1105 – 1112.

Staib, J. L., Quindry, J. C., French, J. P., Criswell, D. S. and Powers, S. K. (2007) Increased temperature, not cardiac load, activates heat shock transcription factor 1 and heat shock protein 72 expression in the heart. *American Jounal of Physiology – Regulatory, Integrative ad Comparative Physiology* **292** (1): R432 – R439.

Staib, J. L., Tümer, N. and Powers, S. K. (2009) Increased temperature and protein oxidation lead to HSP 72 mRNA and protein accumulation in the i*n vivo* exercised rat heart. *Experimental Physiology* **94**: 71 – 80.

Stanley, W. C., Recchia, F. A. and Lopaschuk, G. D. (2005) Myocardial substrate metabolism in the normal and failing heart. *Physiological Reviews* **85**: 1093 – 1129.

Starnes, J. W., Taylor, R. P. and Ciccolo, J. T. (2005) Habitual low–intensity exercise does not protect against myocardial dysfunction after ischaemia in rats. *European Journal of Cardiovascular Prevention and Rehabilitation* **12**: 169 – 174.

Storrow, A. B., Lindsell, C. J., Collins, S. P., Fermann, G. J., Blomkalns, A. L., Williams, J. M., Goldsmith, B. and Gibler, W. B. (2006) Emergency department multimarker point–of–care testing reduces time to cardiac marker results without loss of diagnostic accuracy. *Point of Care: The Journal of Near–Patient Testing and Technology* **5** (3): 132 – 136.

Strimike, C. (2006) B–type natriuretic peptide: An emerging cardiac risk marker. *American Journal for Nurse Practitioners* **10** (3): 27 – 34.

Su, H., Sun, X., Ma, H., Zhang, H. F., Yu, Q., J., Huang, C., Wang, X. M., Luan, R. H., Jia, G. L., Wang, H. C. and Gao, F. (2007) Acute hyperglycemia exacerbates myocardial ischaemia/reperfusion injury and blunts cardioprotective effect of GIK. *American Journal of Physiology – Endocrinology and Metabolism* **293** (3): E629 – E635.

Su, C. Y., Chong, K. Y., Chen, J. Ryter, S., Khardori, R. and Lai, C. C. *(*1999*)* A physiologically relevant hyperthermia selectively activates constitutive HSP70 in H9c2 cardiac myoblasts and confers oxidative protection*. Journal of Molecular and Cellular Cardiology* **31***:* 845 – 855*.*

Sudoh, T., Kangawa, K., Minamino, N. and Matsuo, H. (1988) A new natriuretic peptide in porcine brain. *Nature* **332**: 78 – 81.

Sumeray, M. S., Rees, D. D. and Yellon, D. M. (2000) Infarct size and nitric oxide synthase in murine myocardium. *Journal of Molecular and Cellular Cardiology* **32**: 35 – 42.

Sun, H., Guo, T., Liu, L., Yu, Z., Xu, W., Chen, W., Shen, L., Wang, J. and Dou, X. (2010) Ischaemic postconditioning inhibits apoptosis after acute myocardial infarction in pigs. *The Heart Surgery Forum* **13** (5): E305 – E 310.

Sun, Q., Kang, Z., Cai, J., Liu, W., Liu, Y., Zhang, J. H., Denoble, P. J., Tao, H. and Sun, X. (2009) Hydrogen–rich saline protects myocardium against ischaemia/reperfusion injury in rats. *Experimental Biology and Medicine* **234** (10): 1212 – 1219.

Sung, J. H. and Shuler, M. L. (2009) Prevention of air bubble formation in a microfluidic perfusion cell culture system using a microscale bubble trap. *Biomedical Microdevices* **11**: 731 – 738.

Sutherland, F. J. and Hearse, D. J. (2000) The isolated blood and perfusion fluid perfused heart. *Pharmacological Research* **41**: 613 – 627.

Suzuki, K., Murtuza, B., Sammut, I. A., Latif, N., Jayakumar, J., Smolenski, R. T., Kaneda, Y., Sawa, Y., Matsuda, H. and Yacoub, M. H. (2002) Heat shock protein 72 enhances manganese superoxide dismutase activity during myocardial ischaemia–reperfusion injury, associated with mitochondrial protection and apoptosis reduction. *Circulation* **106**: I270 – I276.

Szabó, C. (2003) Multiple pathways of peroxynitrite cytotoxicity. *Toxicology Letters* **140 – 141**: 105 – 112.

Szabó, I. and Zoratti, M. (1993) The mitochondrial permeability transition pore may comprise VDAC molecules. I. Binary structure and voltage dependence of the pore. *FEBS Letters* **330**: 201 – 205.

Szabó, I., De Pinto, V. and Zoratti, M. (1993) The mitochondrial permeability transition pore may comprise VDAC molecules. II. The electrophysiological properties of VDAC are compatible with those of the mitochondrial megachannel. *FEBS Letters* **330**: 206 – 210.

Tabeling, P. (2005) *Introduction to microfluidics*. US: Oxford University Press.

Taegtmeyer, H. (2000) Metabolism – The lost child of cardiology. *Journal of the Amerian College of Cardiology* **36** (4): 1386 – 1388.

Taha, Z. H. (2003) Nitric oxide measurements in biological samples. *Talanta* **61**: 3 – 10.

Takayama, S., McDonald, J. C., Ostuni, E., Liang, M. N., Kenis, P. J. A., Ismagilov, R. F. and Whitesides, G. M. (1999) Patterning cells and their environments using multiple laminar fluid flows in capillary networks. *Proceedings of the National Academy of Sciences of the United States of America* **96**: 5545 – 5548.

Takeuchi, A., Nakafutami, S., Tani, H., Mori, M., Takayama, Y., Moriguchi, H., Kotani, K., Miwa, K., Lee, J., Noshiro, M. and Jimbo, Y. (2011) Device for co–culture of sympathetic neurons and cardiomyocytes using microfabrication. *Lab on a Chip* **11**: 2268 – 2275.

Takimoto, Y., Aoyama, T., Keyamura, R., Shinoda, E., Hattori, R., Yui, Y. and Sasayama, S. (2000) Differential expression of three types of nitric oxide synthase in both infracted and non–infarcted left ventricles after myocardial infarction in the rat. *International Journal of Cardiology* **76**: 135 – 145.

Takimoto, Y., Aoyama, T., Tanaka, K., Keyamura, R., Yui, Y. and Sasayama, S. (2002) Augmented expression of neunoral nitric oxide synthase in the atria parasympathetically decreases heart rate during acute myocardial infarction in rats. *Circulation* **105**: 490 – 496.

Talukder, M. A. H., Zweier, J. L. and Periasamy, M. (2009) Targeting calcium transport in ischaemic heart disease. *Cardiovascular Research* **84**: 345 – 352.

Tamm, N. N., Seferian, K. R., Semenov, A. G., Mukharyamova, K. S., Koshkina, E. V., Krasnoselsky, M. I., Postnikov, A. B., Serebryanaya, D. V., Apple, F. S., Murakami, M. M. and Katrukha, A. G. (2008) Novel immunoassay for quantification of brain natriuretic peptide and its precursor in human blood. *Clinical Chemistry* **54**: 1511 – 1518.

Tandon, N., Marsano, A., Maidhof, R., Wan, L., Park, H. and Vunjak-Novakovic, G. (2011) Optimization of electrical stimulation parameters for cardiac tissue engineering. *Journal of Tissue Engineering and Regenerative Medicine* **5** (6): e115 – e125.

Tang, W. H., Kravtsov, G. M., Sauert, M., Tong, X. Y., Hou, X. Y., Wong, T. M., Chung, S., K. and Chung, S. S. M. (2010) Polyol pathway impairs the function of SERCA and RyR in ischaemic–reperfused rat hearts by increasing oxidative modifications of these proteins. *Journal of Molecular and Cellular Cardiology* **49** (1): 58 – 69.

Tatsumi, T., Shiraishi, J., Keira, N., Akashi, K., Mano, A., Yamanaka, S., Matoba, S., Fushiki, S., Fliss, H. and Nakagawa, M. (2003) Intracellular ATP is required for mitochondrial apoptotic pathways in isolated hypoxic rat cardiac myocytes. *Cardiovascular Research* **59** (2): 428 – 440.

Thannickal, V. J. and Fanburg, B. L. (2000) Reactive oxygen species in cell signalling. American *Journal of Physiology Lung Cellular and Molecular Physiology* **279**: L1005 – L1028.

Thellin, O., Zorzi, W., Lakaye, B., de Borman, B., Coumans, B., Hennen, G., Grisar, T., Igout, A. and Heinen, E. (1999) Housekeeping genes as internal standards: use and limits. *Journal of Biotechnology* **75**: 291 – 295.

Thygesen, K., Alpert, J. S. and White, H. D. (2007) Universal definition of myocardial infarction. *Circulation* **116**: 2634 – 2653.

Totzeck, A., Boengler, K., van de Sand, A., Konietzka, I., Gres, P., García-Dorado, D., Heusch, G. and Schulz, R. (2008) No impact of protein phosphatises on connexion 43 phosphorylation in ischaemic preconditioning. *American Journal of Physiology – Heart and Circulatory Physiology* **295** (5): H2106 – H2112.

Touchberry, C. D., Wacker, M. J., Richmond, S. R., Whitman, S. A. and Godard, M. P. (2006) Age–related changes in relative expression of real–time PCR housekeeping genes in human skeletal muscle. *Journal of Biomolecular Techniques* **17**: 157 – 162.

Toufektsian, M. C., de Lorgeril, M., Nagy, N., Salen, P., Donati, M. B., Giordano, L., Mock, H. P., Peterek, S., Matris, A., Petroni, K., Pilu, R., Rotilio, D., Tonelli, C., de Leiris, J., Boucher, F. and Martin, C. (2008) Chronic dietary intake of plant–derived anthocyanins protects the rat heart against ischaemia–reperfusion injury. *The Jounal of Nutrition* **138**: 747 – 752.

Tripathi, P. and Misra, M. K. (2009) Therapeutic role of L–arginine on free radical scavenging system in ischaemic heart diseases. *Indian Journal of Biochemistry and Biophysics* **46**: 498 – 502.

Trost, S. U., Omens, J. H., Karlon, W. J., Meyer, M., Mestril, R., Covell, J. W. and Dillmann, W. H. (1998) Protection against myocardial dysfunction after a

brief ischaemic period in transgenic mice expressing inducible heat shock protein 70. *The Journal of Clinical Investigation* **101** (4): 855 – 862.

Trueblood, N. A., Ramasamy, R., Wang, L. F. and Scaefer, S. (2000) Niacin protects the isolated heart from ischaemia–reperfusion injury*. American Journal of Physiology – Heart and Circulatory Physiology* **279**: H764 – H771.

Turer, A. T. and Hill, J. A. (2010) Pathogenesis of myocardial ischaemia–reperfusion injury and rationale for therapy. *The American Journal of Cardiology* **106** (3): 360 – 368.

van Midwoud, P. M., Groothius, G. M. M., Merema, M., T. and Verpoorte, E. (2010) Microfluidic biochip for the perifusion of precision–cut rat liver slices for metabolism and toxicology studies. *Biotechnology and Bioengineering* **105**: 184 – 194.

van Rooij, E., Sutherland, L. B., Liu, N., Williams, A. H., McAnally, J., Gerard, R. D., Richardson, J. A. and Olson, E. N. (2006) A signature pattern of stress–responsive microRNAs that can evoke cardiac hypertrophy and heart failure. *Proceedings of the National Academy of Sciences of the United States of America* **103** (48): 18255 – 18260.

Venugopal, V., Hausenloy, D. J., Ludman, A., Di Salvo, C., Kolvekar, S., Yap, J., Lawrence, D., Bognolo, J. and Yellon, D. M. (2009a) Remote ischaemic preconditioning reduces myocardial injury in patients undergoing cardiac surgery with cold–blood cardioplegia: a randomised controlled trial. *Heart* **19**: 1567 – 1571.

Venugopal, V., Ludman, A. Yellon, D.M. and Hausenloy, D. J. (2009b) 'Conditioning' the heart during surgery. *European Journal of Cardio–Thoracic Surg*ery **35**: 977 – 987.

Vivekananthan, D. P., Penn, M. S., Sapp, S. K., Hsu, A. and Topol, E. J. (2003) Use of antioxidant vitamins for the prevention of cardiovascular disease: meta–analysis of randomised trials. *The Lancet* **361**: 2017 – 2023.

Voldman, J., Gray, M. L. and Schmidt, M. A. (2000) An integrated liquid mixer/valve. *Journal of Microelectromechanical Systems* **9** (3): 295 – 302.

Wakisaka, O., Takahashi, N., Shinohara, T., Ooie, T., Nakagawa, M., Yonemochi, H., Hara, M., Shimada, T., Saikawa, T. and Yoshimatsu, H. (2007) Hyperthermia treatment prevents angiotensin II–mediated atrial fibrosis and fibrillation via induction of heat–shock protein 72. *Journal of Molecular and Cellular Cardiology* **43** (5): 616 – 626.

Wambolt, R. B., Lopaschuk, G. D., Brownsey, R. W. and Allard, M. F. (2000) Dichloroacetate improves postischaemic function of hypertrophied rat hearts. *Journal of the American College of Cardiology* **36**: 1378 – 1385.

Wang, J. (2006) Electrochemical biosensors: towards point–of–care cancer diagnostics. *Biosensors and Bioelectronics* **21** (10): 1887 – 1892.

Wang, J., Bao, N., Paris, L. L., Wang, H., Geahlen, R. L. and Lu, C. (2008) Detection of kinase translocation using microfluidic electroporative flow cytometry. *Analytical Chemistry* **80** (4): 1087 – 1093.

Wang, J., Zhang, Z., Hu, Y., Hou, X., Cui, Q., Zang, Y. and Wan, C. (2007) SEA0400, a novel Na^+/Ca^{2+} exchanger inhibitor, reduces calcium overload induced by ischaemia and reperfusion in mouse ventricular myocytes. *Physiological Research* **56**: 17 – 23.

Wang, P. and Heitman, J. (2005) The cyclophilins. *Genome Biology* **6**: 226.

Wang, X., Hofmann, O., Das, R., Barrett, E. M., de Mello, A., J., de Mello, J., C. and Bradley, D. D. C. (2007) Integrated thin–flim polymer/fullerene photodetectors for on–chip microfluidic chemiluminescence detection. *Lab on a Chip* **7**: 58 – 63.

Wang, Y. and Chen, Z. (2010) A novel poly(cyanocobalamin) modified glassy carbon electrode as electrochemical sensor for voltammetric determination of peroxynitrite. *Talanta* **82** (2): 534 – 539.

Wang, Y., Gao, E., Tao, L., Lau, W. B., Yuan, Y., Goldstein, B. J., Lopez, B. L., Christopher, T. A., Tian, R., Koch, W. and Ma, X. L. (2009) AMP–activated protein kinase deficiency enhances myocardial ischaemia/reperfusion injury but has minimal effect on the antioxidant/antinitrative protection of adiponectin. *Circulation* **119**: 835 – 844.

Wang, Z., Liu, S., Wu, P. and Cai, C. (2009) Detection of glucose based on direct electron transfer reaction of glucose oxidase immobilized on highly ordered polyaniline nanotubes. *Analytical Chemistry* **81** (4): 1638 – 1645.

Webb, A., Bond, R., McLean, P., Uppal, R., Benjamin, N. and Ahluwalia, A. (2004) Reduction of nitrite to nitric oxide during ischaemia protects against myocardial ischaemia–reperfusion damage. *Proceedings of the National Academy of Sciences of the United States of America* **101**: 13683 – 13688.

Webster, A., Dyer, C. E., Haswell, S. J. and Greenman, J. (2010) A microfluidic device for tissue biopsy culture and interrogation. *Analytical Methods* **2**: 1005 – 1007.

Wei, G., Z., Zhou, J., J., Wang, B., Wu, F., Bi, H., Wang, Y. M., Yi, D. H., Yu, S. Q. and Pei, J. M. (2007) Diastolic Ca^{2+} overload caused by Na^+/Ca^{2+} exchanger during the first minutes of reperfusion results in continued myocardial stunning. *European Journal of Pharmacology* **572** (1): 1 – 11.

Wei, H., Fu, Y. and Arora, R. (2005) Intron flanking EST–PCR markers: to gene structure analysis in *Rhododendron*. *Theoretical and Applied Genetics* **111** (7): 1347 – 1356.

Werdich, A. A., Lima, E. A., Ivanov, B., Ges, I., Anderson, M. E., Wikswo, J. P. and Baudenbacher, F. J. (2004) A microfluidic device to confine a single cardiac myocyte in a sub–nanoliter volume on planar microelectrodes for extracellular potential recordings. *Lab on a Chip* **4**: 357 – 362.

Weston, M. C., Anderson, E. C., Arumugam, P. U., Narasimhan, P. Y. and Fritsch, I. (2006) Redox magnetohydrodynamic enhancement of stripping voltammetry: toward portable analysis using disposable electrodes, permanent magnets, and small volumes. *Analyst* **131**: 1322 – 1331.

Weston, M. C., Nash, C. K. and Fritsch, I. (2010) Redox–magnetohydrodynamic microfluidics without channels and compatible with electrochemical detection under immunoassay conditions. *Analytical Chemistry* **82**: 7068 – 7072.

Whitesides, G. M. (2006) The origins and the future of microfluidics. *Nature* **442**: 368 – 373.

Wildhirt, S. M., Weismueller, S., Schulze, C., Conrad, N., Kornberg, A. and Reichart B. (1999) Inducible nitric oxide synthase activation after ischaemia/reperfusion contributes to myocardial dysfunction and extent of infarct size in rabbits: evidence for a late phase of nitric oxide–mediated reperfusion injury. *Cardiovascular Research* **43** (3): 698 – 711.

Williams, I. A., Xiao, X., Ju, Y. and Allen, D. G. (2007) The rise of $[Na^+]i$ during ischaemia and reperfusion in the rat heart–underlying mechanisms. *Pflügers Archiv European Journal of Physoiogy* **454** (6): 903 – 912.

Wiwanitkit, V. (2006) Glass syringes are better than plastic for preserving arterial blood gas for oxygen partial pressure determination: an explanation based on nanomaterial composition. *International Journal of Nanomedicine* **1**: 223 – 224.

Wolfrum, S., Grimm, M., Heidbreder, M., Dendorfer, A., Katus, H. A., Liao, J. K. and Richardt, G. (2003) Acute reduction of myocardial infarct size by a hydroxymethyl glutaryl coenzyme A reductase inhibitor is mediated by endothelial nitric oxide synthase. *Journal of Cardiovascular Pharmacology* **41** (3): 474 – 480.

Wong, S. H., Ward, M. C. L. and Wharton, C. W. (2004) Micro t–mixer as a rapid mixing micromixer. *Sensors and Actuators B* **100** (3): 359 – 379.

Wu, A. H. B. and Feng, Y. J. (1998) Biochemical differences between cTnT and cTnI and their significance for diagnosis of acute coronary syndromes. *European Heart Journal* **19**: N25 – N29.

Wu, Y., Lu, X., Xiang, F. L., Lui, E. M. and Feng, Q. (2011) North American ginseng protects the heart from ischaemia and reperfusion injury via upregulation of endothelial nitric oxide synthase. *Pharmacological Research* **64** (3): 195 – 202.

Xu, K. Y., Huso, D. L., Dawson, T. M., Bredt, D. S. and Becker, L. C. (1999) Nitric oxide synthase in cardiac sarcoplasmic reticulum. *Proceedings of the National Academy of Sciences of the United States of America* **96**: 657 – 662.

Xu, L., Tripathy, A., Pasek, D. A. and Meissner, G. (1998) Potential for pharmacology of ryanodine receptor calcium release channels. *Annals of the New York Academy of Sciences* **853**: 130 – 148.

Yamanaka, K., Takahashi, N., Ooie, T., Kaneda, K., Yoshimatsu, H. and Saikawa, T. (2003) Role of protein kinase C in geranylgeranylacetone–induced expression of heat–shock protein 72 and cardioprotection in the rat heart. *Journal of Molecular and Cellular Cardiology* **35**: 785 – 794.

Yamazaki, K. G., Romero-Perez, D., Barraza-Hidalgo, M., Cruz, M., Cortez-Gomez, B., Rivas, M., Cortez-Gomez, B., Ceballos, G. and Villarreal, F. (2008) Short and long term effects of (−)− epicatechin on myocardial ischaemia reperfusion injury. *American Journal of Physiology – Heart and Circulatiory Physiology* **295**: H761 – H767.

Yan, J., Pedrosa, V. A., Enomoto, J., Simonian, A. L. and Revzin, A. (2011) Electrochemical biosensors for on–chip detection of oxidative stress from immune cells. *Biomicrofluidics* **5**: 032008.

Yang, M. and Zhang, X. (2007) Electrical assisted patterning of cardiac myocytes with controlled macroscopic anisotropy using a microfluidic dielectrophoresis chip. *Sensors and Actuators A: Physical* **135** (1): 73 – 79.

Yang, M., Lim, C. C., Liao, R. and Zhang, X. (2006) Oriented and vectorial patterning of cardiac myocytes using a microfluidic dielectrophoresis chip—towards engineered cardiac tissue with controlled macroscopic anisotropy. *Journal of Microelectromechanical Systems* **15** (6): 1483 – 1491.

Yang, M., Lim, C. C., Liao, R. and Zhang, X. (2007) A novel microfluidic impedance assay for monitoring endothelin induced cardiomyocyte hypertrophy. *Biosensors and Bioelectronics* **22** (8): 1688 – 1693.

Yau, T. M., Weisel, R. D., Mickle, D. A., Burton, G. W., Ingold, K. U., Ivanov, J., Mohabeer, M. K., Tumiati, L. and Carson, S. (1994) Vitamin E for coronary bypass operations: a prospective, double–blind, randomized trial. *The Journal of Thoracic and Cardiovascular Surgery* **108** (2): 302 – 310.

Ye, Y., Wang, C., Zhang, J., Cho, Y. K., Gong, G., Murakami, Y. and Bache, R. J. (2001) Myocardial creatine kinase kinetics and isoform expression in hearts with severe LV hypertrophy. *American Journal of Physiology – Heart and Circulatory Physiology* **281** (1): H376 – H386.

Yellon, D. M. and Hausenloy, D. J. (2007) Myocardial reperfusion injury. *The New England Journal of Medicine* **357**: 1121 – 1135.

Yeon, J. H. and Park, J. (2007) Microfluidic cell culture systems for cellular analysis. *BioChip Journal* **1**: 17 – 27.

Yigzaw, Y., Gordon, L. and Solomon, T. (2002) Optimization of a hydrogel–based bienzyme amperometric sensing device for L–glutamate and β–N–oxalyl–α,β–diaminopropionic acid (β–ODAP) using glutamate oxidase and horseradish peroxidise. *Current Separations* **19**: 119 –125.

Yu, H., Yokoyama, M. and Asano, G. (1999) Time course of expression and localization of heat shock protein 72 in the ischaemic and reperfused rat heart. *Japan Circulation Journal* **63**: 278 – 287.

Yu, J., Zhang, H., Wu, F., Li, Q., Ma, H., Guo, W., Wang, H. C. and Gao, F. (2006) Insulin improves cardiomyocyte contractile function through enhancement of SERCA2a activity in simulated ischaemia/reperfusion. *Acta Pharmacologica Sinica* **27** (7): 919 – 926.

Yu, Z. B., Gao, F., Feng, H. Z., and Jin, J. P. (2007) Differential regulation of myofilament protein isoforms underlying the contractility changes in skeletal muscle unloading. *American Journal of Physiology – Cell Physiology* **292**: C1192 – C1203.

Zachary, I. And Morgan, R. D. (2011) Therapeoutic angiogenesis for cardiovascular disease: biological context, challenges, prospects. *Heart* **97**: 181 – 189.

Zamzami, N. and Kroemer, G. (2001) The mitochondrion in apoptosis: hoe Pandora's box opens. *Nature Reviews Molecular Cell Biology* **2**: 67 – 71.

Zanello, P. (2003) *Inorganic electrochemistry: theory, practice and applications.* Cambridge: The Royal Society of Chemistry.

Zaninotto, M., Altinier, S., Lachin, M., Carraro, P. and Plebani, M. (1996) Fluoroenzymometric method to measure cardiac troponin I in sera of patients with myocardial infarction. *Clinical Chemistry* **42** (9): 1460 – 1466.

Zhang, D., Dougal, S. M. and Yeganeh, M. S. (2000) Effects of UV irradiation and plasma treatment on a polystyrene surface studied by IR–visible sum frequency generation spectroscopy. *Langmuir* **16** (10): 4528 – 4532.

Zhang, S. (2004) Beyond the petri dish. *Nature Biotechnology* **22** (2): 151 – 152.

Zhang, Z., Biesiadecki, B. J. and Jin, J. P. (2006) Selective deletion of the NH2–terminal variable region of cardiac troponin T in ischaemia reperfusion

by myofibril–associated mu–calpain cleavage. *Biochemistry* **45**: 11681 – 11694.

Zhao, B., Moore, J. S. and Beebe, D.J. (2002) Principles of surface–directed liquid flow in microfluidic channels. *Analytical Chemistry* **74**: 4259 – 4268.

Zhao, Z. Q. and Vinten-Johasen, J. (2002) Myocardial apoptosis and ischaemic preconditioning. *Cardiovascular Research* **55** (3): 438 – 455.

Zhu, W., Dong, J., Ding, H., Yang, H. and Zhou, Z. (2004) Postnatal development in intermittent hypoxia enhances resistance to myocardial ischaemia/reperfusion in make rats. *European Journal of Applied Physiology* **91**: 716 – 722.

Zhuo, Y., Yi, W. J., Lian, W. B., Yuan, R., Chai, Y. Q., Chen, A. and Hu, C. M. (2011) Ultrasensitive electrochemical strategy for NT–proBNP detection with gold nanochains and horseradish peroxidase complex amplification. *Biosensors and Bioelectronics* **26** (5): 2188 – 2193.

Zima, A. V., Copello, J. A. and Blatter, L. A. (2004) Effects of cytosolic NADH/NAD^+ levels on sarcoplasmic reticulum Ca^{2+} release in permeabilized rat ventricular myocytes. *The Journal of Physiology* **555***:* 727 – 741.

Zimmer, H. G. (1998) The isolated perfused heart and its pioneers. *News in Physiological Sciences* **13**: 203 – 210.

Zimmermann, J., Fromm, R., Meyer, D., Boudreaux, A., Wun, C. C. C., Smalling, R., Davis, B., Habib, G. and Roberts, R. (1999) Diagnostic marker cooperative study for the diagnosis of myocardial infarction. *Circulation* **99**: 1671 – 1677.

Zimmermann, M., Hunziker, P. and Delamarche, E. (2009) Autonomous capillary system for one–step immunoassays. *Biomedical Microdevices* **11** (1): 1 – 8.

Ziółkowska, K., Kwapiszewski, R. and Brzózka, Z. (2011) Microfluidic devices as tools for mimicking the *in vivo* environment. *New Journal of Chemistry* **35** (5): 979 – 990.

Zweier, J. L. and Hassan Talukder, M. A. (2006) The role of oxidants and free radicals in reperfusion injury. *Cardiovascular Research* **70**: 181 – 190.

Zweier, J. L. and Villamena, F. A. (2003) Chemistry of free radicals in biological systems. In: M. L. Kukin and V. Fuster, eds. *Oxidative stress and cardiac failure*. Armonk, New York: Futura Publishing Company, Inc.